The molecular mechanisms of action of antimicrobial ions released from orthopaedic implants on bone cell function and regeneration

Paul Mark Souter

PhD

University of York

Biology

December 2018

Abstract

Orthopaedic implant infection as a consequence of bacterial adhesion to an inert implant surface occurs in 1.7-40 % of open fractures treated with fixation devices. Prevention of bacterial adhesion that is the nidus for infection, through the addition of silver (Ag^+) to the implant surface could reduce this incidence rate, but should not be detrimental to the biology of the fracture healing cascade. Mesenchymal stromal cells (MSCs) are the source of many progenitors involved in the fracture repair process and the effect of silver on *in vitro* MSC viability and function was studied. The application of Ag^+ at concentrations and timeframes determined from a clinically relevant *in vivo* rat model of intramedullary implantation, did not affect MSC growth when cultured at high density. However, Ag^+ induced a significant reduction in MSC clonogenicity compared to controls, which was abrogated through the co-application of Ag^+ with conditioned media from untreated MSCs. Osteogenic and adipogenic differentiation of MSCs exposed to Ag^+ during and prior to differentiation showed no statistical effect on osteogenesis. However adipogenic differentiation was significantly decreased in the presence of Ag^+, but significantly elevated in its absence when using MSCs that had been expanded at clonal density with Ag^+.

The elevation of oxidative stress as a consequence of Ag^+ treatment and the role of the antioxidant pathway in the neutralisation of reactive oxygen species was determined. Real-time PCR and proteomic analysis of MSCs generated under clonogenic conditions in the presence of Ag^+ confirmed the upregulation of components of the peroxiredoxin/thioredoxin pathway, in addition to the mechanisms involved with glutathione (GSH) synthesis and reduction. Inhibition of GSH synthesis using BSO eliminated MSC clonogenicity in the presence of Ag^+, while recovery was achieved through the concurrent addition of exogenous GSH, verifying the vital role of GSH in MSC tolerance to Ag^+.

Table of Contents

Abstract 2

Table of Contents 3

List of Tables 10

List of Figures 11

Acknowledgements 15

Declaration 16

1 Chapter 1: Introduction 17

1.1 Fracture epidemiology and treatment background 17

1.2 Fracture repair 19

1.3 An introduction to implant infection 23

1.3.1 The use of inert materials and their contribution to the risks of implant associated infections 25

1.3.2 The formation and characteristics of a bacterial biofilm 26

1.3.3 The prevalence and enhanced effects of implant biofilm upon antibiotic resistance 28

1.3.4 The clinical and financial consequences of implant infection 32

1.4 Strategies for biofilm prevention 33

1.4.1 Prevention of biofilm formation 33

1.5 Silver as an antimicrobial 36

1.5.1 Antimicrobial mode of action 36

1.5.2 The current clinical uses of silver 39

1.5.3 Biological prevalence of silver 41

1.6 Effect of silver on eukaryotic cells 42

1.6.1 Ag^+ uptake in to eukaryotic cells 42

1.6.2 The effects of Ag^+ on the generation of reactive oxygen species (ROS) ... 43

1.7 Mesenchymal stromal cells (MSCs) 48

1.7.1 Characteristics and identification 48

1.7.2 MSC Differentiation 49

1.8 Current research on the effects of Ag^+ 59

1.8.1 The effect of experimental design 59

1.8.2 Cell Function and Regulation 60

1.8.3 Effect of Ag^+ on MSC differentiation 60

2 Chapter 2: Materials and Methods 64

2.1 Materials 64

2.2 *In vitro* 64

2.2.1 Cell culture 64

2.3 Statistical analysis 65

3 Chapter 3: *In vivo* evaluation of silver elution and clearance from titanium intramedullary implants in the rat femur 66

3.1 Introduction 66

3.2 Aims 68

3.3 Methods 69

3.3.1 Surgery 69

3.3.2 Silver quantification using Inductively Coupled Plasma Mass Spectrometry (ICP-MS) 70

3.4 Results 72

3.4.1 Rapid elution of Ag^+ from implant results in sort-term peak exposure 72

3.4.2 Maximum intramedullary Ag^+ exposure 76

3.5 Discussion 78

3.6 Conclusion 81

4 Chapter 4: Availability of Ag^+ in cell culture media 82

4.1 Introduction 82

4.2 Aims 85

4.3 Methods 86

4.3.1 Silver ion preparation, media incubation and ICP-MS analysis 86

4.3.2 *In vitro* viability in different cell culture media 86

4.3.3 *In vitro* viability in DMEM and αMEM containing equal sodium chloride and glucose content 87

4.4 Results 88

4.4.1 Analysis of silver from αMEM & DMEM media 88

4.4.2 Cell viability following 24 hour exposure to Ag^+ when cultured in αMEM and DMEM 92

4.4.3 Effect of media NaCl and glucose content on cytotoxicity of Ag^+ to MSCs 95

4.5 Discussion 98

4.6 Conclusion 102

5 Chapter 5: The effect of silver on cell viability and function 103

5.1 Introduction 103

5.1.1 Origin and background to Y201 clonal MSCs 106

5.2 Aims 107

5.3 Methods 108

5.3.1 Viability & Proliferation 108

5.3.2 CFU-f proliferation and CFU-Osteoblastic (CFU-Ob) formation in presence of Ag^+ 109

5.3.3 Differentiation - Osteogenesis 109

5.3.4 Differentiation - Adipogenesis 110

5.3.5 Determination of clonogenicity of MSCs derived from CFU-f formed during Ag^+ exposure 112

5.3.6 CFU-f formation in conditioned media from semi-confluent cultures (Primary MSCs and Y201s) 114

5.4 Results 115

5.4.1 Cytotoxicity – WST-1, EdU assays 115

5.4.2 CFU-f formation 118

5.4.3 Differentiation 122

5.4.4 Determination of clonogenicity of MSCs derived from CFU-f formed during Ag^+ exposure 128

5.4.5 The effect of conditioned media on CFU-f formation during Ag^+ exposure 131

5.5 Discussion 134

5.6 Conclusion 138

6 Chapter 6: Mechanisms of oxidative stress management 139

6.1 Introduction 139

6.2 Aims 144

6.3 Methods 145

6.3.1 qPCR of oxidative stress pathway (Primary MSC) 145

6.3.2 Global proteomic analysis of CFU-f cell lysates (Y201) 146

6.3.3 Inhibition of oxidative stress pathway (Primary MSCs) 147

6.3.4 Addition of exogenous reduced glutathione to cultures treated with the γ-glutamylcysteine synthetase inhibitor, L-Buthionine-sulfoxamine (BSO), and/or 10 μM Ag^+ (Primary MSCs) 147

6.3.5 Immunocytochemistry of CFU-f for the glutathione synthesis subunit, GCLM, and thioredoxin (Primary MSCs) 148

6.3.6 Response of Y201 MSC Wnt reporters to stimulation of the Wnt pathway following CFU-f expansion in the presence of 10 μM Ag^+ 149

6.4 Results 150

6.4.1 Molecular regulation of oxidative stress pathways during CFU-f formation in the presence of 10 μM Ag^+ 150

6.4.2 Protein regulation by MSCs during CFU-f formation in the presence of 10 μM Ag^+ 153

6.4.3 Immunocytochemistry detection of upregulated oxidative stress related proteins, GCLM and TRX 162

6.4.4 Oxidative stress pathway inhibition and recovery through addition of reduced glutathione 165

6.4.5 Wnt signaling pathway reduction in CFU-f expanded in 10 μM Ag^+ (Y201-Wnt) 170

6.5 Discussion 172

6.6 Conclusion 176

7 Chapter 7: General Discussion 177

7.1 Differentiation 178

7.2 Clonogenicity 179

7.3 Oxidative stress pathway identification 180

7.4 Further mechanisms 181

7.5 Limitations 183

7.6 Future directions 184

Appendix 1 188

8 List of Abbreviations 217

9 References 219

List of Tables

Table 1.1: Gustilo-Anderson classification of open fractures with subsequent sub-classification of Grade III injuries. 18

Table 1.2: Classification of infection timings and causative organisms 23

Table 3.1: Calculation of plasma volume, total Ag^+ and maximum Ag^+ concentration within the intramedullary canal for study animals from Day 1. 77

Table 4.1: Measured Ag from DMEM according to target concentration and incubation time 90

Table 4.2: Mean EC_{50} values for Ag^+ cytotoxicity on MSCs and L929 cells. 94

Table 4.3: Expansion time and inclusion in WST-1 viability assay of MSCs cultured in αMEM and DMEM containing low (1 g/L) and high (4.5 g/L) glucose. 96

Table 6.1: Details of significantly upregulated proteins associated with identified KEGG pathways of control and Ag^+ CFU-f (Y201). 158

Table 6.2: Comparison of Y201 protein regulation to corresponding oxidative response genes identified in the primary MSCs of Section 6.4.1. 160

List of Figures

Figure 1.1: Schematic depicting the phases of fracture healing. 22

Figure 1.2: Incidence of implant infection related to Gustilo-Anderson classification of the open fracture separated by region. 24

Figure 1.3: Illustration of biofilm development and maturation. 27

Figure 1.4: Timeline of clinical release and reported bacterial resistance to antibiotics. Note: Penicillin was in limited use prior to 1943. 29

Figure 1.5: Mechanisms of ROS processing for the maintenance of the homeostatic balance between positive cellular ROS and oxidative stress. 44

Figure 1.6: Canonical Wnt signalling pathway. 51

Figure 1.7: Regulation of osteogenesis via activation of Runx2. 53

Figure 1.8: Positive and negative control of adipogenesis through influence on the master regulators, C/EBPα and PPARγ. 55

Figure 1.9: Regulation of chondrogenesis via the Sox9 transcription factor. 58

Figure 3.1: Implantation of silver coated Ti-6Al-4V pin in the rat femoral intramedullary canal (left). Confirmation of placement through medial/lateral X-ray (right). 70

Figure 3.2: Quantification of Ag^{+} from explanted silver coated Ti-6Al-4V implants over a 28 day study period. 73

Figure 3.3: Quantification of Ag^{+} from plasma of rats implanted with a silver coated Ti-6Al-4V implant over a 28 day study period. 74

Figure 3.4: Quantification of Ag^{+} from rat femurs implanted with a silver coated Ti-6Al-4V implant over a 28 day study period. 75

Figure 4.1: Quantification of Ag^+ from cell culture media and deionised water..... 89

Figure 4.2: Quantification of Ag^+ in DMEM cell culture media during 24 hour time period. 90

Figure 4.3: Quantification of Ag^+ from αMEM at short time points..... 91

Figure 4.4: Cell viability of a) MSCs and b) L929 cultured in αMEM and DMEM following 24 hour exposure to Ag^+..... 93

Figure 4.5: MSC viability cultured in DMEM, DMEM spiked with NaCl and αMEM following 24 hour exposure to Ag^+..... 95

Figure 4.6: MSC viability following short (≤11 day) and prolonged (32 day) expansion in low and high glucose DMEM and αMEM following 24 hour exposure to Ag^+..... 97

Figure 5.1: Illustration of two-stage assessment of clonogenicity. 113

Figure 5.2: MSC viability following 24 hour exposure to Ag^+..... 115

Figure 5.3: Cell viability of a) THP-1 human monocytes and b) primary human osteoblasts, following 24 hour exposure to Ag^+..... 116

Figure 5.4: Proliferation of MSCs as determined by the percentage uptake of EdU during 72 hours culture in the presence of Ag^+..... 117

Figure 5.5: Characterisation of colony formation (CFU-f) of MSCs seeded at clonal density and cultured for the initial three days in the presence of ≤10 μM Ag^+..... 119

Figure 5.6: Characterisation of colony formation (CFU-f) of MSCs seeded at clonal density and cultured continuously in the presence of ≤10 μM Ag^+..... 120

Figure 5.7: Characterisation of alkaline phosphatase positive CFU-Ob cultured continuously in the presence of Ag^+..... 121

Figure 5.8: Osteogenic differentiation of culture expanded MSCs in the presence of Ag^+ as determined by normalised ALP activity. 123

Figure 5.9: Adipogenic differentiation of culture expanded MSCs as determined by optical density quantification of lipid deposits stained using Oil Red O. 124

Figure 5.10: Osteogenic differentiation of CFU-f derived MSCs as determined by mean normalised ALP activity. 126

Figure 5.11: Adipogenic differentiation of CFU-f derived MSCs as determined by optical density quantification of lipid deposits stained using Oil Red O. 127

Figure 5.12: CFU-f generation by MSCs during Stage 2 culture following pre-culture at clonal density. 130

Figure 5.13: Flow cytometry analysis of MSC and Y201 conditioned media. 132

Figure 5.14: Effect of Ag^+ on CFU-f number when applied in conditioned media. 133

Figure 6.1: Synthesis of reduced glutathione and the neutralisation of ROS. 141

Figure 6.2: Real-time PCR analysis of oxidative stress gene regulation associated with the response of primary MSCs cultured at clonal density in 10 µM Ag^+ 151

Figure 6.3: Enrichment analysis of oxidative stress genes with mean $\Delta\Delta C_t$ ≥1.5 fold from primary MSCs cultured at clonal density in 10 µM Ag^+. 152

Figure 6.4: Proteomic identification and fold-change of proteins in Ag^+ and control CFU-f (Y201). 154

Figure 6.5: Volcano plot of proteomic data for control and Ag^+ treated CFU-f (Y201). 155

Figure 6.6: Interaction network of significantly upregulated proteins from Ag^+ cultured CFU-f (Y201). 156

Figure 6.7: Protein upregulation in control group CFU-f (Y201) compared to Ag^+ 157

Figure 6.8: Enrichment of correlating gene/protein upregulation in CFU-f under Ag^+ culture conditions. 161

Figure 6.9: Peptide relative abundance of a) GCLM and b) TRX in control and 10 μM Ag^+ cultured CFU-f (Y201, n=3, biological replicates)..... 162

Figure 6.10: Immunostaining of primary MSC CFU-f for the glutathione synthesis protein, GCLM. 163

Figure 6.11: Immunostaining of primary MSC CFU-f for the oxidative stress pathway protein, thioredoxin. 164

Figure 6.12: Potentiation of the Ag^+ induced ROS through addition of the glutathione pathway inhibitor, BSO. 166

Figure 6.13: Potentiation of the Ag^+ induced ROS through addition of the thioredoxin pathway inhibitor, PX-12. 167

Figure 6.14: Mean CFU-f number of MSCs treated with a combination of 10 μM Ag^+, the glutathione pathway inhibitor, BSO, and 2 mM GSH-MEE. 169

Figure 6.15: Response of Y201-Wnt MSCs to Wnt3a following expansion as CFU-f in the presence/absence of 10μM Ag^+. 171

Figure 7.1: Mechanisms of ROS processing as a consequence of Ag^+ exposure. 186

Figure 7.2: DNA repair mechanisms in which protein components were upregulated in MSC CFU-f 187

Acknowledgements

Firstly I would like to thank my supervisors Paul Genever and Alan Horner for their advice and support throughout this project, special thanks to Paul, who agreed to take me on as a student when Alan and I approached him with the proposal. I would also like to thank my colleagues at Smith & Nephew, particularly Tim Morley for his help in gaining support for my PhD application within the company, and Jim Cunningham, Luke Sprakes and John Vaughan for their advice on ideas and technical aspects of the project at its early stages.

My transition from industry to full time academia half way through the project was made easier by the members of the Genever and J0 labs. I must therefore thank both past and present members who were always welcoming and willing to help, making my return to University as a mature student an enjoyable experience that I would recommend to anyone. Outside of the lab group, I have relied on the advice and expertise of the departmental Technology Facility, so thanks goes to those members, especially Graeme Park who has always been on hand to point me in the right direction with confocal microscopy. I must also thank Adam Dowle and Rebecca Preece of Metabolomics and Proteomics, who have helped with the generation of the hugely useful body of data on protein regulation.

Finally, I would like to thank my family for their unwavering support for my decision to pursue this PhD.

Declaration

I declare that this thesis is a presentation of original work performed between April 2014 and May 2018. All experiments were performed by the author except for implant preparation, animal husbandry, surgery and some aspects of ICP-MS during the reported *in vivo* study that were carried out by colleagues at Smith & Nephew Research Centre, York. Dr Adam Dowle of the Metabolomics and Proteomics Department at the University of York performed protein analysis of cell lysates. Preparation and protein analysis of conditioned media was performed by Andrew Stone (University of York) and Dr Adam Dowle, respectively. This work has not previously been presented for an award at this, or any other, University. All sources are acknowledged as References.

1 Chapter 1: Introduction

1.1 Fracture epidemiology and treatment background

Bone fractures are a common clinical occurrence and it is estimated that 38.2 % of the UK population will fracture a bone in their lifetime (1). The prevalence of fractures is altered across gender and age, with the incidence amongst males (4.1 per 100 people) greater than that of females (3.1 per 100 people), and a propensity for fractures in males to decrease with age while those in the female population increases (1,2). This distribution is likely a factor of involvement with high-risk activities in young males and postmenopausal related decreases in bone mineral density in females. Most commonly, fractures occur in the limbs, specifically the long bones of the ulna/radius (21 %) and the tibia/fibula (14 %) (3), treatment of which is through non-fixation (i.e. stabilisation using cast), percutaneous (i.e. pins or external fixation) or internal fixation devices (i.e. screws, plates and intramedullary nails). These treatment regimens are primarily linked to the severity of the fracture and the patient age, with those below the age of 16 years more likely to be treated with casting due to the consideration of continued growth. The most common form of intervention, however, is internal fixation (4).

Internal fracture fixation involves the surgical implantation of 'hardware' such as metal plates, screws and intramedullary nails that supply a degree of mechanical stability while also reducing the fracture i.e. restoring the anatomical relationship between distal and proximal bone fragments. The choice of hardware is related to the fracture type and location, however in the event of fracture repair of the tibial diaphysis, intramedullary nailing is used in 60 % of cases (4). Intramedullary nailing has been practiced since the early part of the 20th century, used initially by G Küntscher during World War II (reviewed in (5,6)). While these techniques proved successful in restoring function to damaged limbs, the incidence of infection was high. Only with developments in technology, techniques and antibiotic therapies was the high rate of infection decreased to what were considered acceptable levels for widespread adoption of the treatment.

However, the treatment of fractures is not a simple case of aligning the broken fragments and expecting the bone to repair. In the 700,000 cases of delayed or non-union reported annually in the USA, there are a multitude of elements that

influence the outcome. These include patient co-morbidities (e.g. diabetes, smoking), surgical factors (e.g. technique, implant suitability) and the severity of the fracture site itself, which is determined in part by the energy that caused the condition (7,8). Fractures are principally categorised as 'closed' or 'open' depending on the presence of a wound at the fracture site. Open fractures are further classified by the degree of soft-tissue damage and contamination. Although several descriptive systems have been developed to allow the accurate classification of such fractures (e.g. AO/OTA classification for fractures), the Gustilo-Anderson classification was the first to be published in 1976, with a subsequent re-classification of Grade III open fractures published in 1984 (Table 1.1). While the classification provides a comprehensive framework from which clinicians can initiate a treatment regime, it also allows for subsequent analysis of outcomes related to the severity of the injury, such as fracture healing success and likelihood of infection.

Table 1.1: Gustilo-Anderson classification of open fractures with subsequent sub-classification of Grade III injuries.

Classification adapted from publications by Gustillo *et al*. (9,10).

Type	Description
I	An open, simple fracture with a clean wound of less than 1cm in length.
II	An open, simple fracture with a wound of >1cm without extensive soft-tissue damage.
III	Either an open segmental fracture, or an open fracture with extensive soft-tissue damage, or a traumatic amputation, or an open contaminated fracture, or vascular injury requiring repair
III A	Adequate soft tissue coverage of fracture despite extensive soft-tissue damage, or high-energy trauma irrespective of wound size.
III B	Extensive soft-tissue loss with periosteal stripping and bone exposure
III C	Open fracture associated with vascular injury requiring repair.

Current standards for the management of open fractures in the UK are detailed in the British Orthopaedic Association Standards for Trauma (BOAST) guidelines authored by the British Orthopaedic Association (BOA) and British Association of Plastic,

Reconstructive and Aesthetic Surgeons (BAPRAS) (11). The guidelines recommend the systemic administration of broad spectrum antibiotics within 3 hours of injury (with additional direct application of antibiotics for Grade III injuries); surgical debridement; fracture stabilisation and soft tissue restoration (flap coverage) (12,13). Where bone loss has occurred, autogenous bone grafts (from the patient) (14), calcium phosphate bone graft substitutes (14), Bioactive silicate glasses (15) and induced periosteum (16) can be used to accelerate bone union.

In a retrospective review of data from a fifteen year study period performed by Court-Brown *et al.* (17), the incidence of open fractures was estimated at approximately 30.7 per 100,000 fractures per year. Mirroring the data previously discussed related to all fractures, there was a greater occurrence in males (69.1 %) than in females, with a decline with age observed for males and an increase with age for females. For open fractures, those of the lower limb are most common (18), although a study in Sweden suggested that the prevalence of such injuries, and consequentially open fractures, are decreasing (19). The Court-Brown data states that approximately 14 % of tibial fractures were classified as 'open' (in part caused by the limited soft tissue), representing 44 % of all long-bone open fractures (17,20). A review of the literature regarding outcomes of open tibial shaft fractures by Papakostidis *et al*. (21) provided a clear examination of the complications related to Gustilo-Anderson score. The incidence of delayed-union, non-union and amputation were all increased in line with a greater open fracture classification, likely a result of reduced periosteal vascularisation, soft tissue damage, insufficient stability or critical sized fracture gap (7). The occurrence of deep infection increased from 1.8 % for Gustilo I to 16.1 % for Gustilo IIIC injuries, an anticipated consequence of the detection of positive microbiological cultures in 70 % of all open injuries (9).

1.2 Fracture repair

Successful fracture repair occurs through one of two distinct routes: primary (direct, cortical) or secondary (indirect, spontaneous) healing (22). Primary healing is the least common form, occurring under conditions of low interfragmentary movement (IFM) or when the fragments of bone resulting from the injury are under compression. Secondary fracture repair, so called due to the secondary transformation of the initial callus in to bony tissue, transpires upon stabilisation of diaphyseal fractures using casting, bracing or intramedullary implantation that allow a controlled degree of IFM (7).

Due to the relevance with intramedullary surgical intervention, secondary healing will be introduced here.

The breaking of a bone initiates a co-ordinated cascade of events that occurs through four recognised phases of repair (Figure 1.1): inflammation, soft callus formation, hard callus formation and bone remodelling (23). The initial fracture causes damage to local tissue and the rupture of blood vessels, resulting in an inflammatory phase that is characterised by the formation of a haematoma and the infiltration of polymorphonuclear neutrophils (PMNs), macrophages and degranulating platelets. In addition, the periosteum and surrounding soft tissue become involved in supplying mesenchymal stromal cells (MSCs, see Section 1.7). Together, these released factors are broadly categorised in to i) pro-inflammatory cytokines, ii) chemokines, iii) members of the transforming growth factor beta (TGF-β) super family (e.g. bone morphogenetic proteins, BMPs) and iv) angiogenic promoters (24–27). The elevation of these factors within the first 24 hours following fracture is the start of the complex molecular co-ordination of fracture repair.

The detection of chemoattractants such as C-C motif chemokine 2 (CCL2) and the elevation of the stromal derived factor (SDF)-1 chemokine (also known as CXCL12) receptor (CXCR4), encourage the localisation of lymphocytes, monocytes, macrophages and MSCs that start the process of fracture stabilisation (27–30). Peaks in pro-inflammatory cytokines (interleukin-1 (IL-1) and IL-6); tumour necrosis factor alpha and beta (TNF-α, -β)), angiogenic factors (angiopoietin, vascular endothelial growth factor (VEGF)) and bone metabolism regulators (e.g. BMP-2 and prostaglandin E_2 (PGE_2)) are indicative of the hypoxic environment that the haematoma now provides (24,31–35). While the production of cytokines is believed to play a further role in recruitment of cells to the site of injury, they are also thought to enhance matrix synthesis and encourage angiogenesis (32). Further angiogenic stimulation is provided by angiopoietin-2 which stimulates the early generation of a pool of endothelial cells in preparation for the rebuilding of vasculature, and angiopoietin-1 that encourages the branching of capillaries from the existing blood supply of the periosteum (24,36). Finally, the members of the TGF-β superfamily (BMP-2, -4, -5 & -6) and PGE_2 promote the generation of the soft callus and the regulation of other BMP signalling (37,38); with the proliferation and survival of required cell populations and mobilisation of calcium reserves controlled by growth factors (PDGF, FGF) (24,30,39).

Secondary healing is characterised by soft callus formation that overlaps with the initial inflammatory phase. This period of repair sees the continued generation of the avascular callus by chondrocytes, a result of the differentiation of invading MSCs in the areas of low oxygen tension, and the stimulation of collagen deposition by TGF-β2 and TGF-β3 (28). During this stage of maximal cartilage formation there is an inhibition of endochondral resorption through an elevated expression of osteoprotegerin (OPG), an inhibitor of receptor activator of NF-κB ligand (RANKL) mediated osteoclastogenesis (32,40). Alongside the generation of the callus, endochondral bone formation commences proximally and distally to the fracture site via MSCs that have localised to the region during the initial stages of repair (30). Although a majority of these MSCs have arrived via the periosteum and existing bone marrow, in the case of a closed fracture, the surrounding muscle also provides osteoprogenitors, a source that is impaired in the event of severe open fractures where the periosteum and soft tissue have been stripped (41,42).

As sufficient stabilisation of the fracture is achieved by enlargement of the soft callus there is a transfer to stage three of the repair process, hard callus formation. Chondrocytes undergo terminal differentiation and become hypertrophic with subsequent calcification of the extracellular matrix (43). The increased levels of VEGF released by the hypertrophic chondrocytes results in enhanced vascularisation of the callus, supported by the now stabilised fracture, providing an increased oxygen tension that allows osteogenic differentiation. At this time, TNF-α levels reach a peak alongside elevated OPG and RANKL, stimulating osteoclastogenesis, promoting MSC proliferation and the apoptosis of the chondrocytes. Without TNF-α, there is a delay in chondrocyte apoptosis and the resorption of the mineralised cartilage, a process that is primarily mediated by matrix metalloproteinase 9 and 13 (36,44,45). The replacement of the collagenous matrix with bone is stimulated by BMPs (BMP-2, -6 & -9) that commit MSCs towards the osteoblastic lineage and ensure maturation of committed osteoblasts, bridging the original fracture with new bone.

Whereas the inflammatory and bridging of fracture sites takes approximately 28 days to complete (42), the final process of bone healing is a remodelling phase that can last for several years. The remodelling of the hard callus is achieved by a balanced removal and replacement of the matrix by osteoclasts and osteoblasts, respectively. The co-ordination of which is through continued elevation of IL-1, TNF-α and BMP-2 (36). Once complete, the biomechanical properties of the fracture site return to that of the original structure.

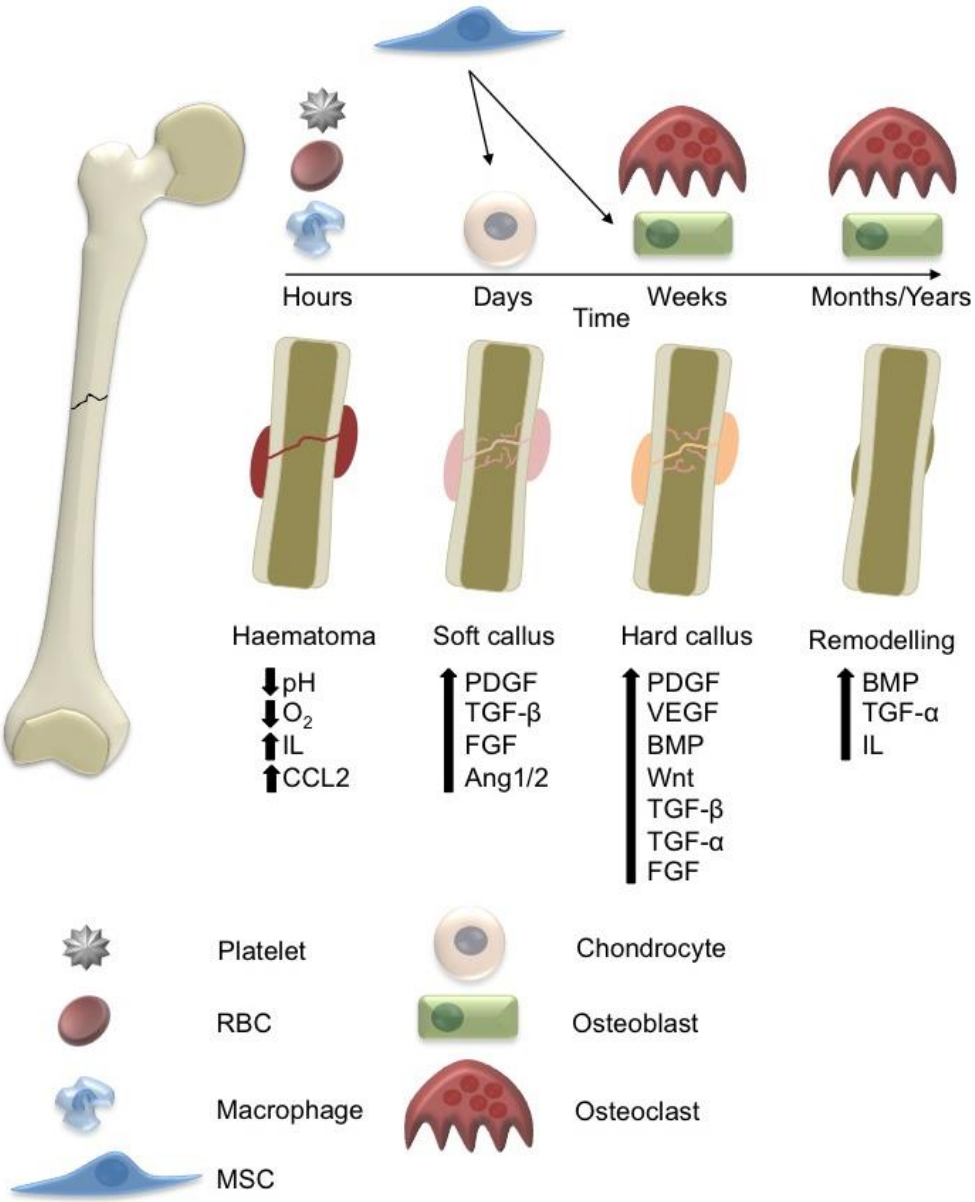

Figure 1.1: Schematic depicting the phases of fracture healing.

The progression from injury to remodelling involves several overlapping processes. Haematoma is characterised by the infiltration of inflammatory cells and a decrease in oxygen tension and pH, the release of pro-inflammatory cytokines results in the recruitment and migration of MSCs to the site of injury. The initiation of the soft callus formation occurs within days, increasing growth factors that promote chondrogenesis; neo-vascularisation can occur due to increased stabilisation of the injury site. Replacement with hard callus progresses from the periphery of the fracture, until bridging occurs with complete hard callus formation completed in 6-8 weeks. The process of remodelling continues for months/years to restore the biomechanical properties of the original bone.

1.3 An introduction to implant infection

Implantation of an inert material in the form of an intramedullary nail can result in infection, one of the most devastating musculoskeletal complications following surgery. In the case of open fractures, the source of infecting bacteria can be from the initiating wound, during insertion of the fixation device e.g. from the patients skin, or post-operatively as a result of disturbances during wound healing (46,47). Approximately 30 % of all cases of fracture fixation device infection are caused by the gram-positive organism, *Staphylococcus aureus*; while coagulase-negative staphylococci (22 %) and gram-negative bacilli (10 %) complete the top three causative agents (46). The timing of infection is classified in to early (<2 weeks post-surgery), delayed (2-10 weeks) or late (>10 weeks) with each primarily caused by variations in the source and virulence of the causative organism (Table 1.2). Early infection presents as local pain, erythema (redness), oedema (local fluid accumulation), incomplete wound healing, haematoma or fever; while delayed or late infection are characterised by increased pain, non-union, implant loosening as a result of osteomyelitis and, in some cases, the development of a sinus tract ('tunnelling wound') (46).

Table 1.2: Classification of infection timings and causative organisms

Table adapted from (46).

Timing	Source and characteristic micro-organism
Early (<2 weeks)	Likely caused through acquisition during initial trauma or surgical intervention. Highly virulent micro-organism (e.g. *Staphylococcus aureus*, gram-negative bacilli e.g. *Enterobacter* spp.)
Delayed (2-10 weeks) & Late (>10 weeks)	Likely caused through acquisition during initial trauma or surgical intervention. Low virulent organisms (e.g. coagulase-negative staphylococci); presence of a low inoculum or incomplete eradication by antimicrobial prophylaxis; in some cases caused by haematogenous seeding from distant infection site.

The risk of infection for closed fractures of the tibia treated with surgical fixation remains low, approximately 1.6 %, however those of open fractures increases to approximately 13.6 % regardless of severity (48). When considering infection rates

related to Gustilo-Anderson classification, Papakostidis *et al*. (21) observed an increase in infection associated with higher Gustilo-Anderson scores when using intramedullary nailing, external fixation and plating. This incidence was reduced when analysing the data for use of intramedullary nailing alone, however the correlation with severity still existed (Mean infection, Gustilo I: 1.7 %, II: 3.1 %, IIIA: 2.4 %, IIIB: 9.2 %). A limitation of these data is the lack of Grade IIIC fractures in which intramedullary nailing was used, however a review of the literature suggests that the mean infection rate associated with Grade IIIC fractures to be 40 % (18,49–65). Also of importance, but not often discussed in the literature, is the geographical influence on the data. While there exists a clear increase related to severity, this is much more pronounced when separating out studies from those countries outside of Europe and North America (i.e. Japan, Malaysia, India) (Figure 1.2).

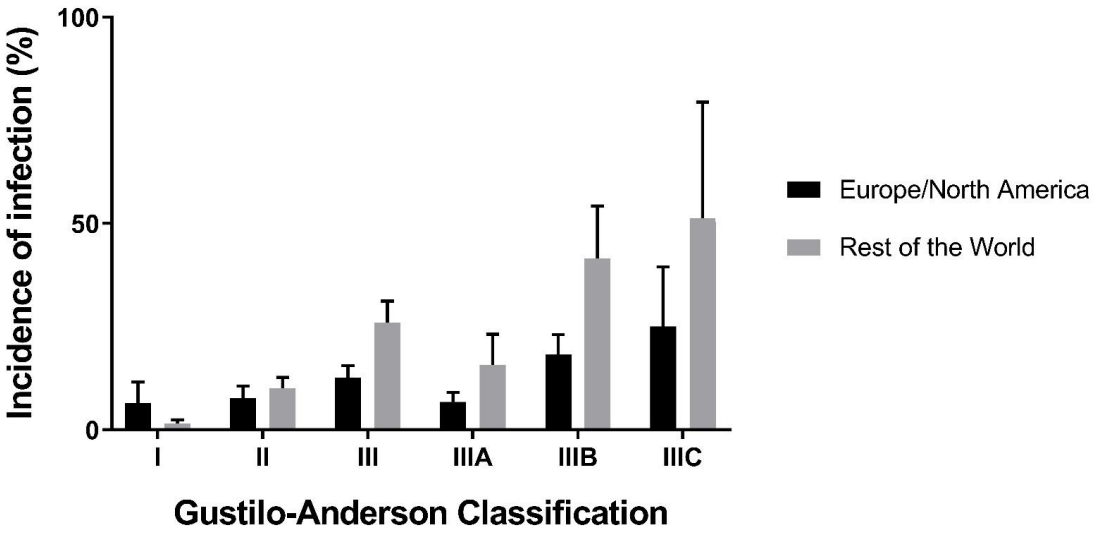

Figure 1.2: Incidence of implant infection related to Gustilo-Anderson classification of the open fracture separated by region.

A marked increase in the rate of infection is observed in all but Grade I cases of open fractures presenting at hospitals outside of Europe & North America (18,49–65). Data presented as mean ±SEM.

1.3.1 The use of inert materials and their contribution to the risks of implant associated infections

The ability of bacteria to generate a local infection is enhanced by the implantation of an inert material. Studies in the 1950s by Elek & Conen (66) demonstrated that the minimum dose of *S. aureus* required to cause a pus-forming wound in healthy human volunteers was greatly reduced when the bacteria were applied sub-cutaneously on a silk suture; a decrease that was not observed when the bacteria were applied to wounds with adjuvants selected to enhance infection. While further studies were hampered by the difficulty in recruiting new volunteers, the results provided evidence that the presence of an inert material enhanced bacterial virulence by the order of 10,000 times. The translation of this work to orthopaedics was primarily recognised by Gristina and colleagues (67) who initially reported on the *in vitro* effects of metal reactivity upon bacterial growth. Their findings showed that inert substrates that had low reactivity and low bacteriotoxic properties provided suitable surfaces on which bacteria were able to proliferate. They therefore speculated that similar effects may be observed if these inert materials were to be implanted *in vivo*. Following these early discoveries and resulting theories, Gristina & Costerton (68) reported on a study of retrieved infected orthopaedic prostheses, culminating in the first evidence that bacterial biofilms forming on inert materials were responsible for the failure of orthopaedic implants. These biofilms were composed of a microcolony surrounded by a protective glycocalyx (see Section 1.3.2). Since these initial publications, further studies have investigated the impact of material selection, surface topography and implant design on the prevalence of bacterial biofilm formation following implantation.

When investigating the effects of implant design on bacterial colonisation, several studies have included surface topography in combination with implant material. Studies to determine the dose of colony forming units (CFU) required to infect 50 % of animals (ID_{50}) in a rabbit tibial fracture model, reported lower ID_{50} for roughened stainless steel and titanium-7% aluminium-6% niobium (TAN) implants compared to smooth controls. While an increased surface roughness might be expected to result in greater bacterial adherence (69), this was not evident *in vivo* for rough commercially pure titanium implants, which returned higher ID_{50} (i.e. a greater number of CFU required for infection) when compared to polished controls (70,71), possibly a result of increased Van der Waals forces on the smoothened surfaces (72,73). Using the same model, Arens *et al*. found that the rate of infection for steel plates (75 %) was significantly greater ($p<0.05$) than that of titanium equivalents (35 %), correlating with the greater

surface energy of stainless steel over that of titanium (74,75). Subcutaneous implantation of stainless steel and commercially pure titanium cylinders with subsequent addition of *Staphylococcus epidermidis* resulted in greater CFU on the stainless steel implants after seven days (76). While within an intramedullary setting, stainless steel implants were also found to be more vulnerable to bacterial adhesion compared to titanium (75,77), however characterisation of the implant surfaces were not performed, therefore the effect of surface topography on these data cannot be determined.

Aside from the material properties and topography, the design of the implant for surgical and mechanical purposes also influences the incidence of infection. Intramedullary nails are cannulated to aide surgical placement especially in the event of comminuted (i.e. a break of multiple fragments) or displaced fractures (i.e. where the bones are separated), however this creates the potential of a 'dead space' within the nail following placement and an increased surface area for colonisation. The resulting area within the centre of the nail is devoid of fluid flow with the consequence being a lack of immune cell and prophylactic antibiotic access. *In vivo* studies comparing the infection resistance of solid nails over cannulated or slotted equivalents reported a >2-fold increase in the infection incidence in the nails that contained the 'dead space' (78,79). Therefore efforts are required to reduce the possibility of bacterial colonisation of this design since it is a feature that ultimately results in greater successful radiographic union (80).

1.3.2 The formation and characteristics of a bacterial biofilm

Biofilms undergo a lifecycle that involves bacterial attachment, biofilm formation and dispersal (Figure 1.3). Their discovery is credited to Van Leeuwenhoek, who initially observed microorganisms on the surfaces of teeth while using simple microscopic techniques (reviewed in (81)). The advent of electron microscopy facilitated the deeper investigation of these structures and was used by Costerton and colleagues (82) to describe the composition of a biofilm in 1978, studying the natural attachment of bacteria to cells and surfaces through the generation of a tangle of polysaccharide fibres across the colony to form a 'glycocalyx' (commonly referred to an extracellular polymeric substance (EPS)). They noted that due to the energy required for the process of forming this beneficial matrix, this had not been observed in the protected environment of the laboratory since it provided no advantage. Since this discovery, controlled laboratory conditions have allowed the extensive understanding of biofilm

formation and development, in addition to *in vivo* studies upon implanted medical devices.

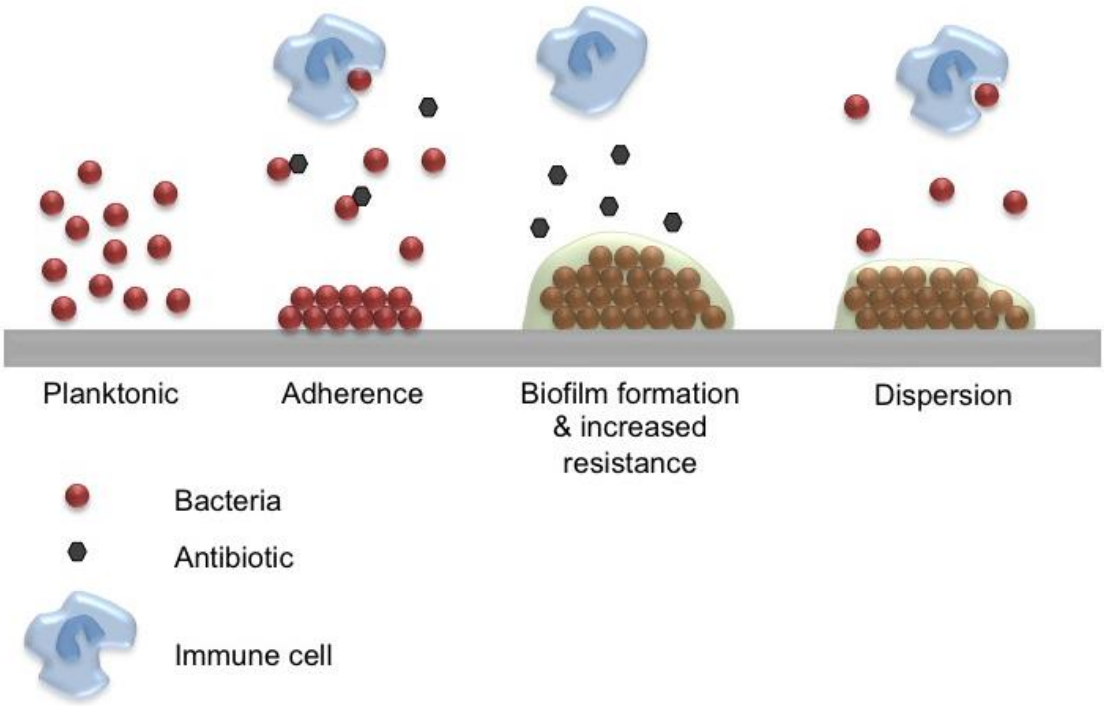

Figure 1.3: Illustration of biofilm development and maturation.

Adhesion of planktonic bacteria leads to the formation of a biofilm consisting of an extracellular polymeric substance (EPS) that contributes to the evasion of host immunity and systemic antibiotics. Eventual dispersion restarts the inflammatory response that can result in osteomyelitis.

The formation of a biofilm starts with the essential process of attachment to a surface, the efficiency of adherence is dependent on the surface topography, substrate and additional, related properties, such as hydrophobicity. In addition, upon implantation a proteinaceous film binds to the surface of the device, facilitating bacterial attachment and the initial stages of biofilm formation (81,83). Division of the bacteria to form a microcolony causes a reduction in the available nutrients and/or accumulation of waste products which in turn enhances stress response genes responsible for, amongst other things, increased EPS synthesis (84,85). The EPS matrix provides stability to the structure, improves adherence to the substrate and surrounding bacterial cells and helps to trap nutrients. The growing biofilm becomes a highly organised structure, containing pores that facilitate the transfer of nutrients and oxygen to its innermost parts, in addition to the transfer of signalling molecules and genetic material (plasmids) that contribute to the properties of this sessile community. As the biofilm matures there is a shedding of individual bacteria and parts of the community held within the EPS. This dispersion or sloughing of the biofilm is affected by a number of independent factors such as nutrient levels, physical forces caused by implant sheer, or quorum sensing that can influence the differentiation of biofilms (81). At this stage, a biofilm that hitherto has caused no clinical symptoms has become a nidus for infection that may result in systemic symptoms. In addition, these bacteria may maintain the antibiotic resistance acquired from the parent biofilm.

1.3.3 The prevalence and enhanced effects of implant biofilm upon antibiotic resistance

The emergence of antibiotic resistant bacteria has become a major concern for public health across the globe. While antibiotic overuse and misuse have been widely reported as the major contributors to this crisis, the decrease in drug development caused by a lack of financial incentive for the pharmaceutical industry, combined with difficult regulatory hurdles, have contributed to the current situation (86). To date, resistance has occurred in nearly all antibiotics, in some cases appearing within twelve months of widespread clinical use (Figure 1.4). Of concern is the developing resistance to drugs of last resort such as vancomycin, an antibiotic originally believed to be difficult to generate resistance to.

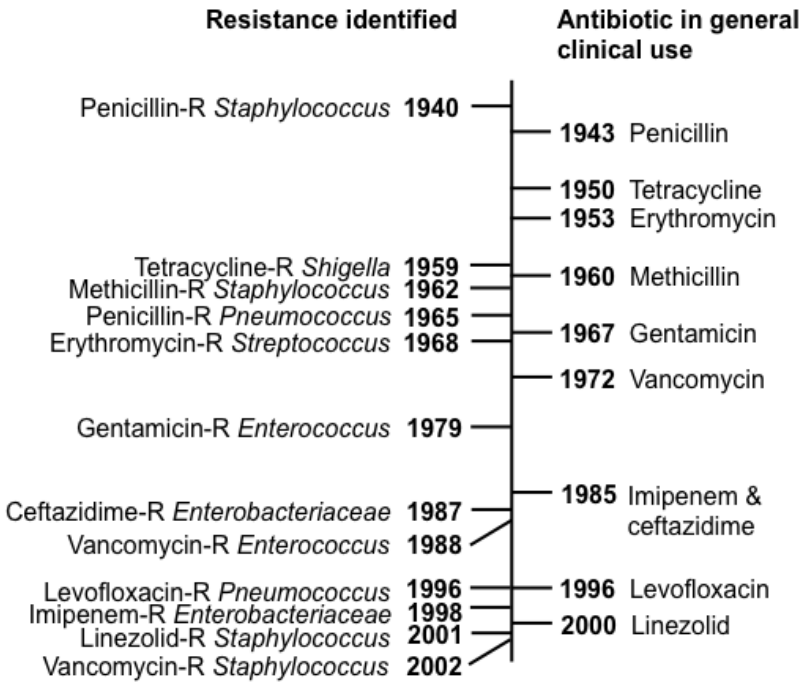

Figure 1.4: Timeline of clinical release and reported bacterial resistance to antibiotics. Note: Penicillin was in limited use prior to 1943.

Adapted from (86).

The inhibitory concentration of antibiotics required for combating established biofilms can be up to 1000 times higher than against their planktonic (freely suspended) equivalents (87). Williams *et al*. (88) reported that 10 times the minimum bactericidal concentration (MBC) of vancomycin and tetracycline were ineffective at killing 7 day *S. aureus* biofilms. However, Rifampicin was effective against the same biofilms at an MBC equivalent to that which was effective against planktonic cultures. In some cases the application of sub-inhibitory concentrations of antibiotics can increase the formation of the biofilm, a defence response of the microorganisms to the onset of chemical attack (89). There are however, a plethora of methods employed to achieve resistance, some being related to the physical nature of the biofilm itself, while others are associated with the development of resistance mechanisms. Although the defence of biofilms is dependent upon the antibiotic agent and the composition of the matrix, the following points outline the generally accepted mode of actions that contribute to the difficulty in combating these infections (90).

The inability of antibiotics to fully penetrate the biofilm, preventing access to the bacterial cells within the matrix, is a major barrier to efficacy. Singh *et al.* (91) reported a decreased capacity of oxacillin, cefotaxime and vancomycin to penetrate the biofilms of *S. aureus* and *S. epidermidis*. This inability may not only be due to the slow diffusion of the chemical through the matrix but also a consequence of the antibiotic being adsorbed by components of the biofilm. Hoye *et al*. (reviewed in (92)) showed that the EPS produced by *Pseudomonas aeruginosa* was able to bind tobramycin, with planktonic cells 15-times more susceptible than those retained within the biofilm. In addition to binding antibiotic agents, Liu *et al.* (93) reported that the deactivation of the antimicrobial oxidant, hydrogen peroxide, by catalase-positive biofilms provided an additional defence mechanism against attack by phagocytes in response to foreign invasion.

A further explanation for the reduced efficacy of antibiotics as a consequence of biofilm formation is the diminished nutrient/oxygen availability to those encased within the EPS. This causes a slowing in the growth of the bacteria, a problem when considering that the effectiveness of many antibiotics is reliant on the growth rate of the target organism. Therefore a transition from logarithmic growth to a stationary phase is detrimental to the bactericidal effect that these agents can impose, further limiting their use (94).

Aside from the physical properties of the biofilm the transfer of extrachromosomal DNA (plasmids) between bacteria of sessile communities appears greater than between their planktonic equivalents (reviewed in (92)). This sharing of genetic material can confer resistance mechanisms upon those bacteria that were previously susceptible to the mode of action of particular antibiotics. Notably, plasmid-encoded resistance has been identified for most classes of commonly used antibiotics (95).

The first evidence of biofilm formation on an implanted medical device (rather than orthopaedic as discussed earlier), and the ineffective treatment with antibiotics, was reported in 1982 by Marrie and colleagues (96). Electron microscopy revealed extensive bacterial biofilm formation on the pacemaker of a patient six years following implantation. The cause was believed to be an infected wound of the elbow received three weeks prior to admission to hospital with nausea, fever and anorexia; blood cultures were positive for *S. aureus*. A four week course of intravenous (i.v.) antibiotics resulted in discharge from hospital, however the patient returned after one week with

severe symptoms. No infection of the pacemaker pocket was noted, and after a second, longer course of i.v. and orally administered antibiotics the patient was allowed home, only to return for a third time nine days later. On this occasion the device was replaced, with i.v. antibiotics continued for four weeks following surgery. Although haematogenous seeding is rare, this clinical evidence first highlighted the problems faced by medicine with regards to bacterial adhesion and the ineffectiveness of antibiotic therapies on an established biofilm.

In the case of open fractures, the inoculation of the implant is likely to occur from the initial injury. Otchwemah and colleagues (97) investigated isolated bacteria from the wounds of patients presenting with open fractures. Their data presented the bacterial species of the fracture, the Gustilo classification and provided details of the resistance to antimicrobials already apparent at surgery. Of the 35 patients from whom swabs were taken, most (n = 17) were from the Gustilo II fractures (Grade I = 6, III = 12). Positive cultures were detected in 50 % of the Grade III swabs and a total of thirteen different pathogens identified (Grade I returned three different pathogens and Grade II, ten). Importantly the corresponding data concerning resistance revealed that ten different antibiotics were ineffective across a range of the isolates from the different fracture severities. While the conclusion stated that the guidelines on antibiotic prophylaxis for open fractures (as reviewed in (98)) were effective in 97 % of cases in the authors local trauma network, the work highlighted the prevalence of microbial contamination of open fractures and the potential for resistant biofilms to form if not dealt with.

As noted above, the current selection of prophylactic antibiotics appears to be appropriate against the strains of bacteria isolated in the study. However, the Otchwemah study did not take in to account the ability of the systemic antibiotics to reach the site of infection at an appropriate concentration and within an appropriate timeframe i.e. before the irreversible attachment of bacteria and subsequent biofilm formation. Where a large degree of soft tissue damage has occurred the systemic antibiotic delivery may be compromised, providing a window of opportunity for colonisation of an implant. In the event that infection does occur, treatment regimes involve high doses of antibiotics, debridement and possible removal of the device. The cultures isolated from the infected device led the selection of appropriate antibiotics and dosages. Treatment can extend for months with i.v. administration likely in many cases (46).

1.3.4 The clinical and financial consequences of implant infection

The costs of infected fracture fixation devices can be viewed from both a clinical and a patient perspective. From a patient perspective there are numerous negative effects of an infection including; pain, increased hospital stay, likely additional surgery, the psychological impact of illness, as well as financial burdens through loss of earnings and in some geographies, the additional healthcare costs where state funded care is not available (99).

Clinically, the cost of surgical site infection (SSI) is measured as the additional financial costs of providing the healthcare and the increase in patient hospitalisation (days), referred to as Length of Stay (LOS). While all publications agree that a consequence of infection is a significant increase in the financial cost and LOS for each patient, there is considerable variation in the degree of change from non-infected controls as a result of geography, follow-up, severity of fracture and inclusion of differing sites of trauma. Thakore *et al*. (100) retrospectively reviewed data from a five-year period collected at their orthopaedic trauma facility (Nashville, USA), calculating costs and LOS for each patient, matching for control and SSI. They concluded that SSI caused an approximate doubling of median hospitalisation costs ($57,418 v $108,782) and LOS (3 v 7 days) compared to controls. While increases observed with these data roughly equated to those of Jenks *et al*. (101) who compared the effects of SSI at a hospital in the UK (although with much reduced costs), they did not include follow-up after the first readmission and are therefore likely to be an underestimation of the true cost. Despite this, Alt (102) used these figures to estimate that the total cost of SSIs, in tibial shaft fractures alone, to be approximately $83.3M annually (closed: $47.2M, open: $36.1M) – the greater cost for closed fractures being a result of their higher annual incidence.

The estimated cost in a European healthcare setting was investigated by Metsemakers *et al*. (48). Using data on tibial shaft fractures at their traumatology centre (Leuven, Belgium), they estimated that the effect of SSI was to increase the cost of healthcare by 6.5-times (median per patient €6,962 v €44,468), with median LOS also increasing (7 days v 54 days). While a majority of the increased cost was related to the LOS, they also showed increases in the median number of operations (1 v 4), consultations (5 v 10) and days on antibiotic therapy (1 v 11), contributing to the additional costs. These data do not separate out the impact of antibiotic resistance (MRSA), however Edwards *et al*. (103) found that this also increased the cost and LOS from those cases of non-MRSA infection in a UK hospital, although each was found to be non-significant.

The benefits, therefore of preventing, or at least reducing, the incidence of infection related to fracture fixation are numerous for both patient and healthcare systems that are already stretched both physically and financially.

1.4 Strategies for biofilm prevention

Arguably, the most effective and efficient way of preventing the onset of infection related to fracture fixation devices is to provide protection for the implant surface against bacterial adhesion (and therefore subsequent biofilm formation), in addition to the current practices employed by first responders and hospitals. By achieving this aim, bacteria within the injury site would continue to be planktonic and therefore remain susceptible to the host immune response and systemic antibiotics. While there may be a degree of extra cost to the purchase price of any implant that comprises a technology designed to do this, it is likely that the increase would be a small percentage of the cost of treating a serious SSI. Nevertheless, for products to be widely used in the clinic rather than just for those patients at most risk, it is likely that manufacturers would endeavour to keep any price increases minimal over that of the untreated device.

1.4.1 Prevention of biofilm formation

The application of biofilm prevention technologies to medical devices requires the consideration of a number of factors other than efficacy, such as biocompatibility, suitability under surgical implantation and ease of incorporation in to manufacturing processes. While these may rule out a number of viable options that otherwise appear promising during *in vitro* testing, they will be included in the following summaries.

1.4.1.1 Low-fouling coatings

As previously discussed (Section 1.3.2), the adhesion of host proteins to the implant surface can provide a favourable substrate upon which invading bacteria are able to attach and form a biofilm. Therefore, in some facture repair environments, the production of a coating that prevents the adhesion of both bacteria and host biomolecules may offer a form of protection from the initiation of an implant infection.

Current strategies are focussed on the addition of various polymers to substrates that provide a hydrophilic surface, thereby resisting the attachment of host cells and non-specific protein adsorption through the generation of a water layer. The

consequence of this coating is therefore to reduce or at least, slow, the attachment of any localised proteins while also repelling any bacteria with coating of a similar charge. While generally gram-negative bacteria have polyanionic EPS, gram-positive bacteria are polycationic, therefore the interaction with these surfaces is highly dependent on the species present within the wound. The difficulty comes however, in instances where the EPS of invading bacterial species contains exopolysaccharide components that are oppositely charged from their generally accepted form (104).

With regards to the clinical suitability of low-fouling coatings, there may be a disadvantage of protecting the surface so directly. Scratches resulting from the abrasion experienced during implantation in to the intramedullary canal could result in areas on the implant surface that are no longer protected. This may provide exposed substrate upon which protein absorption and bacterial adhesion could occur. Quantification of the bacteria within different thicknesses of biofilms reported 3.5 – 7.6 log CFU/cm^2 of substrate surface (105), providing evidence that only a small area of coating removal during surgery could result in the generation of a dangerous biofilm.

With these considerations in mind, it is therefore believed that the design of anti-adhesive surfaces to prevent the attachment of bacterial strains present in a clinical situation may not be possible and that the inclusion of antimicrobial peptides or antibiotics may be necessary for these strategies to be successful.

1.4.1.2 Antibiotic coated surfaces

The application of antibiotics to the surface of implants appears to be an obvious method for preventing the initial adhesion of bacteria while delivering a prophylactic directly to the fracture site. The addition of an eluting antibiotic would provide a halo effect around the implant to kill bacteria while planktonic, nullifying the possible effects of coating removal via abrasion. This approach is commercially available in the form of a biodegradable polymer-coated gentamicin-loaded intramedullary nail (UTN PROtect®, DePuy Synthes). This product releases gentamicin upon degradation of the polymer coating in which the antibiotic is contained. Elution characteristics of the antibiotic from the nail show the release of 70 % within 24 hours in water and published studies report no cases of infection in patients with open or closed tibial fractures (106,107). While these data appear promising, neither study included a matched control group, so baseline infection rates for those institutions are not available.

Antibiotics have also been tethered directly to the surface of implants in an alternative approach to providing antibiotics to the fracture site. This method of application aims to directly protect the surface of the implant, thereby exerting its effect as a barrier to microbial colonisation. Several antibiotics have been attached in this way, with vancomycin (108), minocycline, rifampin (109) tetracycline (110) and enoxacin (111) appearing effective *in vitro* and *in vivo*, however further clinical evidence has not been provided thus far. It also appears that progress towards the clinical use of such implants is beyond the near future. A search of clinical trials (performed on 20th July 2018, www.clinicaltrials.gov) concerning the use of antibiotic coated orthopaedic implants (both fracture fixation and orthopaedic reconstruction) revealed no current or recent trials.

Despite the potential efficacy of these devices, the use of antibiotic coated implants remains controversial. The delivery of additional antibiotics has the potential to cause systemic toxicity to the patient, and while the possibility of this adverse event is low, the benefits of this treatment when given to patients with minimal risk of infection, may not outweigh the possible side effects (112). The significance of using further antibiotics must also be considered in the context of potentially adding to the prospect of resistance. No data are provided on the release of gentamicin from the UTN PROtect® nail following 48 hours, it may therefore be possible that low-level release occurs over a prolonged timeframe. This raises the possibility of providing an environment in which selective-pressures result in the emergence of resistant strains. Evidence of this has been reported following analysis of recovered gentamicin-loaded polymethylmethacrylate beads used to treat bone and soft tissue infections. Residual antibiotic release was detected 5 years following implantation and gentamicin-resistant *Staphylococcal* strains recovered from the bead surfaces (113). While this example focuses on the use of gentamicin, the possibility of similar consequences must be considered with the use of alternative antibiotics and may therefore steer the development of further antibiotic loaded devices.

In addition, the continued efficacy and target specificity of each antibiotic applied to implants must be considered at an early stage of development. For example, the application of vancomycin to implants will only protect against potential infection with gram-positive organisms, while the development of an implant loaded with an antibiotic to which bacterial resistance develops, may also prove worthless. Therefore, the development of technologies using a broad spectrum antimicrobial (effective against a wide variety of gram-negative & gram-positive organisms) with low chance of

resistance is of potential interest to both manufacturers and clinicians alike. With this in mind, attention has increased in recent years in the use of silver as a potent broad spectrum antimicrobial.

1.5 Silver as an antimicrobial

Silver (periodic symbol: Ag; molecular weight: 107.868) is a naturally occurring element that is inert in its non-ionised form. It exists as two isotopes (Ag^{107} and Ag^{109}) and can be found in three oxidation states: Ag^{+}, Ag^{2+} and Ag^{3+}, however only the Ag^{+} format is sufficiently stable for use on medical devices as an antimicrobial (114). The identification of the antibacterial properties of ionic silver was first discovered in the 19th century and is now considered to have broad-spectrum applicability. Initially silver nitrate ($AgNO_3$) was used during the 18th century for the treatment of ulcers, however its acceptance by the US Food and Drug Administration (FDA) in the 1920s cleared its use for the clinical treatment of wounds (115). While the discovery of penicillin reduced the use of silver for the treatment of infections during the 1940s & 1950s, there was an increase in the 1960s as a result of the development of a silver-sulfadiazine cream for the treatment of burns. Since then there has been an explosion in the number of silver containing wound dressings available to wound specialists.

1.5.1 Antimicrobial mode of action

The bactericidal action of silver ions (Ag^{+}) is multi-modal, affecting multiple targets within the molecular machinery of a cell. This provides silver with an advantage over the traditional antibiotics that only target one of a range of specific processes: cell wall, protein, DNA, messenger ribonucleic acid (mRNA) and folic acid synthesis. Whereas the bactericidal effects of Ag^{+} are through its ability to work actively against the cell wall, membrane and cytoplasm; damage bacterial DNA; and denature proteins and enzymes related to cell function and metabolism (116).

The entrance of Ag^{+} in to gram-negative bacteria is enhanced by porins, water filled protein channels of approximately 1 nm diameter that allow the diffusion of solutes through the cell wall and membrane in to the cytoplasm. Radzig and colleagues (117) demonstrated that while these pores were too small for the translocation of silver nanoparticles, bacterial sensitivity to Ag^{+} was reduced in those containing mutations of the porin proteins, therefore indicating at the role of these channels in transfer of silver ions.

The ability of Ag^+ to influence the integrity of bacterial cell walls has been described by various groups. Hachicho and colleagues (118) demonstrated that the application of Ag^+ (through the addition of $AgNO_3$) to *Pseudomonas* strains resulted in the alteration of the *trans/cis* ratio of unsaturated fatty acids within the cell membrane. This ratio has been proposed as a reliable indicator of prokaryotic cell response to stress and is thought to be an effort to decrease the membrane fluidity in response to environmental factors that potentially increase this physiology, thereby affecting the permeability (119). Therefore, the alteration of this ratio is a clear indicator that the action of silver ions is to affect membrane integrity via changes in fluidity. This attack on the structure appears to manifest itself in an increased permeability and a separation of the cell wall from the cell membrane in both gram-positive (*S. aureus*) and gram-negative (*Escherichia coli*) bacteria treated with Ag^+. Images clearly show increases in propidium iodide infiltration and fluorescence from disulphide bond reporter cells of Ag^+ treated cultures indicating increased permeability; in addition to shrinkage of the membrane away from the wall, both effects that ultimately led to the release of cellular components and cell wall degradation (120–122).

The strong binding of Ag^+ with amino acids containing thiols, amino, carboxyl, imidazole and phosphate groups causes their denaturation and inactivation (116). Many of the subsequent biological processes are therefore disrupted, leading to the inhibition of phosphate uptake in *E. coli* in addition to efflux of phosphate, mannitol, glutamine and proline (123); the inhibition of the respiratory chain (124); and inhibition of ribosomal function (125). The negative effect on the ribosome, specifically the expression of the 30S subunit protein S2, is proposed by Yamanaka *et al*. (125) as the prime reason for both the loss of integrity of the cell wall and the collapse of energy metabolism noted by previous researchers. They proposed that the immediate accumulation of Ag^+ was not at the cell periphery, but rather internally having passed through ion channels, and that the denaturing of the ribosome resulted in the prevention of protein and enzyme synthesis. Consequently, the intracellular production of adenosine triphosphate (ATP) was dramatically reduced, thereby compromising cell survival. They stated that this forms the primary bactericidal mode of action of Ag^+.

Despite the belief that the prevention of protein synthesis is the principle biocidal consequence of Ag^+ treatment, other modes of action should not be disregarded. Silver ions are able to bind to DNA resulting in conformational changes to the structure. Feng *et al*. (121) noted electron-light regions in the centre of *E. coli* and *S. aureus* cells correlating to the condensation of DNA in those treated with Ag^+ and a loss of the

ability to replicate. Further genotoxic effects can be attributed to the Ag^+ related generation of reactive oxygen species (ROS) (see Section 1.6.2). Anas *et al.* (126) reported that the DNA of 68 % of *P. aeruginosa* cultures was damaged one hour after Ag^+ treatment, caused by the development of ROS.

As a consequence of the multifaceted bactericidal arsenal of Ag^+, many believe that the possibility of bacterial resistance to silver remains low. However, while there have been few reported cases of silver-resistant clinical isolates, the development of prevalent resistant strains is still considered a future risk (115). Several resistant isolates have been cultured from burns patients where there is widespread use of silver-coated wound dressings to treat the injuries. These, primarily gram-negative bacteria, were found to contain resistance genes on the plasmid DNA. Three different mechanisms of resistance were encoded by these genes: a periplasmic metal-binding protein and two efflux pumps (115,127). While the mechanism for removal of the protein bound Ag^+ from the periplasmic space is yet to be determined, the presence of two parallel encoded efflux pumps potentially provides different mechanisms of Ag^+ removal from the cell. Although these plasmids were transferable to other bacterial species, it was noted that subculture ultimately resulted in a loss of resistance. This loss was also observed upon culture in the absence of Ag^+, suggesting that the resistance was unstable without the selection pressure, possibly the result of a physical cost of maintaining the resistance proteins when not required (115). This evidence therefore suggests that the resistance is through an association rather than a cause of the use of Ag^+.

While using silver on orthopaedic implants is with the aim of preventing biofilm formation, the treatment of established biofilms is of importance in wound management. Although the use of silver dressings has provided limited success in the eradication of mature biofilms (114), some evidence suggests that the application of Ag^+ does negatively affect the integrity of a biofilm. Chaw and colleagues (128) used atomic force microscopy to investigate the intercellular adhesion forces within established *S. epidermidis* biofilms. They showed that the addition of Ag^+ destabilised the biofilm matrix through binding to the electron donor groups of biomolecules, thereby reducing the number of binding sites for hydrogen bonds and electrostatic/hydrophobic forces. Hill *et al*. (129) showed a reduction in viable cells of 3 day old mixed culture biofilms using silver-coated wound dressings, however this was minimal and was ineffective in the more established 7 day biofilms. A finding that supported data from Bjarnsholt and colleagues (130) who concluded that while mature biofilms were

susceptible to the effects of Ag^+, the concentration of silver was 10-100 times greater than that needed to kill planktonic bacteria. The same study also concluded that the amount of Ag^+ on current dressings was below that required to treat chronic biofilms.

With the prevention of biofilm formation the principle aim of an implant coating and systemic antibiotics there must be consideration as to the effects of the combined therapy. It was previously mentioned that the delivery of further antibiotic treatment in the form of an implant coating had the potential to increase the risk of systemic toxicity, an effect that may outweigh any benefits (see Section 1.4.1.2). If the implant coating was comprised of silver that was shown to be biocompatible, there is evidence of improved antimicrobial spectrum and efficacy of the systemically administered antibiotics. Several research groups have observed an increased effect of a combined antibiotic/silver treatment versus antibiotic or silver alone when tested against a range of bacterial species (131–133). Although these results were only proven in bacterial growth inhibition tests, they provide some support to the possible synergistic activity of a combined therapy. These findings were progressed further by Morones-Ramirez and colleagues (122) in both *in vitro* and *in vivo* models of infection. They reported that sub-lethal doses of both Ag^+ and antibiotic result in enhanced antimicrobial activity (the result of increased ROS production). Furthermore, the minimum inhibitory concentration of a resistant *E. coli* strain was returned to that of wild-type when treated with the combination therapy, an effect that they believe to be a result of Ag^+ induced increases in membrane permeability. Finally, they proposed that the combination therapy would allow the use of specific antibiotics across both gram-negative and gram-positive species. For example, the use of vancomycin is limited to the combat of gram-positive infections (e.g. *S. aureus*) through disruption of cell wall synthesis, however the group demonstrated a 100-fold decrease in cell count when *E. coli* (gram-negative) were treated with vancomycin and Ag^+ in an *in vivo* model of intraperitoneal infection. It therefore appears that the potential benefits of applying silver to fracture fixation implants may go beyond its own antimicrobial mode of action.

1.5.2 The current clinical uses of silver

The main clinical use of silver remains in the field of wound management where according to a 2012 report there were approximately 50 silver-containing wound dressings available for clinical use, primarily from eight different companies, applying varying forms of silver to foams, hydrogels and gauzes (134). The use of silver in other areas of medicine is much less widespread, chiefly due to the difficulty of application to

the required materials and the regulatory pathways involved. For example, the pre-clinical testing necessary for inclusion in regulatory submissions for 'permanent' implants (i.e. those residing in the body for >30 days) is greatly more costly and time consuming than for short duration, externally applied wound dressings that can be removed in the case of adverse events (135). The second most commonly found medical use of silver is its incorporation in to catheters to combat catheter-associated urinary tract infections (CAUTI). The risk of CAUTI is calculated at 5 % per day of catheterisation causing it to be the most commonly acquired hospital infection in the United States (136). Disappointingly though, the use of the silver coated devices has shown varying results in the clinic (136,137).

The clinical availability of silver-coated devices in orthopaedics is currently limited to two technologies (Agluna®, Stryker; MUTARS®, Implantcast GmbH) applied to joint reconstruction megaendoprosthesis used for limb salvage in bone oncology patients. Currently there are no silver-coated fracture fixation devices on the market, therefore the following data is only applicable to the joint reconstruction side of orthopaedics, however parallels may be assumed from the results concerning possible infection rates following surgical intervention. Implantation of megaprostheses has proven to be successful in several clinical levels. Reductions in infection rate were observed in all studies investigating the use of silver-coated prostheses, with statistical significance achieved in a retrospective case study, however several datasets appear to be hampered by a small recruitment in patients (138–140). In addition to the reduction of infection rates, there was also a significant decrease in the requirement of two-stage revisions (i.e. two surgical interventions) following the detection of infection, that is to say that treatment with debridement and antibiotics alone (i.e. one-stage) was sufficient to remove evidence of infection (139). In other cases, the full removal of hardware was also not necessary, thereby reducing the surgical trauma and associated costs. A greater success rate for those that did require two-stage revision was also noted compared to those that received control (uncoated) implants (138).

A further consequence of implant infection is the possible risk of amputation. Following implantation of megaprostheses this incidence has been reported as high as 11 %, with the risk associated with tibial prostheses as high as 15.5 % (141,142). With the implantation of silver-coated prostheses, the incidence of amputation was greatly reduced. While the exclusion of control cohorts diminished the impact of some data (143), where non-coated implants were included the need for amputation was reduced or eliminated compared to control groups (138,139). This amputation risk, while not as

high in fracture cases, is still present, and the prospect of reducing it further with the application of silver to the implant surface is an attainable target.

1.5.3 Biological prevalence of silver

If silver is applied to medical devices for permanent implantation it will increase patient exposure to unnaturally high, localised levels, therefore the pharmacological consequences need to be examined. Although silver is not considered to be a trace metal, it is found within the body at low concentrations (<2.3 µg/L) through ingestion, inhalation and industrial exposure (114). The World Health Organisation (WHO) has placed a No Observable Adverse Effect Level (NOAEL) of 10 g over the course of a lifetime (144), approximately three-times greater than the total quantity of silver applied to the MUTARS® device (145). Despite this level being within the recommended limits set by the WHO some side-effects are observed, most commonly a harmless blue/grey coloration on the skin of patients in the region of implantation, termed ‘argyria’. This effect was observed in 23 % of patients that received a silver-coated megaendoprosthesis (146). The colour generally occurred in light-exposed areas, a result of the reaction with ultraviolet radiation of the deposited silver selenide and silver sulphide in the connective tissue of the dermis (147). Although this effect was related to silver exposure, clinical data did not suggest that it was a result of overtly increased concentrations of silver at the wound site, since analysis of biopsy and serum levels did not indicate significantly elevated levels of silver when compared to those who showed no signs of argyria (146).

Silver that is not deposited within the dermis is found to accumulate primarily in the bile, urine and blood of exposed subjects, indicating at the low residence time within the body (144,148). Similar data have been reported in pre-clinical studies of megaendoprosthesis implantation, with the liver and spleen returning the highest silver content of the analysed organs (149). Monitoring of further parameters including liver and kidney function, and haemoglobin and leukocyte values, showed no adverse effects from pre-operative levels after a period of follow-up. Of concern, however, was the identification of a ‘peripheral neurological deficit’ in two patients who experienced argyria, however no further details of this finding were provided (146). Furthermore, the effect on the principle source of reparative cells within bone (e.g. MSCs) was not determined from any of these studies.

1.6 Effect of silver on eukaryotic cells

1.6.1 Ag^+ uptake in to eukaryotic cells

The specific mechanism by which Ag^+ is transported across the cell membrane is currently under debate. Since it is not a required trace metal there are no Ag^+ specific transporters, it is therefore likely that it enters the cell via transporters for other essential metals or through piggybacking upon nutrients (e.g. amino acids). The copper transporter CTR1, involved in copper (Cu^{2+}) homeostasis, is a likely candidate for the passage of Ag^+ in to the cell. The chemical similarity between these two ions allows for use of the same second transmembrane helix lining the trimeric pore structure of CTR1, thereby permitting its transport. The C-terminal structure of the transporter then facilitates the transfer to metallo-chaperones (144,150). This process is believed to be independent of ATP hydrolysis due to the low concentration of free Cu^+ as a consequence of its sequestration by the chaperones in the prevention of copper toxicity, thereby creating a concentration gradient from which the Cu^+ and Ag^+ transport can take advantage. However it is likely that other mechanisms are involved since only a 50 % reduction in Ag^+ uptake was observed in CTR1 deficient embryonic mouse fibroblasts (151).

The question therefore is what allows the transport of Ag^+ in the absence of using CTR1? The divalent metal transporter, DMT1, facilitates the transport of Cu^{2+} in addition to iron and other divalent metals. Research has demonstrated that Cu^{2+} can also be transported in this way but with lower efficiency, with some therefore suggesting that this transporter should be considered as a contributor to the passage of Ag^+ in to cells (152). Further routes of entry have been explored in mouse embryonic fibroblasts, such as the voltage-sensitive potassium ion channel (K_v). Zhan and colleagues (153) monitored the cellular uptake of Ag^+ using scanning electron microscope (SEM) fitted with an Ag^+ ion-selective electrode. They reported that blocking of the K_v channel by 4-aminopyridine (4-AP) resulted in an increase in the influx of Ag^+. While they suggest that the binding of 4-AP caused a conformational change in the channel of *E. coli*, opening the channel as an additional pathway for Ag^+ entry, they do not hypothesise this mechanism for eukaryotic cells.

Finally, transport across proton-coupled Na^+ channels has been proposed as a mechanism of Ag^+ entry across the basolateral membrane of the gills in freshwater fish (154). This ATP dependent mechanism was reduced in the presence of phenamil, a

Na^+ channel blocker, and bafilomycin A1, an inhibitor of V-type ATPases. The involvement of ATP-hydrolysis was also proposed for the transport of Ag^+ in to the eukaryotic intracellular organelle of the lysosome, which, although requires Ag^+ to be present within the cell, indicates that similar mechanisms of entry may exist in mammalian systems (155).

1.6.2 The effects of Ag^+ on the generation of reactive oxygen species (ROS)

Intracellular ROS have historically been perceived as negative factors, by-products of inefficiencies during aerobic metabolism, formed during the mitochondrial mediated generation of ATP via the electron transport chain. During this process, oxygen (O_2) is reduced to superoxide ($O_2^{\bullet-}$), an unstable molecule that is rapidly converted to hydrogen peroxide (H_2O_2) by superoxide dismutases (SOD1 & 2), thereby preventing the damaging actions of $O_2^{\bullet-}$. The removal of hydrogen peroxide is subsequently dealt with by antioxidant proteins such as catalase, glutathione peroxidase (GPx) and peroxiredoxin (Prx), that convert the molecule to water (156). The process of H_2O_2 neutralisation by Prx and GPx involves the active oxidation of their proteins to produce Prx^{ox} and glutathione disulphide (GSSG). Reduction of these molecules must then proceed in order to allow the continued management of intracellular ROS, therefore reduced thioredoxin (Trx^{red}) accepts the oxygen from Prx^{ox} while glutathione reductase (GR) performs the same process, converting GSSG to glutathione (GSH), via oxidation of reduced nicotinamide adenine dinucleotide phosphate (NADPH) (Figure 1.5).

Additional intracellular sources of ROS include: i) the smooth endoplasmic reticulum which detoxifies lipid-soluble drugs and metabolites via enzymes such as cytochrome P450, oxidising unsaturated fatty acids and foreign chemical substances, producing $O_2^{\bullet-}$ and / or H_2O_2 and ii) peroxisomes that contain H_2O_2 producing enzymes to detoxify substances such as ethanol (157). While some evidence exists that these molecules may have indirect negative impacts on cellular function, they are mainly unreactive, however if not controlled they may cause an imbalance in the concentration that leads to oxidative stress. If the cell is unable to deal with the excess ROS they may go on to produce the highly reactive and damaging, hydroxyl radicals (OH^-). Hydroxyl radicals are produced via the Fenton reaction, where the presence of transition metals (e.g. iron and copper) with H_2O_2 results in the generation of OH^-, a destructive molecule that is able to damage DNA, proteins and lipids (158). As a result, mechanisms have developed in order to maintain iron homeostasis and prevent an imbalance that may result in OH^-.

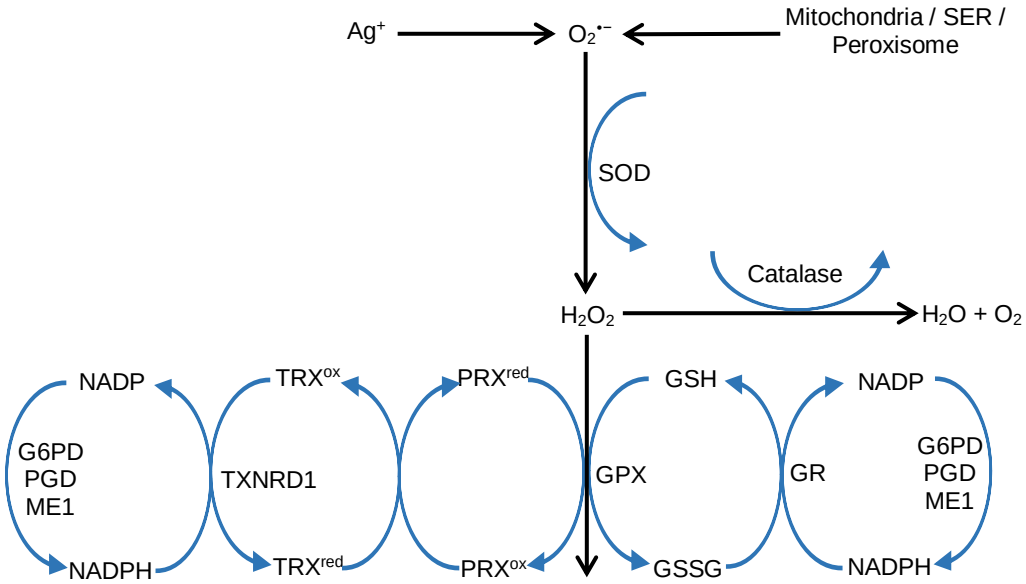

Figure 1.5: Mechanisms of ROS processing for the maintenance of the homeostatic balance between positive cellular ROS and oxidative stress.

TRX – Thioredoxin, TXNRD1 – Thioredoxin reductase, PRX – Peroxiredoxin, GPX – Glutathione peroxidase, GSH – Glutathione, GSSG –Glutathione disulphide, GR – glutathione reductase, ^{ox} – oxidised protein, ^{red} – reduced protein, NADPH - reduced nicotinamide adenine dinucleotide phosphate, NADP - nicotinamide adenine dinucleotide phosphate, G6PD - Glucose-6-phosphate 1-dehydrogenase, PGD – 6-phosphogluconate dehydrogenase, ME1 - NADP-dependent malic enzyme.

Despite the negative characteristics associated with the generation and persistence of ROS, they are also implicated in the important roles of intracellular signalling pathways, response mechanisms and apoptosis. Mitochondrial generated ROS (mtROS) are involved in several mechanisms of ROS-mediated signalling pathways. Hydrogen peroxide is able to readily diffuse across plasma membranes where it can exert an effect on signalling through modification of the cysteine and methionine residues of proteins (159). For example, the response to hypoxic conditions is controlled by the release of mitochondrial H_2O_2 and the stabilisation of hypoxia inducible transcription factors (HIF). These factors have been credited with the upregulation of angiogenesis, the increase in enzymes responsible for glucose metabolism via the glycolytic pathway, the induction of survival factors and red blood cell formation, as well as involvement in the control of apoptosis (160).

Although not directly related to mtROS, other sources of cytosolic H_2O_2 interact with other transcription factors via formation of disulphide-bridges between proteins. The forkhead box O (FOXO) transcription factors are involved with several regulatory mechanisms that include cell cycle progression, metabolism, apoptosis and DNA repair. Crucially they are also involved in stress resistance via the upregulation of the antioxidant enzymes, SOD2 and catalase. Binding of FOXO4 and transportin-1 as a consequence of increased ROS results in the accumulation within the nucleus aiding the activation of FOXO4 as a transcription factor (161). Control of ROS also occurs in a similar format through the release of nuclear factor erythroid 2-related factor 2 (Nrf2). The Nrf2 transcription factor resides with its binding partners, Kelch-like ECH-associated protein 1 (KEAP1) and E3 ubiquitin ligase cullin 3 (CUL3). Under normal conditions, continual ubiquination results in the degradation of Nrf2 via the proteasome, however upon ROS oxidation of the cysteine residues found on KEAP1, Nrf2 is released, with increased levels promoting the accumulation within the nucleus and binding to the antioxidant response element (ARE) promoters. Numerous genes are positively regulated by Nrf2, these include cytochrome P450, NAD(P)H:quinone oxidoreductase 1, proteins of the glutathione and thioredoxin systems and transcription factors (159,162).

Signal transduction via ROS generated from ligand-receptor interactions were originally identified as a result of an increase in ROS prior to tyrosine phosphorylation by growth factor stimulation. The binding of ligands to receptors results in the elevation of ROS production via the activation of the NADPH oxidase family (NOX enzymes), this subsequently causes tyrosine phosphorylation due to the inactivation of protein tyrosine phosphatases (PTP) by the ROS. This inactivation occurs through the familiar binding of ROS to the cysteine residue of the PTP. Reversal of this oxidation state occurs via the Prx enzymes previously encountered, thereby returning the signalling to basal levels (159).

Further examples of ROS mediated signalling are applied across a vast range of cellular responses and functions, such as involvement with PMN cell adhesion to exogenous H_2O_2; endothelial cell permeability through the ROS-enhanced phosphorylation of VE-cadherin via VEGF; and stromal cell differentiation via ROS-induced expression of miRNAs (163,164). The role of ROS in stromal cell function will now be explored further.

1.6.2.1 ROS and their importance in stromal cell function and bone healing

MSCs maintain a balance between a quiescent state that prevents exhaustion in order to allow continued self-renewal, and the ability to proliferate/differentiate in response to the needs of tissue repair. During this quiescent state, MSCs reduce the abundance of mitochondria and use of mitochondrial respiration in comparison to their progenitors, relying instead on the use of glycolysis for their energy requirements, thereby keeping the generation of ROS beneficially low (165). An increase in MSC proliferative activity, such as that promoted during *in vitro* expansion, serves to transfer the energy requirements to that of mitochondrial oxidative phosphorylation, resulting in an increase in the generation of mtROS. However, this comes at the expense of the self-renewal capacity that is characteristic of MSCs, since the increased level of ROS ultimately has a negative impact that has been shown to induce senescence and decrease their differentiation potential (166).

Despite the general negative effects of ROS on the self-renewal of MSCs, their presence is highly influential on differentiation. The consequence of elevated ROS is a decrease in the osteogenic differentiation of MSCs, while this increase appears to favour the adipogenic lineage. Several mechanisms that underlie this fate determination have been proposed. The *in vitro* promotion of osteogenic differentiation of human MSCs has been shown to result in an increase in mitochondrial DNA, respiratory enzymes, oxygen consumption and synthesis of ATP, indicating at transfer to aerobic metabolism that has been shown to elevate mtROS. However, the ROS levels in this research were decreased due to the concomitant upregulation of the antioxidant enzymes, SOD2 (mitochondrial membrane linked) and catalase. In addition, it was found that osteogenic differentiation was reduced if either exogenous H_2O_2 was added to the cultures or if the antioxidant enzymes were inhibited (167). It is therefore clear that MSCs are able to initiate a process of self-regulated management of the ROS generated from the necessary energy production dependent on the differentiation signals received.

In the event that ROS concentrations are raised, then the reduction in osteogenesis is believed to be due to several mechanisms. As previously noted, in times of oxidative stress there is an activation of FOXO for the upregulation of antioxidant enzymes, however in order for this to occur, once within the nucleus FOXO proteins bind with β-catenin, diverting β-catenin from its role as a vital component of the Wnt signalling

pathway necessary for osteogenesis. Almeida and colleagues found that they could reverse this reduction in osteogenesis via the overexpression of β-catenin (168).

Inhibition of hedgehog signalling has been identified as another mechanism of ROS-induced suppression of osteogenesis (169). Proteins of the hedgehog (Hh) family are crucial in directing the differentiation of MSCs between committing to either the osteoblast or adipocyte lineages (170), with sonic hedgehog (Shh) having a synergistic relationship with bone morphogenetic protein 2 (BMP2) in order to achieve the osteogenic phenotype as measured by ALP expression (171). Increases in Shh mRNA (in addition to other members of the hedgehog family) have also been detected during the early stages of fracture healing and the remodelling stages in mouse models of closed fractures (172–174). However, under conditions of exogenous H_2O_2 induced oxidative stress, there is a reduction in Shh stimulated ALP activity and a suppression of osteogenic and Shh signalling target gene mRNA expression (169).

It is therefore possible that the elevation of ROS in the fracture repair environment could result in consequences for bone healing and remodelling. Garrett and colleagues (175) first observed a correlation with oxygen-derived free radical ($O_2^{\bullet-}$) formation and increased bone resorption in neonatal mouse calvariae and foetal rat forearm when cultured with xanthine oxidase/xanthine. They reported an increased number of osteoclasts associated with the treatment that was identical to that observed with the treatment of bones with parathyroid hormone (PTH) and IL-1. These findings were supported by work from Bax *et al*. (176) who demonstrated that the addition of H_2O_2 to rat osteoclasts significantly increased resorption of devitalised bovine bone. Fraser *et al*. (177) later added to this work, reporting however, that the resorption of mouse calvariae was dependent on the elevation of H_2O_2 only, and that the generation of $O_2^{\bullet-}$ via the xanthine system was only effective in enhancing resorption when in the presence of SOD.

This activation of osteoclastogenesis appears to be dependent on the familiar role of ROS as an activator of downstream messaging. The generation of osteoclasts is partly dependent on the activation of RANK by its ligand, RANKL, a member of the TNF cytokine family. The binding of RANKL causes the recruitment of TNF receptor-associated factor 6 (TRAF6) to RANK, activating a signalling cascade via mitogen-activated protein (MAP) kinases such as JNK, p38 and ERK. The signalling capacity of these molecules is then propagated via the association of ROS (178–180).

While in young, healthy individuals, the removal of mineralised matrix is balanced with the generation of new bone, an alteration in the equilibrium of ROS could result in an acceleration of the bone resorption process via the propagation of one of these routes. The *in vitro* elevation of ROS in the human osteoblast-like MG63 cell line and mouse MSCs resulted in an increase in mRNA and protein expression of RANKL. The mechanism of action was identified as the ROS promotion of phosphorylation of cyclic adenosine monophosphate (cAMP) response element-binding protein (CREB)/ATF2 and its binding to the RANKL promoter (181). Further intracellular ROS elevation and related bone loss was observed in the osteoclasts of ovariectomised rats. The researchers concluded that the reduction in oestrogen caused a lowering of the antioxidants within osteoclasts, thereby sensitising the cells to ROS-mediated osteoclastogenic signals (182).

With regards to silver, once within the eukaryotic cell, Ag^{+} has been implicated in the generation of reactive oxygen species (ROS) such as hydrogen peroxide (H_2O_2) and superoxide ($O_2^{\bullet -}$) (183). It is therefore possible that the increase in ROS may lead to the onset of oxidative stress.

1.7 Mesenchymal stromal cells (MSCs)

1.7.1 Characteristics and identification

The ability of cells within the bone marrow to form different tissue was first reported by Friedenstein and colleagues (184). They discovered that ectopic bone formation occurred in mice following the implantation of diffusion chambers containing complete bone marrow. The continuation of this work led to the isolation of fibroblastic cells from the bone marrow stroma via their ability to adhere to glass once disaggregated. Osteogenesis was once again identified as a result of intraperitoneal implantation in diffusion chambers at high density, a result that was not observed in fibroblastic cells from spleen. In addition, they recognised that these fibroblast precursors had the ability to form colonies from individual cells when cultured at low density, terming them colony-forming unit fibroblastic (CFU-f) (185). The CFU-fs isolated from bone marrow represent the heterogeneous nature of the parent tissue, forming colonies of various sizes, growth rates and morphologies, with large differences between donors also apparent. For example, with increasing donor age comes a decrease in the efficiency of CFU-f formation, with humans experiencing approximately an 8-fold decrease in

efficiency over a lifetime (~80 CFU-f per 10^5 nucleated cells at birth to ~10 CFU-f per 10^5 nucleated cells during old age). Despite this however, the formation of CFU-f correlates with the incidence of the progenitors available within a bone marrow sample (186,187).

The formation of ectopic bone by these cells led to the discovery of their potential to generate further tissue types *in vitro*, such as cartilage (chondrogenesis), fat (adipogenesis), muscle, tendon and ligament, leading to the popular term of 'mesenchymal stem cells' (188). However discussions within the literature have questioned the appropriateness of the term, with belief that 'mesenchymal stromal cell' is a more relevant terminology due to the limitations of these cells to form all tissue types *in vivo* (189,190). Despite this, the *in vitro* differentiation through osteogenic, adipogenic and chondrogenic lineages of both cultured and CFU-f expanded MSCs has been shown (191), and it is this feature, plus their isolation via adherence and self-renewal at clonal density, that are the primary characteristics that are often used to define a multipotent stromal cell (164). In addition, molecular markers and combinations thereof are often employed to aid enrichment from heterogeneous populations, however their use in identifying bone derived MSCs is problematic due to the lack of stable, unique markers. In light of this a consensus was published to clarify the situation, identifying a number of markers that could identify MSCs: $CD105^+$, $CD73^+$, $CD90^+$, $CD45^-$, $CD34^-$ $CD14^-$, $CD19^-$, $CD3^-$ (192,193). However, the use of cell surface markers has been used to enhance the CFU-f efficiency from a bone marrow. For example, such an increase was observed versus unsorted bone marrow populations with cells that were $CD146^+$ and $CD45^-$ (194), while CFU-f numbers were also enhanced in populations enriched for those cells that were positive for the alternative markers of STRO-1 and vascular cell adhesion molecule-1 (VCAM-1) (195,196).

1.7.2 MSC Differentiation

MSCs are generally described as having multilineage potential, that is to possess the ability to differentiate into osteoblasts, adipocytes and chondrocytes in order to produce bone matrix, fat and cartilage, respectively. The direction along which the differentiation occurs is a fine balance between actively promoting one while inhibiting another, with an imbalance resulting in differentiation along the promoted lineage. The process of MSC differentiation will now be outlined.

1.7.2.1 Osteogenesis

The Wnt/β-catenin pathway plays a role in osteogenesis via activation of the runt-related transcription factor 2 (Runx2). In total there are nineteen Wnt proteins that signal via the seven transmembrane domain Frizzled (Frz) receptor and its co-receptor, the low-density lipoprotein receptor-related protein (LRP)-5/6. In the canonical pathway (Figure 1.6) Wnts transduce their signal through an alteration in the action of intracellular proteins that ordinarily promote the degradation of β-catenin in the absence of Wnt. Upon Wnt binding, the β-catenin degradation complex comprised of glycogen synthase kinase-3β (GSK3), Axin and Adenomatous Polyposis Coli (APC) is disrupted due to the sequestration of Axin by Dishevelled (Dsh). This results in the inhibition of GSK3 and the dephosphorylation of β-catenin, thereby no longer marking it for ubiquitination by β-TrCP-containing SCF E3 ubiquitin ligase leading to proteasome degradation. β-catenin levels therefore increase and translocate to the nucleus, binding to the TCF/LEF1 factor and directly promoting osteogenic-specific gene transcription via Runx2 (197–199). Of importance though is that not all Wnt proteins promote osteogenesis. While Wnt10b is strongly connected with the increase in bone mass and stimulation of osteoblastogenesis in mouse bone marrow derived ST2 cells, Wnt3a promotes bone cell proliferation but suppresses dexamethasone-induced osteogenic differentiation of MSCs (200,201).

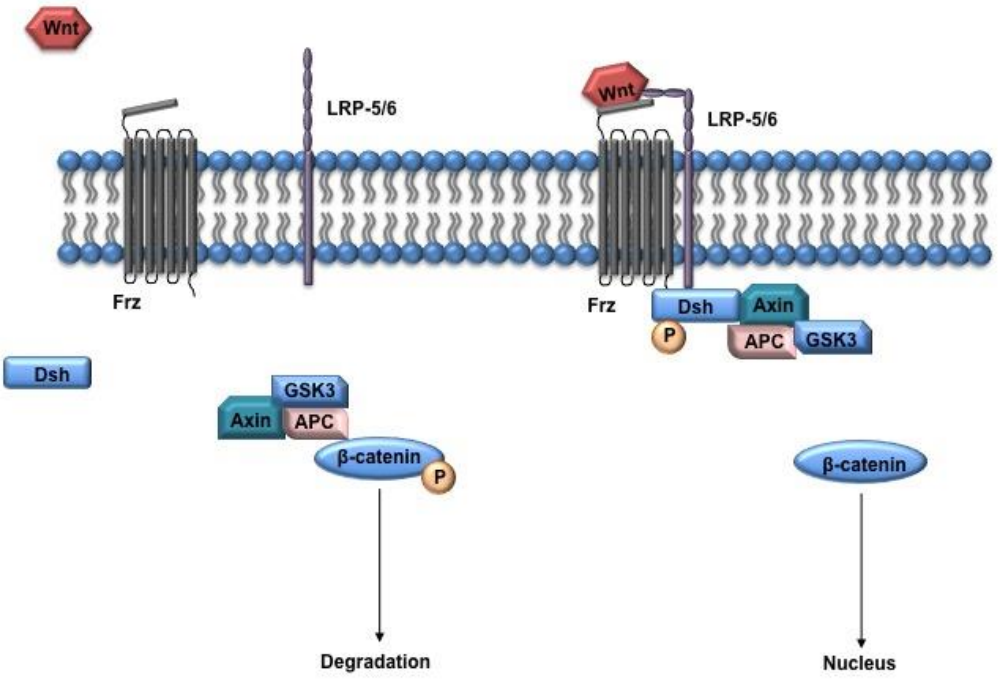

Figure 1.6: Canonical Wnt signalling pathway.

In the absence of Wnt, β-catenin is degraded due to its continued phosphorylation by the degradation complex containing Axin, GSK3 & APC and subsequent ubiquitination. Activation of the pathway is caused via Wnt binding to Frz and the co-receptor LRP-5/6. The degradation complex is then deactivated by Dsh, allowing β-catenin to translocate to the nucleus.

The use of the synthetic glucocorticoid, dexamethasone (Dex), for *in vitro* osteogenesis, in addition to the phosphate donor, β-glycerophosphate (βGP) and the enzyme cofactor, ascorbic acid (AA), is primarily for its control of the Runx2. Runx2 is considered the master regulator of osteogenesis and is a part of the TGF-β/BMP signalling pathway (Figure 1.7). The interaction of TGF-β and BMPs to their respective receptors causes receptor phosphorylation, cascade of the signal via phosphorylation of the related receptor regulated-Smad (R-Smad) proteins (TGF-β: Smad2 & 3; BMP: Smad1, 5 & 8) and common mediator Smad (C-Smad) protein (Smad4) and subsequent activation of Runx2. As a result, Runx2 promotes the transcription of osteogenic genes osteocalcin, osteopontin, bone sialoprotein, alkaline phosphatase (ALP) and collagen 1α via binding to the osteoblast-specific *cis*-acting element (OSE2) (202–204). The addition of Dex promotes osteogenesis by targeting several upstream coactivators of Runx2 while also altering its phosphorylation state. For example, transcriptional coactivator with PDZ-binding motif (TAZ) is a β-catenin-like molecule and a coactivator of Runx2. Studies found that TAZ enhanced the expression of osteocalcin, BMP2 and ALP, and increased calcium deposition during Dex induced osteogenesis. However, these effects were only observed when Dex was applied at physiological concentrations (10^{-8} M), if Dex was applied at ≥10^{-7} M then TAZ expression was decreased along with ALP. As a result of its effects on BMP2 it was hypothesised that high concentrations of Dex decreased osteoblast differentiation via inhibition of the Wnt/β-catenin pathway (205). Recently, research has proven the link between TAZ and β-catenin. In the absence of Wnt signalling, the β-catenin destruction complex maintains the degradation of TAZ by linking it to its ubiquitin ligase, however upon Wnt signalling, β-catenin linked degradation of TAZ is impaired, allowing accumulation of both β-catenin and TAZ, resulting in Runx2 activation (206).

Further regulation of Runx2 has been proposed via its phosphorylation. Phillips *et al*. (207) provided evidence that expression of osteoblast-specific genes and ALP activity were decreased upon inhibition of mitogen-activated protein kinase (MAPK) phosphatase-1 (MKP-1). Therefore, decreased Runx2 phosphoserine levels resulting from increased MKP-1 allowed for elevated Runx2 trans-activation. This effect was enhanced in the presence of dexamethasone.

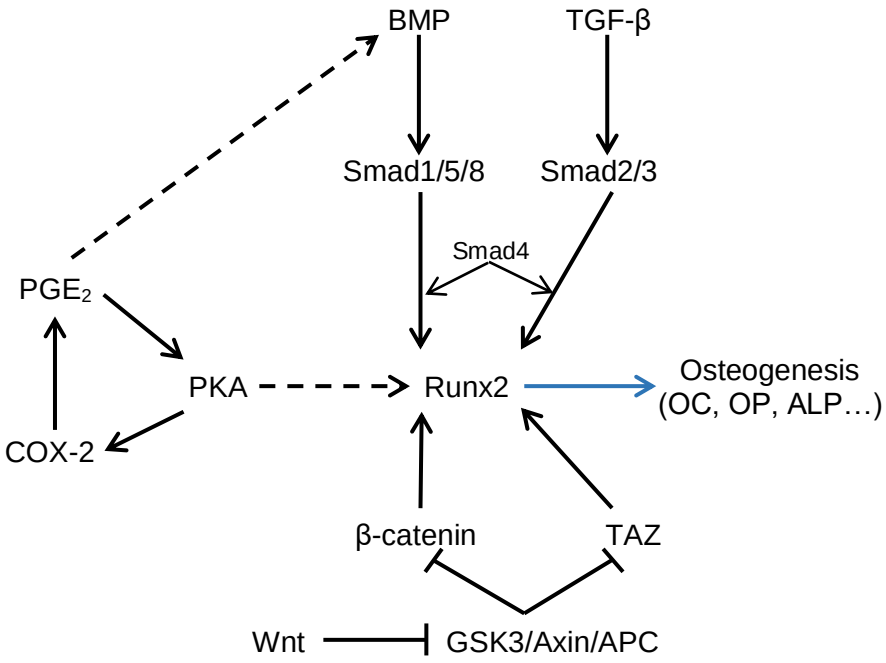

Figure 1.7: Regulation of osteogenesis via activation of Runx2.

Expression of osteogenic proteins via Runx2 is promoted by several routes: TGF- β superfamily signalling through the Smad transcription factors; COX-2 generation of PGE_2 that signals via protein kinase A (PKA) and an unknown mediator; and the Wnt/β-catenin pathway.

1.7.2.2 Adipogenesis

As for osteogenesis, the differentiation of MSCs in to adipocytes is controlled by a master regulator gene, peroxisome proliferator-activated receptor γ (PPARγ), without which adipogenesis is neither initiated or maintained (208). PPARγ is present in two isoforms (PPARγ1 & PPARγ2) that are both able to induce adipogenesis in the absence of the other, however the process is enhanced in the presence of CCAAT-enhancer-binding proteins (C/EBPs). C/EBPs are a family of transcription factors (C/EBPα, C/EBPβ, C/EBPγ & C/EBPδ) that are involved as differentiation progresses from early induction to maturation. This occurs either via direct induction of selected adipocyte-related genes (in the case of C/EBPα) or through promotion of C/EBPα and PPARγ. PPARγ promotes downstream regulators of adipogenesis such as the uptake and metabolism of glucose while C/EBPα is essential for establishing glucose transport in response to insulin (209).

Induction of these proteins is via signalling cascades that are initiated through hormones (e.g. insulin) and growth factors (e.g. insulin-like growth factor and BMPs) (Figure 1.8). While there is a direct positive effect on PPARγ and C/EBPα regulation via signalling through the insulin/IGF1 receptor pathway, further positive regulation can be mediated through growth factor families already encountered for initiating osteogenesis. The addition of BMP4 to C3H10T1/2 mouse multipotent stem cells commits them to becoming preadipocytes that undergo differentiation upon exposure to adipogenic differentiation media, an effect not observed when using BMP2 (210). In contrast, other work has suggested that BMP2 may act synergistically with adipogenic inducers (i.e. Rosiglitazone) to enhance PPARγ expression and lipid metabolism (211), while a dose-dependent effect of BMP2 addition upon adipogenic differentiation was observed by Wang and colleagues using C3H10T1/2 (reviewed in (208)). Finally, adenoviral overexpression of several other BMP molecules in this same mouse stem cell line have also been shown to increase lipid deposition via PPARγ upregulation (212).

Negative regulation of adipogenesis primarily comes from signals that are known to promote osteogenesis such as TGF-β, Wnt and TAZ, however the mechanism of regulation differs for each signal. The addition of TGF-β to pre-adipocytes inhibits their differentiation through activation of Smad3/4 and prevention of C/EBPδ, thereby reducing the activity of the C/EBP transcription factors (213). Similarly, TAZ binds to PPARγ, preventing its ability to stimulate gene expression, even in the presence of

Rosiglitazone, a PPARγ-activating ligand (214). Further negative regulation is via Wnt, where inactivation of the canonical Wnt pathway is required for activation of adipogenic transcription factors (215). Through the addition of Wnt10b and the subsequent elevation of free β-catenin via the canonical pathway, there was a decrease in adipogenesis due to direct prevention of PPARγ and C/EBP transcription, a phenotype that was reversed with the overexpression of the β-catenin degradation complex component, Axin (216,217). In cases where this regulation has occurred it is likely that osteogenic differentiation has been initiated or the MSC status quo maintained.

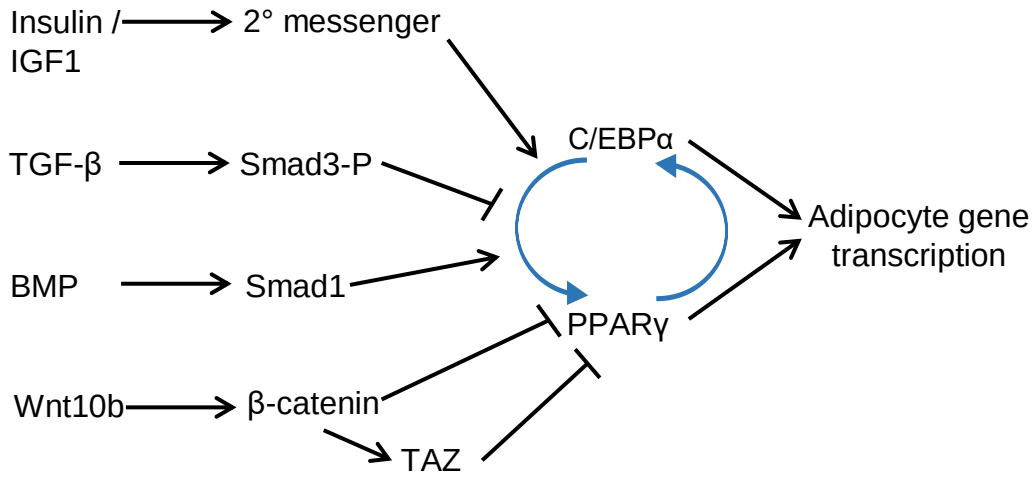

Figure 1.8: Positive and negative control of adipogenesis through influence on the master regulators, C/EBPα and PPARγ.

1.7.2.3 Chondrogenesis

The process of MSC chondrogenic differentiation leads through a number of stages, the proliferative phase as a chondroprogenitor; differentiation as a chondroblast leading to chondrocyte formation; and finally the terminal differentiation as hypertrophic chondrocytes. This process takes place through the fracture healing cascade as discussed in Section 1.2, with the initial chondrocyte matrix formation leading ultimately to the mineralisation and replacement with bone. Due to this transition there are a multitude of varied and complex signals regulating chondrogenic differentiation, with the latter stages closely linked to the osteogenic endpoint; these details will be briefly discussed here.

Characteristic markers of chondrogenesis are considered to be the production of matrix proteins collagen II (Col II) and aggrecan, the most abundant collagen and proteoglycan in articular cartilage. The presence of Col I and Col X are generally accepted as negative markers of early chondrogenesis, but signify the progression towards the terminal differentiation state. The *in vitro* initiation of chondrogenesis from mesenchymal cells is primarily through the addition of TGF-β. Early experiments used TGF-β1 or TGF-β2, however the use of TGF-β3 was later shown to enhance glycosaminoglycan (a component of aggrecan) production and Col II expression over that of the other two TGF isoforms, however an increase in Col X was also observed (218). TGF-β is believed to induce chondrocyte differentiation through independent phosphorylation and stabilisation of the Sox9 transcription factor via Smad2/3 and p38 (219,220).

The activation and upregulation of the transcription factor Sox9 is important in the initiation of chondrogenesis since its expression overlaps with the upregulation of Col II and the subsequent synthesis of further collagens and aggrecan. It also progresses the differentiation process from mesenchymal condensation through targeting Sox5 and Sox6, both enhancers of chondrogenic gene transcription (221,222).

Other members of the TGF-β superfamily have also shown involvement in chondrogenic differentiation. Several BMP proteins have enhanced chondrogenesis as indicated through alcian blue (glycosaminoglycan) matrix staining, likely through the upregulation of Sox9. In this respect BMP-2, -6 and -7 have all demonstrated increases in chondrogenesis, although in the case of BMP-2 this was shown to be dose and time dependent (223) or when applied in addition to TGF-β3 supplementation (224).

Other factors affecting chondrogenesis include induction via activation of the HIF1α transcription factor. An upregulation in HIF1α activity is observed through the generation of hypoxic conditions found in the foetal growth plate during endochondral bone development and in the environment created at fractures sites (225,226). Under these conditions, elevated HIF1α directly binds to the Sox9 promoter region, regulating its expression and that of the downstream proteins of aggrecan and Col II (227,228).

Finally, progression to the mature and hypertrophic stages of the chondrocyte lifecycle are characterised by the synthesis of Col X. While Sox9 ordinarily represses Runx2 through active β-catenin degradation, thereby protecting chondrocytes from entering a prehypertrophic state, it has also been found to contribute to the promotion of the hypertrophic marker, Col X, during this latter stage. This control of hypertrophy through its continued presence is believed to allow the preservation of the differentiation decision of the chondrocytes (229). Eventually Runx2 expression overrides that of Sox9, promoting the terminal differentiation of the chondrocytes and expression of BMPs, osteopontin, bone sialoprotein and collagenase 3 (230). Figure 1.9 provides a summary of the regulation of chondrogenesis.

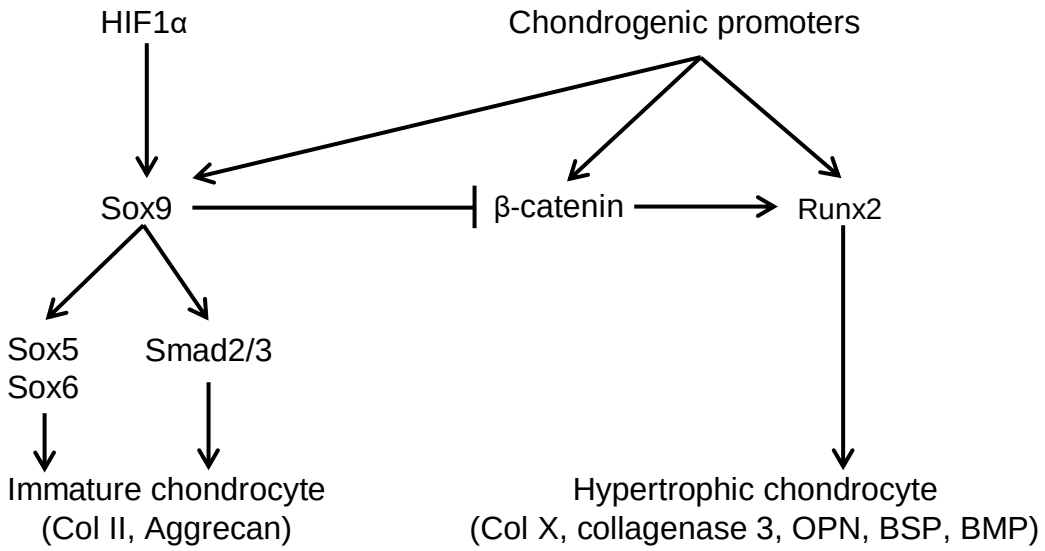

Figure 1.9: Regulation of chondrogenesis via the Sox9 transcription factor.

Promotion of Sox9 results in the upregulation of both Smad proteins and further members of the Sox family, while also suppressing β-catenin. Progress through to terminal differentiation results in the upregulation of Runx2, previously repressed by Sox9, and the expression of genes promoting hypertrophy.

1.8 Current research on the effects of Ag^+

1.8.1 The effect of experimental design

The use of *in* vitro assays to determine the toxicity of silver on eukaryotic cell types has taken a number of forms, with differences between the use of cells from animal or human sources and primary or immortalised cells combining to have an effect on the outcome. For simplicity, the effects on viability (i.e. metabolism) are frequently observed and provide numerous examples of the effects of variation both between researchers and even within research groups. For example, Wataha *et al*. published EC_{50} values (the concentration that provides a 50 % response) based on metabolism data for 24 hour exposure of Balb/c 3T3 mouse fibroblasts to Ag^+. Under the same culture conditions they determined EC_{50}s of 5.8 μM (231) and ~10 μM (232), a 42 % decrease in the reported value. While this is one example of the variation experienced within the literature, it also serves to prove that this method of analysis, while valuable in obtaining preliminary working ranges, is very sensitive to the severe drop in metabolism experienced with some cytotoxic substances.

Wataha *et al.* (233) also provided data on the possible differences caused by variables within the experimental design. They investigated the effects of using different cell lines on the toxicity of silver (as measured using succinic dehydrogenase activity), detailing that Balb/c 3T3 mouse fibroblasts were more sensitive to Ag^+ than L929 mouse fibroblasts, with EC_{50} of 25.5 μM and 30.1 μM respectively. In the same publication they find that the human fibroblast cell line, WI-38, was not sensitive at the concentrations tested (EC_{50} >38 μM). While they suggest that this is linked to doubling time, with the shorter replication time of the Balb/c 3T3 a potential cause for the increased sensitivity, they do not suggest whether the difference in species may be of importance. It also highlights the requirement to conduct *in vitro* testing in the most appropriate cells for the application of the medical device in research.

As if to confirm this further, it is apparent that primary cells react differently to Ag^+ exposure than cell lines (234,235), however, where direct comparison has been performed, both positive and negative effects have been reported. While Boonkaew *et al*. (236) provide evidence that primary keratinocytes are more resistant to the effects of Ag^+ than the immortal equivalents (HaCaT); Schedle *et al*. (234) showed the opposite, with an increase in the Ag^+ EC_{50} for L929 fibroblasts compared to primary human fibroblasts (once again, the difference in species is not considered) and

increased histamine release from primary human basophils & mast cells compared to their cell line equivalents (237). These examples show that while the use of cell lines is clearly an extremely useful tool for the study of eukaryotic cells due to their availability and potential for manipulation, the data gained from such investigations should be supported by equivalent testing in primary cultures to confirm initial findings.

Although, as discussed, cytotoxicity is unquestionably tied to experimental factors, the effect of exposure time to a chemical entity on cellular response is undoubtedly one area through which the most significant impacts can be investigated. In cases where multiple time points have been examined, all authors report a degree of negative impact of increased exposure time to Ag^+ (238–245). These reports imply that there are instances of a level of resistance to immediate cytotoxicity, raising the suggestion that a silver coated device that is to be in contact with eukaryotic cells could potentially have its antimicrobial effects over a short time period provided that the level of silver is high enough to be efficacious, while below the limit that is cytotoxic at the short timeframe. This endurance may be caused by inherent resistance to the exposure, the cell cycle/division rate (as previously stated) or variations in the rate of uptake within the cell (231).

1.8.2 Cell Function and Regulation

Although the overall effect on viability is an important consideration when assessing Ag^+ on eukaryotic cells, the effect on function and regulation is of equal interest; a cell that appears to be viable in terms of metabolism may not be functioning as for the unexposed controls.

Several areas of function and regulation have been repeatedly investigated *in vitro*. Gene expression (183,238,241,246–248), differentiation (238,249), DNA fragmentation (239,248), apoptosis/necrosis (239,250–252), cell cycle (252) and oxidative stress (183,247,248,250,252–255) have all shown deleterious outcomes of silver ion exposure on eukaryotic cells.

1.8.3 Effect of Ag^+ on MSC differentiation

Available literature on the relationship between Ag^+ exposure and differentiation of MSCs is limited. A recent search (August 2018) of PubMed retrieved 87 publications under the search terms ‘mesenchymal AND differentiation AND silver’. Of the relevant

published data (e.g. excluding the use of nanoparticles that is not the basis of this research project) much involves investigating the incorporation of Ag^+ into orthopaedic related surfaces such as hydroxyapatite (HAp) (256–259) or titanium (246,260).

The expression and activity of ALP is an accepted measure of osteogenesis. Where ALP activity has been analysed following direct ion exposure from silver (rather from exposure to a combination coating e.g. Ag/HAp) we see a dose response as previously observed for viability. Hardes *et al*. (261) exposed a human osteosarcoma cell line (HOS-58) to a specified weight of silver powder and showed no effect on osteocalcin but a dose-dependent decrease in ALP, accompanying a decreased metabolism. However, they also observed an increase in ALP against controls at the lowest silver quantities, despite significant decreases in metabolism at these same concentrations. Disappointingly, however, no further information on the silver was provided, therefore the actual molar content of the media cannot be ascertained.

Quantifiable silver doses have been provided by other research, for example, UMR106 rat osteoblasts cultured in the presence of silver ions released from wire exhibited a decrease in ALP while only showing a small decrease in cell survival. The researchers quantified the silver ion release over the 48 hour time period at a maximum of 9.2 µM (262). In contrast, Qin *et al*. (263) observed no effect on ALP activity from differentiated primary human urine derived stem cells exposed to 18.5 µM Ag^+ (in the form of $AgNO_3$), a dose that they had previously observed to be non-cytotoxic. The same result was reported by Pauksch *et al*. when culturing MSCs and osteoblasts to sublethal Ag^+ doses ($\leq$9.3 µM) for up to 35 days (238).

Data recording chondrogenic differentiation in the presence of Ag^+ is relatively scarce, likely due to the primary use of silver being in wound management and interest in orthopaedics. As a result, the analysis of chondrogenesis falls behind that of wound healing and osteogenic related measures. Despite this, some data exists showing that Ag^+ at 9.3 µM had no significant effects on aggrecan synthesis over a 21 day period, although a mean decrease of approximately 20 % was observed from control (264). This team also investigated the effects of the same Ag^+ concentration (9.3 µM) on adipogenic differentiation over 14 days, concluding that there was a significant decrease in both lipid deposition and adiponectin expression (an adipogenic differentiation marker). This finding is interesting since the elevation of intracellular ROS is considered to favour adipogenesis through FOXO mediated inhibition of

β-catenin, thereby promoting adipogenic gene transcription as observed by He *et al*. (164,265). However, the increased adipogenesis reported by He was using samples coated with silver nanoparticles (AgNP) that released little Ag^+ in to the media (~46 nM) and were weakly antimicrobial. This suggests that the divergence to adipogenesis may occur even in the presence of low levels of silver.

While it is clear that there is an extensive body of published work on the effects of silver ions, those relating to the field of orthopaedic trauma are limited to the basic understanding of cell viability and differentiation. These findings are undoubtedly of use to determine the *in vitro* sensitivity of various cell types to Ag^+, however a majority of them are simply standalone publications with little justification for their study design or translation to clinical applications. Given that the primary goal of much of the research is to progress scientific understanding for the benefit of the patient, there exists a need to translate the findings of the bench to the advances for the bedside. It is therefore clear that analysing the effects on cells using Ag^+ concentration and exposure timeframes that are relevant to potential technology developments is of importance to our understanding.

While there does appear to be an effect of Ag^+ exposure on the *in vitro* differentiation of MSCs as a result of increased ROS generation, the effect on the vital property of self-renewal has not been investigated. I therefore hypothesised that the oxidative stress caused by clinically relevant concentrations of Ag^+ would reduce the self-renewal capacity and affect the subsequent differentiation potential of those clonal cells. As part of this work I also planned to investigate the mechanisms by which they are able to tolerate the Ag^+ and importantly, relate this to clinically relevant exposure concentrations, a factor that is vitally important if laboratory based research is to progress to effective treatments.

Project aims

The aim of this thesis was to investigate the effects of a clinically relevant concentration of Ag^+ on MSC clonogenicity, differentiation and the mechanisms employed by MSCs to manage the related elevation in ROS as a consequence of exposure. Establishment of culture conditions and subsequent *in vitro* analysis aimed to:

- determine the maximum intramedullary Ag^+ exposure, and subsequent clearance from the surrounding tissue, through the use of a relevant *in vivo* model
    - Data presented in Chapter 3 reports the measured Ag^+ release from the implant surface, the plasma and bone concentrations during the study period in addition to the theoretical maximal release in to the free canal volume.

- determine the efficiency of MSC differentiation under conditions of Ag^+ exposure
    - Using the media selection determined in Chapter 4, MSC differentiation during and following maximal Ag^+ exposure is reported in Chapter 5

- assess MSC clonogenicity and the mechanisms involved in CFU-f management of ROS
    - The effect on MSC clonogenicity was determined (Chapter 5), with proteomic and pharmacological confirmation of the oxidative stress pathways employed by tolerant MSCs provided in Chapter 6

2 Chapter 2: Materials and Methods

2.1 Materials

Cell culture was performed on tissue culture grade plasticware purchased from Corning Lifesciences (Corning, NY, USA). All culture media and supplements were purchased from Invitrogen (Paisley, UK) unless otherwise stated. Foetal bovine serum (FBS) purchased from Labtech International (Heathfield, UK) was batch tested for proliferation and differentiation and used for these purposes. Media used in assays set up at clonal density for colony-forming unit fibroblastic (CFU-f) assessment was supplemented with 20 % HyClone Foetal Bovine Serum (GE Healthcare, Cat: SV30160.03) in place of the 10 % FBS used elsewhere. All *in vitro* applications of silver ions were using silver sulphate (Ag_2SO_4, CAS: 10294-26-5, Alfa Aesar, Cat: 41443, Ag content ≥68.9 %, 99.9 % metal basis).

2.2 *In vitro*

2.2.1 Cell culture

2.2.1.1 Cell origin

All primary MSCs were of human origin, isolated from bone marrow aspirate (Lonza, Walkersville, USA) or excised bone donated by patients undergoing primary arthroplasty surgery (NHS, Clifton Park Hospital, UK). Procured tissues were done so under the Smith & Nephew Human Tissue Authority Licence (Research No. 12252 & Anatomy No. 12576), while donated samples were collected under ethical approval from the University of York Biology (07/Q1105/9). In total, seven primary MSC donors were used throughout this thesis, with an age range of 18-74 years (median 25 years), 3 were male (43 %) and 4 were female (57 %). A minimum of three donors were used in each experiment, chosen at random from those available, and are identified via their human tissue sample number 'HS###' or 'K###'. Information for individual MSC donors can be found in Appendix 1.

Clonal MSCs, termed Y201, generated from primary bone marrow derived MSCs engineered to overexpress human telomerase reverse transcriptase (hTERT) (266), were used as a model cell system in some assays and has been stated where appropriate.

2.2.1.2 Expansion and preparation

MSCs and Y201s were expanded in DMEM (high glucose) supplemented with 10 % Foetal Bovine Serum (FBS), 100 Units/mL Penicillin and 100 µg/mL Streptomycin and passaged once 80-90 % confluency was achieved. The maximum passage of primary MSCs for experimental use was passage 7.

2.2.1.3 *Mycoplasma* testing

Cultures were regularly tested for mycoplasma contamination during expansion and prior to experimentation. Cells were seeded in to 4-well plates for a minimum of 24 hours, rinsed with PBS, fixed with methanol, washed with deionised water and stained with 2 µg/mL 4', 6-diamidino-2-phenylindole (DAPI). Cultures were inspected using the Leica IRB inverted microscope for the punctate fluorescent staining within the cytoplasm that is indicative of contamination.

2.2.1.4 Crystal violet staining

To visualise colony formation media was removed and replaced with 0.05 % w/v crystal violet (1xPBS, 1 % formaldehyde, 1 % methanol) for 20 minutes at room temperature after which plates were washed with tap water to remove background staining. Plates were left to air dry before imaging using a flatbed scanner.

A primary measure of CFU-f number was employed across all experiments with a colony defined as being ≥50 cells, this criteria was also employed for inclusion in the secondary measure of colony diameter (manually attained using Zeiss Zen 2.3 Lite) that was performed for some experiments. A further measure of total colony area (determined using ImageJ macro (267)) was also analysed for some experiments.

2.3 Statistical analysis

Data were expressed as the mean ±SEM. Unless otherwise specified, experiments were performed with a minimum of three primary donors. Data were interrogated as stated in the individual methods using appropriate post-hoc multiple comparison test. Statistical analysis was performed using GraphPad Prism 7 software (GraphPad Software, La Jolla, California, USA).

3 Chapter 3: *In vivo* evaluation of silver elution and clearance from titanium intramedullary implants in the rat femur

3.1 Introduction

The elution profile of any antimicrobial from an implant is of paramount importance with respect to both efficacy and safety. While information regarding the peak local concentration will inform as to the ability to reach minimum bactericidal concentrations (MBC), the duration of the release may also have implications regarding the efficacy in the event of continued microbial challenge. Both of these properties apply to the evaluation of safety, however the duration with which the antimicrobial resides in the local area is also an important consideration with regards to tissue repair and regeneration (remodelling).

In vitro determination of an elution profile is beset with complications primarily related to the composition of the eluent (262,268,269). This situation is exacerbated with Ag^+ due to complexing with ligands within the solutions such as chloride, sulphides and thiols, such as cysteine, that bind strongly to Ag^+ (152,262). This therefore renders the simple use of phosphate buffered saline (PBS) (270,271), water (272,273) or simulated body fluid (274,275) for the assessment of Ag^+ elution as irrelevant due to their lack of protein content, especially where subsequent efficacy and biocompatibility testing contains this important constituent.

In eluents that contain protein, the source (for example, Foetal Bovine Serum (FBS) or bovine serum albumin (BSA)) greatly influenced the elution profile (268), while the selection of a physiologically relevant concentration is not always standardised or difficult to ascertain (262,276). Further variation would also undoubtedly come from the batch and supplier of the inherently capricious FBS. While the components of the eluent play a role in the release kinetics, a saturation effect related to the eluent volume should also be considered but is rarely noted by researchers (272). This phenomenon, combined with the influences outlined above, highlight the artificial nature of *in vitro* elution studies. While they play an informative role in the early development of elution-dependent technologies, the true elution profile can only be obtained *in vivo*.

The use of clinically relevant *in vivo* models (i.e. those that make use of an appropriate anatomical site) for determining the elution profile of medical devices provide data that account for the effect of implantation abrasion, shear forces, fluid flow and environmental milieu. The use of such a model therefore provides an accurate representation of the release kinetics of an active ingredient. Furthermore, the design of the study can additionally inform of the distribution and excretion from tissues of the eluted molecule – pre-clinical data that is vital for determining the safety profile necessary for progressing a product towards the clinic. With this in mind, the work performed in this chapter will primarily detail the silver elution from intramedullary implants, while also allowing peak concentrations and exposure durations to be elucidated, providing the framework from which further *in vitro* investigations can be translated from an accurate *in vivo* setting.

3.2 Aims

The aims of the study presented in this chapter were to provide information on the performance of the silver coating, specifically analysis of the elution of silver ions from the implant surface within the intramedullary environment.

Specific aims of this chapter are to:

- Determine the release kinetics of silver ions from a coated implant in a physiologically relevant setting.
- Ascertain the duration of silver persistence within the femur and circulatory system.
- Calculate the maximal silver exposure within the intramedullary canal to enhance the translation between the *in vivo* and future *in vitro* experimental designs.

3.3 Methods

3.3.1 Surgery

3.3.1.1 Test material

Titanium alloy (Ti-6Al-4V) rods (20 mm length x 1.1 mm diameter) were prepared at Smith & Nephew Research Centre (York, UK) using a proprietary method to achieve a targeted silver dose. All implants were individually packaged and gamma sterilised prior to surgery.

3.3.1.2 Animal model

Twelve male Sprague Dawley rats, each weighing 250-300 g, were randomised in to four groups consisting of three animals per group. Each group was allocated to a time point of 24, 48, 72 hours or 28 days. Animals were group housed in temperature controlled rooms at 21 °C ± 2 °C with a relative humidity of 55 % ± 10 % and artificial lighting cycle of 12 hours light/dark. The study design was approved by the Smith & Nephew Research Centre Animal Welfare Ethical Review Board, taking into consideration the requirements for reduction, replacement and refinement.

3.3.1.3 Surgical procedure

Prior to surgery, animals were given a sub-cutaneous injection of Septrin (24 mg/kg, containing trimethoprim & sulphonamide) as an antibiotic prophylaxis, a dose that was provided twice per day for the initial two days of the study. In addition, intra-peritoneal injections of Buprenorphine analgesia (0.05 mg/kg) and medetomidine sedative (0.1 mg/kg) were provided. Following surgery, Buprenorphine (0.05 mg/kg) was administered every eight hours for a minimum of 48 hours.

The animals were anaesthetised using an Isoflurane/Oxygen/Nitrous oxide mixture and the left hind limbs were shaved and the skin washed with antiseptic scrub. Rats were placed in the dorsal recumbency and a 1-2 cm incision made long the front of the knee. The patella was moved to allow access to the inter-condylar notch where an entry hole was drilled in to the femoral canal. The test article was inserted, the patella repositioned and the wound closed using absorbable sub-articular sutures (Figure 3.1). Following surgery, the animals underwent X-rays (Figure 3.1) and were returned to individual housing until fully recovered from anaesthesia, after which they were

returned to the group. Appropriately trained and Home Office licenced personnel performed all surgical procedures and anaesthesia.

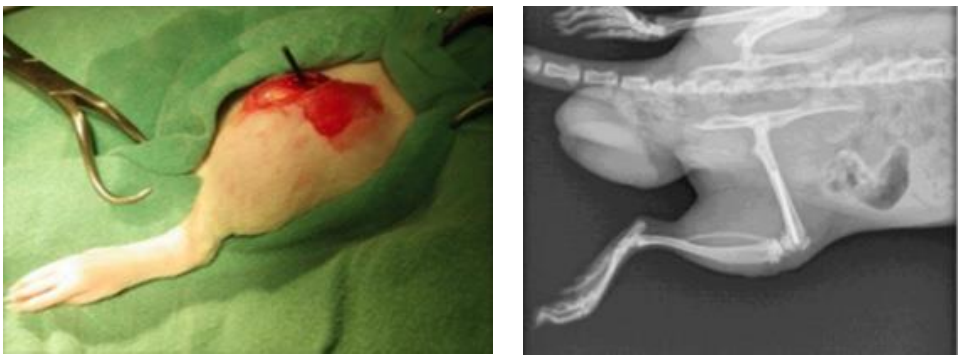

Figure 3.1: Implantation of silver coated Ti-6Al-4V pin in the rat femoral intramedullary canal (left). Confirmation of placement through medial/lateral X-ray (right).

3.3.1.1 Termination and specimen preparation

At each time point the animals were sacrificed and plasma samples prepared from whole blood collected in heparin sodium salt anticoagulant (Sigma, Cat: H4784). Blood was centrifuged at >530 x g for 15 minutes (4-8 °C), the plasma fraction removed and stored at ≤ -20 °C.

The femur was removed, stripped of soft tissue and the implant pushed through in a retrograde action. The femur was stored at ≤ -20 °C and the implant at 2-8 °C until each was analysed for silver.

3.3.2 Silver quantification using Inductively Coupled Plasma Mass Spectrometry (ICP-MS)

Samples, described below, were analysed against Ag standard curves prepared from a commercially available single element standard (Ag, 1,000 µg/mL in 5 % HNO_3, Agilent, Cat: 5190-8524) using the Agilent 8800 ICP-MS Triple Quad. To monitor drift during analysis, a 500 ppb rhodium internal standard (Agilent, Cat: 8500-6945) was included in addition to a final sample Ag control. In brief, diluted samples were injected with argon, and Ag (molecular weight, 107.9) detected within the resulting plasma following filtration of interfering ions. Data was provided as parts per billion (ppb) and

converted to mass. Statistical analysis was by two-way ANOVA using Tukey's correction for multiple comparisons.

3.3.2.1 Implant

Total silver analysis of pins was determined pre- and post-implantation. At both stages, individual pins were placed in 10 mL 1:2 (v/v) nitric acid/dH_2O and incubated overnight at room temperature (RT). Solutions were vortexed and diluted 1:1000 (v/v) in 1 % nitric acid. Silver content was determined against an Ag^+ standard (0.2 - 20 ppb).

3.3.2.2 Plasma

Plasma samples were diluted 1:25 (v/v) in 1 % nitric acid and the Ag^+ content determined against an Ag^+ matrix matched (4 % rat plasma (Innovative Research, Cat: IRT-N)) standard (0.05 - 2 ppb).

3.3.2.3 Femur

Rat femurs were transferred to individual glass vials and heated to 700 °C for four hours after which each was mixed with a 1:2 (v/v) nitric acid/dH_2O solution and left overnight at RT. Samples were diluted 1:200 (v/v) in 1 % nitric acid and Ag^+ content determined against an Ag^+ standard (0.2 - 20 ppb).

3.4 Results

3.4.1 Rapid elution of Ag^+ from implant results in sort-term peak exposure

The elution kinetics of silver from Ti-6Al-4V pins implanted within rat femoral intramedullary canals was successfully plotted over 28 days. A burst release of silver was observed within the initial 24 hour period following implantation (Figure 3.2). This equated to a mean release of 25.15 µg Ag^+ (SEM±1.45 µg; range: 22.8 - 27.8 µg) in to the canal, approximately 70 % of the pre-implantation Ag^+ content of each implant (p<0.0001). No additional significant Ag^+ release was observed over the remaining course of the study, with the mean total release at Day 28 equating to 28.16 µg (SEM±1.76 µg; range: 24.8 - 30.8 µg).

Paralleling the rapid release of Ag^+ from the implant was an increase in Ag^+ detected in both the plasma (Figure 3.3) and femur (Figure 3.4), however, the residence time in both tissues was very different. Baseline silver content of plasma was below 0.00125 µg/mL (the limit of detection). A maximum concentration of Ag^+ was detected in plasma at Day 1 (0.019 µg/mL, SEM±0.004 µg/mL), after which a steady state decline was observed over the first three days of the study (R^2=0.874). While only approximately 9 % of the Ag^+ was removed from the plasma at Day 2, this clearance rapidly increased to 52 % at Day 3. Circulating silver detected at Day 28 decreased to a mean 0.0016 µg/mL (SEM±0.0003 µg/mL), approximately 7 % of the reported Day 1 value (p<0.05) and was not significantly different to that of the baseline measurement (p=0.999).

The study design demonstrated the persistence of silver within the femur for the first three days following implantation (Figure 3.4). Although a significant initial increase from Day 0 was detected in total Ag^+ at Day 1 (6.00 µg, SEM±2.00 µg; range: 2 – 8 µg; p<0.01), peak total Ag^+ did not occur until Day 3 (7.00 µg; SEM±0.58 µg; range: 6 – 8 µg; p<0.01) before significantly declining over the remaining study period (Day 28, 2.00 µg; comparison to Day 2 & 3, p<0.05). There was no statistical difference between the Ag^+ content of the femurs at Day 28 and baseline (p=0.58).

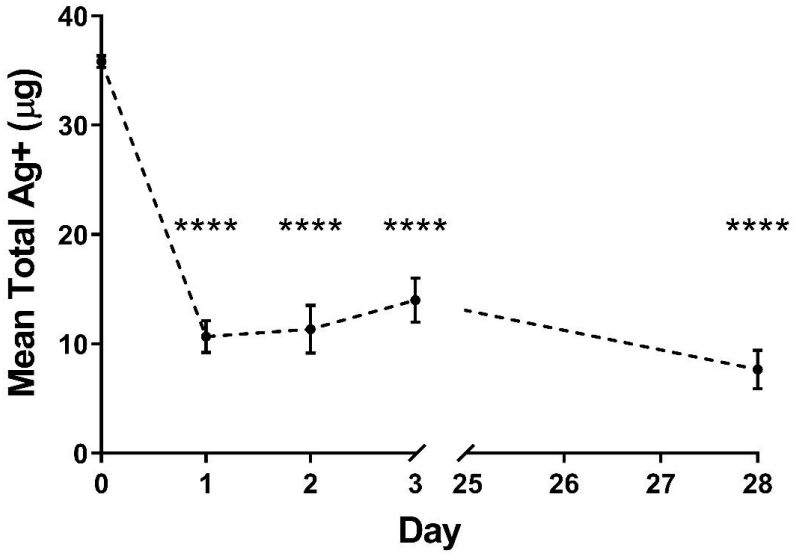

Figure 3.2: Quantification of Ag^+ from explanted silver coated Ti-6Al-4V implants over a 28 day study period.

Mass of silver on implants was determined prior to implantation, Day 0. At time points following surgery (Day 1, 2, 3 & 28), implants were excised and the quantity of remaining Ag^+ determined by ICP-MS. Mean Ag^+ (µg) is presented ±SEM (n=3 implants per time point). Statistical analysis against Day 0 by one-way ANOVA using Tukey's correction for multiple comparisons, **** $p<0.0001$. No significance detected between subsequent time points.

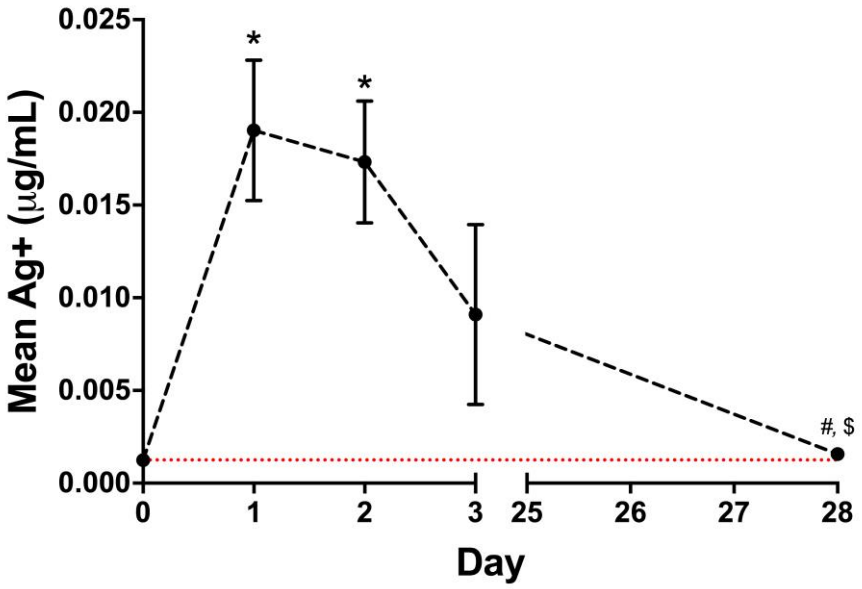

Figure 3.3: Quantification of Ag^+ from plasma of rats implanted with a silver coated Ti-6Al-4V implant over a 28 day study period.

The Ag^+ concentration within plasma was determined via ICP-MS for samples taken at termination. Mean Ag^+ (µg/mL) is presented ±SEM (n=3 plasma samples per time point). Statistical analysis against Day 0 by one-way ANOVA using Tukey's correction for multiple comparisons, * $p<0.05$. Significance against Day 1 represented by # = $p<0.05$ and against Day 2 represented by $ = $p<0.05$. No significance detected against Day 3. Red line represents limit of detection (= 0.00125 µg/mL).

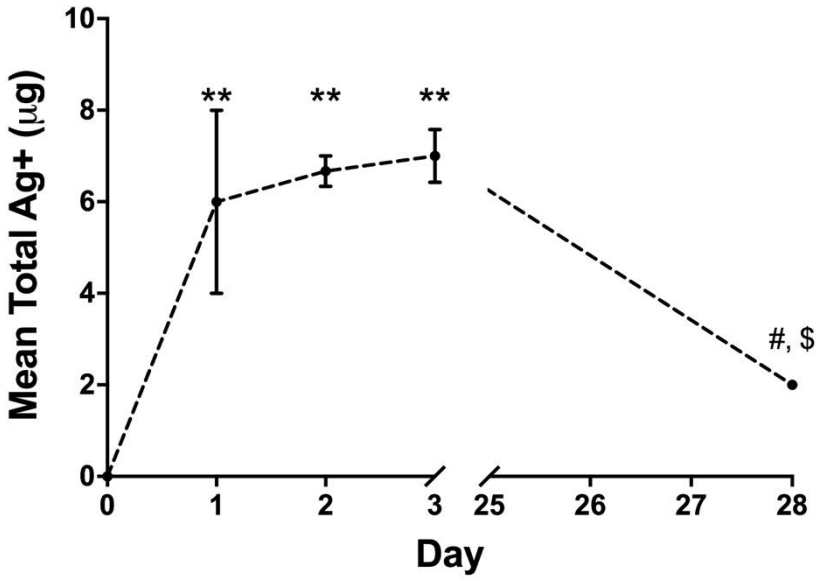

Figure 3.4: Quantification of Ag^+ from rat femurs implanted with a silver coated Ti-6Al-4V implant over a 28 day study period.

Total silver for operated femurs following the removal of the implant was quantified via ICP-MS. Day 0 baseline data obtained from non-implanted animals. Mean Ag^+ (μg) is presented ±SEM (n=3 femora per time point). Statistical analysis performed between all time points by one-way ANOVA using Tukey's correction for multiple comparisons. Significance against Day 0 represented by * $p<0.05$; significance against Day 2 represented by # $p<0.05$ and Day 3 by $ $p<0.05$.

3.4.2 Maximum intramedullary Ag^+ exposure

From these data, further analysis was performed regarding the maximum potential Ag^+ concentration within the canal and total circulating Ag^+ in plasma. Additional information obtained from the study and available information regarding femoral canal volume (Smith & Nephew internal data) and estimated plasma volumes for male Sprague Dawley rats, was used for this purpose (Table 3.1).

Since minimal Ag^+ release was observed after Day 1, this time point was analysed further to determine the maximum Ag^+ concentrations within the free canal volume (i.e. the canal volume available while the implant was *in situ*) with the assumption that the observed elution occurred instantaneously. For each of the animals allocated to the Day 1 time point it was clear that variation existed with the quantity of Ag^+ eluted from the implant and residing within the femurs following removal. This discrepancy was particularly highlighted by Animal 2, which had the lowest Ag^+ retention within the femur (2 µg) while also returning the highest Ag^+ elution from the implant (27.8 µg) over the 24 hour period. Therefore the maximum concentration of Ag^+ within the free canal volume was calculated as 6.00 µM. Lower concentrations were returned for the remaining animals (4.92 µM & 5.35 µM) giving a mean Ag^+ of 5.42 µM (SEM±0.31 µM). In addition, a calculation of the mean Ag^+ concentration within the canal in the event of instant release of the total Ag^+ from the implant was determined as 7.72 µM (range: 7.33 – 7.97 µM).

Having determined the concentration of Ag^+ within the free canal volume, further information regarding the transfer of Ag^+ into the circulatory system and subsequent redistribution/excretion could be ascertained. To determine, as far as possible from the study data, the total Ag^+ that may be accounted for in each animal, total plasma Ag^+ was determined. Using the animal weight, recorded prior to surgery, and a plasma constant value of 4.1 mL/100 g, determined for male Sprague Dawley rats (277), the total Ag^+ within the circulatory system was calculated (Table 3.1). Consequently, assuming that each pin contained the mean quantity of 35.83 µg Ag^+ when implanted, approximately 14 – 25 µg Ag^+ cannot be accounted for, with the assumption being that this was either redistributed within the organs of the animal or excreted within the 24 hour timeframe following surgery.

Table 3.1: Calculation of plasma volume, total Ag^+ and maximum Ag^+ concentration within the intramedullary canal for study animals from Day 1.

Maximum Ag^+ concentration (μM) within the free canal space was calculated for each animal using a canal volume measurement of 62.4 μL and an implant volume of 19 μL (molecular weight of silver = 107.9). Total plasma Ag^+ (μg) determined using volume constant 4.1 mL/100g, allowing total accounted Ag^+ measurement (μg) for each animal at Day 1.

	Replicates				
	1	2	3	Mean	SEM
Animal weight (g)	289	290	332		
Total plasma volume (mL)	11.85	11.89	13.61		
Ag^+ remaining on implant (μg)	13	8	11	10.7	1.45
Ag^+ in plasma (μg/mL)	0.0154	0.0266	0.0151	0.019	0.004
Total Ag^+ from femur (μg)	8.00	2.00	8.00	6.00	2.00
Ag^+ eluted from implant (μg)	22.8	27.8	24.8	25.16	1.45
Ag^+ concentration within free canal volume (μM)	4.92	6.00	5.35	5.42	0.31
Total plasma Ag^+ (μg)	0.182	0.316	0.206	0.235	0.072
Total Ag^+ accounted for (μg)	21.18	10.32	19.21	16.90	3.34
Total Ag^+ unaccounted for (μg)	14.65	25.51	16.62	18.93	3.34

3.5 Discussion

While elution studies performed through *in vitro* methods provide early stage information on the release kinetics from an implant surface, they do not offer reliable data related to a clinically relevant environment (270–272). Therefore, in order to achieve an improved degree of translation between *in vivo* and *in vitro* data it was important to understand the performance of the technology in a relevant setting before undertaking further detailed analysis of its biocompatibility. The primary objective of the study design was to provide a clinically representative reproduction of the implant and intramedullary environment, whilst measuring a number of parameters regarding the release of silver and the transfer/persistence in the circulatory system and surrounding implant site. The data obtained provided important evidence that facilitated the design of further *in vitro* experiments.

The bolus release of Ag^+ observed following the intramedullary implantation of this technology appears to be characteristic of the profile observed with other silver anti-microbial coatings (272) and those of clinically available antibiotic eluting intramedullary nails (106). With approximately 70 % of the Ag^+ eluting within the initial 24 hours the potential maximum local concentration at a fracture site was calculated at 6.00 µM. For the purposes of safety, the maximum concentration in the event of implant failure should be used as a benchmark for analysis and in the context of the implants prepared for this study, that maximum increased to 7.97 µM. However, further considerations may influence this maximum. For example, continued product development may necessitate an elevation of the Ag^+ content of each implant to increase anti-biofilm efficacy (initial *in vivo* infection data provided evidence of a 33 % reduction in the number of colonised implants, p=0.22; Smith & Nephew internal data). Furthermore, the target Ag^+ and acceptable quality assurance ranges applied during manufacturing may result in implants that contain a greater Ag^+ content than those tested here (e.g. the required percentage of hydroxyapatite applied to hip prosthesis is simply stated as >50 % (278)). It is therefore clear that both scenarios could result in a higher level of Ag^+ being applied to the implants, thus data from a broader investigation will be of benefit. As a result, initial *in vitro* investigations will interrogate a dose response based around these initial concentration findings.

While vastly reduced elution from the implant over the remaining study period was observed, this should not be dismissed during the consideration of *in vitro* testing. Although this low level may in itself have little impact with regards biocompatibility, the prolonged nature and effects on cells within the canal that have been pre-exposed to high concentrations as a result of the initial burst release, may be of consequence.

Aside from the dose response of eukaryotic cells to Ag^+, the duration of exposure will greatly affect the biocompatibility, with the effects of Ag^+ on *in vitro* cell survival to be highlighted (see Section 5.4.1). To reliably determine a clinically relevant duration of local exposure from the study data, both the femoral and plasma information needs to be considered in parallel. As expected, the spike in plasma Ag^+ is related to the burst release from the implant, however the exhaustion of Ag^+ elution results in the delayed but rapid removal from the circulatory system. Day 28 readings confirm a continued presence of Ag^+ within the plasma and while no direct baseline concentration for this study is available, data collected during method development allows us to presume the level to be below detection for unexposed laboratory animals (Smith & Nephew internal data). The continued detection of Ag^+ must therefore be attributable to a slow biological release (see below) resulting from its persistence within the femur following the rapid increase after implantation. While the duration of Ag^+ within the bone and surrounding tissue cannot be accurately predicted due to the limitations of the study i.e. 3 day initial time frame, we can presume from the lack of further Ag^+ release from the implant and the decreasing Ag^+ content of the plasma that the levels contained within the bone will not increase above those observed at Day 3.

Despite the encapsulation of the implant within the intramedullary cavity, the maximum accumulation of Ag^+ within the bone is secondary to the quantity that is unaccounted for within the initial 24 hour period of the study. While the excretion and localisation of Ag^+ was not investigated here, it is likely that this can be accounted for through the primary routes of faecal excretion or deposition within the kidneys and liver (149,279). These components of the hepatic system are the major contributors for dealing with metal toxicity through their elevated levels of metallothioneins (MTs). MTs are primarily involved in the homeostatic regulation of intracellular copper and zinc, with a subsequent fortuitous ability to sequester heavy metal contaminants such as cadmium (280,281) and silver (147,282). Once the metals have bound to the cysteine residues within the MT proteins they are degraded via the lysosome. Their half-life (t½) is dependent on the metal to which they are bound, with those sequestering heavy metals such as cadmium and silver increasing the t½ (283,284). However, of importance with

relation to the persistence of Ag^+ within bone and the presumed excretion of Ag^+ through hepatic routes, is the differential expression of MTs. While MT synthesis is observed in both kidney and liver upon administration of silver, there is no additional synthesis detected within the bone, potentially accounting for the high concentration of heavy metals found in these organs, relative to bone (285,286). It is likely, therefore, that the quantity of Ag^+ sequestered within bone may partly be limited by predetermined MT levels (287). In addition, studies involving cadmium showed that approximately 80 % of the metal ion was adsorbed to proteins of a high molecular weight rather than MT (285). While the removal of this bound form of Ag^+ may be relatively fast via the circulatory system, a slower degradation of the MT bound Ag^+ may be the cause of the persistence at Day 28 of approximately 33 % of the Ag^+ originally detected at Day 1.

It should be acknowledged that an improved understanding of the elution, accumulation and excretion of Ag^+ could be achieved with increased time points immediately following implantation. However, these data have provided a suitable background from which to determine the critical aspects of Ag^+ release, persistence and maximal concentrations in the intramedullary setting.

3.6 Conclusion

These data have provided evidence of a rapid release of Ag^+ from an intramedullary device within the initial 24 hours of implantation. The maximum intramedullary concentration for the current technology is 7.97 µM, however *in vitro* investigations should ensure that a range of Ag^+ concentrations are tested to gain maximal evidence for further developments. As far as is determinable, persistence within the bone suggests that *in vitro* testing use a three day window of exposure as a guideline for biocompatibility assessment, however, as with the concentration data, the investigations should not be limited to this timeframe.

4 Chapter 4: Availability of Ag^+ in cell culture media

4.1 Introduction

The development of cell culture media during the 1950s has led to the plethora of formulations that are available today. Many of these have been adapted from the original requirements for mammalian cell culture listed by Harry Eagle in his Eagle's basal media (BME) for the culture of fibroblasts and are modified to enhance the culture of specialised cells (288). For example, subsequent alterations of BME led to the creation of minimal essential medium (MEM) to more closely resemble the protein content for cultured human cells (289), Dulbecco's modified Eagle's medium (DMEM) for the culture of mouse embryonic cells (290,291) and minimal essential medium Eagle, alpha modification (αMEM) for the culture of mouse-hamster hybrid cells (292). Since these original adaptations, selection has continued to be based on improved cellular characteristics, such as proliferation, when using one media type over another (239,293).

Investigation of the *in vitro* cytotoxicity of scientific and medical developments is of paramount importance for the progression of technologies to the bedside. While the International Standards Organisation (ISO) have published guidance on the methods and reagents for biological safety testing of medical devices, the majority of published work on cytotoxicity is based on the practices employed within the particular research group. The extent of this variation is apparent in the use of cell culture media, where a review of the literature for MSC based assays resulted in Roswell Park Memorial Institute (RPMI), DMEM, DMEM/F-12 & αMEM all being selected as the basal media (238,260,294–297). A situation that is complicated further by changes between media type depending on whether cultures were being expanded or differentiated (297–300). While the selection can be justified on the basis of the previously mentioned improved cellular characteristics and differentiation, this variation is often accepted without consideration of the effect on the activity of the test compound and the resulting output.

Literature reporting the biocompatibility of silver have presented both positive and negative data regarding cytotoxicity, however as outlined above, the research has employed various cell specific media types. As a consequence, comparison of the biocompatibility reported between e.g. mouse pre-osteoblasts and human osteoblasts is difficult (239,262,274). In order for this research to progress effective therapies to the

clinic, it is important that the data are consistent during this *in vitro* stage of experimentation, however the continuity and consistency of the conclusions drawn from data between laboratories may be compromised through the variations in media choice. While ionic silver is effective as an antimicrobial, it rapidly forms silver chloride (AgCl) in biological systems, reducing its bioavailability and preventing its bactericidal activity (301). This situation also conversely applies to its biocompatibility on mammalian systems as demonstrated through reduced cytotoxicity following the formation of AgCl in chloride controlled test media (152,302). Of interest, is that extreme increases in the chloride content of bacterial culture media (i.e. NaCl ≥20 g/L) can result in the generation of water soluble anions, $AgCl_2^-$ and $AgCl_3^{2-}$ that are bactericidal (303). This phenomenon is unlikely in cell culture media due to the lower chloride component, therefore insoluble AgCl precipitates of 200-350 nm diameter form, restricted in size by the generation of a 'protein corona' (296).

Additional reductions in cytotoxicity were reported by Zuberek and colleagues (304). They observed an increased tolerance of HepG2 cells (human hepatocyte cell line) to silver nanoparticles (AgNP) as a result of long-term (>1 month) culture expansion in low glucose DMEM (there is no data presented for long-term culture in high glucose DMEM). The increased viability was determined to be a result of reduced mitochondrial H_2O_2 production (presented as a percentage of control) and elevated antioxidant protein activation in DMEM containing 1 g/L (low) compared to that containing 4.5 g/L (high). However, the report states that the rise in antioxidant enzyme activity was accompanied by an increase in ROS production, a consequence of the switch in metabolism caused by the transfer to low glucose medium. It therefore appears that the reported reduction in mitochondrial H_2O_2 and the increased ability to tolerate AgNP is likely to be a consequence of the increased oxidative stress that the cells find themselves under and the subsequent priming of the ROS pathways. This therefore serves as an example of how culture technique can influence the outcome of data.

With these examples in mind, it was important to determine whether the various media used during MSC culture and differentiation would affect the characteristics of Ag^+ exposure, with results potentially able to direct the selection of media during the *in vitro* testing phase of the study. To achieve this, analytical and *in vitro* cytotoxicity testing in the presence of Ag^+ was performed using media most commonly applied for MSC culture and differentiation, αMEM and DMEM. Alongside these cultures, an immortalised cell line recommended for use by ISO 10993-5 (Biological evaluation of

medical devices – Part 5: Tests for *in vitro* cytotoxicity) was employed as a control. Biocompatibility data were then used to correlate the findings of the analytical studies.

4.2 Aims

The aims of the experimental work presented here were to standardise the MSC expansion and differentiation basal media for future *in vitro* investigations.

Specific aims of the study are to:

- Determine the bioavailability of Ag^+ in the most commonly used basal media for the expansion and differentiation of MSCs.
- Correlate analytical data to MSC viability in DMEM and αMEM through application of an Ag^+ dose response.

4.3 Methods

4.3.1 Silver ion preparation, media incubation and ICP-MS analysis

Stock solutions of 35 mM Ag^+ were prepared in distilled water using polypropylene volumetric flasks (Nalgene). Solutions were sonicated to aide dissolution before filter sterilisation (0.2 µm, Sartorius Minisart) and subsequent dilution to 10 mM working stock. Working stocks were stored at 2-8 °C for a maximum of 7 days.

Silver was spiked in to 2 mL αMEM +10 % FBS[1], DMEM +10 % FBS[1] or deionised water (dH_2O, 15 MΩ) to give an Ag^+ of 25, 250, 400 & 600 µM. Samples were incubated at 37 °C, 5 % CO_2 for 0, 1, 3 & 24 hours, with additional time points of 20, 40, 60 & 80 minutes performed in αMEM for Ag^+ ≥250 µM.

At each time point the solutions were filtered (0.2 µm, Phenomenex, UK, Cat: AF0-1202-12), prepared for analysis by dilution in 1 % nitric acid and analysed using Agilent Technologies 8800 ICP-MS triple quad. Samples were measured against appropriate matrix (αMEM/DMEM cell culture media) matched Ag^+ standard curves using a 500 ppb rhodium internal standard (see Section 3.3.2). Results were generated as parts per billion and converted to moles. Data were analysed by two-way ANOVA, Tukey's correction for multiple comparison.

4.3.2 *In vitro* viability in different cell culture media

Viability was assessed using ISO10993-5 as a guideline (305). MSCs and the immortalised mouse connective tissue cell line, L929 (ECACC, Cat: 85011425), were seeded in to 96-well plates at $3.125x10^4$ cells/cm^2 leaving the outermost wells in to which sterile PBS was added. After 24 hours incubation (37 °C, 5 % CO_2) media were removed and an Ag^+ dose response (range 8.75 – 100 µM (DMEM) or 50 – 700 µM (αMEM)) added in triplicate (100 µL/well). A further 24 hour incubation was followed by the addition of WST-1 reagent (Roche Diagnostics, Cat: 11644807001) and the optical density read at 440 nm & 600 nm after a 1 hour incubation. Optical density was converted to viability as a percentage of the untreated control and EC_{50} concentrations

[1] FBS added to αMEM and DMEM was from the same source and batch to allow for equal comparison of effects.

(the concentration that provides a 50 % response) calculated. Data were analysed by one-way ANOVA, Sidak's correction for multiple comparison.

4.3.3 *In vitro* viability in DMEM and αMEM containing equal sodium chloride and glucose content

4.3.3.1 NaCl supplementation

Following initial cell viability testing the assay was repeated in DMEM and αMEM media containing equal concentrations of sodium chloride (NaCl) to determine if the difference was responsible for the decrease in Ag^+ cytotoxicity. The difference in NaCl content between the two basal media was 0.4 g/L (DMEM, 6.4 g/L; αMEM, 6.8 g/L), therefore an appropriate volume of filter sterilised NaCl (prepared in DMEM) was added to DMEM+10 % FBS.

MSCs were seeded as before, in their respective test medium (DMEM, DMEM+NaCl, αMEM), after which an Ag^+ dose response was added. Viability was assessed as previously described.

4.3.3.2 Glucose supplementation

DMEM is available as either low (1 g/L) or high (4.5 g/L) glucose, however αMEM is only available at a glucose content equivalent to that of the low glucose DMEM (i.e. 1 g/L), therefore the deficit was rectified by supplementing αMEM with D-(+)-Glucose (Sigma, Cat: G7528). DMEM+10 % FBS and αMEM+10 % FBS preparations were therefore available in 'Low' (1 g/L) and 'High' (4.5 g/L) versions.

Replicating the work by Zuberek *et* al. (304), MSCs were expanded in the four different media types before testing in their respective medium as previously described (see Section 4.3.2).

4.4 Results

4.4.1 Analysis of silver from αMEM & DMEM media

Inductively coupled plasma mass spectrometry (ICP-MS) detection of Ag in the dH_2O solutions was in agreement with the target molar concentrations at all time points (Figure 4.1). At T0 (Figure 4.1a), culture media concentrations of ≥250 µM were significantly lower than detected in dH_2O (p<0.0001), but were equivalent to each other (p>0.05). After one hour incubation, the measured Ag in αMEM (250 & 400 µM) was significantly decreased further from that of water (p<0.0001) and DMEM (p<0.0001), a trend that was maintained at all subsequent time points. This decline was not observed at 600 µM, with the measured concentration exceeding that of DMEM in all cases after T0 (Figure 4.1b-d).

The variation in measured Ag for DMEM samples related to time point is presented in Figure 4.2 and Table 4.1. At a target Ag^+ of 25 µM, mean Ag (±SEM) during the 24 hour period of analysis equated to 23.00 µM (±1.07 µM), with the range between time points of 18.53 µM (at T0) and 27.07 µM (at T1). With increasing target concentration came an increase in the overall spread of data. Furthermore, despite the measured Ag providing a linear result from the target Ag^+ values over the range tested (R^2=0.998), the measured Ag equated to approximately 70 % of target value at concentrations ≥250 µM, while the mean was 92 % of the target value at 25 µM.

Analysis of shorter time points in αMEM highlighted the time frame at which the availability of the lower Ag^+ concentrations (250 & 400 µM) was altered. While little variability was observed over the 80 minute time frame for samples containing 600 µM Ag^+ (Figure 4.3), a reduction from T0 was recorded after 20 and 40 minutes for 250 µM and 400 µM Ag^+, respectively.

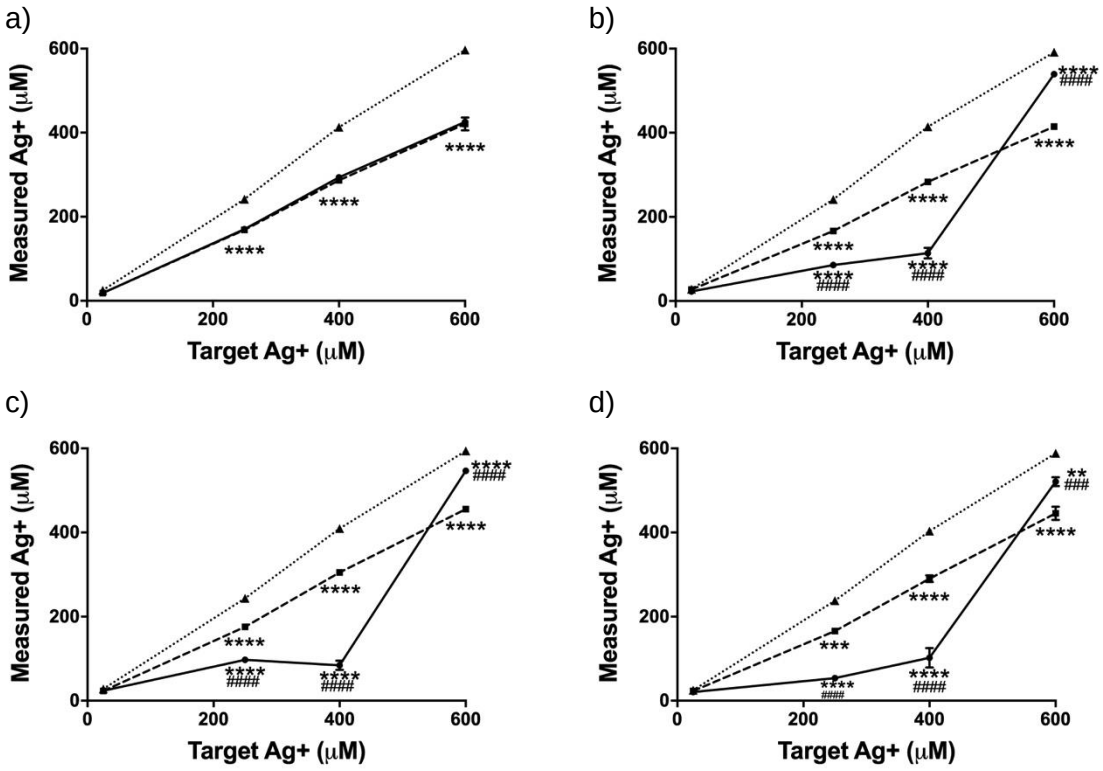

Figure 4.1: Quantification of Ag^+ from cell culture media and deionised water.

Measured Ag^+ from αMEM (—), DMEM (----) and dH_2O (-----) determined at a) 0, b) 1, c) 3 & d) 24 hours, using ICP-MS and following incubation at 37°C, 5 % CO_2. Data presented as target Ag^+ against mean Ag^+ concentration ±SEM (n=3, independent replicates per concentration). Significance against dH_2O represented by ** p<0.001, *** p<0.005, **** p<0.0001, significance between DMEM and αMEM represented by ### = p<0.005, #### = p<0.0001.

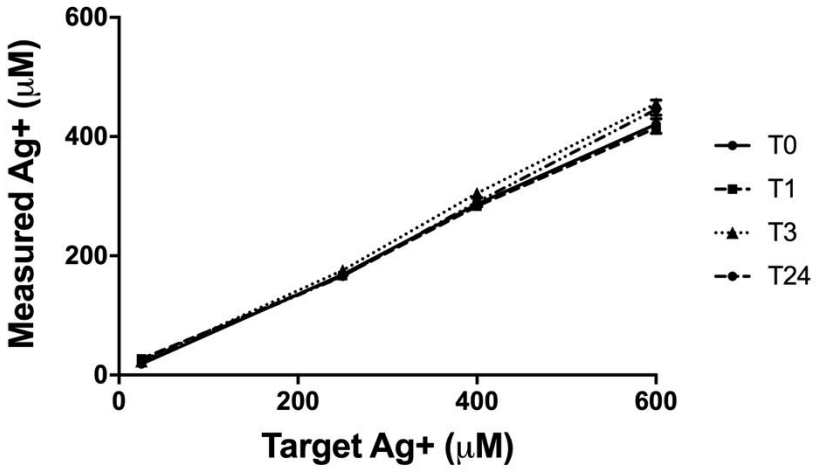

Figure 4.2: Quantification of Ag^+ in DMEM cell culture media during 24 hour time period.

Measured Ag^+ from DMEM following incubation at 37°C, 5 % CO_2 for: 0 (—), 1 (----), 3 (**------**) and 24 hours (**----**). Data presented as mean ±SEM (n=3, independent replicates per concentration).

Table 4.1: Measured Ag from DMEM according to target concentration and incubation time.

Mean Ag from DMEM as measured by ICP-MS. Data provided in relation to target Ag^+ concentration (μM) and incubation time (hours).

	Time point									
	T0		T1		T3		T24		Ag conc. across time points	
Target Ag^+ conc. (μM)	Mean	SEM	Mean	SEM	Mean	SEM	Mean	SEM	Mean	SEM
25	18.53	0.23	27.07	2.17	23.10	1.37	23.30	0.31	23.00	1.07
250	168.57	1.38	166.53	1.11	175.70	2.17	165.50	1.93	169.08	1.40
400	286.73	3.27	283.03	5.34	305.00	4.42	290.03	7.84	291.20	3.44
600	421.00	15.20	414.87	2.84	455.63	3.51	445.83	16.01	434.33	7.00

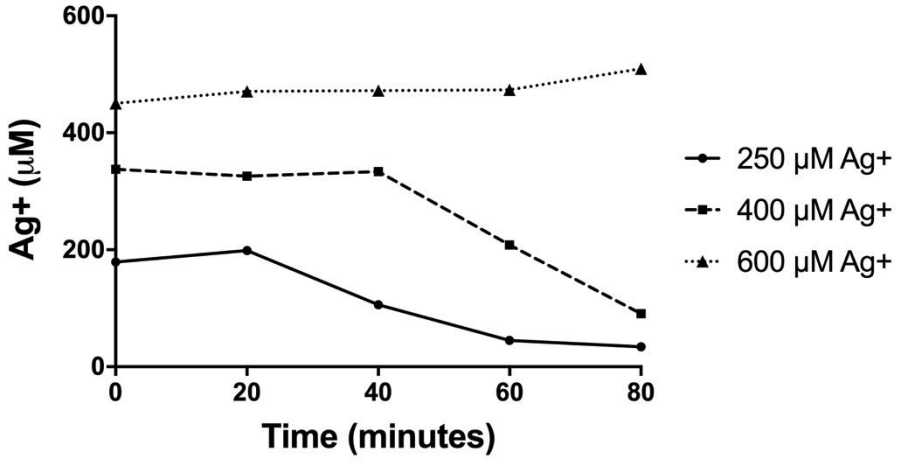

Figure 4.3: Quantification of Ag^+ from αMEM at short time points.

Measurement of Ag^+ at 0, 20, 40, 60 and 80 minutes from αMEM samples spiked at 250 μM (—), 400 μM (----) and 600 μM (**------**) Ag^+ (n=1).

4.4.2 Cell viability following 24 hour exposure to Ag^+ when cultured in αMEM and DMEM

Cell viability in the presence of an Ag^+ dose response was determined through the conversion of WST-1 to soluble formazan products by metabolically active cells. During culture in DMEM, both primary MSCs and the immortalised L929s were susceptible to Ag^+ at concentrations of ≥25 μM and ≥10 μM, respectively. However, the detrimental effects were only observed in αMEM cultured MSCs and L929s during exposure to >400 μM Ag^+ (Figure 4.4).

Analysis of the EC_{50} data for each cell type and media combination further confirmed the effect of media selection on Ag^+ cytotoxicity (Table 4.2). The culture of cells in αMEM resulted in approximately 13-fold increase in the EC_{50} for MSCs and L929s compared to culture in DMEM (MSCs, DMEM: 33.06 μM, αMEM: 444.1 μM, $p<0.0001$; L929, DMEM: 16.78 μM, αMEM: 451.9 μM, $p<0.0001$).

A difference in the viability between cell types was also observed within the culture media test groups. While L929 cells showed a greater tolerance to Ag^+ in αMEM compared MSCs ($p=0.995$), this trend was reversed during analysis of the DMEM data, although this was not statistically significant ($p=0.503$).

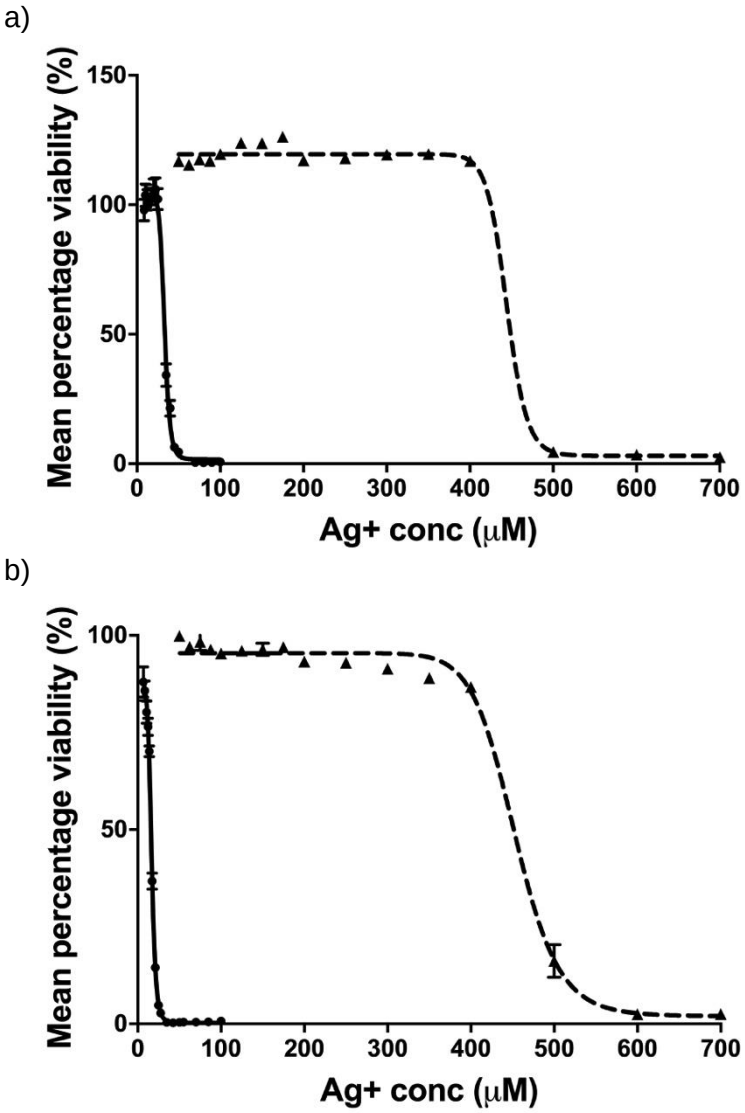

Figure 4.4: Cell viability of a) MSCs and b) L929 cultured in αMEM and DMEM following 24 hour exposure to Ag^+.

Viability of a) MSC and b) L929 cultures as a percentage of untreated control determined via WST-1 conversion. Dose response to silver determined for both cultures in αMEM (----) and DMEM (—). Results are presented as mean percentage viability ±SEM and represent duplicate (αMEM) or triplicate (DMEM) biological replicates from three independent MSC donors (K224, HS509, HS739) or L929 cultures.

Table 4.2: Mean EC_{50} values for Ag^+ cytotoxicity on MSCs and L929 cells.

MSCs and L929 cultures were treated with a concentration range of Ag^+ for 24 hours, after which EC_{50} values were calculated from WST-1 viability assays. Data represents the mean (±SEM) of the three MSC or L929 cultures represented in Figure 4.4.

	MSC	L929
αMEM	444.1 µM (±8.98)	451.9 µM (±11.87)
DMEM	33.06 µM (±0.65)	16.78 µM (±0.06)

4.4.3 Effect of media NaCl and glucose content on cytotoxicity of Ag^+ to MSCs

To determine the role of NaCl in the reduced cytotoxicity of Ag^+ to MSCs, sodium chloride was spiked in to DMEM to provide an equivalent concentration to αMEM for comparison. Viability of MSCs in DMEM was unaffected by the addition of NaCl, with overlying dose response curves observed with DMEM and DMEM+NaCl (Figure 4.5). The equivalent αMEM data showed the expected increased Ag^+ concentration required to reduce MSC viability.

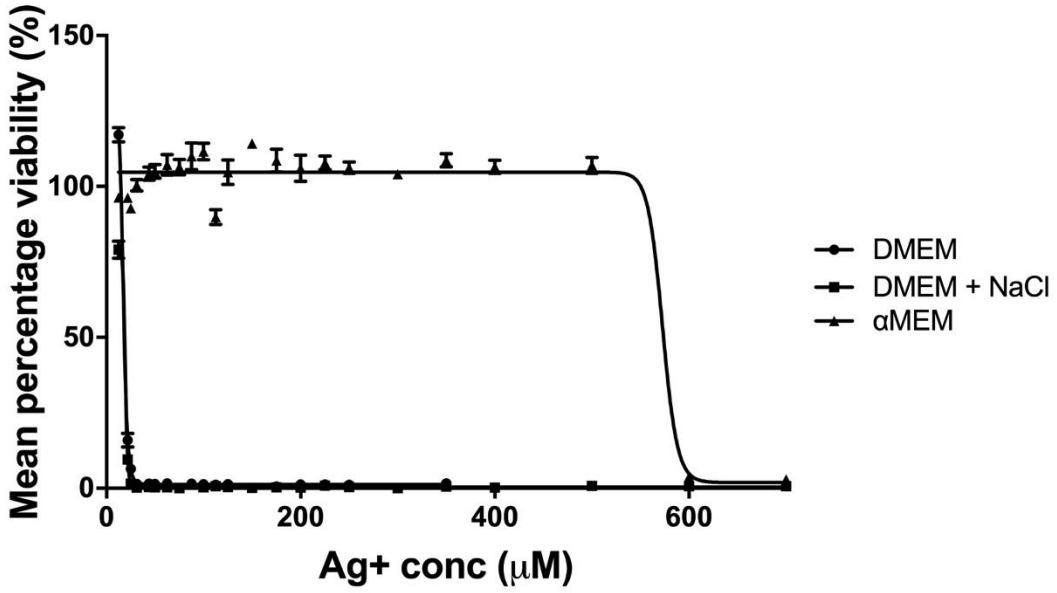

Figure 4.5: MSC viability cultured in DMEM, DMEM spiked with NaCl and αMEM following 24 hour exposure to Ag^+.

Viability of MSC cultures as a percentage of untreated control determined via WST-1 conversion. Dose response to silver determined for cultures in DMEM and DMEM spiked with NaCl equating to that contained in αMEM. Results are presented as mean percentage viability ±SEM and represent triplicate biological replicates from one MSC donor.

The susceptibility of MSCs to Ag^+ following culture and testing in media with different glucose availability was determined. MSCs were expanded in appropriate media for the time periods outlined in Table 4.3. The parallel testing of low glucose αMEM from 32 day expanded cultures was not possible due to inadequate cell number.

Table 4.3: Expansion time and inclusion in WST-1 viability assay of MSCs cultured in αMEM and DMEM containing low (1 g/L) and high (4.5 g/L) glucose.

	HS674		HS739
	Short culture	Prolonged culture	Short culture
	Time in culture (days) / no. of passages	Time in culture (days) / no. of passages	Time in culture (days) / no. of passages
αMEM Low αMEM High DMEM Low DMEM High	11 days / 2 passage	32 days / 5 passage	8 days / 1 passage

The effect of the glucose content of media on the cytotoxicity of Ag^+ is evident in Figure 4.6. The viability of MCSs was unaffected by the expansion time when performed in low glucose DMEM media (equivalent comparison unavailable for αMEM, graph of short term expansion provided for information). There was however a shift in viability following expansion in both DMEM and αMEM containing high levels of glucose. For high glucose DMEM, the shift in mean EC_{50} between short- and long-term expansion was 26.60 µM and 16.16 µM, respectively, while the equivalent EC_{50} values for αMEM were 476.0 µM (short) and 418.1 µM (long). Note should be made of the low donor numbers for each condition, n=2 for short-term expansion, n=1 for long-term expansion.

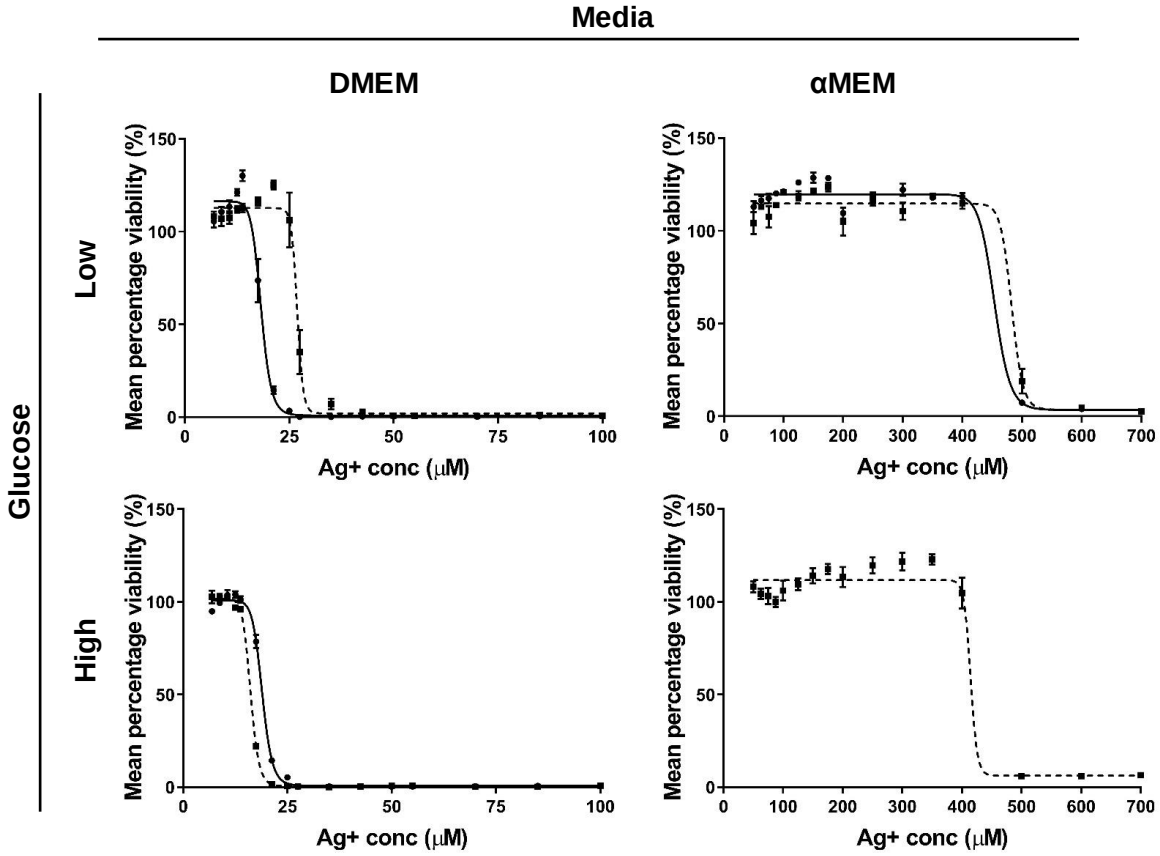

Figure 4.6: MSC viability following short (≤11 day) and prolonged (32 day) expansion in low and high glucose DMEM and αMEM following 24 hour exposure to Ag^+.

Viability of MSC cultures as a percentage of untreated control determined via WST-1 conversion. Dose response to silver determined for cultures in low and high glucose DMEM and αMEM following short (—) and long (----) term expansion. Results are presented as mean percentage viability ±SEM and represent triplicate biological replicates from two donors (HS674 & HS739) for short-term expansion and one MSC donor (HS674) for long-term.

4.5 Discussion

With the increased interest in silver as a broad spectrum antimicrobial agent, the reporting of *in vitro* efficacy and cytotoxicity testing of its application in varying therapies has expanded in recent years. From these studies there have been reports of detrimental outcomes (306) countered by studies reporting minimal biological adverse effects when applied at appropriate concentrations (238,260,295), with benefits to osteogenesis also reported (258,263).

Of importance when reviewing the data from publications that investigate the effects of silver is the understanding that the properties of this element are dependent on its environment. The container within which the activity is performed and the solution within which the silver is applied may reduce the bioavailability (and thereby increase cell viability) through the adherence of the silver ions to different substrates, through the interaction with protein or the formation of inactive silver chloride precipitates (307–310). Although in the current experiments the percentage serum content was standardised to remove any variability that this may have caused, other components of media were identified as possible sources of inactivation.

The reduction of quantifiable silver in αMEM through the formation and subsequent filtration of silver precipitates was highlighted through the ICP-MS analysis, however the surprising factor was that the highest Ag^+ dose (600 µM) returned measured values higher than that of the DMEM and nearing those of the water control. While the shortfall of using ICP-MS is the inability to determine the format of silver within the test solution, the expectation was that the components within the αMEM that caused the decrease at lower values would still exert their effect, but once exhausted, would result in an increase that would continue to be below that of the DMEM. Instead, it appears that high silver concentrations bypass the same particulate formation that occurs at ≤400 µM, thus allowing the silver ions to remain available in solution following 0.2 µm filtration. With this in mind, it is therefore of no surprise that the elevated availability has resulted in the reduced viability observed in αMEM+10 % FBS at Ag^+ >400 µM (Figure 4.4).

The analysis of the filtrate from the shorter time points translates the findings of Zhang *et al.* (302) to that of the cell culture environment. These results confirmed that the formation of silver particulates within αMEM was concentration and time dependent, replicating the trends reported when using silver nitrate spiked phosphate buffered

saline. It appears that the formation of particulates from the 250 µM sample did not occur until after 20 minutes incubation, while a further delay was evident as the Ag^+ concentration increased. An explanation for the delay was not forthcoming, however the suggestion by Zhang that in their experience, an increase in Ag^+ caused a more rapid formation of primary colloids did not correlate with these data. Biologically, the evidence for the delay in Ag^+ precipitation suggested that the detrimental effect on L929 and MSCs was not instantaneous since viability in αMEM at 24 hours was maintained at bioavailable silver concentrations for different timeframes during the first hour, that were ultimately cytotoxic when applied in DMEM.

These findings on the cytotoxicity of silver (in DMEM+10 % FBS) to primary (EC_{50} = 33.06 µM) and immortalised cells (EC_{50} = 16.78 µM) compare to those of other researchers using similar cell types (232,311,312), however no equivalent dose response could be found for parallel cultures tested in αMEM. As a result, the differences in the direct cytotoxic response to Ag^+ in different media have not been properly highlighted. These data from parallel αMEM cultures have provided EC_{50} values of 448.3 µM and 451.9 µM for primary and immortalised cells, respectively, a 13-fold and 27-fold change in EC_{50} value for Ag^+ cytotoxicity caused by the change in media type alone. Importantly, the decline in viability responsible for the calculated EC_{50} concentrations from αMEM cultured cells, correlates with the concomitant rise in Ag^+ quantified from filtered αMEM at concentrations >400 µM.

While a limitation of this study is the accuracy of the EC_{50} values at the greater concentration range, a result of reduced number of Ag^+ test concentrations above 400 µM, these data still highlight the dramatic effects of culture media selection. Therefore, an emphasis must be placed on the behaviour of the test material, especially when assessing the biocompatibility of silver containing medical devices under development, and should potentially be considered for other innovations containing similar reactive metal ions.

Notwithstanding the linearity of Ag^+ quantification from DMEM, the reduction in measured Ag^+ compared to target should not be ignored. While these data confirm that the availability of Ag^+ is consistent, there is clearly a discrepancy between that of the target and measured concentrations. As with all *in vitro* models, while it is important to ensure the accuracy and potential clinical translation, it should always be considered as a model. While the normal functioning of this system (i.e. cell proliferation) should

not be compromised in order to enhance the action of the chemical substance, there should be an awareness of the potential effects that the model can exert. The data presented here therefore provides evidence that the selection of cell culture media is vital to the outcome of cytotoxicity studies of silver, in addition to linking this outcome to the bioavailability of this compound within the cell culture system.

With this in mind, the previous reports highlighting the effect of individual components on the availability of free Ag^+ and cytotoxicity was investigated with respect to NaCl and glucose. Firstly, the data presented here hypothesised a reduction of cytotoxicity as a result of increased chloride concentration. While the chloride (Cl^-) content of DMEM (119.3 mM) and αMEM (126.2 mM) media is derived from several sources e.g. potassium chloride and calcium chloride, the main contributing factor is primarily in the form of NaCl (Cl^-, DMEM = 109 mM; αMEM = 116 mM) (313). The equilibration of the NaCl content between DMEM and αMEM in this work was found to have no effect on viability (either positive or negative), suggesting that this component alone was not responsible for the significant differential in viability between the normal basal media.

The generation of AgCl and effects on cytotoxicity were investigated by Kaiser *et al* (308). The group used MEM (Cl^- = 124.5 mM) to represent their highest chloride containing test medium, with reductions therefrom. Interestingly results showed that MEM caused a decrease in monolayer cell viability compared to media of reduced Cl^- (≤87.3 mM). They proposed that an increased Cl^- in the MEM resulted in an increased sedimentation of dissolved silver through the generation of AgCl precipitates. Cell viability declining as a result of engulfment of the agglomerates. Intriguingly, the increased viability observed at lower Cl^- is not countered by an increase in free Ag^+, even when the amount of dissolved silver in the medium rose in the lowest chloride group (0.05 mM). This therefore indicates, as does our own data, that the formation of AgCl alone is not the only contributing factor involved with the reduced cytotoxicity of Ag^+ when using αMEM.

The availability of glucose during expansion of cultures has been shown to affect susceptibility to silver (304). This component differs between standard αMEM (1.0 g/L) & DMEM (1.0 g/L or 4.5 g/L) and a reduction in the EC_{50} was observed in the data presented here when MSCs were expanded over a period of 32 days (5 passages) in high glucose media (DMEM & αMEM). Unlike the work presented by Zuberek, no effect was observed with extended culture in low glucose DMEM. While this cannot be

explained by the data presented here, the interpretation of their data of increased viability through enhanced antioxidant protein activity as a consequence of altered metabolism in low glucose medium does not appear to transfer to this work. With regards to our reported observations with decreased MSC viability following prolonged expansion in high glucose medium, it must be presumed that the difference lay partly due to the use of primary cells rather than the HepG2 immortalised cell line; with the former potentially undergoing the process of *in vitro* cellular ageing that must not be ignored with regards to increased susceptibility to Ag^{+}.

From these investigations, the NaCl data should be considered as appropriate for providing evidence that the disparity between media may not be a consequence of one individual component, and that to fully elucidate the causes of the reported differences would require a full analysis of each constituent. The study of the effects of glucose availability during expansion serves to highlight the need for rigorous culture technique and to minimise the time of primary MSC culture prior to analysis.

Ultimately, this work has demonstrated the effect of specific cell culture media on the cytotoxicity of silver ions on primary (MSC) and immortalised (L929) cells and has examined the availability of the silver over a range of concentrations and time frames. It has also provided evidence that the potential bioavailability of silver is altered by *in vitro* culture conditions and experimental design.

4.6 Conclusion

The availability of Ag^+ to *in vitro* test systems is significantly altered by the selection of cell culture media. These data have highlighted the reduction of bioavailable Ag^+ when applied in αMEM and the presence of a concentration dependent variability. The findings of which also correlate with cell viability.

The increased viability at low Ag^+ concentrations observed with αMEM is in contrast to that of DMEM. While the measured Ag^+ in DMEM was below that of the target Ag^+, it remained linear at the concentrations and time points tested. Furthermore, the data provide confirmation that the lower EC_{50} was a result of constant, increased Ag^+ availability within the medium.

As a result of this study, future *in vitro* assessments will be made using DMEM as the basal test media.

5 Chapter 5: The effect of silver on cell viability and function

5.1 Introduction

The cascade of events that occur following bone fracture are essential for union and subsequent remodelling, involving the co-ordination and functionalisation of a plethora of cell types. While MSCs provide the platform from which to supply cells of the skeletal lineage, their viability in the presence of Ag^+ may be altered while in this undifferentiated state.

The use of *in vitro* assays to determine the toxicity of silver on eukaryotic cell types frequently takes the form of investigating the effects on viability (e.g. metabolism using MTT). With respect to the viability of primary MSCs under Ag^+ exposure, Pauksch *et al*. (238) observed a 24 hour EC_{50} of 20 µg/mL (approximately 185 µM) when applying either silver nitrate ($AgNO_3$) or silver sulphate (Ag_2SO_4), a result greatly in excess of that reported by Greulich *et al*. (294) at 13.8 – 25 µM. The data from Greulich however is in line with that of Gao *et al*. (314) who reported cytotoxicity on embryonic stem cells (EC_{50} = ~18 µM) and Qin *et al*. (263) when studying urine-derived stem cells (EC_{50} = 37 µM). These examples serve to highlight the variation within the literature, and when investigating the effects on other cell types it is clear that further disparity exists. For example the EC_{50} for osteoblasts ranges from 9.6 – 57 µM when allowing for media type (239,315). Similar data also exists for THP-1 monocytes with reported EC_{50} of 6 µM (253) and 10 – 20 µM (316). In comparison to these data, I reported an EC_{50} of 33.06 µM (±0.45 SEM) for primary MSCs (Chapter 4), therefore it will be of interest to test both human osteoblast and THP-1 monocytes (*in vitro* osteoclast-like precursor cells) in this system to provide an outline of data for those cells important for fracture repair.

Although the overall effect on viability is a key consideration when assessing Ag^+ on eukaryotic cells, the effect on function and regulation is of equal interest; a cell that appears to be viable in terms of metabolism may not be functioning as for the unexposed controls. As previously discussed (see Section 1.8.3), much of the literature surrounding the use of Ag^+ in orthopaedics is focussed on the incorporation of silver with hydroxyapatite, with orthopaedic reconstruction the clinical aim. These therefore are assessing the cellular responses when cultured in direct contact with the silver incorporated surface, a different scenario to that primarily found in orthopaedic trauma

where cell adherence to the implant surface is not required. Additional sources have detailed the effects of silver ions alone, with some showing positive osteogenic properties with regards to ALP expression (238,263). While these data appear positive, there is a fine balance between osteogenic and adipogenic differentiation. Although this is well maintained by MSCs, differentiation is often balanced towards the adipogenic lineage as a result of age. Increases in the adipose content of bone, with a corresponding decrease in trabecular bone volume have been observed in patients as a consequence of advancing years (317). This observation corresponded with a reduction in osteoblast number and the proliferative and differentiation capacity of MSCs in older subjects (318–320). This change has been linked to a decreased expression of the bone morphogenic protein (BMP) receptor-1B, a reduction in the BMP regulator Smad6 and an increase in the expression of PPARγ; all factors that contributed to the increased potential of MSCs from aged mice to undergo spontaneous adipogenic differentiation in a study by Moerman *et al*. (319). Furthermore, with increased adipogenesis linked to elevated oxidative stress via inhibition of β-catenin by FOXO (164,265), there is undoubtedly an important role of ROS on differentiation.

Further evidence for the 'oxidative stress theory of ageing' and the promotion of adipogenesis in older cells that was reported by Moerman, was the discovery of decreased superoxide dismutase (SOD) expression in "old" MSC donors (i.e. >40 years) that exhibited decreased osteogenic differentiation (321). This supported the theory that elevated ROS were responsible for the decline in bone formation and that its reduction could protect against the dysfunction observed with cell age (reviewed in (322)). With this in mind it is therefore important to determine the impact of device related Ag^+ exposure and the accompanying elevation in ROS upon the differentiation of MSCs. For this to be studied it is important that the possible effects of device related Ag^+ release be simulated, therefore data from the previous metabolism and *in vivo* study will be employed during differentiation. Additionally, the effect on differentiation will be assessed in Ag^+-free conditions following expansion of MSCs exposed to Ag^+, thereby simulating the effects of the continued process of bone synthesis during fracture healing once the elution of Ag^+ from the implant surface in to the surrounding tissue has ceased.

Further to the ability of MSCs to differentiate during and following exposure to Ag^+, their ability to continue their self-renewal is also paramount to maintaining a viable population of progenitors. The use of the CFU-f assay, specifically the generation of

colonies from individual cells seeded at low density, is the gold standard *in vitro* method to assess clonogenicity (185). While the determination of this capacity during Ag^+ elution from an implant is of importance, the requirement for this ability does not diminish once Ag^+ elution is exhausted. It is therefore vital that both the continued generation of MSC derived colonies and the differentiation capacity following their clonal expansion in the presence of clinically relevant Ag^+ concentrations is determined. To date, no studies have investigated the effect of prolonged Ag^+ mediated ROS elevation on the generation of CFU-f. Therefore, the impact of this environment on the clonogenicity of MSCs will be examined. In addition, the analysis of CFU-f generated during secondary seeding from original colonies will be employed to assess the properties of those cells that tolerated Ag^+ exposure. This analysis will take the form of an assay adapted from that reported by Sengers, Dawson & Oreffo in their determination of the bone marrow stromal cell heterogeneity (323). While this publication set out to ascertain the heterogenic characteristics of individual colonies, the work presented here will establish the effects on the overall CFU-f derived MSC population.

It is known that CFU-f formation is enhanced by factors contained within the serum that is added to cell culture media. The requirements and increases in efficiency for CFU-f formation from human bone marrow aspirates have been linked to: fibroblast growth factor-basic (bFGF), TGF-β, epidermal growth factor (EGF) and platelet-derived growth factor (PDGF) (324,325). In the case of human embryonic stem cell (hESC) cultures the maintenance and proliferation is partially facilitated by the presence of a mouse embryonic fibroblast (MEF) feeder layer that provides additional cues. However, MSC conditioned media (MSC-CM) has also been proven to provide sufficient factors to allow feeder-free hESC culture (326). This effect of MSC conditioned media identifies a potential role stromal cells play in cell survival, proliferation and disease (327–329). Furthermore, subsequent research has provided evidence that the characteristics of diseased cells are improved when cultured in the presence of MSC-CM (330,331). Investigations have revealed that the signals isolated from the MSC-CM have been in the form of paracrine factors and those found in exosomes (extracellular vesicles released from the plasma membrane that have been found to contain protein, lipid and RNA (332)). Additionally, with conditioned media found to contain not only those factors that have already been illustrated to improve CFU-f efficiency (333), but also members of the superoxide dismutases (330,334), its use will be of interest while investigating any possible negative effects of Ag^+ on CFU-f formation.

The relevance of the *in vitro* work with the previously reported *in vivo* data is important for its translation. From the data reported in Chapter 3, the rate of elution from the implant and the residence time within the bone highlighted that the greatest Ag^+ concentration would be within the initial three days following implantation. In addition to this, the highest possible Ag^+ release from the current technology would equate to approximately 8 μM, a concentration that data from Chapter 4 confirmed is below the *in vitro* cytotoxic concentration of MSCs. Therefore, aside from the viability assays performed on osteoblasts and monocytes, the Ag^+ concentration for future assays was set at a maximum of 10 μM to allow for flexibility with manufacturing acceptable ranges. With regards to exposure times, this was for the initial three days of an assay (to mirror that of the *in vivo* implant release profile) or for the duration of the assay to determine the effect should Ag^+ clearance be impeded by the local environment or physiology.

5.1.1 Origin and background to Y201 clonal MSCs.

Whilst the majority of the *in vitro* cell culture was performed using primary human MSCs, the availability of an immortalised MSC meant that this was selected for some analyses. These experiments were chosen in instances where the reproducibility provided by a clonal cell line was advantageous over the variation encountered with primary donors, or when their use allowed potential comparison between datasets.

The “Y201” MSC was generated by overexpression of human telomerase reverse transcriptase (hTERT), a protein that allows the maintenance of telomere length via addition of the telomere repeat sequence. Following transduction, the Y201 line was selected through clonal expansion from a range of hTERT-MSCs (266). Characterisation of the Y201 line revealed the expression of expected MSC surface markers ($CD73^+$, $CD90^+$, $CD105^+$, $CD34^-$, $CD45^-$) and tri-lineage differentiation potential.

5.2 Aims

The experimental work presented in this chapter aimed to examine the impact that silver has on fracture healing by determining the *in vitro* tolerance and susceptibility of MSCs to Ag^+ and their ability to differentiate both during and following exposure.

Specific aims of the study were to:

- Determine the limits of Ag^+ cytotoxicity through analysis of metabolism and proliferation, relating this to the *in vivo* release and excretion profile of Chapter 3.
- Assess MSC osteogenic and adipogenic differentiation during exposure to Ag^+.
- Determine the effects of Ag^+ on CFU-f and CFU-Ob generation by MSCs at clonal density and investigate the importance of extracellular signalling.
- Investigate the effects of Ag^+ with respect to the surviving CFU-f population and their continued clonogenic and differentiation capacity.

5.3 Methods

5.3.1 Viability & Proliferation

5.3.1.1 WST-1 viability assay

Cell viability in the presence of Ag^+ was determined for human monocytic cell line, THP-1, and human primary osteoblasts (hObs, PromoCell, Cat: C-12720), using WST-1 as outlined in Section 4.3.2.

5.3.1.2 EdU proliferation assay

DNA synthesis in proliferating cells was assessed by determining the incorporation of the thymidine analogue, 5-ethynyl-2´-deoxyuridine (EdU), during S-phase, and its subsequent detection through application of an Alexa Fluor 488 azide (Invitrogen, Cat: C10337) (335).

MSCs were seeded in to 24-well plates at $2.5x10^3$ cells/cm^2 (37 °C, 5 % CO_2). Twenty-four hours after seeding, media was replaced for DMEM+10 % FBS containing Ag^+ at 0, 0.1, 0.5, 1, 5 & 10 µM, with EdU included at a final concentration of 10 µM. After 72 hours, plates were treated according to the manufacturer's protocol (Invitrogen). In brief, cultures were fixed with 3.7 % formaldehyde/PBS (15 minutes at RT) after which the wells were rinsed twice using 3 % BSA/PBS. Cells were permeabilised with 0.5 % Triton X-100/PBS (20 minutes at RT) and rinsed twice, as before. Reaction cocktail (Click-iT reaction buffer, $CuSO_4$, Alexa Fluor azide & reaction buffer additive) was applied (30 minutes at RT, protected from light) followed by another wash with 3 % BSA/PBS and finally PBS alone. Cultures were treated with a 1:2000 dilution of Hoechst (30 minutes at RT, protected from light) and washed twice with PBS. PBS was added for storage at +4 °C.

Five separate areas of each well were imaged and analysed using ImageJ to calculate the number of EdU (488 fluorescent) positive and Hoechst nuclear stained cells (DAPI). Data were calculated as the number of EdU incorporated cells as a percentage of the total cell number for each image and statistical analysis performed by one-way ANOVA with Dunnett's correction for multiple comparisons.

5.3.2 CFU-f proliferation and CFU-Osteoblastic (CFU-Ob) formation in presence of Ag^+

Colony-forming unit fibroblast (CFU-f) assays were established using MSCs at a clonal seeding density of 10 cells/cm^2 in 6-well plates. The media was changed 24 hours after seeding for that containing Ag^+ (0, 0.1, 0.5, 1, 5 & 10 µM). Media was changed twice per week on CFU-f plates with one subset of plates only receiving Ag^+ for the first three days, after which media was without silver (DMEM+20 % HyClone FBS only). CFU-f were cultured for 14 days post-seeding and stained with crystal violet.

The formation of CFU-Ob was as for CFU-f, applying osteogenic additives (see Section 5.3.3) to DMEM+20% HyClone following the media change 24 hours after seeding. Media was changed twice per week with analysis of colonies after two weeks. ALP positive colonies were identified using Fast Red TR/Naphthol AS-MX method. In brief, colonies were washed twice with PBS before addition of ALP detection solution for 2 minutes (0.2 mg/mL naphthol AS-MX (Sigma, N4875), 1 mg/mL Fast Red TR (Sigma, F6760), 10 µL/mL N,N-dimethylformamide (Sigma, D4551), 0.1 M Tris base pH 9.2). Cultures were then washed twice in PBS and stored in 20 % glycerol/PBS.

Analysis of all CFU data was against control (0 µM) by one-way ANOVA using Dunnett's correction for multiple comparisons.

5.3.3 Differentiation - Osteogenesis

MSCs were culture expanded, seeded in to well-plates (DMEM+10 % FBS) and incubated (37 °C, 5 % CO_2) for 24 hours prior to the addition of osteogenic media (DMEM, 10 % FBS, 100 units/mL Penicillin, 100 µg/mL Streptomycin, 50 µg/mL L-Ascorbic acid 2-phosphate sesquimagnesium salt hydrate (Sigma, Cat: A8960), 10^{-8} M Dexamethasone (Sigma, Cat: D2915), 3 mM β-glycerophosphate (Sigma, Cat: G9422)) ±10 µM Ag^+. Media was changed after three days in one Ag^+ treated group for osteogenic media only while maintaining 10 µM Ag^+ in the second treatment group. Media were changed twice per week with time points for analysis at seven and 14 days post-seeding. Non-osteogenic (basal media) controls underwent the same media changes (with/without Ag^+) and time points.

To determine the effects of Ag^+ on CFU-f expanded MSCs, cells were seeded at clonal density (see Section 5.3.2) in T175 flasks (and additional six-well plates to allow confirmation of detrimental mean CFU-f number in the presence of Ag^+) and treated

with 10 µM Ag^+ for 14 days. Following expansion, MSCs were seeded and osteogenic media added as previously stated, but without the addition of Ag^+ during differentiation.

Alkaline phosphatase (ALP) activity was used as a marker of osteogenesis and was determined through the colorimetric change that occurs with the dephosphorylation of a p-nitrophenyl-phosphate substrate (pNPP) by ALP. At the specified time points, cultures were washed three times with 0.2 M carbonate buffer and lysed with 0.1 % Triton X-100/0.2 M carbonate buffer. Lysis was completed through five freeze/thaw cycles. A p-nitrophenol standard (pNP, 0-250 nmol/mL, 100 µL/well) was applied to a 96-well plate alongside 50 µL of each sample, diluted in 0.1 % Triton X-100/0.2 M carbonate buffer where necessary. To each sample, 50 µL of a pNPP substrate (5 mM pNPP, 3.3 mM $MgCl_2$ in 0.2 M carbonate buffer, protected from the light) was added and the plate incubated (1 hour, 37 °C). Optical density measurements were taken at 405 nm using the Multiskan GO microplate spectrophotometer (Thermo Fisher, UK). Calculation of the unknown samples was performed in Microsoft Excel.

All ALP data were normalised to the double stranded deoxyribonucleic acid (dsDNA) content for individual wells, determined using the fluorescent probe, PicoGreen (Thermo Fisher, Cat: P7581). Cell lysates were diluted as necessary in 0.1 % Triton X-100/0.2 M carbonate buffer and added to the wells of a 96-well plate (50 µL/well) alongside a Salmon sperm dsDNA standard curve (0 – 4 µg/mL) prepared in 0.1 % Triton X-100/0.2 M carbonate buffer. PicoGreen reagent was diluted 1/100 in 1xTE buffer (10 mM Trizma base, 1.25 mM EDTA in dH_2O, pH 7.5) and added to the wells containing samples and standards (50 µL/well). Fluorescence was read at 485 nm excitation and 538 nm emission and unknowns calculated against the standard curve using Microsoft Excel. Statistical analysis of data from culture expanded MSCs was performed between all groups within each time point by two-way ANOVA using Dunnett's correction for multiple comparisons. Data from CFU-f expanded MSCs underwent pairwise comparison within time points by one-way ANOVA using Sidak's correction.

5.3.4 Differentiation - Adipogenesis

MSCs were culture expanded, seeded in to well-plates and incubated (37 °C, 5 % CO_2) for 24 hours prior to the addition of adipogenic media (DMEM, 10 % FBS, 100 units/mL Penicillin, 100 µg/mL Streptomycin, 10^{-6}M Dexamethasone (Sigma, Cat: D2915),

500 µM 3-Isobutyl-1-methylxanthine (Acros, Cat: 228420010), 1 µg/mL Insulin from bovine pancreas (Sigma, Cat: I5500), 100 µM Indomethacin (Sigma, Cat: I7378)). Media was changed after three days in one Ag^+ treated group for adipogenic media only while maintaining 10 µM Ag^+ in the second treatment group. Media was changed twice per week with one time point of 21 days. Non-adipogenic (basal media) controls underwent the same media changes (with/without Ag^+) and time points.

To determine the effects of Ag^+ on CFU-f expanded MSCs, cells were seeded at clonal density (see Section 5.3.2) in T175 flasks (and additional six-well plates to allow confirmation of detrimental mean CFU-f number in the presence of Ag^+) and treated with 10 µM Ag^+ for 14 days. Following expansion, MSCs were seeded and adipogenic media added as previously stated, but without the addition of Ag^+ during differentiation.

Adipogenesis was confirmed and quantitatively analysed by staining the lipid deposits with Oil Red O (Sigma, Cat: O0625). The Oil Red O working solution was prepared by a 6:4 mix of Oil Red O stock solution (0.3 g Oil Red O in 100 mL 99 % Isopropanol) and dH_2O. The solution was left to stand for ten minutes before filtering (Whatman No. 1) and was used within 2 hours of preparation. All of the following procedures were performed ensuring that the cultures were not at risk of drying, thereby protecting the lipid vacuoles from lysis. Media was removed from cultures and the monolayers rinsed once with PBS. Cells were fixed for ten minutes in 10 % formaldehyde (Polysciences, Cat: 04018-1) followed by a rinse with dH_2O and the addition of Oil Red O working solution for five minutes. The stain was removed and the wells washed with 60 % Isopropanol. Finally, wells were rinsed with tap water. Water was left on the cultures to prevent desiccation during imaging.

To quantitate the extent of the lipid bound stain, the Oil Red O was removed through two washes with 200 µL 99 % Isopropanol. Each wash was added to individual Eppendorf tubes (one per well) which were vortexed and the destain solution added in triplicate to 96-well plates (100 µL/well). Optical density was measured at 520 nm (Multiskan GO, Thermo Fisher, UK,). Statistical analysis of the differentiation of culture expanded MSCs was performed between all test groups under both non-adipogenic and adipogenic conditions by two-way ANOVA using Tukey's correction for multiple comparisons. Analysis of CFU-f was as for the culture expanded but using Sidak's correction.

5.3.5 Determination of clonogenicity of MSCs derived from CFU-f formed during Ag^+ exposure

A two-stage assay was devised, outlined in Figure 5.1, to evaluate the clonogenic capacity of MSCs following CFU-f culture with Ag^+. In addition, the assay would establish whether an Ag^+ tolerant sub-population existed that maintained CFU-f number (equivalent to control) under further clonogenic Ag^+ culture.

In brief, primary MSCs were seeded at clonal density in to 6-well plates and assigned as 'Stage 1' of the experiment. After 24 hours, media was changed for that containing 0, 1 or 10 µM Ag^+ and changed twice per week thereafter. After two weeks, wells from the same treatment group (e.g. control) were trypsinised, pooled and counted for re-seeding in to further 6-well plates at clonal density ('Stage 2'). As previously, they were incubated for 24 hours before the media was changed (0, 1 or 10 µM Ag^+). After two weeks, the 'Stage 2' plates were stained with crystal violet and the number of colonies and their diameters were measured. Assessment of CFU-f diameter was performed using the Zeiss Zen 2.3 Lite software. Statistical analysis of CFU-f number was between all groups and conditions by two-way ANOVA; analysis of CFU-f diameter was by one-way ANOVA; both methods used Tukey's correction for multiple comparisons.

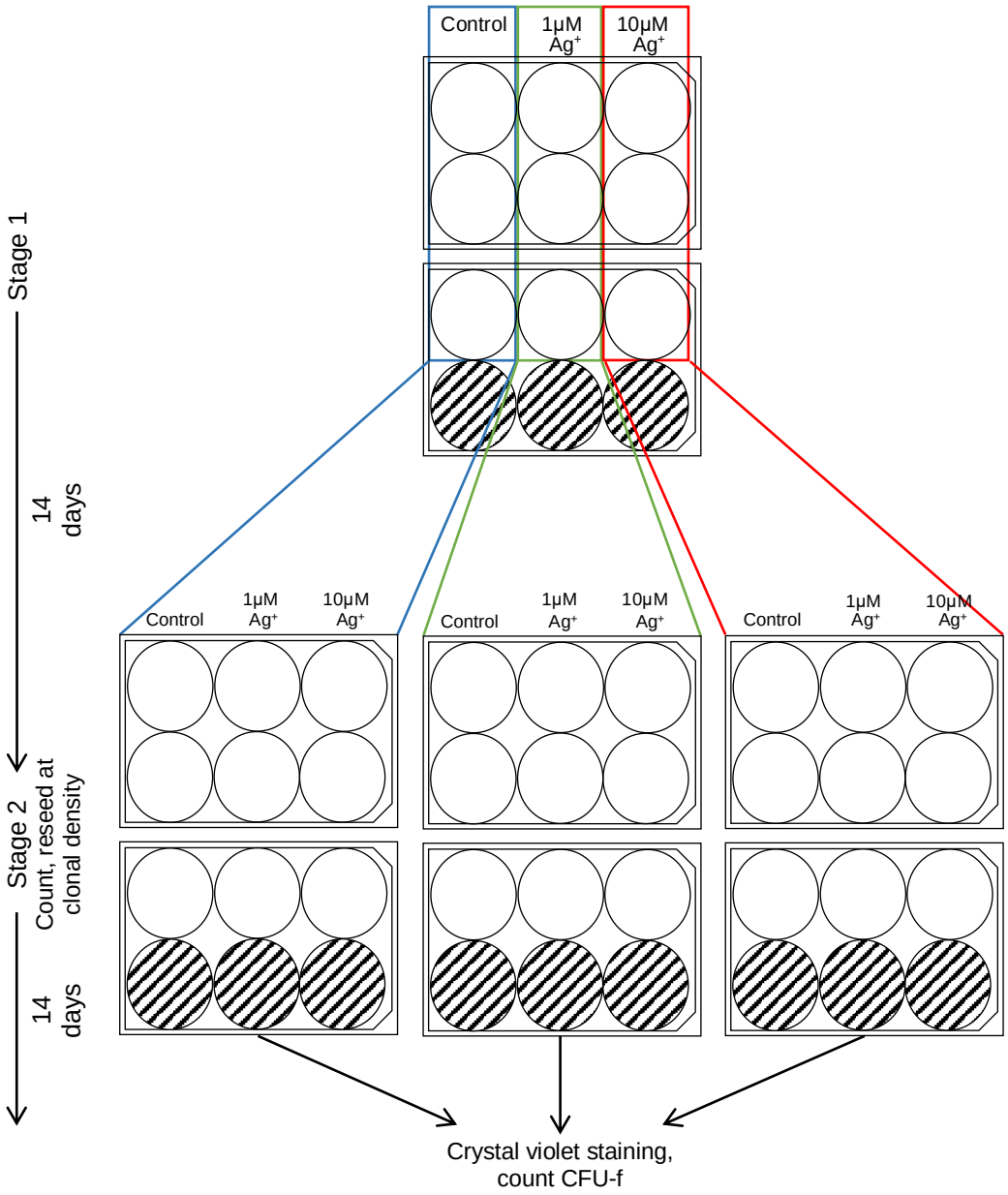

Figure 5.1: Illustration of two-stage assessment of clonogenicity.

MSCs seeded at clonal density and cultured for two weeks in the absence/presence of Ag^+ (Stage 1). CFU-f from wells of the same culture condition (e.g. control) were resuspended and counted before reseeding at clonal density and subsequent culture for two weeks in the absence/presence of Ag^+ (Stage 2). CFU-f generated during Stage 2 culture are counted after crystal violet staining. Hashed lines indicate empty wells.

5.3.6 CFU-f formation in conditioned media from semi-confluent cultures (Primary MSCs and Y201s)

To determine the effect of environmental signals on MSC clonogenicity, primary MSCs and Y201s were expanded to provide sufficient T175 tissue culture flasks for the preparation of plates and conditioned media. At Day 0, one flask was used to seed MSCs at clonal density in to two 6-well plates per donor, while remaining flasks were rinsed with PBS and 20 mL serum free DMEM (100 Units/mL Penicillin and 100 µg/mL Streptomycin) added to each. After 24 hours the serum free media was removed, centrifuged and filtered (0.45 µm), at this stage an aliquot of each was separated for flow cytometry confirmation as being cell free. HyClone FBS was added to the remaining serum free media to provide a 20 % growth media and stored at 2-8 °C. The MSC containing 6-well plates were allocated to one of two groups, 'Non-conditioned media' or 'Conditioned media' and wells within each divided equally between control and 10 µM Ag^+ treatments. Media was changed twice per week as appropriate, with colonies stained using crystal violet after 14 days. Statistical analysis of both the 'Non-conditioned media' and 'Conditioned media' groups was a simple control versus Ag^+ within each, performed using two-way ANOVA with Sidak's correction for multiple comparisons.

5.4 Results

5.4.1 Cytotoxicity – WST-1, EdU assays

The viability of MSCs was determined during Chapter 4, providing an EC_{50} equating to 33.06 µM (Figure 5.2). Equivalent data for both THP-1 and hOb was determined as for MSCs using WST-1. The data revealed that the primary human osteoblasts exhibited greater tolerance to Ag^{+} than the monocyte cell line, with calculated EC_{50} values for THP-1 and hOb being 11.9 µM and 41.4 µM, respectively (Figure 5.3). The sensitivity of osteoblasts is therefore close to that of MSCs, while that of the non-adherent THP-1 cells is three-fold lower than its adherent counterparts.

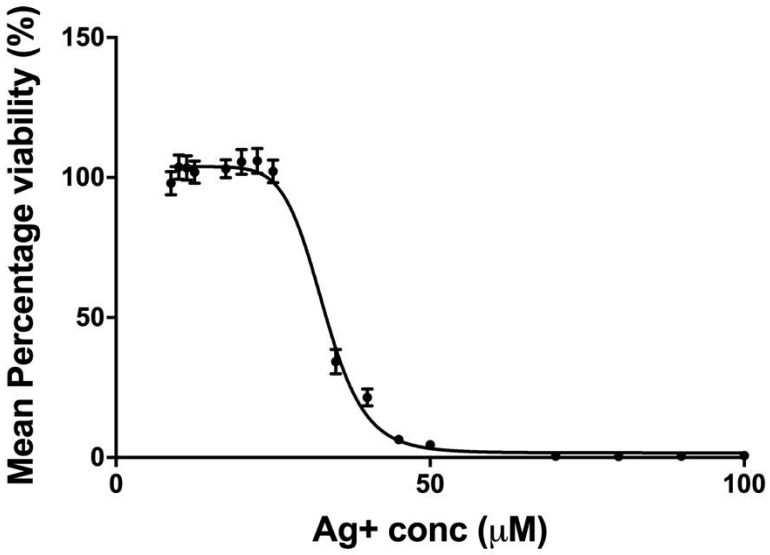

Figure 5.2: MSC viability following 24 hour exposure to Ag^{+}.

Viability of MSCs as a percentage of untreated control determined via WST-1 conversion. EC_{50} value of 33.06µM. Results are plotted as mean percentage viability ±SEM of triplicate biological replicates from three primary MSC donors (K224, HS509, HS739).

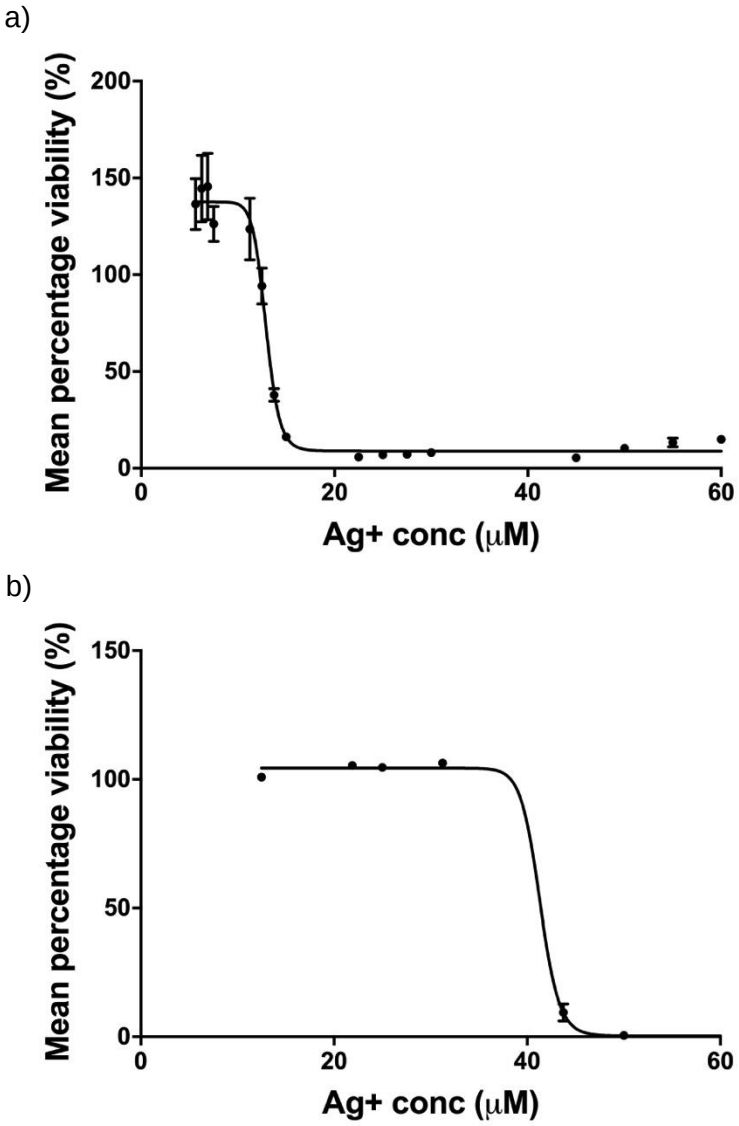

Figure 5.3: Cell viability of a) THP-1 human monocytes and b) primary human osteoblasts, following 24 hour exposure to Ag^+.

Viability of a) THP-1 and b) hOb cultures (HS781) as a percentage of untreated control determined via WST-1 conversion. EC_{50} values were calculated as THP-1 = 11.9 µM and hOb = 41.4 µM. Results are plotted as mean percentage viability ±SEM and represent triplicate biological replicates.

The proliferation of MSCs in the presence of Ag^+ over a 72 hour assay period was determined by the detection of incorporated EdU. The mean percentage of EdU-positive cells for each donor was calculated from a total of fifteen images across three technical replicates. The mean from three donors is presented in Figure 5.4 and shows that proliferation is unaffected from control at concentrations of ≤10 μM Ag^+. These findings confirm the viability data from WST-1 conversion by MSCs that these concentrations were determined as sub-toxic.

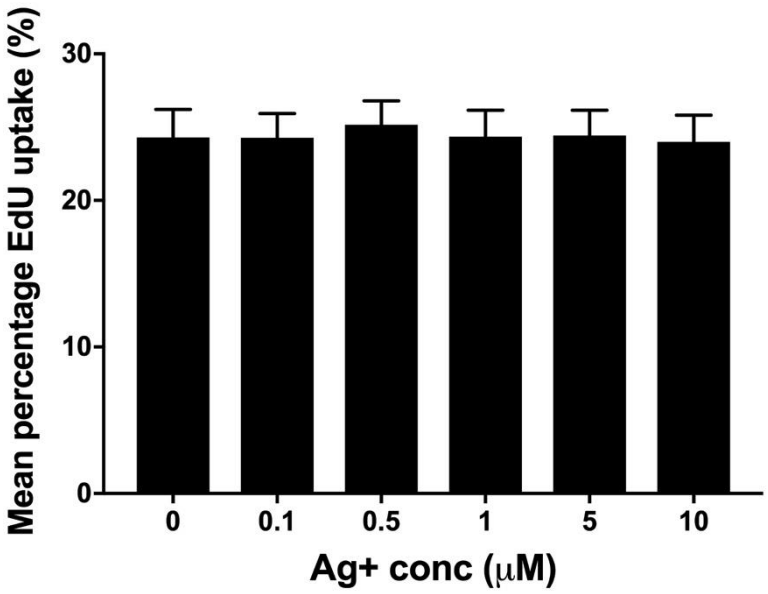

Figure 5.4: Proliferation of MSCs as determined by the percentage uptake of EdU during 72 hours culture in the presence of Ag^+.

Proliferation assessed by incorporation of EdU at the thymidine bases during S-phase. Results are presented as the mean percentage of cells detected using a secondary fluorescent probe ±SEM, and represent data from forty-five images (five images from each of three biological replicates, for each independent donor (HS674, HS681, HS729)). Statistical analysis was performed for all Ag^+ groups compared to control (p>0.05, by one-way ANOVA using Dunnett's correction for multiple comparisons).

5.4.2 CFU-f formation

The formation of CFU-f from cells plated at low density represents the ability of clonogenic replication of MSCs, a characteristic that defines them against other cell types. The effect of Ag^+ on both CFU-f number and total colony area was determined using a dose response assay, with maximum Ag^+ and exposure as defined in Section 5.1.

The ability of MSCs to form CFU-f was unaffected by any of the Ag^+ concentrations applied to the media when given during the first three days of culture. This is highlighted by the equivalent mean CFU-f number across the Ag^+ dose range (Figure 5.5a). The mean total percentage area of the same colonies exhibited a decrease compared to control for those of the 10 µM Ag^+ treatment group (Figure 5.5b). The decline in area equated to approximately 30 % of the control, however this was not statistically significant (p=0.64).

The formation of colonies during Ag^+ treatment for the duration of the 14 day assay was reduced with regards to both CFU-f number and total percentage area (Figure 5.6). Mean CFU-f number (Figure 5.6a) experienced a dose related decline, culminating in approximately 50 % reduction to control in the 10 µM Ag^+ treatment group (p<0.01). The decline in CFU-f area was more marked, with a steady decline observed for all Ag^+ treatment doses compared to control. A 50 % reduction in mean total percentage area was observed at 5 µM (p<0.05), increasing to 83 % from control for those cultures treated with the maximum Ag^+ (p<0.001) (Figure 5.6b).

The formation of CFU-Ob in the presence of Ag^+ was determined through positive Fast Red/Naphthol staining for ALP. A 62 % decline in the mean number of positively identified colonies was observed for those cultured in the presence of 10 µM Ag^+ compared to control (Figure 5.7a), however this was not statistically significant (p=0.11). No notable decrease in CFU-Ob number was observed for the other Ag^+ concentrations tested. The analysis of mean total percentage CFU-Ob area revealed a decline across Ag^+ concentrations of 0.5-10 µM (Figure 5.7b). Despite this, the 88 % reduction from control at the highest Ag^+ concentration was the only point at which this was statistically significant (p<0.05).

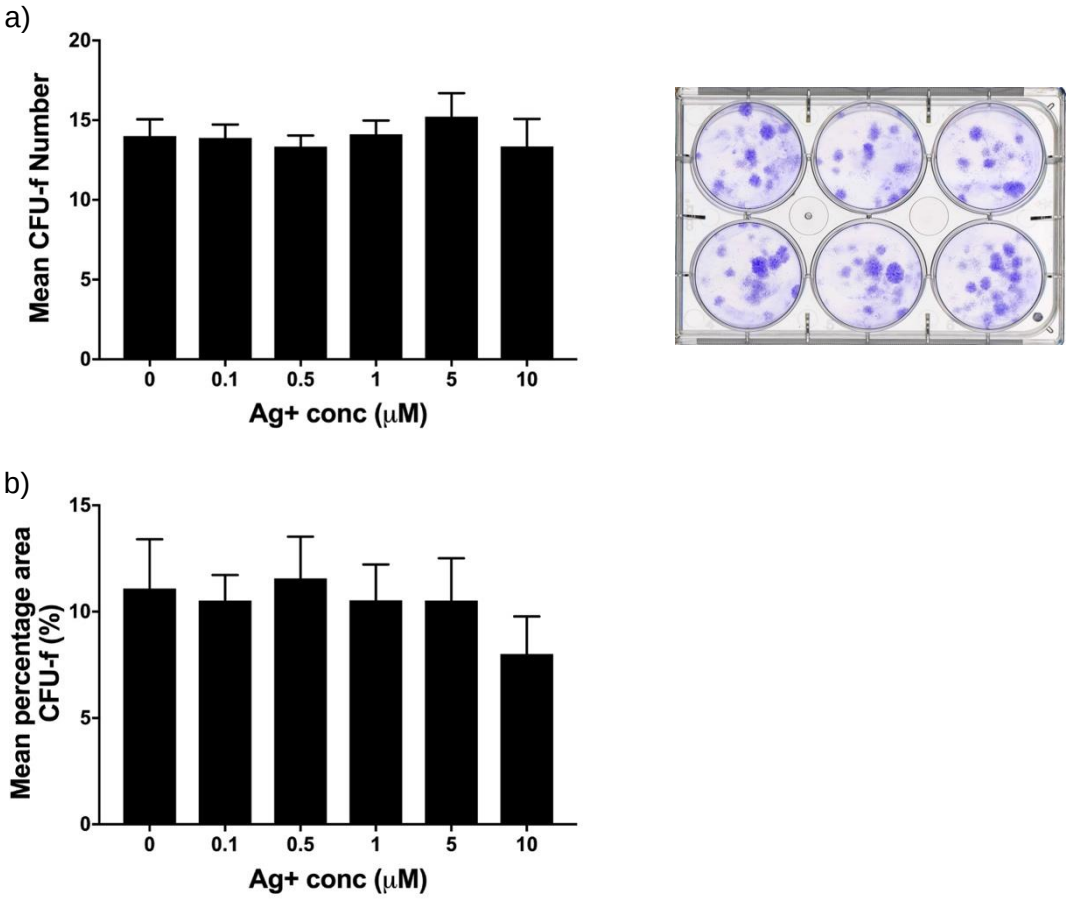

Figure 5.5: Characterisation of colony formation (CFU-f) of MSCs seeded at clonal density and cultured for the initial three days in the presence of ≤10 μM Ag^+.

Measurement of a) CFU-f number and b) total percentage CFU-f area. Data are presented as mean ±SEM of three donors (HS674, HS681, HS729), determined from three biological replicates for each donor. Statistical analysis performed for all Ag^+ groups against control (0 μM) by one-way ANOVA using Dunnett's correction for multiple comparisons. Representative images (HS729) of crystal violet stained CFU-f (top) and associated image for area calculation generated using ImageJ (bottom); Ag^+ concentrations for plate (L-R): top row, 10, 5, 1 μM; bottom row, 0.5, 0.1, 0 μM.

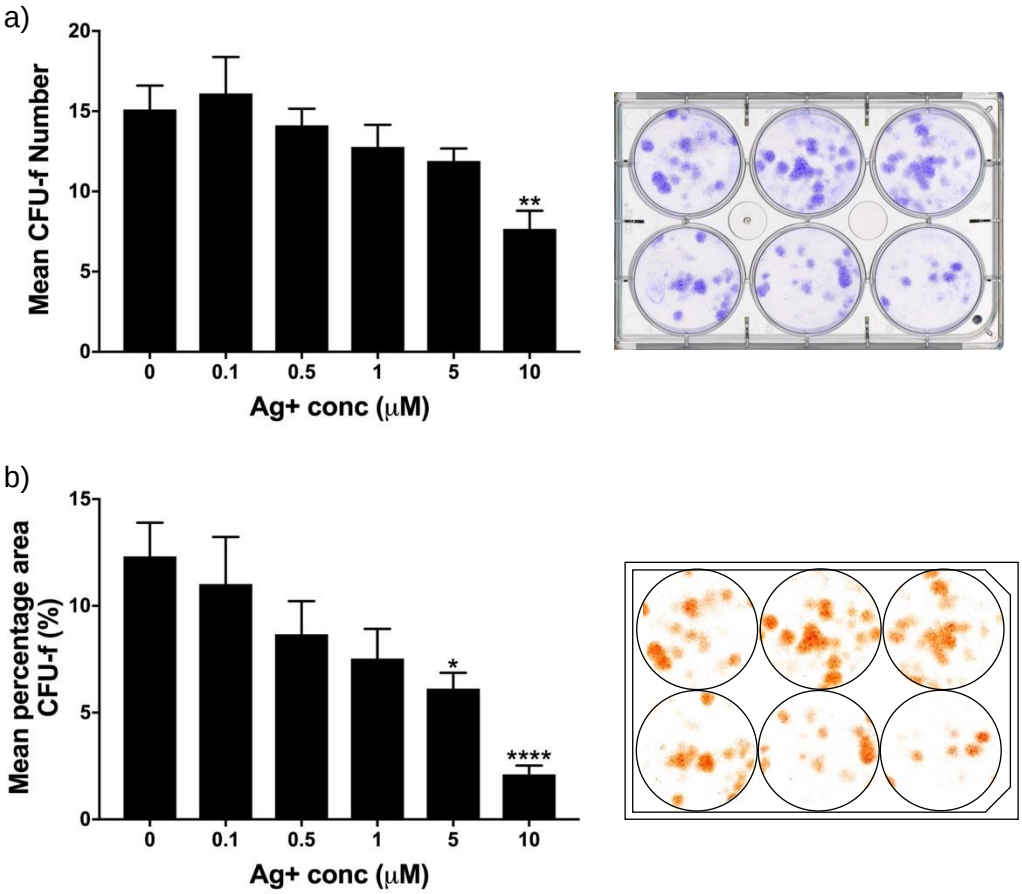

Figure 5.6: Characterisation of colony formation (CFU-f) of MSCs seeded at clonal density and cultured continuously in the presence of ≤10 μM Ag^+.

Measurement of a) CFU-f number and b) total percentage CFU-f area. Data are presented as mean ±SEM of three donors (HS674, HS681, HS729), determined from three biological replicates for each donor. Statistical analysis performed for all Ag^+ groups against control (0 μM) by one-way ANOVA using Dunnett's correction for multiple comparisons. * p<0.05, ** p<0.01, **** p<0.0001. Representative images (HS729) of crystal violet stained CFU-f (top) and associated image for area calculation generated using ImageJ (bottom); Ag^+ concentrations for plate (L-R): top row, 10, 5, 1 μM; bottom row, 0.5, 0.1, 0 μM.

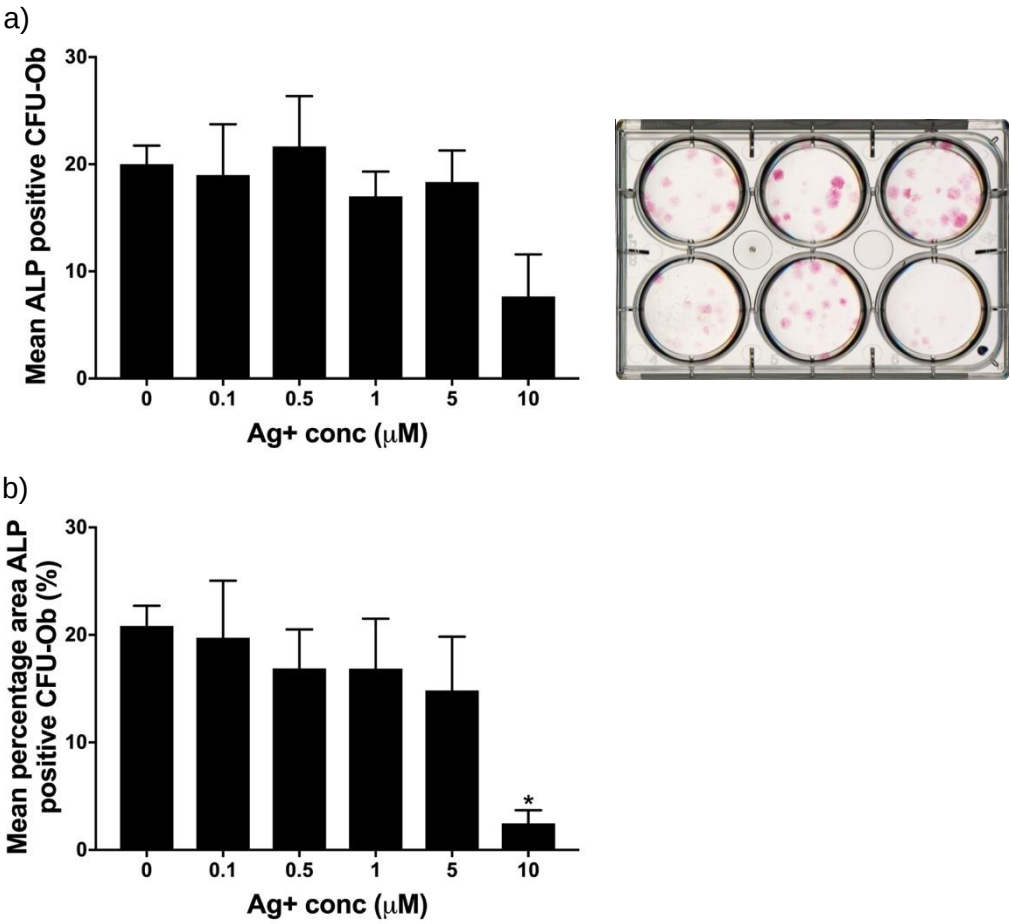

Figure 5.7: Characterisation of alkaline phosphatase positive CFU-Ob cultured continuously in the presence of Ag^+.

Measurement of a) CFU-Ob number and b) total percentage CFU-Ob area presented as mean ±SEM. Data determined from three donors (HS674, HS729, HS738). Statistical analysis performed for all Ag^+ groups against control (0 μM) by one-way ANOVA using Dunnett's correction for multiple comparisons. * $p<0.05$. Representative image (HS738) of ALP positive CFU-Ob; Ag^+ concentrations for plate (L-R): top row, 10, 5, 1 μM; bottom row, 0.5, 0.1, 0 μM.

5.4.3 Differentiation

5.4.3.1 Differentiation post-expansion

Evidence suggests that the elevation of ROS causes a decrease in osteogenic differentiation and a propensity towards the adipogenic lineage, therefore the analysis of MSC behaviour in the presence of appropriate Ag^+ concentrations and exposure times is relevant for the fracture healing application.

The MSC osteogenic response to Ag^+ as evaluated by normalised ALP activity is depicted in Figure 5.8a, and shows the effect of both short term (0-3 Day) and continual exposure over the seven and 14 day assay period. Measurement at seven days revealed that the presence of Ag^+ for any time period in the culture media had little effect on mean normalised ALP activity. Although a small decrease was observed in those cultures that were exposed to Ag^+ for the initial period, the difference between this and control was not statistically significant (p>0.05). At 14 days there was a noticeable decrease in mean ALP activity compared to control for both Ag^+ exposed test groups. The reduction in activity corresponded to the duration of the exposure, with those cultures treated with Ag^+ for the initial three-day period (218.9 nmol/µg/mL ±17.26 SEM) exhibiting a smaller decline to control (260.7 nmol/µg/mL ±32.84 SEM) compared to those treated throughout the 14 days (192.6 nmol/µg/mL ±24.55 SEM). Despite the observed reduction for both Ag^+ treatment groups, neither the three-day exposure (p=0.58) or continual exposure (p=0.25) were significantly different to control. Analysis of the individual ALP and DNA quantification data showed that the trend towards decreased normalised ALP activity was the result of a decline in ALP rather than an alteration in the cell number, with DNA quantification remaining consistent between test groups (Figure 5.8b & c). This maintenance of DNA quantity served to show that cell number was not adversely affected by 14 day exposure to 10 µM Ag^+.

The equivalent adipogenic assay revealed that lipid deposition was not initiated by the addition of Ag^+ in the absence of adipogenic stimuli ('Non-adipogenic'; p>0.05) (Figure 5.9). In the presence of *in vitro* adipogenic additives there was no positive or negative effect of short term Ag^+ treatment on lipid deposition as quantified by Oil Red O staining (p>0.05). The continued Ag^+ treatment of MSCs in adipogenic cultures did result in a decrease in lipid formation that was significant compared to both control and short term Ag^+ exposure (p<0.0001).

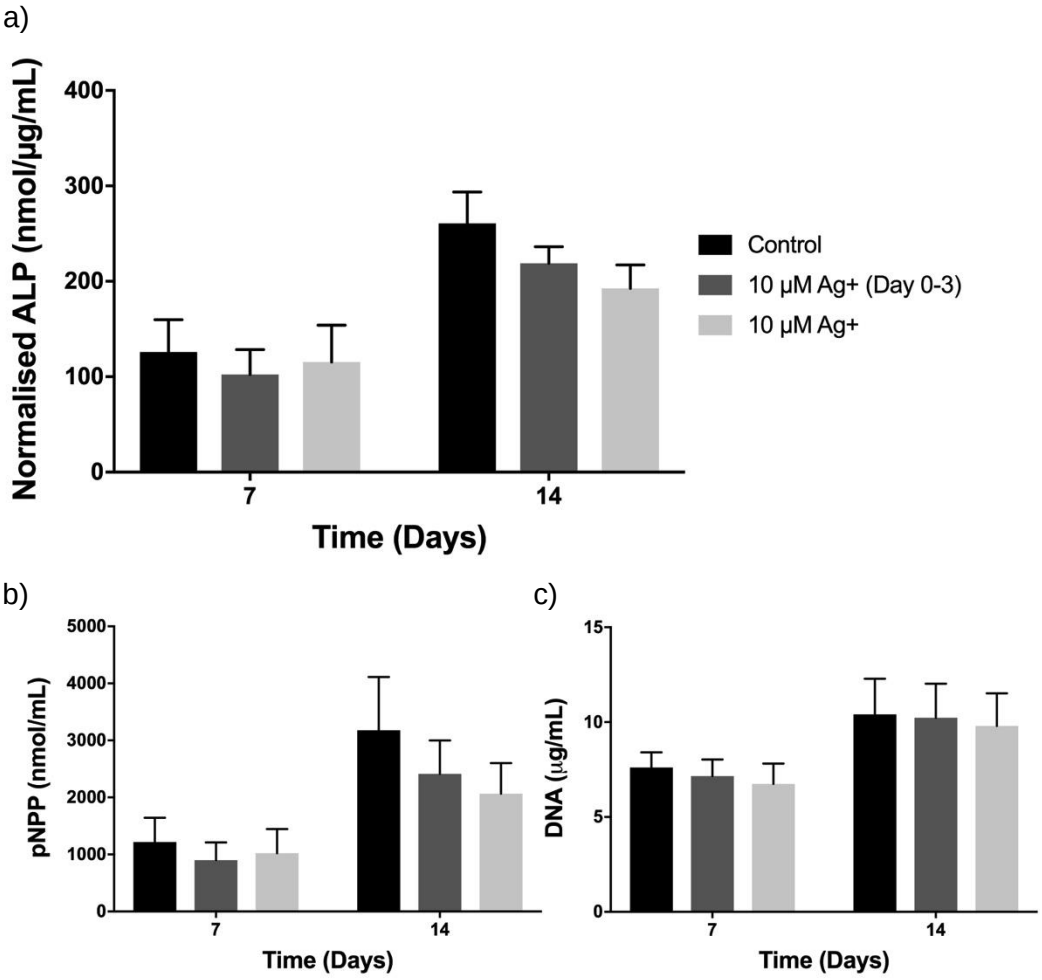

Figure 5.8: Osteogenic differentiation of culture expanded MSCs in the presence of Ag^+ as determined by normalised ALP activity.

Osteogenic differentiation was performed in the presence of 10 µM Ag^+ for either the initial three days of culture (Ag^+ 10 µM (Day 0-3)) or for the entire differentiation period (Ag^+ 10 µM). Control cultures received Ag^+ free osteogenic differentiation media only. ALP activity (b) and DNA quantification (c) were measured from cell lysates, providing normalised ALP (a). The results are presented as the mean ±SEM of three donors (HS674, HS729, HS739), determined from three biological replicates for each donor. Statistical analysis performed between all groups within each time point by two-way ANOVA using Dunnett's correction for multiple comparisons.

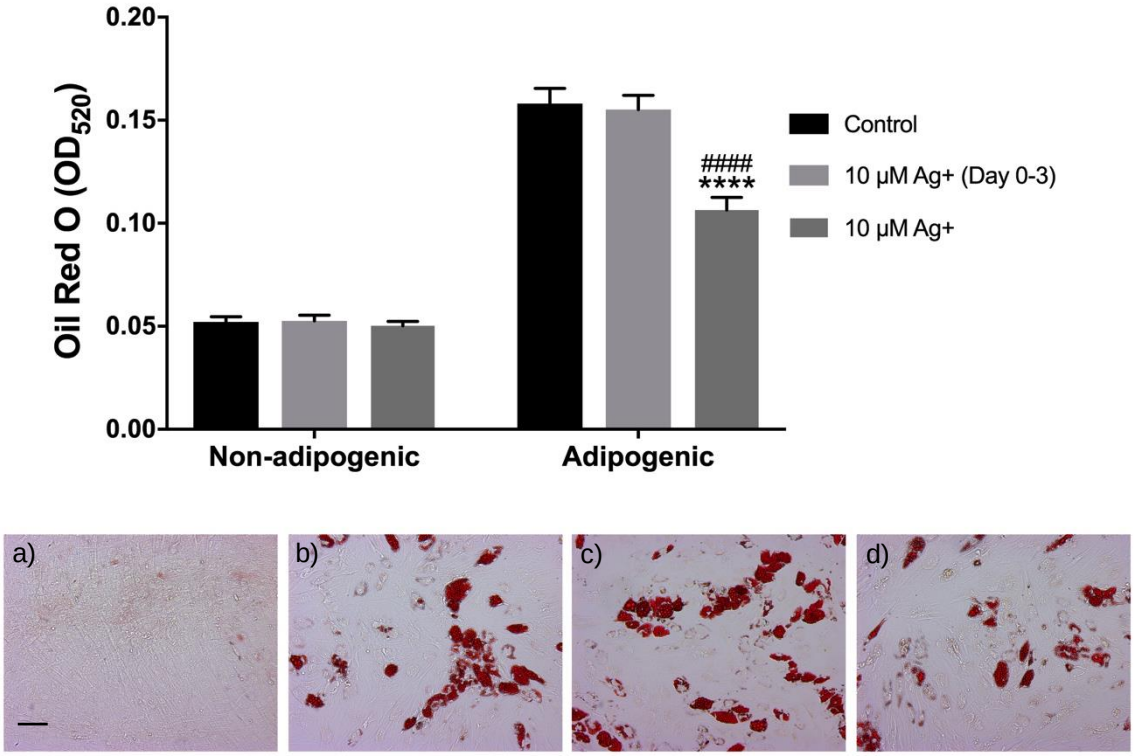

Figure 5.9: Adipogenic differentiation of culture expanded MSCs as determined by optical density quantification of lipid deposits stained using Oil Red O.

Adipogenic differentiation was performed in the presence of 10 µM Ag^+ for either the initial three days of culture (10 µM Ag^+ (Day 0-3)) or for the entire differentiation period (10 µM Ag^+). Control cultures received Ag^+ free adipogenic differentiation media only. Non-adipogenic cultures received basal media ±Ag^+ as appropriate. Lipid bound Oil Red O was removed and measured by optical density (520nm). The results are presented as the mean OD_{520} ±SEM of four donors (HS674, HS681, HS738, HS739), determined from three biological replicates for each donor. Statistical analysis performed between all groups for both non-adipogenic and adipogenic by two-way ANOVA using Tukey's correction for multiple comparisons. Significance against control represented by **** p<0.0001, significance against 10 µM Ag^+ (Day 0-3) represented by #### = p<0.0001. Representative images of Oil Red O stained cultures (HS738) are provided as follows: a) non-adipogenic, 10 µM Ag^+; b) adipogenic, control; c) adipogenic, 10 µM Ag+ (Day 0-3); d) adipogenic, 10 µM Ag^+; (scale bar = 100 µm).

5.4.3.2 Differentiation post-CFU-f formation

With elevated ROS associated with *in vivo* ageing of MSCs and a decline in cellular function, the effects on MSC differentiation following Ag^+ exposure were determined. Following the expansion of MSCs at clonal density while in the presence/absence of 10 µM Ag^+ ('Ag^+ CFU-f'/'Control CFU-f'), the cultures underwent osteogenic and adipogenic differentiation in Ag^+ free media (Figure 5.10 & Figure 5.11).

All CFU-f check plates established for each donor during expansion confirmed a statistically significant decrease in mean CFU-f number against control, permitting the use of the colonies in the differentiation assays. A decline in mean normalised ALP activity was observed under osteogenic conditions at both seven and 14 days for those MSCs that had been exposed to Ag^+ during their expansion as CFU-f (Figure 5.10). Compared to control CFU-f cultures, this decline in osteogenesis was not statistically significant at either time point (7 Days: p=0.63; 14 Days: p=0.11). Analysis of the contributing data (ALP activity (Figure 5.10b) and DNA quantification (Figure 5.10c)) revealed that the ALP activity from the Ag^+ CFU-f MSC group was no different to control at either time point, however a significant increase in DNA quantification was observed for the Ag^+ CFU-f MSCs at 14 days (p<0.01).

In contrast, adipogenic differentiation was enhanced in those MSCs that had been cultured in the presence of Ag^+ (Figure 5.11). Although the increase in mean lipid deposition appeared small compared to control MSCs, the difference was determined as significant (p<0.05). There was no significant alteration in the quantity of Oil Red O staining in the non-adipogenic group, signifying that spontaneous differentiation was not promoted in those MSCs that had undergone Ag^+ expansion.

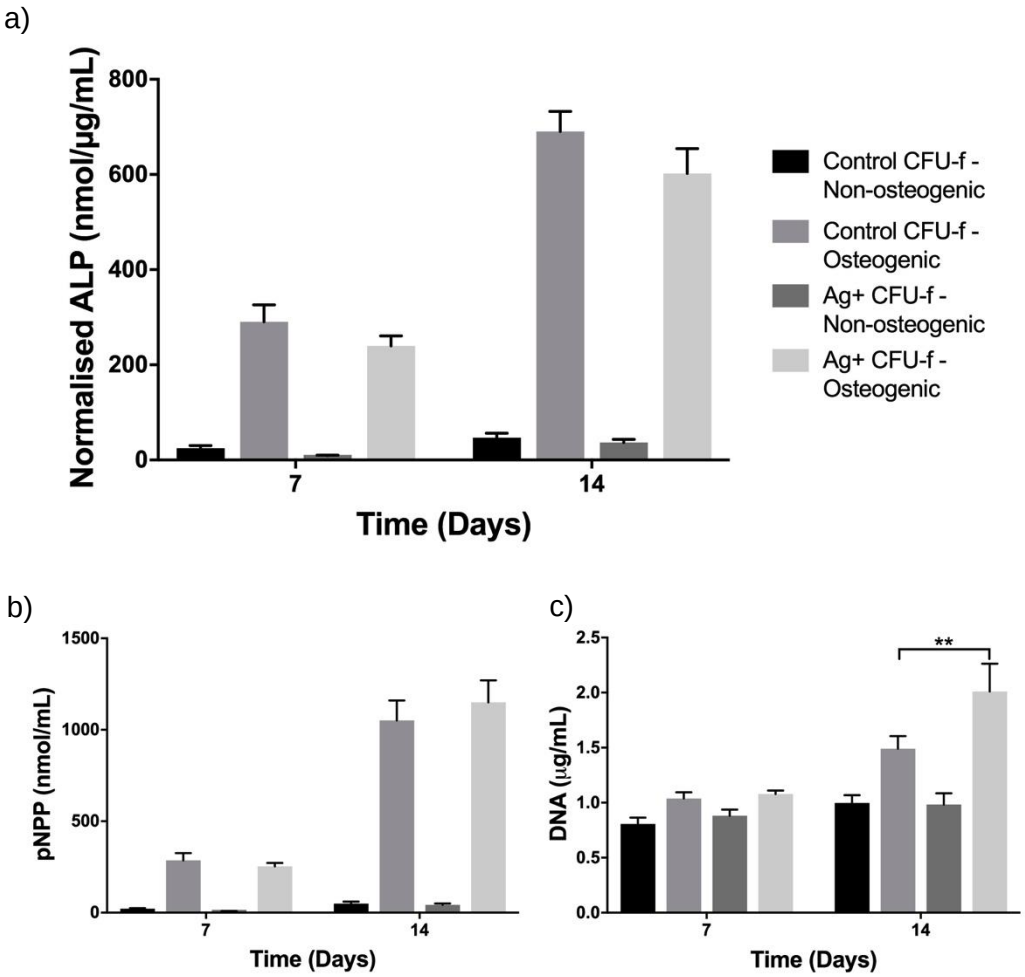

Figure 5.10: Osteogenic differentiation of CFU-f derived MSCs as determined by mean normalised ALP activity.

CFU-f derived MSCs were cultured in the presence/absence of 10 µM Ag^+ prior to osteogenic differentiation in Ag^+ free media. ALP activity (b) and DNA quantification (c) were measured from cell lysates, providing normalised ALP (a). The results are presented as the mean ±SEM of three donors (HS674, HS738, HS739), determined from three biological replicates for each donor . Paired statistical analysis of non-osteogenic and osteogenic groups within time point, by one-way ANOVA using Sidak's correction for multiple comparisons. ** p<0.01.

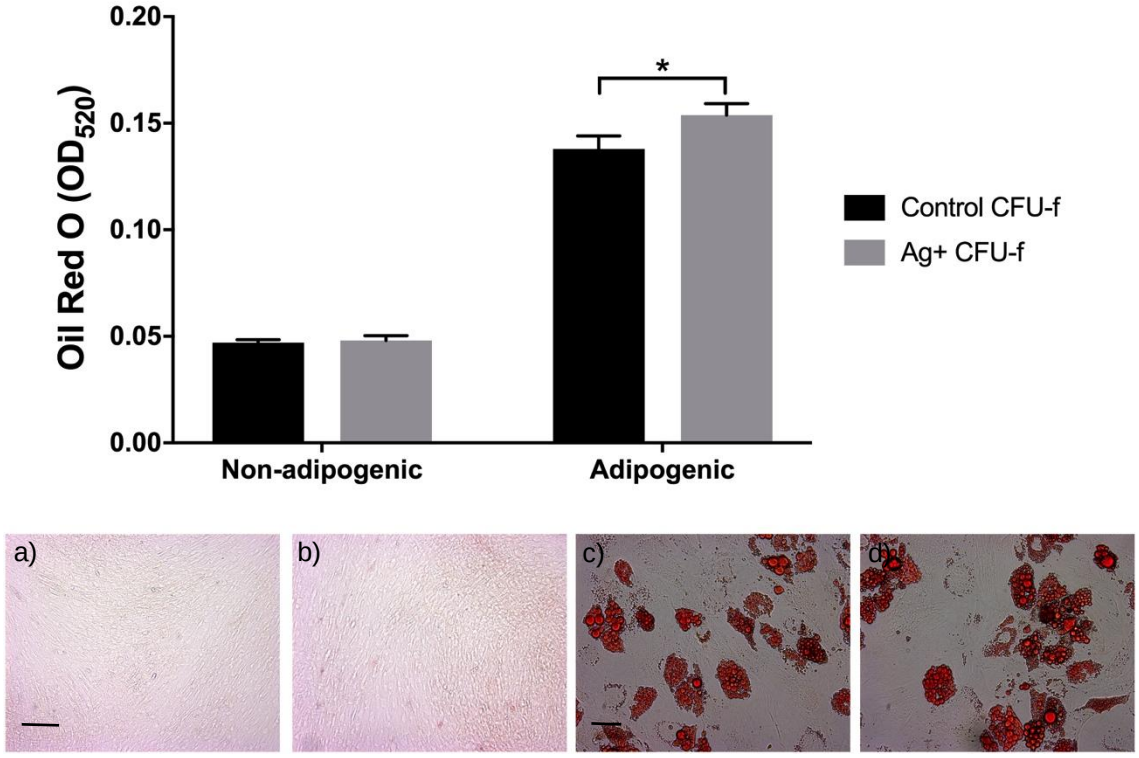

Figure 5.11: Adipogenic differentiation of CFU-f derived MSCs as determined by optical density quantification of lipid deposits stained using Oil Red O.

CFU-f derived MSCs were cultured in the presence/absence of 10 µM Ag^+ prior to adipogenic differentiation in Ag^+ free media. Lipid bound Oil Red O was measured by optical density (520 nm). The results are presented as the mean OD_{520} ±SEM of three donors (HS674, HS738, HS739), determined from three biological replicates for each donor. Statistical analysis by two-way ANOVA using Sidak's correction for multiple comparisons. * $p<0.05$. Representative images of Oil Red O stained cultures (HS7674) are provided as follows: a) non-adipogenic, control CFU-f; b) non-adipogenic, Ag^+ CFU-f; c) adipogenic, control CFU-f; d) adipogenic, Ag^+ CFU-f; (scale bar: non-adipogenic = 250 µm, adipogenic = 50 µm).

5.4.4 Determination of clonogenicity of MSCs derived from CFU-f formed during Ag^+ exposure

The retention of the clonogenic capacity of MSCs is of importance following exposure to Ag^+ and the potential elevation in ROS associated with this contact. The generation of CFU-f in the presence of Ag^+ illustrated a decline in CFU-f number when cultured with the previously proven (for near confluent cultures) sub-toxic dose of 10 µM Ag^+ (see Section 5.4.2). Using this finding, CFU-f produced in the presence of Ag^+ were re-seeded at clonal density in order to identify any detrimental effect on continued clonogenicity and also to test the hypothesis that Ag^+ was promoting the selection of a tolerant sub-population. Mean number and diameter of the Stage 2 CFU-f are represented by the graphs of Figure 5.12, with the original Stage 1 culture conditions represented on the *x*-axis.

When comparing to the 'Stage 1' control group (red box, Figure 5.12a) it is clear that the MSCs from CFU-f of 'Stage 1' Ag^+ treatments have retained their clonogenic capacity during 'Stage 2'. Evidence for this lies in that no statistically significant decline in mean CFU-f number was observed for 'Stage 2' control groups (black bars) generated from 'Stage 1' Ag^+ treatments. Further comparison with the Stage 1 control group shows that a statistically significant reduction was observed in CFU-f number for those MSCs from the 1 µM Ag^+ treatment of Stage 1 that were subsequently cultured in 1 µM Ag^+ during 'Stage 2' ($p<0.05$). This was not the case for those MSCs from the 10 µM Ag^+ group of 'Stage 1' that underwent secondary culture in 10 µM Ag^+.

When comparing within each 'Stage 1' condition, the detrimental effect of 10 µM Ag^+ on mean CFU-f number was as previously observed (Figure 5.6). Mean CFU-f number significantly declined against control regardless of pre-exposure to Ag^+ ($p<0.0001$).

Analysis of CFU-f diameter (Figure 5.12b) was performed as for CFU-f number, with determination of statistical significance carried out between, and within, initial culture treatments from Stage 1. No statistical differences were detected between equivalent 'Stage 2' treatments. When comparing to controls within 'Stage 1' groups, significant change was observed in the colony size of 10 µM Ag^+ CFU-fs (dark grey bars) for those MSCs that had been exposed to Ag^+ during the initial 'Stage 1' culture. In these cases a consistent decline in mean diameter occurred as a consequence of the Ag^+ treatment. An 8.5 % ($p=0.078$) decrease in CFU-f size was calculated for those MSCs exposed to 10 µM Ag^+ that had no previous Ag^+ exposure during 'Stage 1', while the

diameter of CFU-fs from MSCs previously cultured in 1 μM and 10 μM Ag^+ were reduced by 13.5 % (p<0.001) and 14 % (p<0.0001), respectively. CFU-fs from 'Stage 1' 10 μM Ag^+ group were the only colonies to show a significant reduction in diameter between Ag^+ treatments during 'Stage 2' (p<0.005).

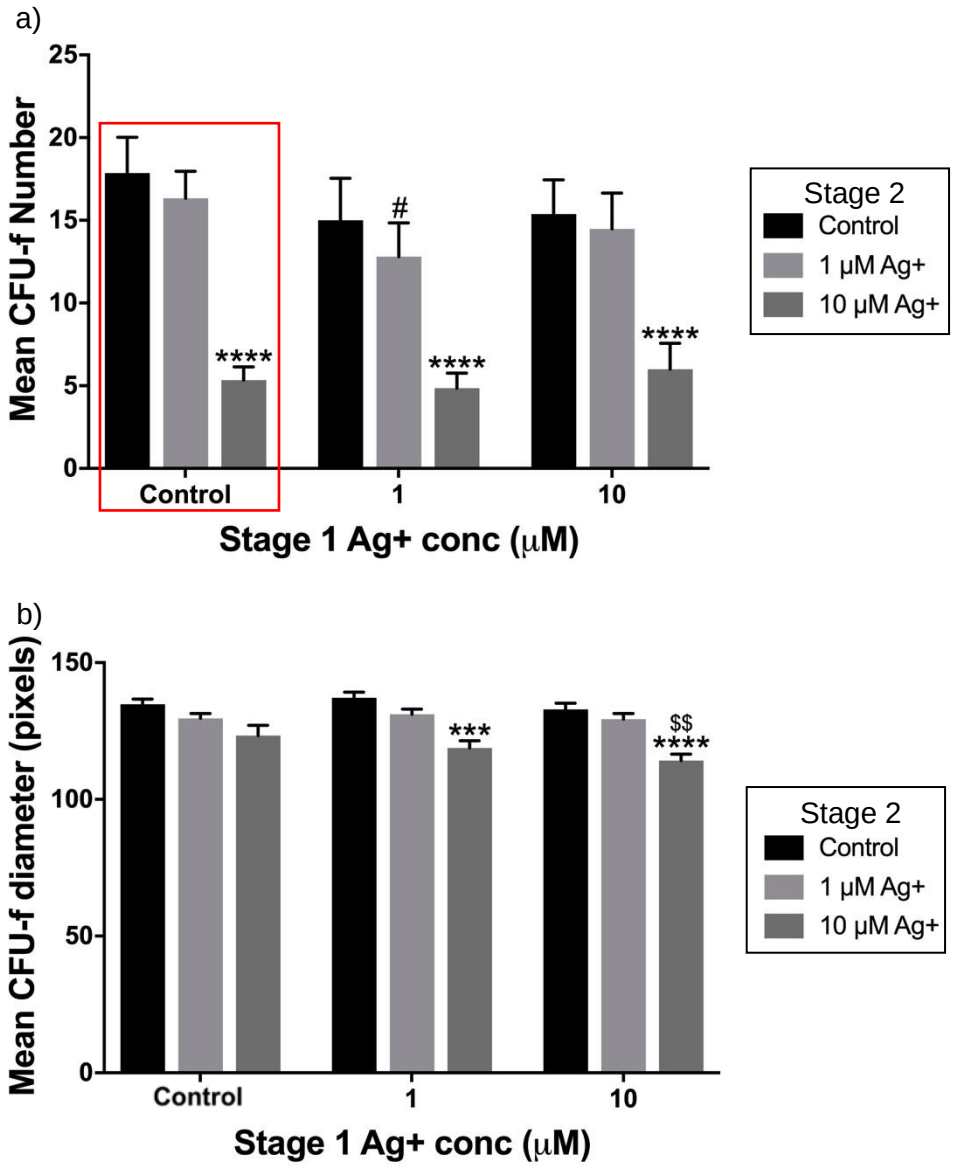

Figure 5.12: CFU-f generation by MSCs during Stage 2 culture following pre-culture at clonal density.

Ag^+ exposure during initial culture is represented on the x-axis with different Ag^+ exposures during Stage 2 displayed using individual bars, identified by the key.

CFU-f number (a) and CFU-f diameter (b) presented as mean ±SEM. Data collected from three donors (HS674, HS726, HS738), determined from ≥6 biological replicates per donor. Statistical analysis of CFU-f number by two-way ANOVA; analysis of CFU-f diameter by one-way ANOVA; both using Tukey's correction for multiple comparisons. Analysis performed for data within each 'Stage 1' Ag^+ concentration, comparing against control, represented by *** $p<0.001$, **** $p<0.0001$; and against 1 μM Ag^+ represented by $$ $p<0.005$. Comparison of each 'Stage 2' Ag^+ treatment to its equivalent from the 'Stage 1' control group (# $p<0.05$).

5.4.5 The effect of conditioned media on CFU-f formation during Ag^+ exposure

The reduced formation of CFU-f under Ag^+ conditions that are sub-toxic to MSCs at greater density highlighted the potential role of trophic factors and cell communication in tolerance to Ag^+, factors that have limited availability at clonal density. The application of conditioned media derived from MSCs at higher density could therefore supply these factors, promoting CFU-f formation despite exposure to Ag^+.

In addition to the 'Conditioned media', each of the MSC and Y201 test groups were set up with a 'Non-conditioned media' control, allowing the expected effects of an Ag^+ induced reduction in CFU-f number to be confirmed.

All conditioned media was confirmed to be cell free, thereby removing the possibility that any increase in CFU-f number was a result of cell transfer from the feeder cell flasks to those wells seeded at clonal density (Figure 5.13). The data illustrated in Figure 5.14 confirmed the expected decline in CFU-f number for the non-conditioned media group, with the number of colonies generated by both the primary MSCs and Y201s significantly reduced in the presence of 10 µM Ag^+ (MSC, $p<0.001$; Y201, $p<0.05$). When 10 µM Ag^+ was added to cultures for the duration of the assay in combination with conditioned media, the reduction in the number of CFU-f was abrogated, with only a small decrease from controls observed in both the primary MSC and Y201 cultures. As a consequence there was no significant decline between control and Ag^+ treatments of the conditioned media groups (primary MSC, $p=0.52$; Y201, $p=0.81$). Also of note was the increased colony size generated by both control and Ag^+ treated MSCs.

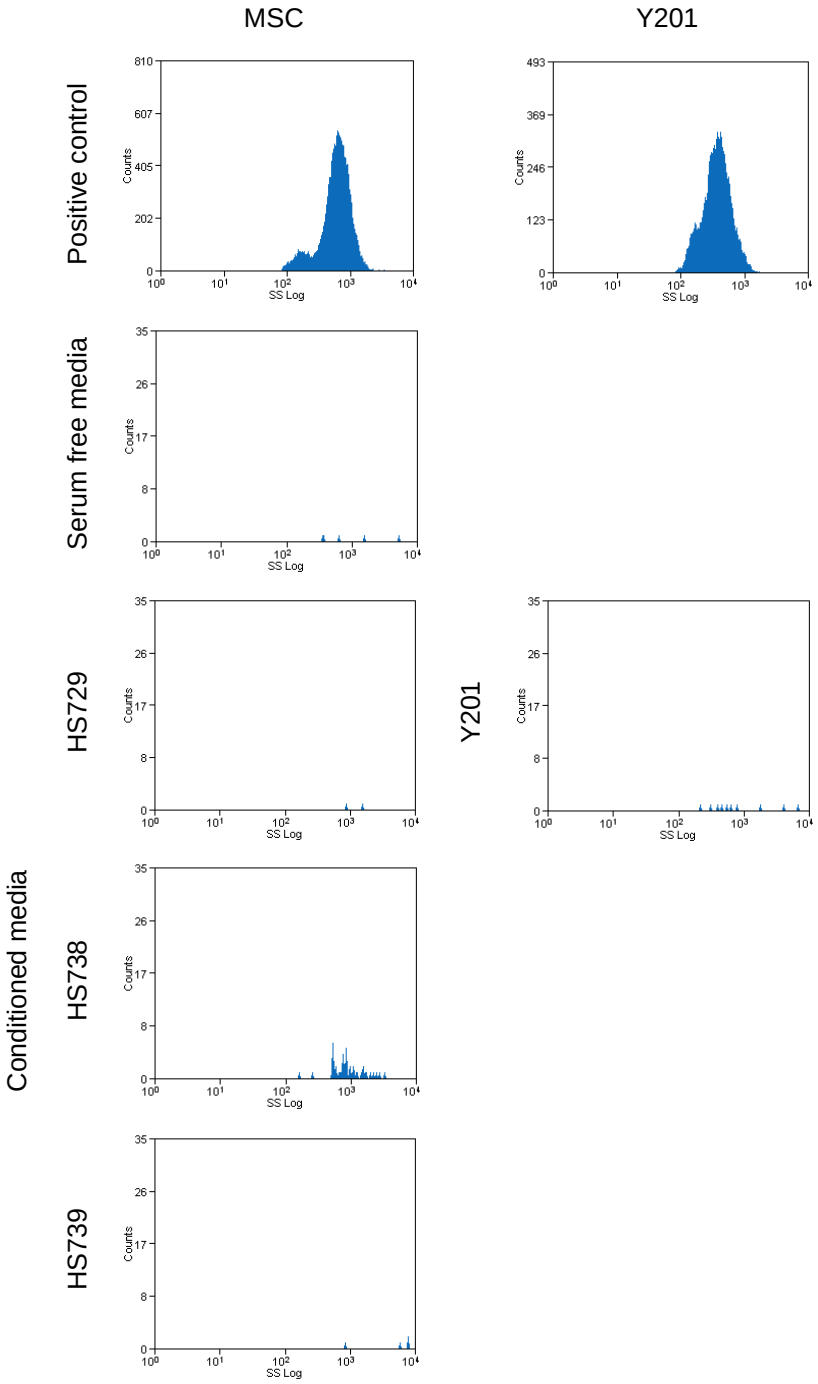

Figure 5.13: Flow cytometry analysis of MSC and Y201 conditioned media.

MSC and Y201 conditioned media was centrifuged and filtered (0.45 µm) prior to analysis to confirm that MSC-CM was cell free. Histograms show data for serum free media positive control containing MSC or Y201, serum free media negative control and conditioned media for each donor as appropriate.

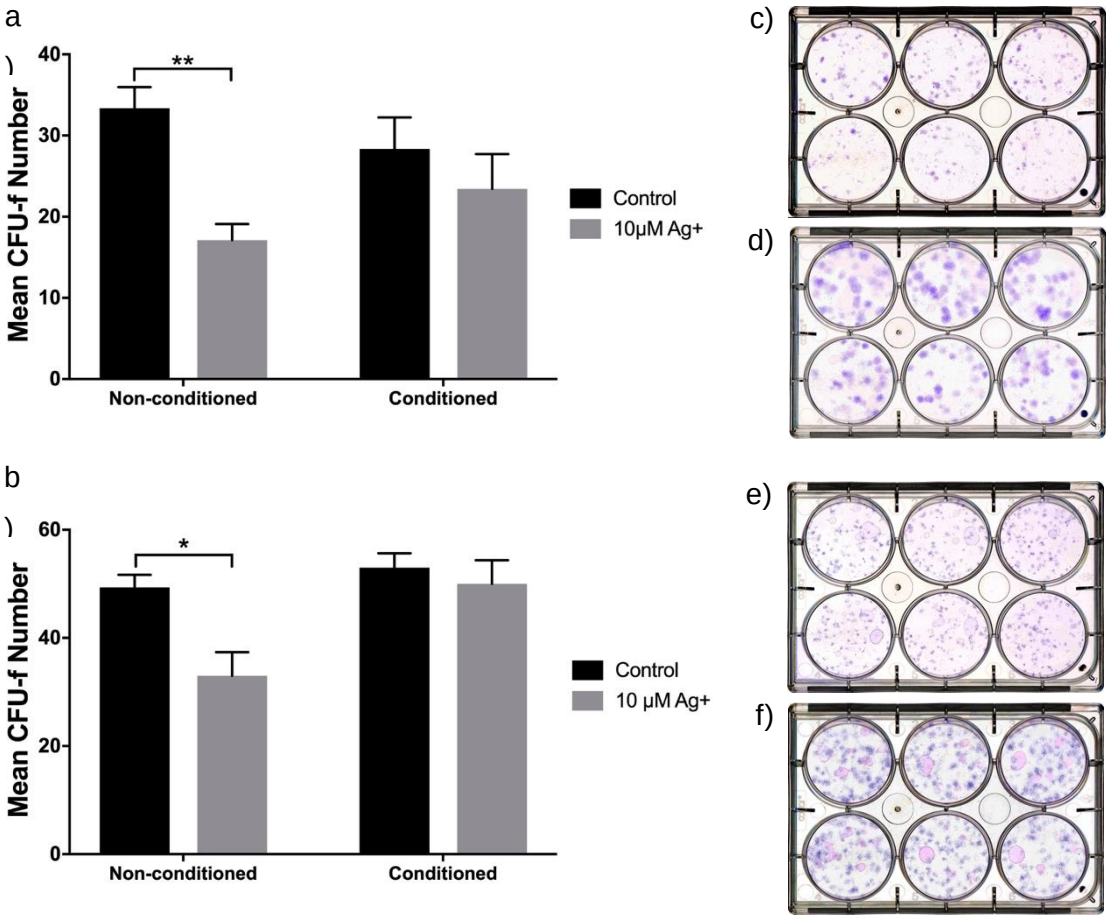

Figure 5.14: Effect of Ag^+ on CFU-f number when applied in conditioned media.

The mean CFU-f number ±SEM for a) primary MSCs (three donors repeated in triplicate, HS729, HS738, HS739) and b) Y201 (n=3, biological replicates). Expected reduction in CFU-f number observed for MSCs treated with Ag^+ applied in non-conditioned media (MSC, ** p<0.001; Y201, * p<0.05), while no statistically significant reduction in colony number was observed when Ag^+ was applied in conditioned media (by two-way ANOVA using Sidak's correction for multiple comparisons). Representative images of crystal violet stained CFU-f for primary MSCs (HS729) (c-d) and Y201s (e-f), cultured with either control (c & e) or conditioned medium (d & f); Ag^+ concentrations for each plate: top row, control; bottom row, 10 μM.

5.5 Discussion

The viability of eukaryotic cells in the presence of Ag^+ has been extensively studied due to the rise in interest in this transition metal for antimicrobial applications. However, results detailing the susceptibility of different cells have varied due to experimental design (e.g. media selection, as discussed in Chapter 4) and the source of cells to be tested. It was therefore important to establish the level of cytotoxicity of further fracture related cell types in this system while also expanding the knowledge of MSC properties in response to Ag^+ exposure.

Calculation of EC_{50} data for primary human osteoblasts, in the same system as previously used for MSCs, has provided confirmation that the cytotoxicity is in line with that of previous researchers (294,336), but not with those data reported by Pauksch *et al*. (238). We must therefore surmise that experimental differences are the cause of this discrepancy, but that the data generated here are reproducible. They also confirm that the Ag^+ concentration calculated for the maximal intramedullary release, while closer to the cytotoxic levels than would be proposed by Pauksch, remain sub-toxic to both hObs and MSCs. Further confirmation that the Ag^+ concentration associated with maximal intramedullary release was below that found to be toxic for MSCs was through the incorporation of EdU. This assay is generally reported as a measure of proliferation, however some data suggests that the EdU reagent can cause the accumulation of cells at the G_2/M phase of the cell cycle (337). With this in mind, while these data individually cannot fully confirm the continued proliferation of MSCs under conditions of Ag^+ exposure, they do demonstrate that MSC progression through S-phase at ≤10 μM was in line with that of the control over the 72 hour period of assessment.

The data for THP-1 cells, however has raised the question of possible differences in *in vitro* susceptibility between adherent and non-adherent cultures to Ag^+. The EC_{50} for the suspension cultured THP-1 cells was approximately in line with the previously reported findings of Lewis *et al*. (316), equating to a three-fold reduction in Ag^+ tolerability than the currently tested adherent cells. It therefore suggests that differences may exist in the susceptibility of this cell type or possibly as a result of cell to cell contact and communication or extracellular matrix adhesion experienced by adherent cultures. However, the significance of this finding to the *in vivo* setting is undetermined and further *in vitro* investigation was not carried out within this thesis.

While viability testing confirmed that Ag^+ at 10 μM was sub-toxic, the focus of attention turned towards the characterisation of MSC properties and function at this concentration. The capacity of MSCs to generate CFU-f and CFU-Ob was reproducibly decreased at 10 μM Ag^+, with mean CFU-f number significantly reduced at this concentration but at no others. At 10 μM Ag^+, mean CFU-f and CFU-Ob area was also significantly affected, a decline also observed across a number of Ag^+ exposures, with further statistical significance shown at 5 μM for CFU-f. This suggests that while MSCs were able to initiate the formation of a colony at clonal density (thereby maintaining mean CFU-f number), the ability to proliferate within that colony was decreased. When considering this information with that of viability and proliferation, where both were found to be unaffected at 10 μM Ag^+, it suggests that this susceptibility may be a result of the clonal seeding density of the MSCs within this assay and that intercellular signalling or released factors may play a role in the maintenance of viability. This may also add weight to the hypothesis that a lack of cell to cell contact or communication is the cause of the low EC_{50} value calculated here and by other research groups for the non-adherent THP-1 cells.

Differentiation of MSCs in the presence of Ag^+ resulted in a decline in *in vitro* osteogenesis when Ag^+ was applied for both the 14 day assay period and for the shorter three-day period. Although neither decline was statistically significant, the data raised interesting considerations about the effect of short term Ag^+ exposure on ALP activity. Specifically the apparent inability of those MSCs to recover the level of ALP activity during the remaining 11 day period following Ag^+ removal. This may be the result of the continued effect and recovery from the elevation in ROS after withdrawal or the consequence of a lag period in osteogenesis during Ag^+ treatment. This decline in ALP was also observed for the CFU-Ob colonies, where the addition of continual 10 μM Ag^+ had a detrimental effect on this marker of osteogenesis. These data therefore corroborate with literature reports of a decline in osteogenesis in the presence of Ag^+ and elevated ROS (262). However, the move towards adipogenic differentiation under conditions of oxidative stress did not occur, instead confirming those data reported by Sengstock *et al*. (264) with a significant decrease in Oil Red O detection of lipid for the continuously exposed cultures. The short-term addition of Ag^+ at the commencement of adipogenesis did not affect the differentiation process, suggesting that any increase in Ag^+ related ROS was not sufficient to either positively or negatively alter the regulation of adipogenesis. Explanation for the observed declines in both osteogenic and adipogenic differentiation, would require further investigation of both oxidative stress levels and the timing of molecular regulators such

as *Runx2* and *PPARγ*. This would be especially interesting for the decline observed for the short-term Ag^+ exposure of osteogenic cultures.

The trend towards a decline in mean ALP activity in those MSCs that were expanded as colonies in the presence of Ag^+, and subsequently assessed under Ag^+ free osteogenic differentiation was as for the culture expanded MSCs. While this reduction was not statistically significant from control, pNPP and DNA quantification data from which the normalised ALP activity was generated showed that, while there was a small increase in ALP activity for the Ag^+ CFU-f expanded MSCs, there was a significant increase from control in the cell number for this group. While other researchers have observed a hormetic response as a consequence of cellular stress, this is usually reported as viability (247,338), whereas the effect reported here is a consequence of cell number, indicating that this is a result of proliferation rather than increased metabolism. It may therefore be possible that the stress endured during CFU-f expansion acted as a priming agent that promoted proliferation in the presence of the osteogenic additives. With regards to adipogenesis, of note was the reversal in the decrease in lipid deposition that occurred with culture expanded MSCs in the presence of Ag^+. The small, but statistically significant rise in Oil Red O staining could suggest that the differentiation of MSCs along the adipogenic lineage is enhanced by this pre-exposure. Taken together, these data suggest that the exposure of MSCs to Ag^+, and the likely elevation of intracellular ROS, may tip the balance of differentiation towards adipogenesis once the source of Ag^+ is removed.

While the effects of Ag^+ on MSC differentiation have been thoroughly investigated, further assessment of the decline in CFU-f number and the continued ability of some cells to generate colonies during exposure to Ag^+ was required. The primary MSCs used within this thesis were a heterogeneous population isolated from bone marrow aspirates. However, testing the hypothesis of Ag^+ mediated selection of a tolerant sub-population was not demonstrated through the re-seeding of surviving colonies in a two-stage assay. The reduction in mean CFU-f number was consistently observed at 10 μM Ag^+ in those groups established with MSCs that had previously been exposed and subsequently cultured in the presence of Ag^+. However, this theory cannot be completely dismissed based on this evidence alone. The two-stage assay employed by Sengers *et al*. (323) showed that the population of cells within individual colonies, when re-plated, were still found to generate colonies of varying sizes, consisting of different cell numbers and comprising a heterogeneous capacity for osteogenic differentiation. All of this despite originating from the same colony derived from a single MSC. With

this in mind, it may therefore be conceivable that the ability to undergo normal clonogenic replication in the presence of 10 μM Ag^+ *is* possessed by a sub-population of MSCs, but that this competence is not held by all daughter cells. As a result, without the isolation of these capable cells the return of mean CFU-f number to that of the controls was lost due to experimental design and the dilution effect of pooling cultures. Despite this, the assay was able to demonstrate the retention of the clonogenic capacity of CFU-f derived MSCs following withdrawal of Ag^+ culture conditions.

The reduction of CFU-f diameter during Stage 2 was also in line with the previous findings that the mean CFU-f area was diminished at 10 μM Ag^+. However, should this hypothesised sub-population of MSCs exist, it may be possible that the decline in area is also reversible. Of course, the question therefore is that, if not all daughter cells possess the ability to generate Ag^+ tolerant colonies (possibly as a result of lacking the cellular mechanisms required to do this) how were they able to be part of colonies grown in Ag^+ containing media? Although a substantiated answer is currently not possible, it may once again lie in the immediate environment within which the cell resides and being surrounded by cells that do possess this capacity.

To demonstrate the potential impact of the cellular environment, specifically trophic factors and extracellular signalling molecules released in to media, MSC-CM containing Ag^+ was applied to clonogenic assays, with interesting results. While the hypothesis originally related to the observed decreases in viability of THP-1 cells and CFU-f number by MSCs seeded at clonal density, the absence of a recovery in CFU-f number and area when using pre-exposed MSCs further added to the theory. Although no work was performed to determine the validity of the hypothesis with regards to THP-1 monocytes, the recovery of CFU-f number as a result of applying Ag^+ in MSC-CM suggested that intercellular signalling or released factors may play a role in cell survival.

5.6 Conclusion

These data have shown that treatment of MSCs with Ag^+, while causing a trend to decreased ALP activity, does not significantly affect osteogenesis, however it does cause a decline in lipid deposition as a result of differentiation during exposure and an increase in adipogenesis following exposure. These data should be considered during *in vivo* study design with respect to fracture repair.

The work here could not definitively prove the existence of a sub-set of Ag^+ tolerant MSCs within the heterogeneous population. However it has provided evidence that the release of extracellular molecules from an untreated population can positively affect the survival and proliferation of MSCs exposed to Ag^+ at clonal density.

6 Chapter 6: Mechanisms of oxidative stress management

6.1 Introduction

An action of silver exposure on eukaryotic cells is undoubtedly the elevation of ROS (183,253,339,340). It is therefore important for the cells exposed to oxidative stress to have the capacity to adapt rapidly, activating mechanisms to protect the normal functioning of the cellular systems vital for regular continuation within the cell cycle. The effect of prolonged ROS on CFU-f formation assessed in Chapter 5, determined that a reduction in mean CFU-f number occurred at a concentration of Ag^+ that was specified following calculation of the maximum released concentration from the technology currently in development at Smith & Nephew. It is therefore of interest to elucidate the mechanisms involved in allowing the continual clonogenicity of the tolerant sub-population of MSCs under these conditions.

Evidence for the mechanisms upregulated in response to silver exposure have been primarily in the form of quantification of mRNA through polymerase chain reaction techniques (PCR), such as real-time PCR (qPCR). Investigations have principally focussed on the regulation of individual genes. Examples of such include the cysteine-rich metal homeostasis protein, metallothionein (MT), that is targeted due to its capacity to sequester Ag^+ (241,245,341). In addition, evidence of the cellular mechanisms involved in dealing with the consequences of Ag^+ generated ROS have also focussed on, and shown positive regulation of, selected genes of interest such as glutathione peroxidase (*GPX*), catalase (*CAT*), *SOD1*, glutamate cysteine ligase (*GCLC*), NADPH quinone oxidoreductase 1 (*NQO1*) and the regulator of oxidative stress response genes, *NRF2* (183,238,248). However, analysis of individual genes can provide only a snapshot of the full picture, therefore Dekkers *et al*. (342) performed total RNA analysis of the Ag^+ induced ROS response of human lung epithelial cells (A549). This allowed the analysis of all gene responses, and as a result identified an array of differentially expressed genes over a time course of exposures (≤ 24 hours), with maximal expression at 6 hours. At this time point, *SOD1,* thioredoxin (*TRX*) and glutamate-cysteine ligase, modifier subunit (*GCLM*) were significantly, but mildly upregulated. However, *GCLC,* glutathione reductase (*GR*) and *PRDX1* were all marginally repressed, with an increased vulnerability to further stress a possibility due to the subsequent reduction in reduced glutathione (GSH) synthesis. While these data therefore suggest that the response to ROS is not sustained in this cell type, the ability

of a subpopulation of MSCs to tolerate a prolonged (14 days) exposure to Ag^+ makes further investigation an interesting prospect.

Alongside the use of molecular analysis for the identification of gene upregulation in response to environmental stress, examination of the whole proteome provides another untargeted approach to identify the cellular responses to stimuli. This method enables the identification of new candidate regulators as well as providing confirmation of expected changes. This whole cell analysis has been used by researchers investigating the effects of metal ions e.g. cadmium, on the expression of intracellular and secreted proteins. The resulting data of differentially regulated proteins then allows the identification of cellular processes and pathways (e.g. Kyoto Encyclopaedia of Genes and Genomes, KEGG). This is performed through the use of Gene Ontology (GO) tools, mapped as a consequence of multiple protein changes related to that system. The use of proteomics when analysing the effects of Ag^+ on cellular responses has been limited. Georgantzopoulou *et al*. (343) primarily focused on the effects of AgNP on an *in vitro* co-culture model of gastrointestinal epithelium but included $AgNO_3$ as a Ag^+ comparator. Their limited analysis identified only 16 proteins of interest in the Ag^+ group, with a significant downregulation of PRX6 being the most relevant discovery. A broader assessment of protein regulation was performed by Juling *et al*. (344), analysing liver samples from rats fed silver acetate over a 28 day period. They identified approximately a 1:3 ratio split of up/downregulated proteins. Upregulated proteins of the oxidative stress response were catalase and glutathione S-transferase (GST, an enzyme that facilitates the conjugation of GSH to electrophiles to detoxify xenobiotics and neutralise free radicals from lipid peroxidation), however downregulated proteins included SOD1, PRX2 and PRX6 (confirming the data of Georgantzopoulou *et al*.). While these data provide a window on the somewhat surprising downregulation of the antioxidant pathway in the presence of Ag^+, there remains a large knowledge gap with regards the global effects on MSCs.

Reduced glutathione (GSH) is the predominant form of glutathione in the eukaryotic system, located primarily within the cytosol. This hydrophilic antioxidant protects cells from internal and external sources of ROS. Its synthesis (Figure 6.1) is initially via the action of glutamate–cysteine ligase (GCL), an ATP-dependent enzyme composed of modulatory (GCLM) and catalytic (GCLC) subunits that is regulated by NRF2. The secondary step in GSH production is through ATP-dependent modification of the γ-glutamylcysteine by glutathione synthase (GS) to form L-γ-glutamyl-L-cysteinyl-glycine (GSH). The action of GSH to neutralise hydrogen peroxide is via the enzymatic

action of glutathione peroxidase (GPX) and catalase, resulting in the oxidised form of GSH, glutathione disulphide (GSSG). The recycling of GSSG back to GSH is via the NADPH-dependent action of GSH reductase (GR), allowing the maintenance of this vital oxidative stress response protein. Evidence shows that GSH is also able to neutralise sudden increases in $O_2^{\bullet-}$ that accumulate while SOD1 production is initiated. This process is independent of enzyme activity and serves to highlight the important role that GSH plays as a front line defence against ROS (345,346).

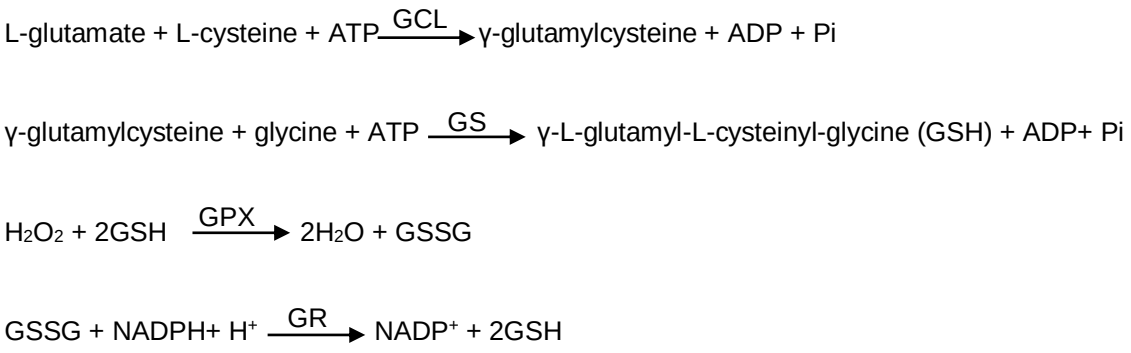

Figure 6.1: Synthesis of reduced glutathione and the neutralisation of ROS.

GCL, glutamate–cysteine ligase; GS, glutathione synthase; GSH, reduced glutathione; H_2O_2, hydrogen peroxide; GPX, glutathione peroxidase; GSSG, glutathione disulphide; GR, glutathione reductase.

Investigating the pharmacological inhibition of the glutathione pathway is commonly achieved via the administration of L-buthionine-sulfoximine (BSO), an inhibitor of GCL that thereby prevents the production of GSH (347). *In vitro* administration of BSO (7.8 – 1000 μM) results in an elevation of intracellular ROS when applied for time-periods up to 72 hours. Following exposure, the cell viability of J774.1 mouse macrophage was maintained when treated with 500 μM BSO alone for six hours, and there was no significant alteration in the expression of *Gpx*, *Sod1* or *Cat* in hepatic stellate cells treated with 200 μM BSO (20 hours) (341,348). However there are reports of side effects, for example, when applied to C3H10T1/2 MSCs for five days (50 μM), authors observed a significant decrease in proliferation (349). With regards to BSO treatment and the determination of clonogenicity in the form of colony formation there have been

few reports, however this was assessed by Ito *et al*. (350) using haematopoietic stem cells (HSCs). They observed no effects of 1 mM BSO (48 hours) in haematopoietic methylcellulose colony-forming assays (no details provided on endpoint timing), yet revealed a statistically significant reduction in the recovery of BSO treated donor derived HSCs following implantation in to irradiated mice. This evidence suggesting that the BSO induced elevation of intracellular ROS was detrimental to the process of hematopoietic reconstitution.

As for the co-treatment of cultures with BSO and Ag^+, work by Shim *et al*. (341) did show a reduction in viability of mouse macrophage culture using the combined treatment. However, Arai and colleagues (351) reported no additional loss of viability of J774.1 cells following a four hour BSO pre-treatment (500 µM) prior to a 24 hour $AgNO_3$ exposure. Aside from this, there have been few reports of further experimental work using this pharmacological inhibitor and Ag^+.

The artificial elevation of intracellular GSH levels can enhance the protective effects and the recovery of glutathione dependent cellular characteristics. This is achieved through the administration of the membrane permeable form of glutathione, glutathione monoethyl ester (GSH-MEE). Once transported in to the cell, the molecule is converted to GSH by cellular esterase and has proven more effective than the simple application of exogenous GSH (347,352). Treatment with 2 mM GSH-MEE enhanced proliferation, telomerase activity and cholinergic neuron differentiation in aged rat MSCs (353) and restored GSH and ROS levels in various hepatic cell lines in which glutathione synthesis was disrupted (354). Recovery of BSO inhibited GSH production was successfully achieved by Lu *et al*. (355), who co-treated cells with BSO (100 µM) and GSH-MEE (2 mM) in order to confirm the role of the glutathione pathway in breast cancer stem cell pluripotency. Results proved the involvement of glutathione in this area of biology and confirmed that this method of inhibiting glutathione synthesis could be nullified by the addition of an external source of GSH.

As previously discussed (see Chapter 1), the neutralisation of H_2O_2 also involves the antioxidant protein, peroxiredoxin (PRX). Oxidised Prx can be reduced by thioredoxin (TRX), thereby returning it to its reduced state (356). Inhibition of this pathway by pharmacologically inactivating TRX is possible by using 1-methylpropyl 2-midazolyl disulphide (PX-12). PX-12 irreversibly inhibits the TRX1 isoform found within the cytoplasm, thereby preventing the reduction of oxidised PRX. Although the *in vitro*

treatment of cells causes dose dependent cell-cycle arrest (357,358), its use at non-cytotoxic doses may provide evidence of the role of PRX/TRX in MSC tolerance to Ag^{+} induced ROS.

6.2 Aims

The experimental work presented in this chapter aimed to investigate the mechanisms employed by MSCs at clonal density that allow them to tolerate the maximum 10 μM Ag^+ exposure.

Specific aims of the study are to:

- To identify the molecular mechanisms by which a subpopulation MSCs at clonal density are able to survive clinically relevant concentrations of Ag^+.
- Confirm the findings of the molecular analysis using proteomic, pharmacological and imaging techniques.
- Provide information of further areas of interest arising from the proteomic analysis of Ag^+ cultured CFU-f.

6.3 Methods

6.3.1 qPCR of oxidative stress pathway (Primary MSC)

6.3.1.1 CFU-f culture and lysis

MSCs were seeded at clonal density in ten 100 mm diameter petri dishes for each of three primary donors. Half of the cultures for each donor were treated with 10 µM Ag^+ with media changes occurring twice per week. After 14 days, one dish from each treatment group and donor was stained using crystal violet to confirm the effects of Ag^+ on CFU-f reduction. The cells from the remaining dishes were trypsinised, centrifuged (130 x g for 5 minutes, RT), rinsed once with PBS and centrifuged for a second time. The resulting pellets were lysed with 600 µL Buffer RLT (Qiagen RNeasy Mini Kit; Qiagen, Cat: 74104).

6.3.1.2 RNA isolation

RNA isolation was performed according to the RNeasy Mini Kit protocol. In brief, following lysis, one volume of 70 % ethanol was added to the pellets with the sample mixed via pipetting. The lysate was added to an RNeasy Mini Spin column and centrifuged for 15 seconds at ≥8000 x g. Buffer RW1 (700 µL) was added to the column and centrifuged again, as before. The column underwent two washes with 500 µL Buffer RPE centrifuging between each for 15 seconds and two minutes at ≥8000 x g. A final centrifugation was performed (1 min, ≥8000 x g) without buffer to dry the membrane before elution of the RNA in 30 µL RNase-free water. RNA quality was determined by measuring the absorbance at 230/260/280 nm using the Nanodrop ND-1000 (Thermo Fisher, UK).

6.3.1.3 cDNA synthesis

cDNA synthesis was performed with 500 ng mRNA per sample reaction using RT^2 First Strand Kit (Qiagen, Cat: 330401). Genomic elimination was achieved using 2 µL Buffer GE per sample, with total sample volume equating to 10 µL. The Genomic elimination mix was incubated at 42 °C for five minutes followed by one minute on ice. To each sample, 10 µL reverse-transcription mix was added and tubes incubated at 42 °C for a further 15 minutes. The reaction was stopped by incubating the sample at 95 °C for five minutes. All samples were diluted with 91 µL RNase-free water and stored at ≤-20 °C.

6.3.1.4 Real-time Polymerase Chain Reaction (qPCR)

Real-time PCR (qPCR) was performed using the RT^2 Human Oxidative Stress PCR Array (Qiagen, Cat: PAHS-065Z), allowing detection of 84 genes related to oxidative stress pathways. Each cDNA sample was prepared for application across all wells, with one sample run on individual 96-well plates. In brief, 1350 µL SYBR Green Mastermix (Qiagen, Cat: 330524) was mixed with 102 µL cDNA and 1248 µL RNase-free water, votexed and 25 µL added per well. QPCR was run on the Thermo Fisher Quantstudio 3 Real-Time PCR System (95 °C for 10 minutes followed by 40 cycles of 95 °C for 15 seconds, 60 °C for one minute, a final melt curve of 95 °C for 15 seconds, 60 °C for one minute, 95 °C for one second). Fold-changes were calculated for each gene for each donor: delta (Δ) C_t values for all genes were determined by normalising the C_t data to β-2-microglobulin (B2M) for each sample, selected from the available housekeeping genes (B2M, GAPDH, β-actin, HPRT1 & RPLP0). $\Delta\Delta C_t$ were calculated for each gene in the Ag^+ treatment groups using the equivalent gene from the control group of that donor. Fold-changes were reported using $2^{(-\Delta\Delta Ct)}$. Finally, the $2^{(-\Delta\Delta Ct)}$ was calculated for each gene as a mean across donors, using the mean control ΔC_t to calculate the $\Delta\Delta C_t$ of each gene replicate from each donor in the treatment group. From this data statistical analysis was performed using multiple t-test of the ΔC_t value (using the original FDR method of Benjamini and Hochberg for multiple comparisons, FDR<0.05). Enrichment analysis was performed using the online tool, STRING (http://string-db.org) (359,360).

6.3.2 Global proteomic analysis of CFU-f cell lysates (Y201)

Clonal MSC line, Y201, were seeded for CFU-f in six T175 flasks. After 24 hours, media was changed to DMEM+20 % HyClone FBS ±10 µM Ag^+ (n=3/group) and exchanged twice per week for 14 days. Alongside the flasks, a six-well plate was cultured under the same conditions to allow a visual confirmation of the colony numbers after the culture period using crystal violet. At 14 days, cells were harvested using trypsin and centrifuged (130 x g for five minutes, RT). The supernatant was removed, the pellet washed once with PBS and the resulting suspension centrifuged as before. The supernatant was removed and urea lysis buffer (20 mM HEPES pH 8.0, 9 M urea, 1mM sodium orthovanadate, 2.5 mM sodium pyrophosphate, 1 mM β-glycerophosphate) added at 5:1 (v:v) of the cell pellet. The slurry was pipetted several times and samples stored at -70 °C.

Samples were warmed to room temperature before being transferred to the Proteomics Laboratory (University of York, Technology Facility) for analysis. Each sample underwent three bursts of microtip sonication at 15 watts, cooling on ice for one minute between each burst. Lysates were transferred to Eppendorf tubes and centrifuged (20,000 x g, 15 minutes, RT) to remove debris. Supernatant was transferred to a LoBind Eppendorf tube.

Proteomics data were provided detailing the relative protein quantification calculated using relative peak areas of non-conflicting peptides. Analysis was performed using online tools: STRING (http://string-db.org) and DAVID Bioinformatics Resource 6.8 (https://david.ncifcrf.gov) (361,362).

6.3.3 Inhibition of oxidative stress pathway (Primary MSCs)

MSCs were seeded at clonal density in to six-well plates. After 24 hours, media were changed to contain Ag^+ (0, 1, 5 & 10 µM) in the presence/absence of either L-Buthionine-sulfoxamine (BSO; Sigma, Cat: B2515) or PX-12 (Tocris, Cat: 2954) – pharmacological inhibitors of γ-glutamylcysteine synthetase and thioredoxin, respectively. Sterile filtered (0.2 µm) stock solutions of BSO and PX-12 were prepared fresh for each media change in dH_2O (eliminating the requirement for vehicle controls) before diluting to the required concentrations (BSO, 0.01, 0.1 & 1 µM; PX-12, 0.1, 1 & 10 µM). A control group of DMEM+20 % HyClone was included for comparison. Media were changed twice per week for 2 weeks after which colonies were stained with crystal violet and CFU-f counted. Statistical analysis of CFU-f numbers was performed against control and conditions of similar Ag^+ concentration by one-way ANOVA using Sidak's correction for multiple comparisons.

6.3.4 Addition of exogenous reduced glutathione to cultures treated with the γ-glutamylcysteine synthetase inhibitor, L-Buthionine-sulfoxamine (BSO), and/or 10 µM Ag^+ (Primary MSCs)

Primary MSCs were seeded at clonal density in 6-well plates and media changed after 24 hours for the following groups:

i. Control
ii. 10 µM Ag^+
iii. 1 µM BSO

iv. 1 μM BSO + 10 μM Ag^+
v. 2mM GSH-MEE
vi. 2mM GSH-MEE + 10 μM Ag^+
vii. 2mM GSH-MEE + 1 μM BSO
viii. 2mM GSH-MEE + 1 μM BSO + 10 μM Ag^+

Stock solutions of BSO and 2 mM GSH-MEE (Sigma, Cat: G1404) were prepared fresh at the time of each media change. Compounds were dissolved in serum free media and filter sterilised (0.2 μm pore size) before the addition of HyClone FBS to provide a 20 % growth media. Media were changed twice per week for 14 days at which point colonies were stained using crystal violet and CFU-f numbers determined. Statistical analysis by one-way ANOVA using Sidak's correction for multiple comparisons.

6.3.5 Immunocytochemistry of CFU-f for the glutathione synthesis subunit, GCLM, and thioredoxin (Primary MSCs)

MSCs were seeded at clonal density on to sterile glass coverslips in 24-well plates and cultured for 14 days in the presence/absence of 10 μM Ag^+. Cells were rinsed once with PBS and fixed with ice cold 100 % methanol (10 minutes) before a further rinse with PBS and storage at 2-8 °C. HeLa cells acted as a positive control for the detection of γ-glutamylcysteine synthetase (GCLM) and thioredoxin (TRX) and were seeded on to coverslips for 24 hours before being fixed as described for CFU-f. Following a one hour incubation with 5 % goat serum/PBS at room temperature, cells underwent a further incubation of one hour with the appropriate primary antibody and concentration. Antibodies used were as follows: 10 μg/mL polyclonal rabbit anti-GCLM IgG (Novusbio, Cat: NBP1-33405) and 4 μg/mL polyclonal rabbit anti-thioredoxin IgG (Novusbio, Cat: NBP2-48873), a rabbit IgG control (Vector, Cat: I-1000) was used alongside all staining. Cells were rinsed five times in three separate solutions of PBS before incubation with 10 μg/mL Alexa Fluor 647-conjugated goat anti-rabbit IgG (H+L) cross adsorbed (1 hour, RT; Invitrogen, Cat: A-21244). Cells were rinsed as before and the nuclei counterstained with 2 μg/mL DAPI before a final PBS rinse. Coverslips were mounted in aqueous mounting media (Abcam, Cat: ab104131) and stored in the dark until analysis. All immunofluorescence imaging was performed using the Zeiss Axio Imager.M2 LSM 710 confocal microscope (Carl Zeiss, Germany). Image processing was performed using Zeiss Zen 2.3 Lite.

6.3.6 Response of Y201 MSC Wnt reporters to stimulation of the Wnt pathway following CFU-f expansion in the presence of 10 μM Ag^+

Following the use of the Y201 hTERT-MSC in Chapter 5, a Wnt reporter Y201 MSC was employed for assessing the effect of Ag^+ on canonical Wnt signalling. The 'Y201-Wnt' MSC was established via transduction of the previously described Y201 MSC. In brief, enhanced green fluorescent protein (eGFP) is synthesised through the minimal CMV (Cytomegalovirus) promoter and TCF/LEF transcriptional response element (TRE). Expression of eGFP occurs through stimulation of the canonical Wnt pathway and activation of TCF/LEF TRE. Osteogenic and adipogenic characterisation of the Y201-Wnt cells was successfully performed as part of the validation (363).

Y201-Wnt MSCs were expanded for 14 days at clonal density in the presence/absence of continual 10 μM Ag^+ containing media. Growth media were replaced for that containing Wnt3a (R & D Systems, Cat: 5036-WN) at 100, 200 or 300 ng/mL ±10 μM Ag^+. Sixteen hours after Wnt3a treatment, the wells were rinsed three times using PBS and lysed using 50 μL/well of 0.1 % Triton X-100/0.2 M carbonate buffer, with plates undergoing three freeze/thaw cycles. After complete lysis, 20 μL from each lysate was transferred in duplicate to a 384-well black flat-bottomed plate and the fluorescence read at 472 nm excitation and 515 nm emission, providing a measure of the level of eGFP synthesis (BMG Labtech, Clariostar). The lysates were returned to their original wells and 60 μL 0.1 % Triton X-100/0.2 M carbonate buffer added to increase the available volume. Total protein was quantified from each well using the BCA enhanced assay (Thermo, Cat: 23227). In brief, working reagent (WR) and a bovine serum albumin standard curve (5 – 250 μg/mL) were prepared according to the manufacturer's instructions. To individual test-tubes, 100 μL of each standard and sample were added in addition to 2 mL WR. The tubes were covered and warmed to 60 °C for 30 minutes in a water bath after which they were cooled to RT and duplicate absorbance readings for each sample taken at 562 nm. Unknowns were calculated against the standard curve using Microsoft Excel from which normalised eGFP for each sample and a mean for each condition was determined. Statistical analysis of mean normalised eGFP performed against control for each Wnt3a concentration, by two-way ANOVA using Sidak's correction for multiple comparisons.

6.4 Results

6.4.1 Molecular regulation of oxidative stress pathways during CFU-f formation in the presence of 10 μM Ag^+

Real-time PCR was performed using the oxidative stress pathway array to identify the response of Ag^+ tolerant MSCs at clonal density to elevated ROS, allowing the recognition of those aspects of the pathway that were responsive in supporting MSC tolerance and allow further work to assess their importance.

The fold-change responses of three primary MSC donors were calculated relative to the B2M house-keeping gene and changes depicted in Figure 6.2a. Collectively, 56 genes (67 % of those tested on the array) were upregulated by ≥1.5 fold in the Ag^+ treatment group in at least one donor, compared to its untreated control. This reduced to 37 % where upregulation was observed in two or more donors for individual genes, indicating at the variable response of primary cells to Ag^+. As a consequence, statistical significance was observed in only one gene when analysing ΔC_t values, thyroid peroxidase (*TPO*) (p<0.001). A mean fold-change of ≥1.5 was calculated for 39 genes (Figure 6.2b) and enrichment analysis based on interaction evidence highlighted strong connection between those genes of the thioredoxin, peroxiredoxin and glutathione pathways (Figure 6.3). In addition, there were increases in heme oxygenase-1 (*HMOX1*), NAD(P)H:quinone oxidoreductase-1 (*NQO1*) and *SOD1*, all indicating at the involvement of the NRF2 transcription factor that is regulated by interaction with sequestosome 1 (SQSTM1) (upregulated in all donors).

Several genes showed no connection with other upregulated areas, such as oxidation resistance gene 1 (*OXR1*); the metal ion transporter, metallothionein 3 (*MT3*); the DNA repair protein, nudix hydrolase 1 (*NUDT1*); and the cytosolic enzyme, sirtuin 2 (*SIRT2*), however this should not distract from the potential importance of their role within the oxidative stress response.

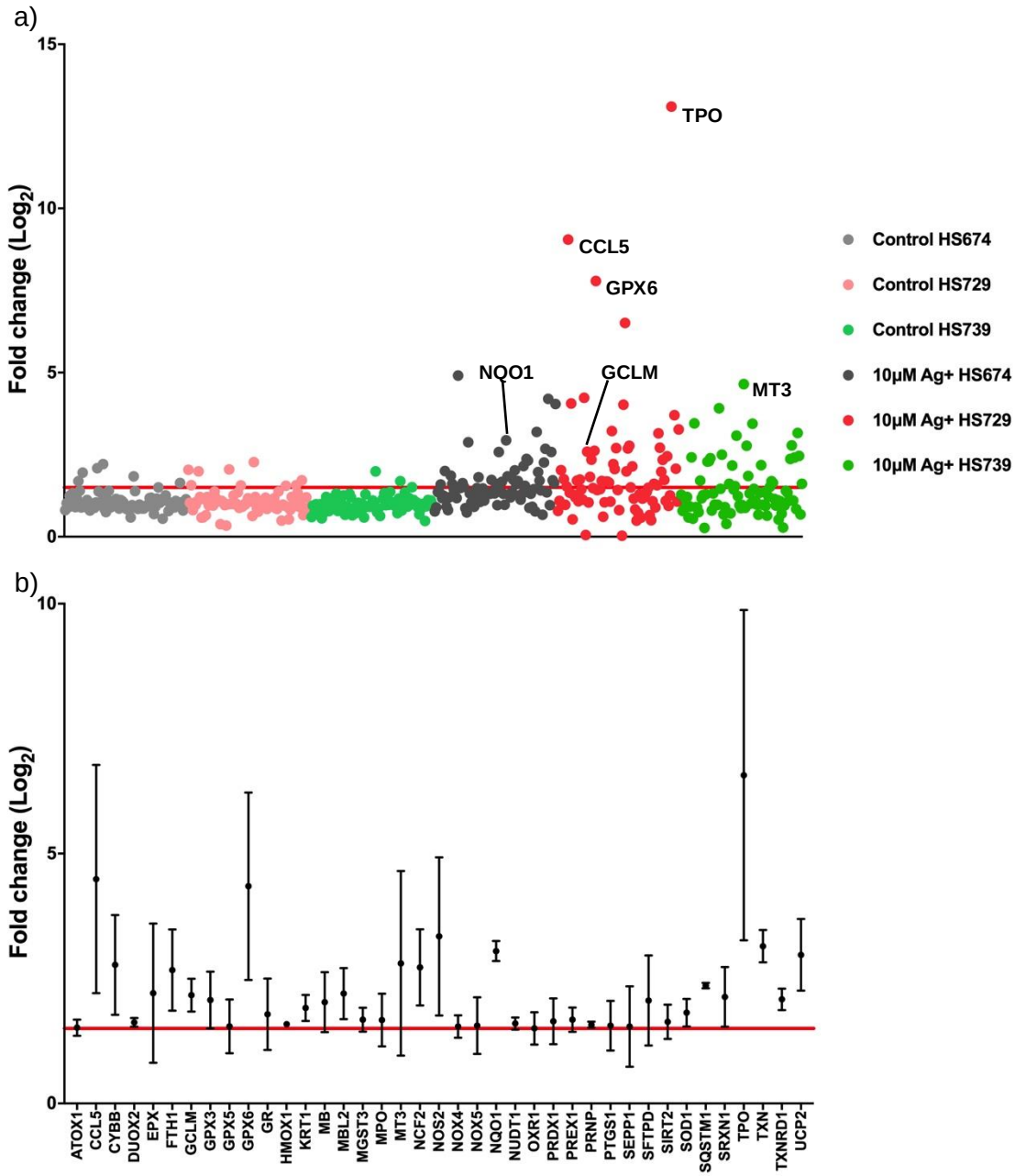

Figure 6.2: Real-time PCR analysis of oxidative stress gene regulation associated with the response of primary MSCs cultured at clonal density in 10 μM Ag^+.

MSCs from three donors (HS674, HS729, HS739) underwent CFU-f culture for 14 days. cDNA was generated and analysed using qPCR array for oxidative stress related genes. a) Scatter plot of data from individual donors (control and Ag^+ treated). Expression data were normalised to the housekeeping gene, B2M, and made relative to their equivalent control. Fold change was calculated as $2^{(-\Delta\Delta Ct)}$. b) Mean data (±SEM) from all donors that exhibited ≥1.5 fold-change is provided. Red line indicates 1.5 fold-change.

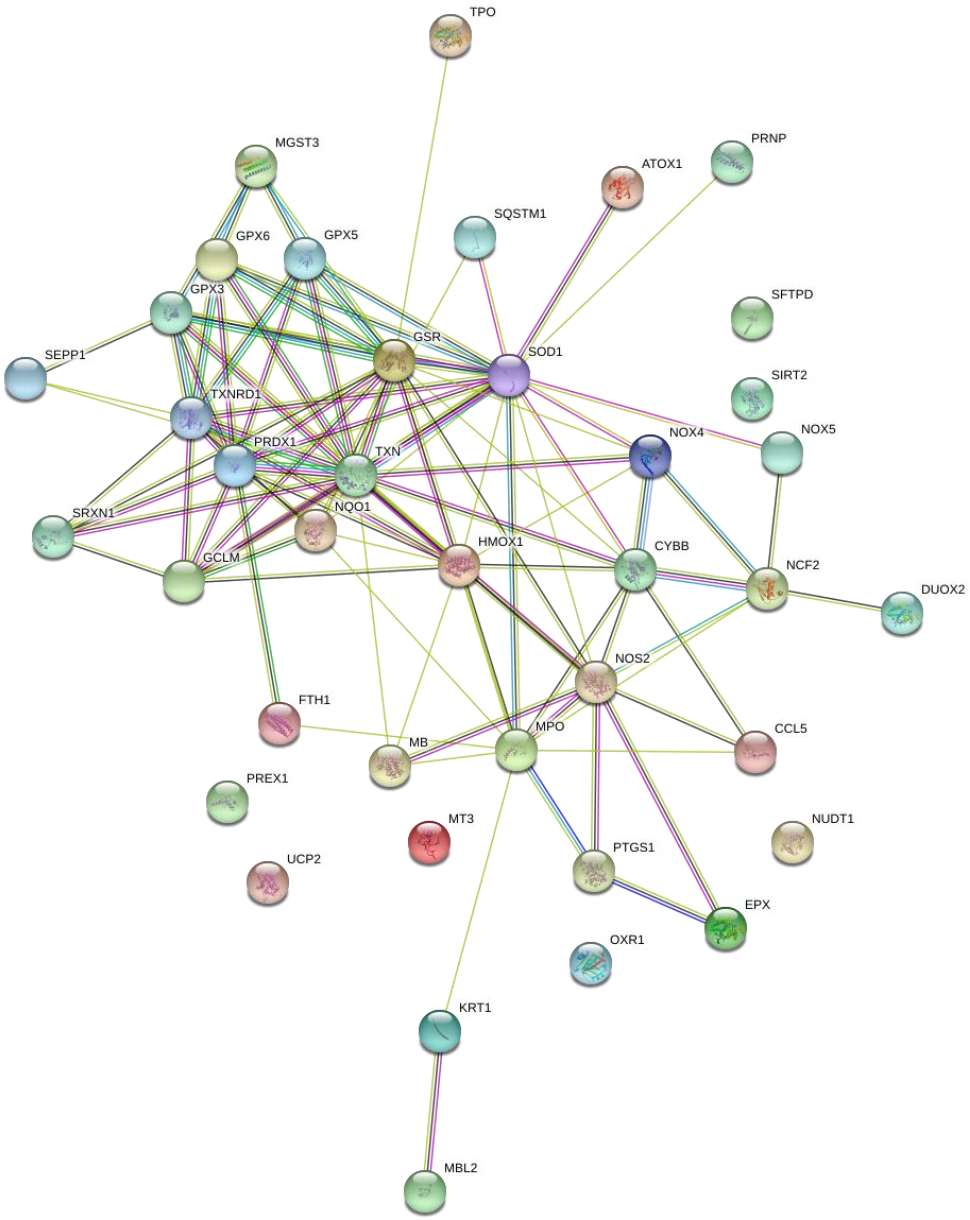

Figure 6.3: Enrichment analysis of oxidative stress genes with mean $\Delta\Delta C_t$ ≥1.5 fold from primary MSCs cultured at clonal density in 10 μM Ag^+.

Enrichment based on interaction evidence highlighted the strong relationship between several genes upregulated in those MSCs exposed to Ag^+. These genes were primarily of the glutathione, peroxiredoxin and thioredoxin pathways and their associated intermediaries, active in the neutralisation of oxidative stress. Network generated using STRING Database (v10.4).

6.4.2 Protein regulation by MSCs during CFU-f formation in the presence of 10 µM Ag^+

A mechanistic understanding of the effects of Ag^+ on MSCs was provided through proteomic analysis of Y201 generated CFU-f after 14 days. In total, 5050 proteins were identified through spectra matching against the UniProt database of human proteins. Relative protein quantification was performed following normalisation to total ion intensity, with fold differences and post-analysis performed thereafter. Overall, 1511 proteins were considered to be differentially expressed (i.e. <-0.5 and >0.5 log_2 fold-change), of which 534 were downregulated in the Ag^+ treatment group (i.e. greater expression in control) and 977 were upregulated (Figure 6.4). From this, 206 and 561 were significantly downregulated and upregulated, respectively (q<0.05) (Figure 6.5). Of the 206 downregulated proteins, 21 were significantly downregulated following statistical correction for multiple comparison (q<0.05, green triangles), while of 561 upregulated proteins, 89 were significant following correction. The proteins identified following correction were then analysed further.

Interaction networks were generated for significantly regulated proteins using the STRING database to allow visualisation of the related proteins, while KEGG pathway enrichment identified the major pathways involved with MSC tolerance to Ag^+ during CFU-f generation. The upregulated proteins showed evidence of a close relationship between several proteins involved with both the glutathione pathway (black circle) and DNA repair mechanisms (red circle) as a consequence of Ag^+ treatment (Figure 6.6). Parts of the glutathione mechanism (GCLC, GSTM3, MGST1, AKR1 (aldo-keto reductase)) of ROS and xenobiotic neutralisation are emanating from the upregulation of NQO1, while the centre point of the DNA repair mechanisms is proliferating cell nuclear antigen (PCNA) that also included the DNA ligase (LIG1), cullin 4A (CUL4A) and ribonucleoside-diphosphate reductase (RRM1). Also upregulated was the AKT serine/threonine kinase 1 (AKT1), a molecule that is activated by phosphatidylinositol 3-kinase (PI3K) and is an anti-apoptotic factor. In addition, KEGG analysis identified the metabolism of xenobiotics by cytochrome P450 as an activated pathway during culture with Ag^+ (Table 6.1).

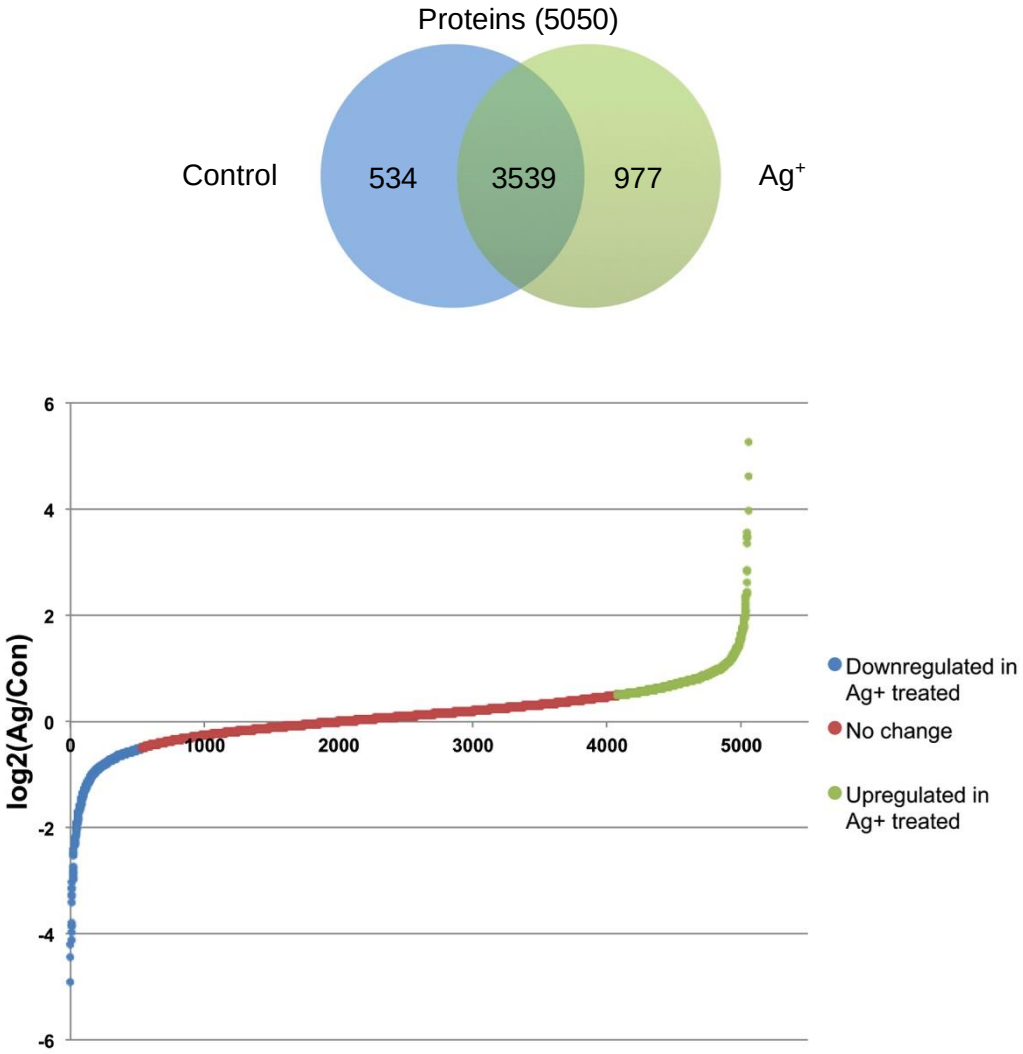

Figure 6.4: Proteomic identification and fold-change of proteins in Ag^+ and control CFU-f (Y201).

Representations of protein fold-changes (< -0.5 - >0.5) following Ag^+ treatment. Venn diagram (upper) indicating total number of proteins dependent on treatment. Change in protein levels as a consequence treatment (lower). Less than 0.5-fold increase/decrease determined as 'No change'.

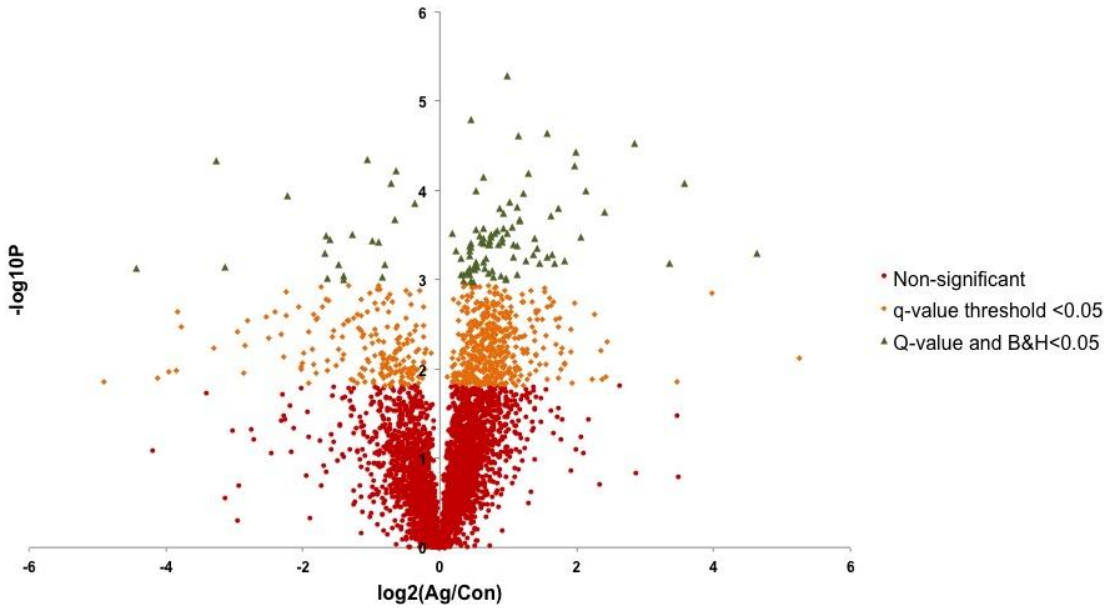

Figure 6.5: Volcano plot of proteomic data for control and Ag^+ treated CFU-f (Y201).

Proteomic identification of 5050 proteins identified in both control and Ag^+ cultured CFU-f illustrated according to statistical significance. Negative/positive log_2 data equate to Ag^+ group down/upregulated, respectively. 15.19% of proteins were significantly differentially regulated assuming a q-value of <0.05 (orange), reducing to 2.17% (green) when allowing for correction (Benjamini & Hochberg).

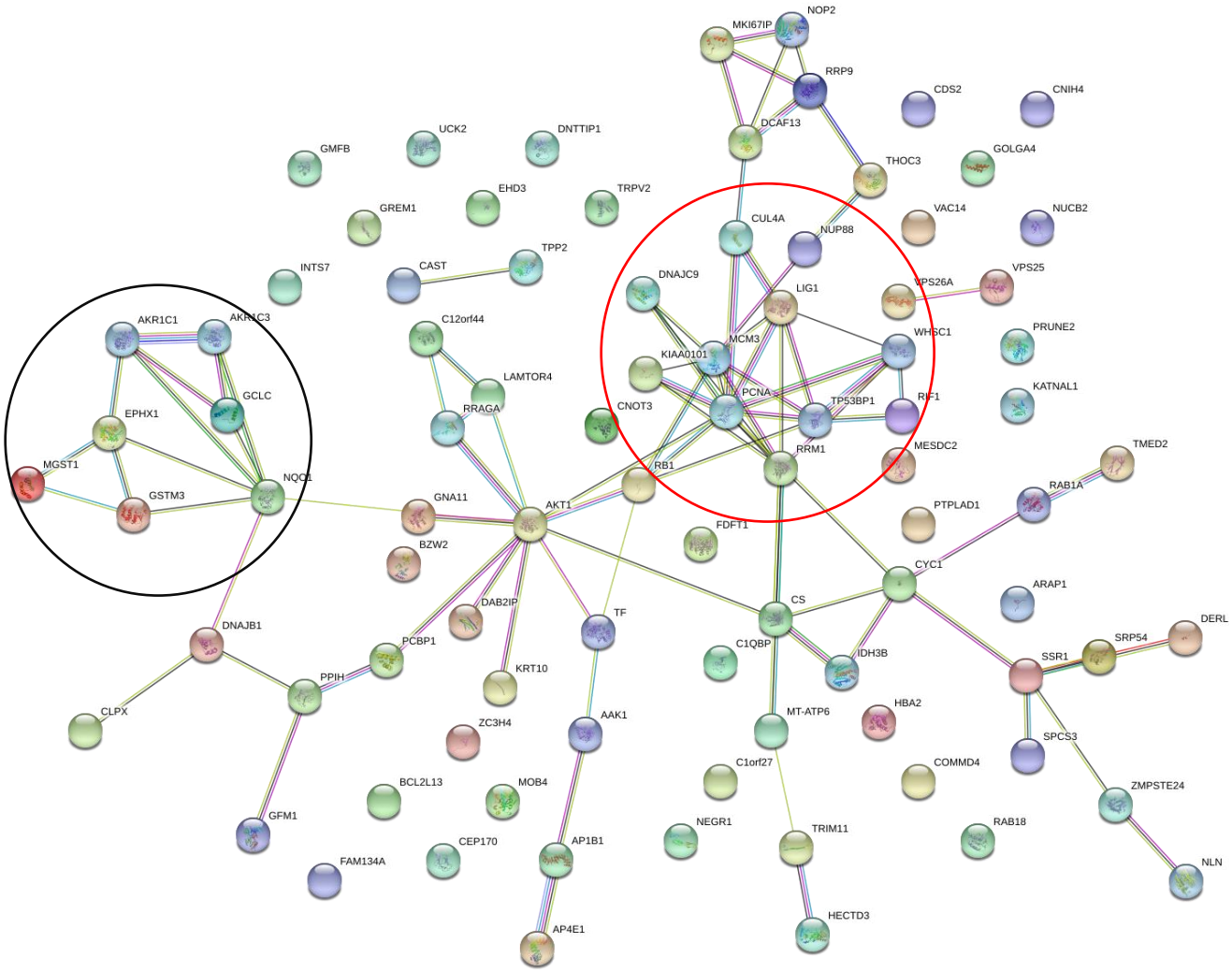

Figure 6.6: Interaction network of significantly upregulated proteins from Ag^+ cultured CFU-f (Y201).

Multiprotein network analysis of significantly upregulated proteins from Y201 CFU-f cultured in the presence of 10 µM Ag^+. Interconnecting lines indicate the level of evidence behind the relationship founded upon publications, co-expression, biochemical data and database associations. Grouping of proteins is dependent upon these associations. Highlighted groupings relate to glutathione metabolism and metabolism of xenobiotics by cytochrome P450 (black circle) and DNA replication (red circle). Network generated using STRING Database (v10.4) from significantly upregulated proteins corrected for false discovery rate (q<0.05, Benjamini and Hochberg).

Few interactions between downregulated proteins were found (i.e. those with greater abundance in the control group). However, those with associations were related to mitochondrial ribosomal transcription and glutathione metabolism (Figure 6.7), with the KEGG pathway of glutathione metabolism identified as the only pathway of significance with reduced activation (Table 6.1). The association with glutathione is contradictory to those data of the Ag^+ group due to the upregulation of the machinery of glutathione synthesis and function as a result Ag^+ exposure. A further inconsistency comes with the downregulation of the replication stress response regulator (SDE2) (an unconnected node within Figure 6.7), which is involved with preventing the replication of damaged DNA through interaction with PCNA, a protein that was upregulated in the Ag^+ group.

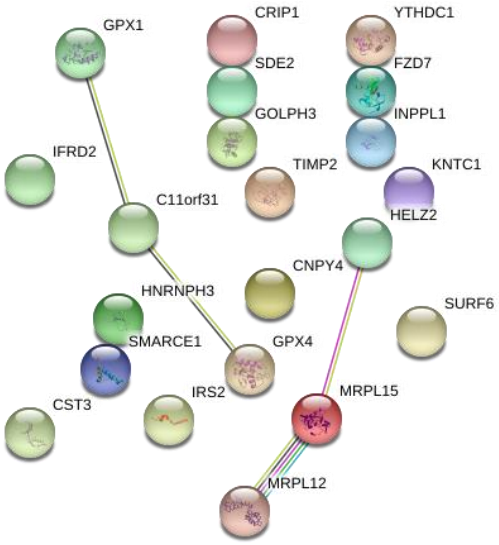

Figure 6.7: Protein upregulation in control group CFU-f (Y201) compared to Ag^+.

Multiprotein network analysis of upregulated proteins from Y201 CFU-f control cultures. Interconnecting lines indicate the level of evidence behind the relationship founded upon publications, co-expression, biochemical data and database associations. Grouping of proteins is dependent upon these associations. Network generated using STRING Database (v10.4) from significantly upregulated proteins corrected for false discovery rate (q<0.05, Benjamini and Hochberg).

Table 6.1: Details of significantly upregulated proteins associated with identified KEGG pathways of control and Ag^+ CFU-f (Y201).

Proteins associated to KEGG pathways (q<0.05). Analysis revealed the cellular processes upregulated between control and Ag^+ culture conditions. Glutathione metabolism was identified under both conditions, however with different protein regulation observed in each.

	KEGG Pathway	Protein name	HGNC Nonmenclature	Uniprot Accession number	FDR
Control	Glutathione metabolism	Glutathione peroxidase 1	GPX1	P07203	0.0041
		Glutathione peroxidase 4	GPX4	P36969	
	Glutathione metabolism	Glutamate-cysteine ligase catalytic subunit	GCLC	P48506	0.0175
		Glutathione S-transferase mu 3	GSTM3	P21266	
		Microsomal glutathione S-transferase 1	MGST1	P10620	
		Ribonucleotide reductase catalytic subunit M1	RRM1	P23921	
Ag+	Metabolism of xenobiotics by cytochrome P450	Aldo-keto reductase family 1 member C1	AKR1C1	Q04828	0.0299
		Epoxide hydrolase 1	EPHX1	P07099	
		Glutathione S-transferase mu 3	GSTM3	P21266	
		Microsomal glutathione S-transferase 1	MGST1	P10620	
	DNA replication	DNA ligase 1	LIG1	P18858	0.0451
		Minichromosome maintenance complex component 3	MCM3	P25205	
		Proliferating cell nuclear antigen	PCNA	P12004	

Further proteins of interest that were differentially regulated compared to control, but were not statistically significant, included the downregulation of the apoptotic promoter Bcl2-associated agonist of cell death (BAD, *q*=0.851) and the upregulation of cytoprotective, anti-apoptotic heat shock protein 90 (HSP90) family and constitutive coactivator of PPAR-gamma-like protein 1 (FAM120A, *q*=0.871). Furthermore, there was an upregulation of proteins involved with the reactive oxygen species pathway, thioredoxin (*q*=0.055), GR (*q*=0.051), the NADPH production enzymes, PGD (*q*=0.056) & G6PD (*q*=0.813) and all GST enzymes detected; increased DNA mismatch repair, MSH2 (*q*=0.328) & MSH3 (*q*=0.063); DNA damage binding protein 2 (DDB2, *q*=0.077) & replication protein A (RPA, *q*=0.135); DNA excision repair, RAB23B (*q*=0.308), Ligase 3 (LIG3, *q*=0.170), XRCC1 (*q*=0.216), ERCC1, 2, 3 (*q*=>0.05), RFC1, 2, 4, 5 (*q*>0.05), & Flap endonuclease 1 (FEN1, *q*=0.056); DNA base excision repair, polynucleotide kinase 3'-phosphatase (PNKP, *q*=0.528), AP endonuclease 1 (APEX1, *q*=0.519), N-methylpurine-DNA glycosylase (MPG, *q*=0.144); and subunits of the 26S proteasome responsible for degradation of misfolded proteins. A reduction in collagens I, II, V & VI (*q*>0.05) and DNA damage binding protein 1 (DDB1, *q*=0.364) were also noted.

With regards to those proteins of interest that may impact MSC clonogenicity, differentiation and fracture repair, Ag^+ cultured CFU-f exhibited a decreased expression of the chemokine, CXCL12 (*q*=0.282); receptors, PDGF receptor β (PDGFRB, *q*=0.372), EGF receptor (EGFR, *q*=0.492), Frizzled 2 (FZD2, *q*=0.203), Frizzled 7 (FZD7, *q*<0.05); and signalling cascade proteins, SMAD1 (*q*=0.436) and SMAD3 (*q*=0.084) compared to untreated controls.

In addition to identifying new mechanisms employed by MSCs under oxidative stress, the data also added detail to some of the results from the qPCR. For each of the 39 genes with ≥1.5 fold-change identified in Section 6.4.1 a search of the proteomics data was performed and the direction of protein regulation recorded, irrespective of the statistical correction (Table 6.2). There was a corresponding protein match for 17 of those genes, however six were calculated to be downregulated (red highlight) in the Ag^+ Y201 CFU-f, with 11 being upregulated (green). There was no corresponding protein identified for the remaining 22 genes (white). Of the upregulated genes, only two, *NQO1* and *KRT1*, were significantly upregulated at the protein level. The use of primary and clonal MSCs for qPCR and proteomics has not been taken in to consideration.

Enrichment analysis of the correlating upregulated gene/protein matches once again highlighted glutathione metabolism as the most significantly activated KEGG pathway in those CFU-f cultured in the presence of 10 μM (Figure 6.8). All genes/proteins (excluding SQSTM1 & MGST3) were involved with the two Gene Ontology Biological Processes of the removal of superoxide (GO: 0019430) and the response to oxidative stress (GO: 0006979).

Table 6.2: Comparison of Y201 protein regulation to corresponding oxidative response genes identified in the primary MSCs of Section 6.4.1.

Gene upregulation (≥1.5 fold) matched with protein alteration (irrespective of significance) in 17 cases. Where significance was achieved during proteomic detection (corrected for multiple comparison) this has been indicated as appropriate. Protein downregulation (red) occurred for six of the genes previously shown to be upregulated at the molecular level. Protein upregulation (green) was identified for 11 genes, with no protein equivalent available for the remaining genes (white).

Gene	Ag^+ group protein regulation
ATOX1	
CCL5	
CYBB	
DUOX2	
EPX	
FTH1	
GCLM	
GPX3	
GPX5	
GPX6	
GR	
HMOX1	
KRT1	q<0.05
MB	
MBL2	
MGST3	
MPO	
MT3	
NCF2	
NOS2	

Gene	Ag^+ group protein regulation
NOX4	
NOX5	
NQO1	q<0.05
NUDT1	
OXR1	
PRDX1	
PREX1	
PRNP	
PTGS1	
SEPP1	
SFTPD	
SIRT2	
SOD1	
SQSTM1	
SRXN1	
TPO	
TXN	
TXNRD1	
UCP2	

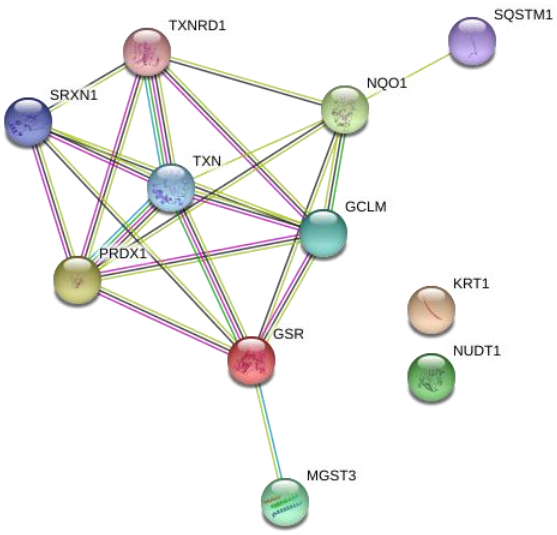

Figure 6.8: Enrichment of correlating gene/protein upregulation in CFU-f under Ag^+ culture conditions.

Glutathione metabolism was identified as the only significant KEGG pathway (FDR<0.001) for which both gene (primary MSC) and protein (Y201) upregulation was detected. The biological processes of the removal of superoxide (GO: 0019430) and the response to oxidative stress (GO: 0006979) encompassed all but two genes (*SQSTM1* and *MGST1*). Network generated using STRING Database (v10.4). Note: due to limitations with the database, the abbreviation 'GR' is referred to as 'GSR' in this diagram.

6.4.3 Immunocytochemistry detection of upregulated oxidative stress related proteins, GCLM and TRX

Validation of the molecular and proteomic analysis was performed by immunocytochemistry of CFU-f from primary MSCs. Two proteins upregulated during Ag^+ exposure, GCLM and TRX, were selected for identification (Figure 6.9). Both proteins were detected during confocal microscopy, with Ag^+ cultured CFU-f exhibiting greater staining compared to control cultures (Figure 6.10 & Figure 6.11). The detection of the glutathione synthesis protein, GCLM, was minimal in control cultures, with increased expression observed evenly between all primary donors under conditions of oxidative stress caused by Ag^+ (Figure 6.10).

Visualisation of TRX was variable between donors (Figure 6.11). Where expression was high in the control CFU-f of HS674, treatment with Ag^+ appeared to result in an increased intensity of staining. Instances of low level expression in the control CFU-f of HS729 & HS738 became greater following Ag^+ treatment, however the localisation and intensity observed with donor HS674 was not as apparent.

Analysis of whole colonies did not reveal any alteration in the quantity of staining. This suggested that the capacity to produce both proteins under conditions of oxidative stress was held by all MSC within a colony rather than by some that were consequently able to protect daughter cells that did not hold this ability.

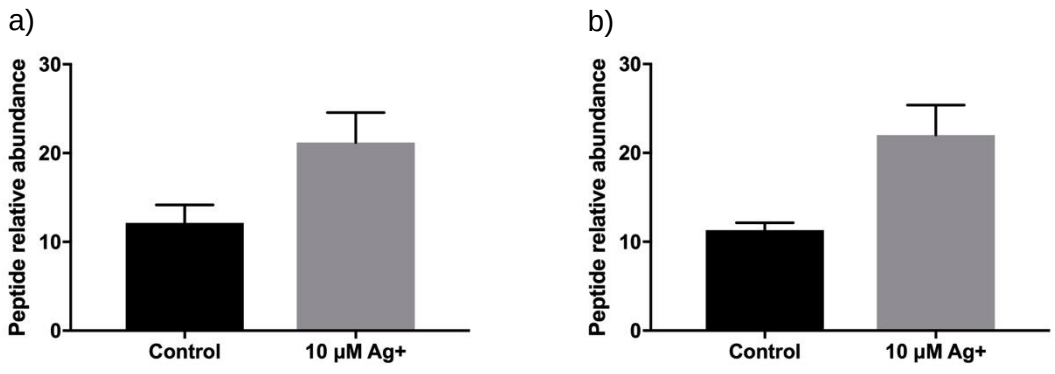

Figure 6.9: Peptide relative abundance of a) GCLM and b) TRX in control and 10 µM Ag^+ cultured CFU-f (Y201, n=3, biological replicates).

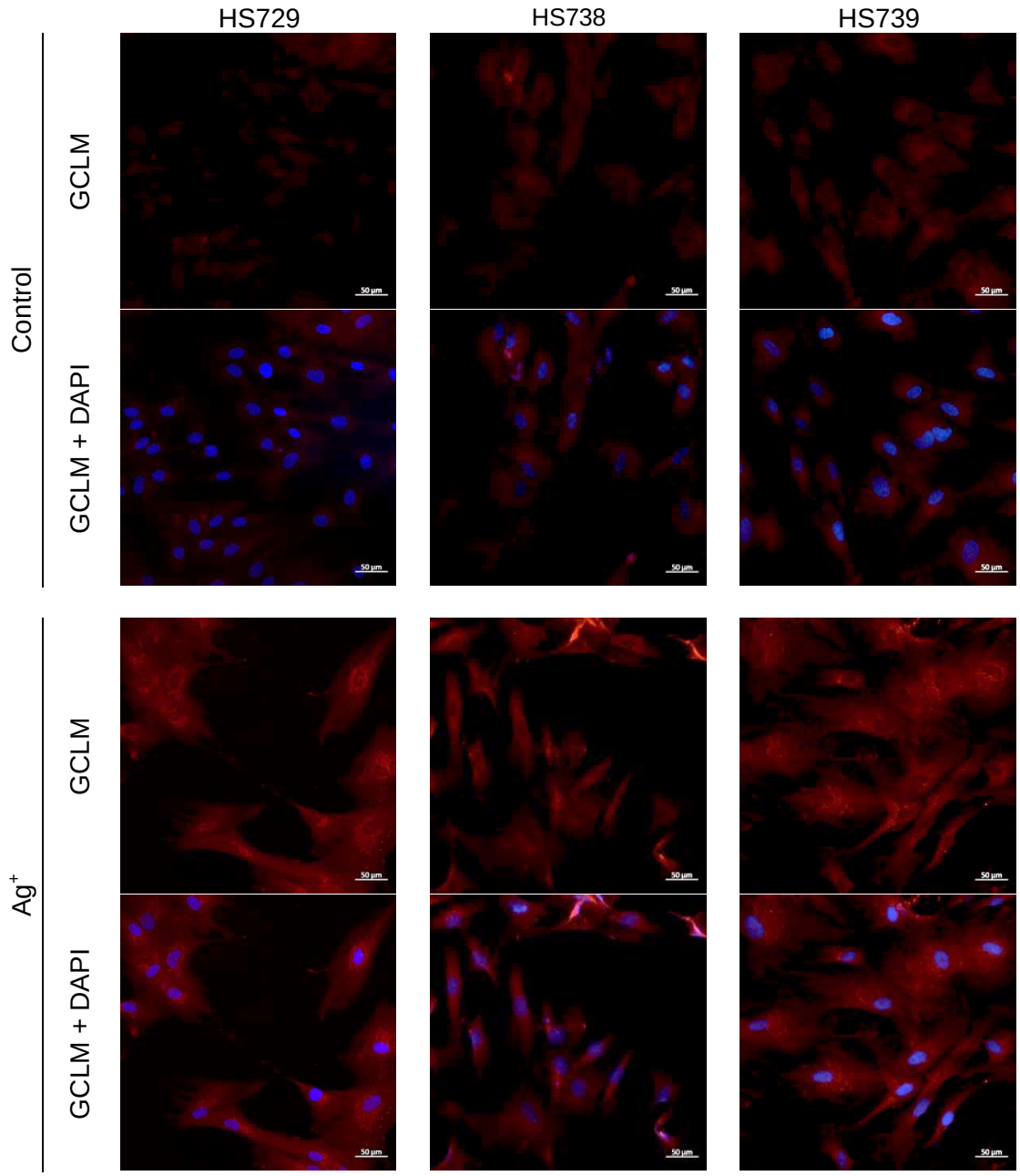

Figure 6.10: Immunostaining of primary MSC CFU-f for the glutathione synthesis protein, GCLM.

MSCs cultured on glass coverslips at clonal density in the presence/absence of 10 µM Ag^+. CFU-f were fixed and stained for GCLM (red) and counterstained with DAPI (blue). A positive control of HeLa cells was included, as were secondary antibody only and IgG controls which were negative for red staining. All images were captured using confocal microscopy using the same parameters.

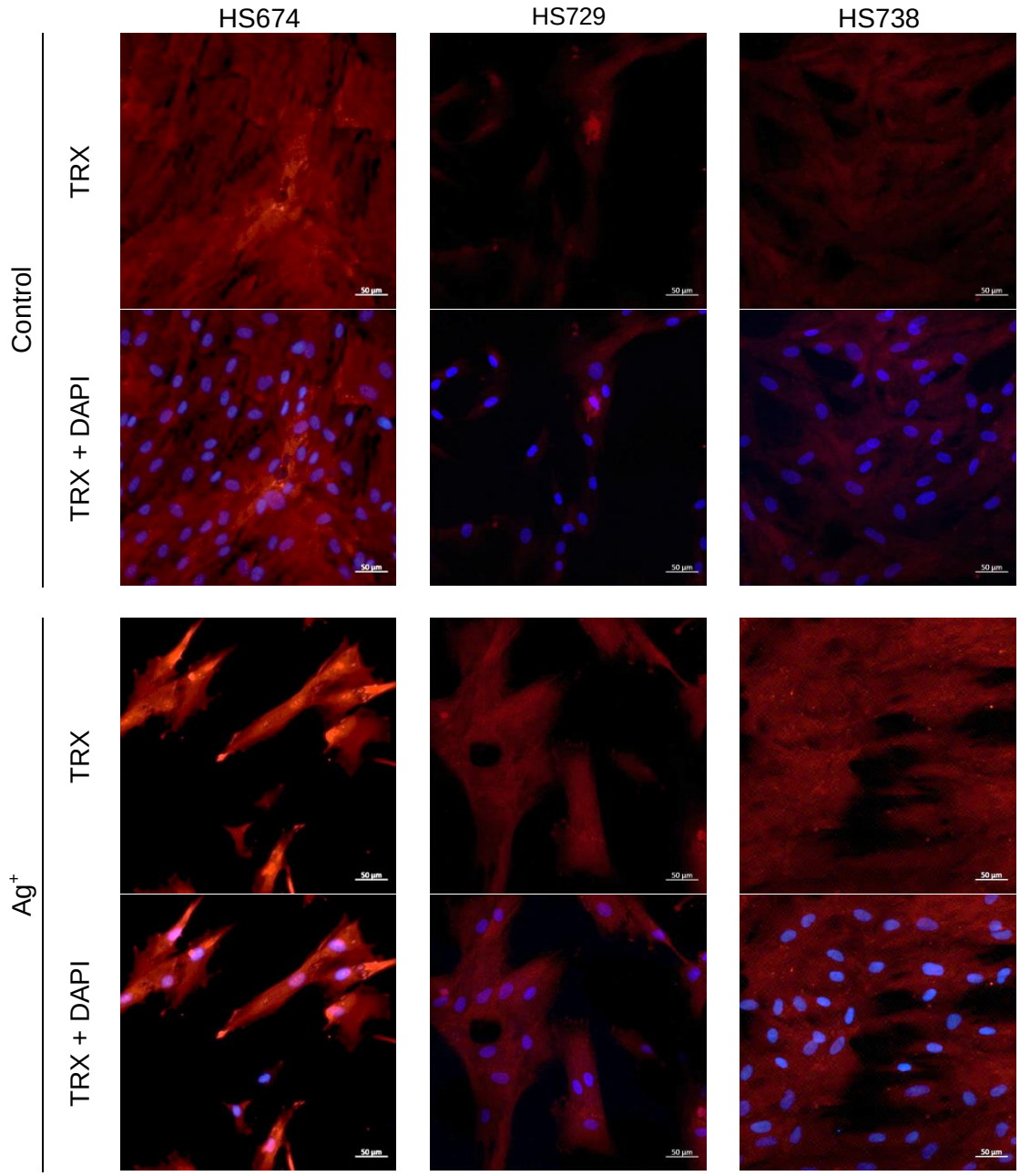

Figure 6.11: Immunostaining of primary MSC CFU-f for the oxidative stress pathway protein, thioredoxin.

MSCs cultured on glass coverslips at clonal density in the presence/absence of 10 µM Ag^+. CFU-f were fixed and stained for TRX (red) and counterstained with DAPI (blue). A positive control of HeLa cells was included, as were secondary antibody only and IgG controls which were negative for red staining. All images were captured using confocal microscopy using the same parameters.

6.4.4 Oxidative stress pathway inhibition and recovery through addition of reduced glutathione

Inhibition of both the glutathione and thioredoxin antioxidant pathways was performed through administration of the pharmacological agents, BSO and PX-12. Dose responses of both the inhibitors and Ag^+ provided CFU-f data that dictated further experimental design.

Oxidative stress pathway inhibition and recovery assays required a statistically significant decline in mean CFU-f number for 10 μM Ag^+ (against control), before data was included for analysis. This acceptance criteria was achieved with three individual donors for each assay.

6.4.4.1 Oxidative stress pathway inhibition

A reduction in mean CFU-f number was observed for those cultures receiving 1 μM BSO compared to control (p=0.16), no discernible decrease was noted for either of the lower concentrations (0.1 & 0.01 μM) of BSO applied (Figure 6.12). When in combination with Ag^+, a potentiation of the negative effects of Ag^+ on CFU-f number was observed. At 1 μM BSO, a statistically significant reduction was determined for those cultures receiving 5 μM Ag^+ (p<0.005, 5 μM Ag^+ v 1 μM BSO/5 μM Ag^+) and 10 μM Ag^+ (p<0.05, 10 μM Ag^+ v 1 μM BSO/10 μM Ag^+). No further decline in mean CFU-f number was observed compared to Ag^+ equivalent controls for any instance where a reduced concentration of BSO was used.

The detected reduction in CFU-f number when MSCs were treated with 1 μM BSO and Ag^+ provided evidence of the importance of the glutathione system in tolerating ROS generated by Ag^+. As a result, these conditions were selected for analysis of the potential recovery of mean CFU-f number upon co-administration of GSH-MEE.

The application of PX-12 to the culture system resulted in an uncompromising effect on CFU-f generation. There was a complete elimination of CFU-f formation for all groups treated with 10 μM PX-12. While a small reduction was observed for those receiving the lower doses of 1 & 0.1 μM, this was not significant (p>0.05) (Figure 6.13). As a result, the use of PX-12 in the investigation of the mechanisms of MSC tolerance to Ag^+ induced ROS was not taken forwards.

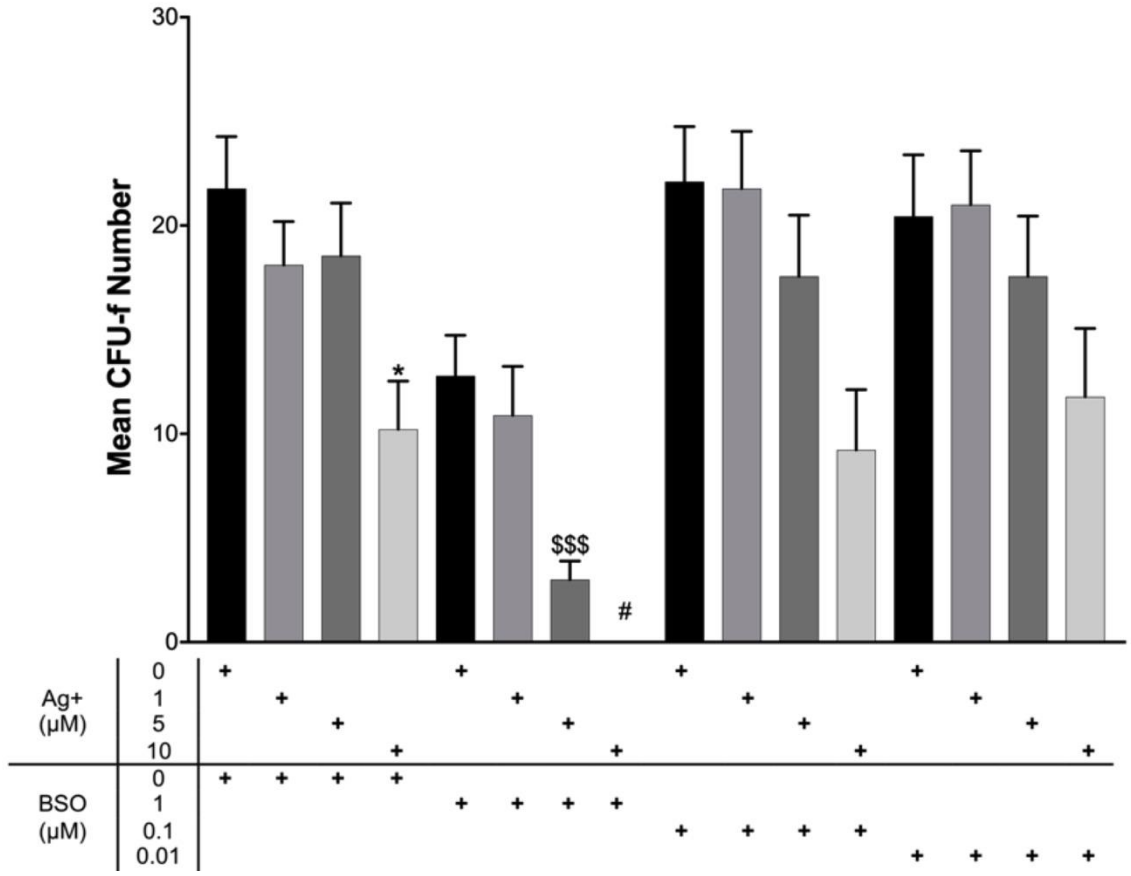

Figure 6.12: Potentiation of the Ag^+ induced ROS through addition of the glutathione pathway inhibitor, BSO.

Dose response of Ag^+ and BSO. The results are presented as the mean CFU-f number ±SEM for three donors (HS674, HS726, HS739), determined from three biological replicates for each donor. Statistical analysis by one-way ANOVA using Sidak's correction for multiple comparisons. Comparisons performed against control represented by asterisks (* p<0.05, ** p<0.01, *** p<0.005). Additional comparisons made against different treatment groups containing the same level of Ag^+ (e.g. 1 μM Ag^+ v 1 μM Ag^+/1 μM BSO), significance indicated compared to 1 μM Ag^+ (~), 5 μM Ag^+ ($) and 10 μM Ag^+ (#).

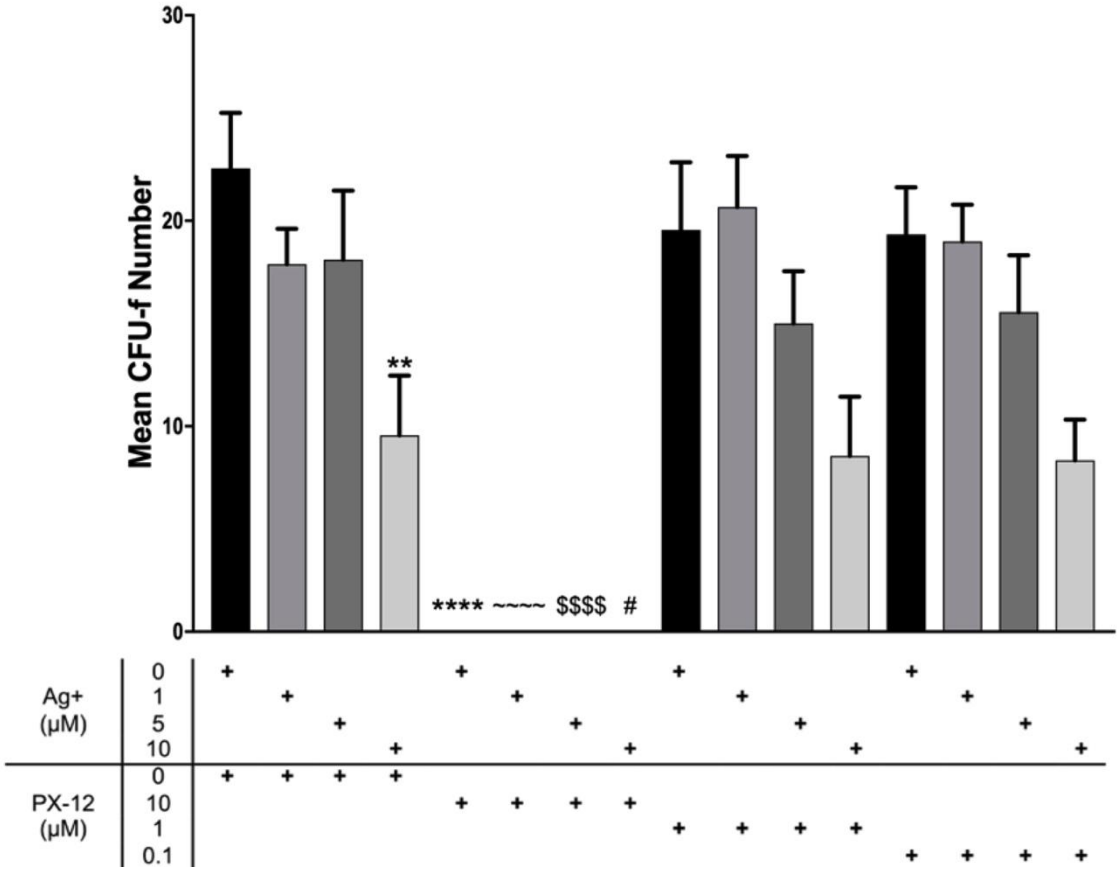

Figure 6.13: Potentiation of the Ag^+ induced ROS through addition of the thioredoxin pathway inhibitor, PX-12.

Dose response of Ag^+ and PX-12. The results are presented as the mean CFU-f number ±SEM for three donors (HS674, HS726, HS739), determined from three biological replicates for each donor. Statistical analysis by one-way ANOVA using Sidak's correction for multiple comparisons. Comparisons performed against control represented by asterisks (* p<0.05, ** p<0.01, **** p<0.0001). Additional comparisons made against different treatment groups containing the same level of Ag^+ (e.g. 1 μM Ag^+ v 1 μM Ag^+/0.1 μM PX-12), significance indicated compared to 1 μM Ag^+ (~), 5 μM Ag^+ ($) and 10 μM Ag^+ (#).

6.4.4.2 Oxidative stress pathway recovery through addition of GSH-MEE

Culture supplementation with exogenous reduced glutathione was performed in order to assess the importance of this element of the oxidative stress pathway in the ability of MSCs to tolerate Ag^+ exposure during CFU-f formation. GSH-MEE was therefore added to cultures treated with 10 µM Ag^+, 1 µM Ag^+ BSO and combinations thereof.

When added individually, all treatments resulted in significant reductions in mean CFU-f number compared to control (2 mM GSH-MEE, $p<0.0001$; 10 µM Ag^+, $p<0.01$; 1 µM BSO, $p<0.0001$) (Figure 6.14). Inhibition of glutathione synthesis during exposure to 10 µM Ag^+ resulted in the elimination of colony formation, significantly potentiating the negative effects of individually applied Ag^+ ($p<0.0001$) and BSO ($p<0.005$).

The addition of GSH-MEE to MSCs treated with either Ag^+ or BSO did not significantly recover the mean CFU-f number compared to either untreated control or individual treatments. While GSH-MEE co-treatment with Ag^+ resulted in a small additional decline in mean CFU-f number compared to Ag^+ alone ($p=0.214$), supplementation to BSO treated cultures did cause a small recovery of CFU-f number compared to BSO only ($p=0.716$).

The significant recovery of mean CFU-f number was achieved through the addition of GSH-MEE to MSCs treated with both Ag^+ and BSO when compared to the co-treatment (Ag^+/BSO) alone ($p<0.05$). Furthermore, the increase in colony formation was statistically equivalent to that of the BSO treatment ($p=0.999$). However, the recovery in mean CFU-f number in the GSH-MEE/Ag^+/BSO treatment group was still significantly below that of the cultures exposed to Ag^+ alone ($p<0.01$) and control ($p<0.0001$).

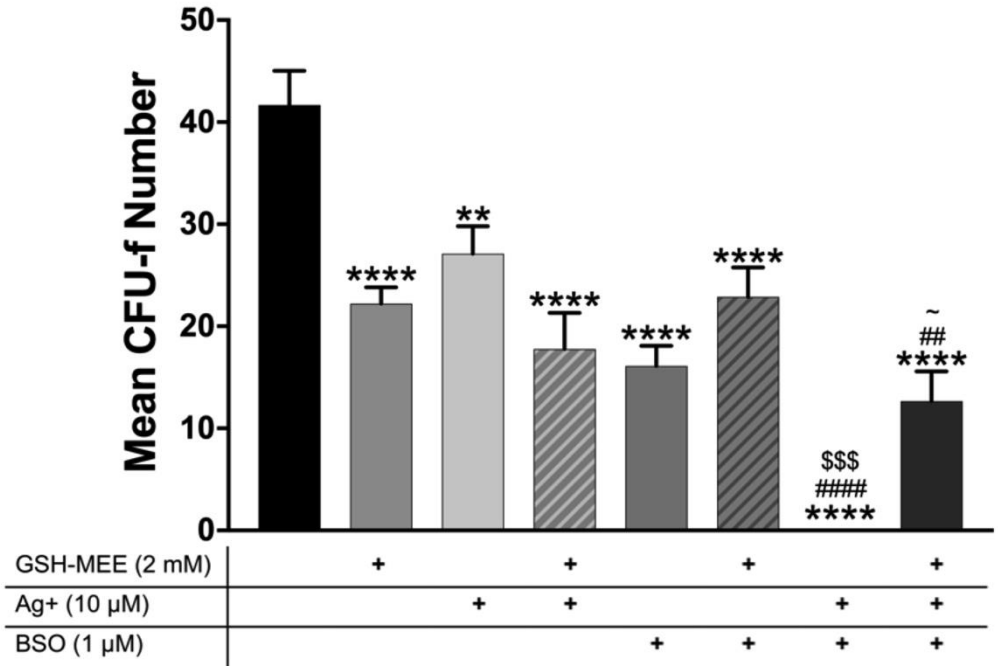

Figure 6.14: Mean CFU-f number of MSCs treated with a combination of 10 µM Ag^+, the glutathione pathway inhibitor, BSO, and 2 mM GSH-MEE.

Ag^+ elevation of ROS and inhibition of the glutathione antioxidant pathway using BSO resulted in a decline in CFU-f number that was partially recovered following addition of exogenous GSH.

The results presented as the mean ±SEM for three donors (HS729, HS738, HS739), determined from three biological replicates for each donor. Statistical analysis of CFU-f number by one-way ANOVA using Sidak's correction for multiple comparisons. Comparisons performed against control represented by asterisks (* p<0.05, ** p<0.01, *** p<0.005, **** p<0.0001). Additional comparisons made against different treatments, significance indicated compared to Ag^+ (#), BSO ($) and Ag^+/BSO (~).

6.4.5 Wnt signaling pathway reduction in CFU-f expanded in 10 μM Ag^+ (Y201-Wnt)

To test the biological impact of the proteomic report of a decline in Ag^+ treated CFU-f of the canonical Wnt receptor, FZD7, and to a lesser extent, FZD2, an assay was designed using Wnt reporter Y201-Wnt cells. Following culture in the presence/absence of 10 μM Ag^+, CFU-f were treated with Wnt3a and the response measured in order to assess a potential decline as a consequence of the treatment.

A clear dose response was apparent in the expression of eGFP from the control CFU-f following stimulation with Wnt3a (Figure 6.15b). Total protein levels for the control group were also stable showing consistency in CFU-f formation under normal culture conditions (Figure 6.15c). While a Wnt3a dose response was evident from those CFU-f cultured in the presence of Ag^+, there was a decline in mean normalised eGFP from control at each dose of Wnt3a (Figure 6.15a). When assessed individually, the difference in mean normalised eGFP between the control and the Ag^+ group at each Wnt3a dose was reduced in relation to increased Wnt3a stimulation. That is to say, the percentage response of Ag^+ CFU-f to control for each Wnt3a concentration was: 100ng/mL = 37.7%, 200ng/mL = 44.0%, 300ng/mL = 52.2%.

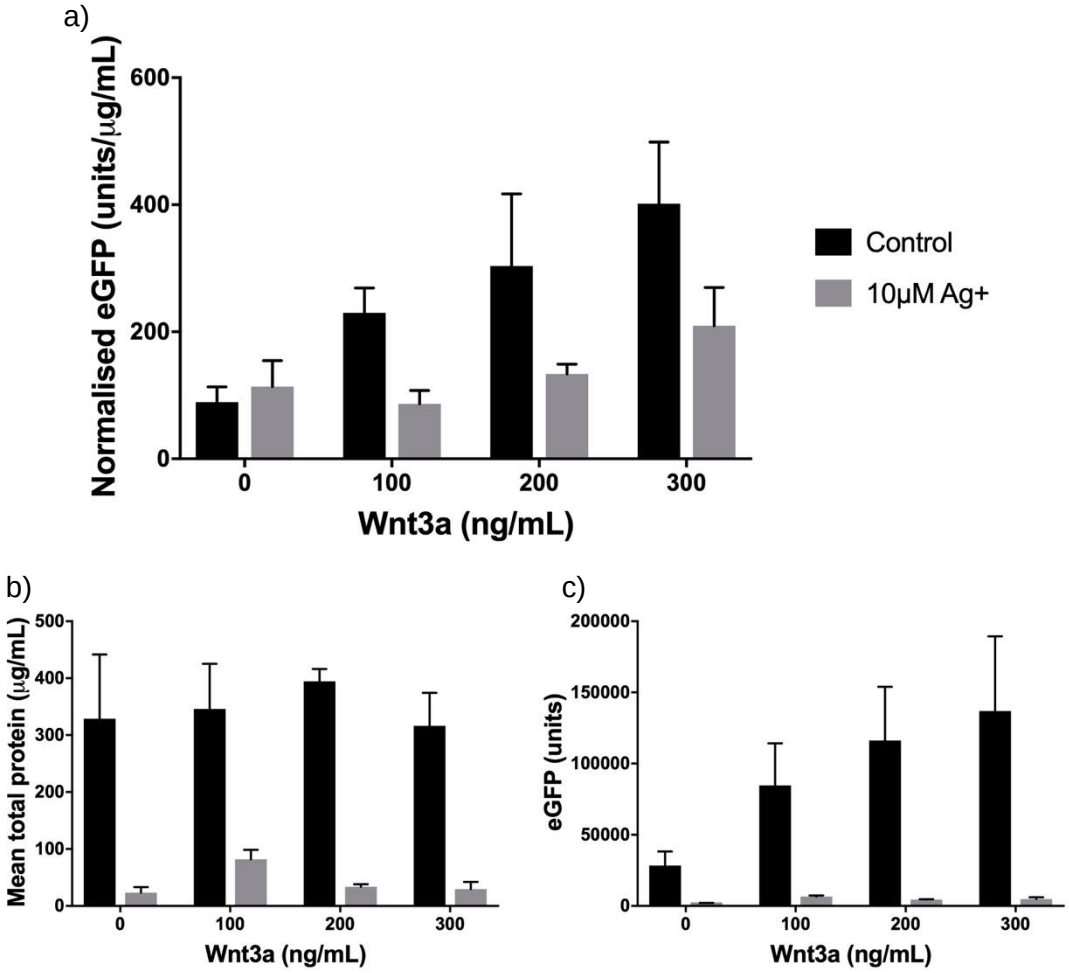

Figure 6.15: Response of Y201-Wnt MSCs to Wnt3a following expansion as CFU-f in the presence/absence of 10μM Ag^+.

Response of Y201-Wnt reporters to Wnt3a stimulation assessed via eGFP production. eGFP activity (b) and total protein quantification (c) were measured from cell lysates, providing normalised eGFP (a). The results represent the mean ±SEM, n = 3 (biological replicates). Statistical analysis of mean normalised eGFP performed against control for each Wnt3a concentration, by two-way ANOVA using Sidak's correction for multiple comparisons.

6.5 Discussion

The ability of MSCs to generate CFU-f from seeding at clonal density was diminished at concentrations of Ag^+ found to be subtoxic to confluent cultures. While previous data (Chapter 5) has provided evidence that the release of extracellular molecules may negate this effect, some CFU-f were still generated in the absence of these external stimuli. It was therefore hypothesised that the capability of these cells to survive was through the employment of mechanisms to neutralise the oxidative stress resulting from exposure to Ag^+. Initial investigation through the use of a qPCR array selected to identify alterations in oxidative stress response genes highlighted glutathione, thioredoxin and peroxiredoxin as areas of enrichment. Combining these data with that of the proteomics further suggested that these three elements of the oxidative stress pathway were employed in reducing oxidative stress. Although not confirmed as part of this thesis, the control of these pathways was likely via SQSTM1 (and NRF2) that was upregulated in all donors (by qPCR and proteomics). Further evidence of the role of NRF2 in the regulation of Ag^+ induced oxidative stress was the proteomic upregulation of GCLC, GSTM3, MGST1, EPHX1, NQO1, GR, PGD & G6PD, of which EPHX1 and NQO1 were statistically significant. Alongside the role of NQO1 as a reductase enzyme, usually involved in the reduction of quinones that are able to react with DNA, NQO1 also scavenges $O_2^{\bullet-}$ (thereby generating H_2O_2) and is especially prominent in tissues of low SOD activity (364). In contrast, the decline in the NRF2 regulated HMOX-1 protein was observed despite elevated expression at the molecular level, suggesting that under conditions of Ag^+ exposure, HMOX-1 expression was controlled by post-transcriptional regulation via miRNA (365). This protein has been identified as playing a role in the release of iron from intracellular stores that, like NQO1, results in the conversion of $O_2^{\bullet-}$ to H_2O_2 and while some components of this process were upregulated, these data would suggest that this is not fully employed by MSCs in their tolerance of Ag^+.

Alongside this, the dual detection of Ag^+ associated upregulation of NUDT1 also signified an increase in DNA repair mechanisms. NUDT1 minimises the accumulation of oxidised guanine (8-oxo-dG) in the genome. This damage is caused by OH^- and occurs within the genome on a daily basis, but is elevated *in vitro* by exposure to AgNP (366). Additionally, the significant upregulation of PCNA, CUL4A and LIG1 combined with the increases in the nucleotide excision repair substrate protein, DDB2; the single strand DNA stabilising protein, RPA; and mismatch repair proteins indicated at the

greater activity by Ag^+ exposed MSCs to manage the oxidative stress induced DNA damage.

Further insights in to the mechanisms used to deal with the stress of Ag^+ exposure showed that while MSCs are attempting to reduce the level and consequences of oxidative stress, they are also making efforts to avoid apoptosis through a protein reduction in Bcl-2-associated death promoter (BAD), thereby promoting the anti-apoptotic action of BCL-2. Increases in the levels of Akt1 could also suggest at the phosphorylation and subsequent inhibition of BAD, however confirmation of this process was not performed as part of this thesis (367).

With regards to protein regulation and the clonogenicity and differentiation of MSCs under Ag^+ exposure, there were several interesting findings from the proteomic data. The significant downregulation of FZD7 and to a lesser extent, FZD2, in combination with the data reported in this thesis showing a decline in Wnt signalling in MSCs cultured with 10 µM Ag^+, could impact the fracture healing process through a decrease in chondrogenic or osteogenic differentiation.

Published data has revealed that MSCs with downregulated FZD7 underwent osteogenesis with enhanced ALP and osteocalcin expression but showed reduced proteoglycan and collagen type II synthesis during chondrogenesis (368). Furthermore, the presence of FZD2 was elevated during the early stages of fracture repair (369). Therefore, it is reasonable to propose that a downregulation of signalling through these receptors may impact the natural regulation of the secondary fracture healing cascade. The direction of differentiation may be further complicated by the decreased expression of SMAD1 & 3 in Ag^+ treated MSCs. As previously discussed (Chapter 1), both proteins positively and negatively influence differentiation: inhibiting the progression of adipogenesis via PPARγ; enhancing the stabilisation of SOX9 during chondrogenesis; and activating *RUNX2* for the promotion of osteogenesis.

Further impacts on MSC proliferation and function may be through the decline in EGFR, PDGFRB and CXCL12. A decrease in the EGF signalling pathway may lead to a decline in MSC proliferation, while the reduction in PDGFRB has been implicated in reduced proliferation and migration, but increased osteogenic markers, ALP and osteonectin mRNA (370,371). Decreased CXCL12 may also contribute to a reduced migration of MSCs, an important component of the fracture repair process, as well as

having further implications on the dynamics of the haematopoietic niche. Investigations using mouse haematopoietic stem cells showed that CXCL12 provided protection from BSO-induced ROS, independent of the glutathione pathway (372). While not investigated further here, this reduction in receptor and ligand expression could also be responsible for the observed decline in CFU-f number/diameter reported in Chapter 5.

Confirmation of the qPCR and proteomic findings took the form of blocking the oxidative stress pathway through pharmacological inhibition of both glutathione synthesis and thioredoxin. The significant detrimental effect of 1 µM BSO on CFU-f formation in the presence of both 5 & 10 µM Ag^+ confirmed the importance of this mechanism to the Ag^+ tolerance of MSCs during CFU-f formation. The decline observed with the addition of BSO alone, even though at a concentration 200-fold lower than applied in some research (348), could have been a consequence of placing the MSCs under conditions of long-term oxidative stress. An elevation in the ROS generated naturally may therefore have been detrimental due to the inhibition of GSH synthesis.

While the inhibition of thioredoxin confirmed the importance of this protein to the continued viability of MSCs, the impact of its role in the tolerance of MSCs to Ag^+ could not be elucidated using the assays performed here. Complete inhibition of CFU-f formation at 10 µM PX-12 and no potentiation effect when applied at lower concentrations in conjunction with Ag^+ meant that the evidence of its involvement can only be provided by the previous qPCR and proteomic data.

The important role of reduced glutathione in colony formation during Ag^+ exposure has been proven through the significant recovery of CFU-f number by MSCs supplemented with GSH-MEE whilst exposed to Ag^+ and BSO treatment. While CFU-f formation was eliminated as a result of concurrent Ag^+ exposure and inhibition of glutathione synthesis, recovery of clonogenicity was observed to return to levels observed with BSO alone (p=0.999), and was a significant improvement from Ag^+/BSO (p<0.05). These data therefore indicate that the addition of GSH-MEE allowed MSCs to tolerate the elevated ROS that were the result of Ag^+ treatment. However, the inability to elevate CFU-f number to control levels when GSH-MEE was added individually to either Ag^+ or BSO suggested that glutathione alone was not the only protein required for CFU-f formation, whether it be under normal culture conditions or those of additional Ag^+ generated oxidative stress.

The negative effect on clonogenicity experienced with the addition of 2 mM GSH-MEE have not been previously reported. The addition of exogenous glutathione ordinarily counters the effects of disruption to glutathione synthesis, therefore the adverse effects observed here are unexpected (348,353–355). One major difference between published reports compared to this investigation was the length of exposure, with treatment for ≤4 days commonly assessed, rather than the 14 day application used here. Nevertheless an adverse effect was reported at a higher concentration (20 mM GSH-MEE) by Chen and colleagues (373), who observed a small decline in BEAS-2B human bronchial epithelial cell viability over 36 hours following a one hour treatment.

To further add to the work of Chapter 5 that investigated the effect of Ag^+ on the differentiation capacity of MSCs during and following silver treatment, it was shown that there was a decrease in the MSC (Y201-Wnt) response to Wnt3a stimulation after expansion in 10 µM Ag^+. The decline in normalised eGFP from Ag^+ Y201-Wnt generated CFU-f indicated at an overall negative effect upon the MSC response. However, this negative effect was reduced at higher Wnt3a concentrations, indicating that MSCs exhibit a reduced sensitivity to Wnt signalling that can in part be nullified by intensifying the stimulatory signal.

6.6 Conclusion

These data have confirmed that MSCs that generate CFU-f in the presence of 10 μM Ag^+ do so primarily by activating the major components of glutathione metabolism and of supplementary proteins, thioredoxin and peroxiredoxin. Evidence suggests that this process is likely to be through activation of the NRF2 transcription factor that also elevates the production of additional ROS scavenger NQO1. Further cytoprotective mechanisms that allow tolerance to Ag^+ are DNA repair proteins and apoptosis pathway regulation. Combined, the increased expression of such processes provides evidence of the mechanisms that allow MSCs to tolerate clinically relevant Ag^+ doses at low density, while also maintaining their clonogenic capacity. It is these properties that may be lacking in those MSCs that are unable to maintain CFU-f formation under these conditions.

Furthermore, MSCs from CFU-fs generated in the presence of Ag^+ display a reduced ability *in vitro* to express proteins that may influence their function within the fracture healing cascade. A diminished sensitivity to Wnt3a stimulation, likely through the reduced expression of frizzled receptors 2 & 7, alongside downregulation of signalling cascade proteins (SMAD1 & 3) and the MSC chemokine, CXCL12, could combine to reduce the efficiency of *in vivo* fracture repair.

7 Chapter 7: General Discussion

The impact of orthopaedic device related infection on both the patient and the health service can be costly on many fronts. While the patient can experience many physical and psychological consequences, such as pain, further surgery, increased hospitalisation and concerns of potential financial repercussions; the clinic has the difficulty of treating such a problematic occurrence and the associated costs (99). With current treatment options of surgical intervention and extensive antibiotic administration, prevention of infection is undoubtedly the primary aim, an objective that is even more pertinent in light of the rise of antibiotic resistance. With this in mind, new technologies aim to prevent the bacterial adherence to implant surfaces that becomes the nidus of infection.

The technology investigated as part of this thesis involves the application of silver to the surface of intramedullary nails, making use of its properties as a broad spectrum antimicrobial to provide unfavourable conditions for bacterial adhesion. While this element has been used extensively on wound dressings, its application within orthopaedics has been limited to reconstruction megaprostheses for oncology patients. Pre-clinical and clinical studies have provided evidence of reduced implant infection rates in subjects receiving such devices, while accompanying toxicological data have detailed the release of Ag^+ in to the surrounding tissue and organs (102,149), with some data reporting release in to the circulatory system at >24 months (145,148). These megaprostheses undergo non-biological, cemented fixation, with the primary aim of reconstruction and restoration of function to a diseased limb. In contrast, the purpose of intramedullary nailing is to provide stability for the primary benefit of fracture repair through active osteogenesis. The consequence of silver release into the surrounding tissue is therefore of high importance to orthopaedic trauma, since the prevention of infection should not come at the cost of impeding fracture repair. With regards to this, the thesis determined the intramedullary release kinetics of Ag^+ (Chapter 3) and the subsequent effects on fracture repair via MSC differentiation/function (Chapter 5) and tolerance mechanisms (Chapter 6).

In order to determine accurately the effect on *in vitro* osteogenesis, preliminary data was necessary to translate Ag^+ exposure from a clinically relevant environment to the *in vitro* setting. The data presented in this thesis confirmed the elution of Ag^+ in to the surrounding tissue and circulatory system from silver coated pins implanted in to rat femoral intramedullary canals. The short time period of maximal exposure (three days)

that was determined as part of the standard implant release profile was incorporated in to MSC differentiation protocols. Additionally, the detection of baseline concentrations of Ag^+ at 28 days provided confidence of limited potential exposure of the fracture sites. Notwithstanding the determined release profile, a prolonged exposure was also adopted into *in vitro* methods to account for instances of reduced clearance, while also applying a maximal intramedullary concentration equating to 10 µM Ag^+. This concentration corresponded to instant total release of Ag^+ and was found to be non-cytotoxic to confluent MSCs. These parameters therefore provided the most accurate translation of intramedullary conditions for the assessment of biological processes involved in fracture healing and MSC function.

7.1 Differentiation

Investigations by Pauksch *et al*. (238) reported no decline in ALP activity during MSC osteogenesis for short (24 hour) or long term (35 day) exposure to 10 µM Ag^+. Work presented in this thesis confirmed the lack of a statistically significant effect, but showed a decline in mean ALP regardless of exposure time, a finding that was more in line with the decline in osteocalcin (a late stage marker of osteogenesis) reported by Sengstock (264). This downward trend, albeit non-significant, was also observed in mean ALP during Ag^+-free osteogenic differentiation by MSCs expanded through CFU-f culture in Ag^+. This decline may, in part, have been caused by a reduction in canonical Wnt signaling that can induce ALP expression (374). As shown in this thesis, the expression of eGFP by Y201-Wnt reporters following Wnt3a treatment was reduced in Ag^+ generated CFU-f. This model therefore indicates at the potential effect of Ag^+ on the wider canonical signaling pathway which is implicated in osteogenesis and facture repair and would be an interesting direction for future research (375,376).

The oxidative stress that is a consequence of Ag^+ exposure has been identified as a causative agent that leads to decreased osteogenesis. The transcription factor, NRF2, which is responsible for the promotion of several elements of the antioxidant system, has been reported to directly inhibit Runx2-dependent osteogenesis in mouse osteoblasts (377). While neither Pauksch nor Sengstock specifically identified increases in NRF2 expression, Pauksch did show upregulation of the NRF2 regulated antioxidant enzyme, *NQO1*, in both the short and prolonged (p<0.001) Ag^+ test groups (162,378). Molecular and proteomic data generated within this thesis also showed an upregulation in transcription and translation of genes that are positively regulated by NRF2 (*SQSTM1*, a promoter of NRF2 release from KEAP1; GCLC; EPHX1; GR and

SOD1 (162,378)), and therefore may indicate at its involvement in the observed trends. However, we should be mindful that these data relate to CFU-f expanded MSCs in 10 μM Ag^+ and therefore can only indicate at a possible mechanism resulting in the reduction of ALP as a consequence of Ag^+ exposure during expansion.

Further evidence of the possible influence of NRF2 on the differentiation of MSCs from Ag^+ expanded CFU-f was during adipogenesis. Although a decline in lipid deposition was observed during exposure to Ag^+, confirming data by Sengstock (264), the significant promotion of adipogenesis was found following MSC CFU-f expansion with Ag^+. Data has linked the deficiency of NRF2 with impaired adipogenesis in human preadipocytes and mouse embryonic fibroblasts (379,380), while exposure of mouse hepatoma cells to cadmium reportedly increased the synthesis and stabilisation of this transcription factor (381). It may therefore be possible that silver promoted a similar stabilisation of NRF2, with the result being that Ag^+ expanded MSCs were potentially primed with the transcription factor that promoted the expression of PPARγ and C/EBP.

7.2 Clonogenicity

The most striking effect on MSCs was the consistent decline in colony formation at 10 μM Ag^+ despite this same concentration showing no effect on confluent cell viability and when applied during differentiation. This lead to the hypothesis for the existence of an Ag^+ tolerant fraction of MSCs and/or the need to be at higher population density in order to survive exposure to Ag^+. No experimental evidence was found for an Ag^+ tolerant MSC sub-group that may have potentially accounted for the survival of a fraction of the originally seeded heterogeneous population. However, further results did suggest that secreted molecules within MSC-CM from unexposed MSCs could restore Ag^+ cultured CFU-f numbers to that of control, possibly through replicating the milieu of a higher population density. MSC conditioned media contains multiple secreted factors that include chemokines, anti-apoptotic factors and proteinase inhibitors (333,334,382,383). Also within this cocktail lie the growth factors identified by Gronthos & Simmons (324) and Kuznetsov *et al*. (325) that enhance CFU-f formation by MSCs. It therefore appears that within the secreted factors found in MSC-CM lie some clues as to why clonally seeded cultures are susceptible to concentrations of Ag^+ that would otherwise pose no problems to those MSCs at higher density.

Ultimately, the effect on MSC clonogenicity found following Ag^+ exposure highlighted that the testing of future antimicrobial technologies on MSC differentiation alone may

not reveal the true extent of the biological impact on fracture healing. However, the experiments described here, and those of future studies (discussed in Section 7.6), may better inform investigations as to the consequences of, and potential solutions to, such deleterious outcomes.

7.3 Oxidative stress pathway identification

Antioxidant protein upregulation was identified in the molecular and proteomic analysis of MSC colonies formed in the presence of Ag^+. Components of glutathione metabolism were identified in all analyses providing irrefutable evidence of the importance of this system in MSC tolerance to silver. Confirmation of the important role of this mechanism was shown through BSO inhibition of GSH synthesis that eliminated the generation of CFU-f when in combination with Ag^+ treatment. That recovery from the elimination of CFU-f was achieved through media supplementation of GSH-MEE served to further highlight its necessity for tolerance to Ag^+ at clonal density. Similarities with this mechanism can be drawn from data regarding the toxicity of cadmium (Cd). Singhal and colleagues (384) identified GSH as a 'first line of defense' against cadmium induced cytotoxicity in mice. They showed lethality of sublethal doses of Cd in those where GSH synthesis was inhibited with BSO, results that were reversed with GSH-MEE pretreatment. These data were replicated *in vitro* by Chen and colleagues (373), who also added that secretion of proteins related to antioxidant enzymes, glutathione metabolism and tumour suppressors, from Cd exposed controls, was not observed in those pretreated with GSH. The time course analysed by Chen *et al*. determined that much of the machinery (GSTP1, PRDX1) was not upregulated until ≥24 hours post-exposure. Therefore it could be presumed that when applied with Ag^+, the components of MSC-CM may provided support during this lag phase of MSC oxidative stress pathway upregulation at clonal density.

Of interest were the unexpected decline in CFU-f of the GSH-MEE control group and the lack of positive effect upon CFU-f number when applied with Ag^+. Explanation of these results may lie in two experimental design factors. Firstly, since Ag^+ was provided in the culture media throughout the 14 day experimental period, it was believed that this should be the case for the glutathione supplementation, however this prolonged exposure may have contributed in some way to the observed reduced colony formation. As a consequence the recovery of CFU-f in cultures treated with BSO, Ag^+ and GSH-MEE was likely limited to that of the GSH-MEE treatment alone. Secondly, the incorporation of a GSH-MEE pretreatment may have positively affected

tolerance to Ag^+. The addition of GSH-MEE prior to inducement of ROS was performed by Chen *et al*. (373) during their experiments with cadmium, and Mulier *et al*. (385) when assessing the effect of H_2O_2 treatment on epithelial cells. This has the potential effect of priming cultures for the onset of ROS, resulting in the positive outcome of their analyses.

Despite this, the significant recovery of CFU-f with GSH treatment confirms the necessary function of this molecule. The roles of GSH in facilitating cell survival under Ag^+ exposure and conditions of oxidative stress are several-fold. GSH is able to directly bind metals through their high affinity for the thiols contained within GSH; convert superoxide in the absence of SOD; act as a substrate for GPX, and as a conjugate for GST to neutralise secondary reactive species (346,386,387). Of these modes, although no light can be shed on the direct binding of GSH to Ag^+, the molecular and proteomic data of this thesis provides an insight of the potential mechanisms employed by MSCs.

Indicated by the decreased SOD1 protein expression in Ag^+ cultured MSCs, the data presented here suggests that under the experimental conditions set out in this thesis, GSH could be the main factor in converting cytosolic superoxide to H_2O_2. In contrast, SOD2 protein was increased, signifying that mitochondrial stress remained elevated in MSCs under prolonged Ag^+ exposure. No evidence existed for the conversion of H_2O_2 by catalase, however several peroxiredoxins and thioredoxin were consistently upregulated at both the molecular and protein level in MSCs from surviving CFU-f. Additionally, glutathione and thioredoxin reductases were also elevated, implying the use of GSH during the activation of both ROS pathways in neutralising hydrogen peroxide as a result of Ag^+; although it must be noted that the upregulation of the detoxifying enzyme, GPX, was inconsistent. Finally, all identified GST and MGST proteins were upregulated in Ag^+ treated CFU-f compared to control. These enzymes conjugate GSH to the products of ROS-mediated lipid peroxidation (i.e. the reaction of lipid and molecular oxygen), thereby reducing the harmful effects of secondary by-products of oxidative stress (387), making this mechanism a clear requirement for the survival of MSCs during colony formation. The role of the oxidative stress pathways and the upregulated proteins within them are outline in Figure 7.1.

7.4 Further mechanisms

Despite the upregulation of ROS defence, the colony forming MSCs were clearly under continued oxidative stress, however the consequences of such conditions on cell

function were minimised through further reactive mechanisms. DNA integrity was managed through the activation of DNA repair mechanisms, allowing passage through the cell cycle and the generation of viable colonies. Oxidative stress affects DNA integrity directly through hydroxyl-mediated addition to double bonds between DNA bases that can result in base transversions (388). Indirect effects of ROS are a consequence of harmful secondary molecules resulting from lipid peroxidation that can cause base lesions (389). As previously discussed, while cellular processes aim to reduce the quantity of potentially damaging ROS, DNA repair mechanisms are activated in the event of such damage. Although no definitive conclusion can be drawn on the particular mechanism, the data presented here suggests that single stranded DNA repair processes, specifically components of the nucleotide excision repair (NER), base excision repair (BER, via the monofunctional DNA glycosylase, APEX1) and mismatch repair (MMR) mechanisms were upregulated in MSCs cultured with Ag^+. The recognition of DNA damage leading to NER is through two systems that subsequently use much of the same machinery to complete repair. Of these surveillance pathways, global genome repair (GG-NER) is likely to have been employed by Ag^+ exposed MSCs due to upregulation of RAD23B that is unique to this system, and the lack of Ag^+-related elevated protein expression of the alternative CSA/CSB controlled mechanism, transcription-coupled NER (TC-NER)[2] (389,390). The implementation of BER and MMR was identified as a result of MPG/APEX1 and MSH2/3, respectively. The outline of DNA repair mechanisms is provided and highlights the extent of upregulated components of the repair processes that were detected in Ag^+ cultured MSCs (Figure 7.2).

The basis of this thesis was to profile the effect of a clinically relevant Ag^+ concentration and pharmacokinetic profile on MSCs with regards to their role in fracture healing and mechanisms of tolerance. Although previous studies have shown that inducing oxygen-free radicals impairs fracture healing in rats (391), no biological reasoning was provided for this outcome. While the induction of ROS in this thesis is through alternative methods to that used in the fracture healing study of oxidative stress, the data provided here suggests that a detrimental effect on MSC clonogenicity and subsequent alterations in their osteogenic and adipogenic differentiation as a consequence of exposure may result in a similar outcome. Alteration of the differentiation potential of MSCs is a clear route to changing the fracture repair process, however the reduction in clonogenicity is also of equal importance. Clinical

[2] TC-NER detects and repairs lesions in actively transcribed genes.

evaluation on the progenitor cell requirements for successful treatment of aseptic non-unions determined that application of >1500 progenitors/cm^3 and an average of 54,962 ±17,431 progenitors/site resulted in successful healing (392). A correlation was also found between the volume of the mineralised callus and the number and concentration of CFU-f applied to the fracture. Treatment that potentially causes a decline in MSC numbers at the fracture site may therefore determine the biological properties and success of the repair. However, as elucidated here, glutathione response to Ag^+ mediated ROS and the upregulation of proteins related to DNA repair mechanisms provide MSCs with the capacity to tolerate clinically relevant concentrations of Ag^+ while maintaining their clonogenic capabilities.

7.5 Limitations

Although it is felt that the data presented here are a thorough examination of the effects of a clinically relevant Ag^+ concentration on MSC function and mechanisms of tolerance, there are limitations that should be considered.

Despite the molecular and protein upregulation of the oxidative stress pathways suggesting that Ag^+ exposure has generated ROS, no direct evidence has been provided within this *in vitro* investigation. While Ag^+ associated generation of cellular ROS has been determined elsewhere (183,253), such evidence could have been provided for this experimental model. The application of ROS sensitive fluorescent probes is one method of detection that would have allowed for the generalised and/or organelle specific identification of ROS (e.g. CM-H_2-DCFDA, MitoSOX) (reviewed in (393)).

Further to the Ag^+ induction of ROS, an oxidative stress control group (e.g. H_2O_2) in addition to the neutralisation of ROS (e.g. vitamin C, E and beta-carotene (394)), may have provided evidence that the decreased CFU-f were related to the elevation of ROS.

The desire to reduce the biological variability that is inherent in primary cells resulted in the use of the Y201 MSC clonal line during proteomic investigations. While data show that the Y201 MSC characteristics replicate that of primary cultures (266), and with a silver induced reduction in CFU-f also replicating that observed with primary MSCs,

they are considered a model cell line and it would be pertinent to further confirm the proteomic findings in primary cultures.

The importance of basal media on Ag^+ availability was highlighted in Chapter 4, however further investigation of this observation in both osteogenic and adipogenic media would have been of interest. Additionally, analysis of Ag^+ in the CFU-f media that contains 20 % FBS may have added further detail to the observation of reduced colony formation, especially considering the effect of protein concentration on Ag^+ bioavailability (395).

7.6 Future directions

The work presented here has focussed on MSC differentiation and clonogenicity, relating that to the process of fracture repair, however the influence of other cell types throughout the healing process, and the effect of Ag^+ exposure on those cells, would produce a more complete picture of the biological impact. For example, the consequences of Ag^+ on the immune system that provides cues to manage the initial stages of repair, and later, during osteoclastic remodelling, should not be ignored and would provide further fascinating insights in to the effects of Ag^+ on the fracture healing cascade.

Related to the impact on alternative cellular involvement, while this thesis has determined the effects of Ag^+ on MSC osteogenesis and adipogenesis, the progression of secondary fracture healing is also dependent on chondrogenic differentiation and the callus formation that provides initial stability to the fracture site. Difficulties in achieving repeatable *in vitro* chondrogenesis meant that the initial findings on the effects of Ag^+ on glycosaminoglycan deposition could not be progressed and have therefore not been submitted. However, this line of analysis would potentially provide an interesting focus, while also completing a clear gap in the current data.

Analysis of the Ag^+ cultured CFU-f was far from exhaustive. Further investigation of the surviving colonies, for example their surface marker expression, cellular ageing defence mechanisms and secretome (i.e. secreted proteins), may all be of interest under conditions of silver exposure. And while the reduced CFU-f resulting from the inhibition of GSH pointed to the role of this oxidative stress pathway in MSC tolerance to Ag^+, the absence of a positive response following GSH supplementation (of the Ag^+

group) that has shown efficacy elsewhere (354,355), may indicate that other tolerance mechanisms are necessary. For example, modification of sulferedoxin activity, a protein vital to the reactivation of PRX under times of severe oxidative stress (396); or NADPH, for the reduction of TRX and GSSG, may highlight deficiencies that become limiting factors in MSC tolerance to Ag^+. Of course, these pathways are related through their regulation via NRF2, inhibition of which would potentially highlight the involvement of global oxidative stress pathways in the continued clonogenicity of a subset of MSCs exposed to Ag^+. Additionally, elucidating the importance of the DNA repair mechanisms would also provide a fascinating expansion to the initial findings highlighted here.

Determining which elements of MSC-CM are important to the recovery of CFU-f would provide a further direction for elucidating the impact of Ag^+ on MSC clonogenicity. This investigation in combination with determining the oxidative stress response of confluent cultures (that exhibit no loss of cell number under exposure to 10 µM Ag^+) may help to clarify whether CFU-f are reduced due to an increased sensitivity to Ag^+ at clonal density or through an inability to form colonies resulting from the reduced proliferative signalling cascade that is potentiated by the stress of the Ag^+ environment.

Finally, these *in vitro* investigations have looked at the cellular response to Ag^+ in isolation, therefore the completion of an appropriate *in vivo* study would confirm the effects on fracture healing in the complex biological environment that is found in such trauma sites. Such an investigation would confirm the translation of the benchside findings to the *in vivo* situation. Therefore, the completion of an appropriate *in vivo* model, monitoring the progression/quality of, and the cellular response to fracture repair would reveal the clinical impact of the Ag^+ released from orthopaedic implants.

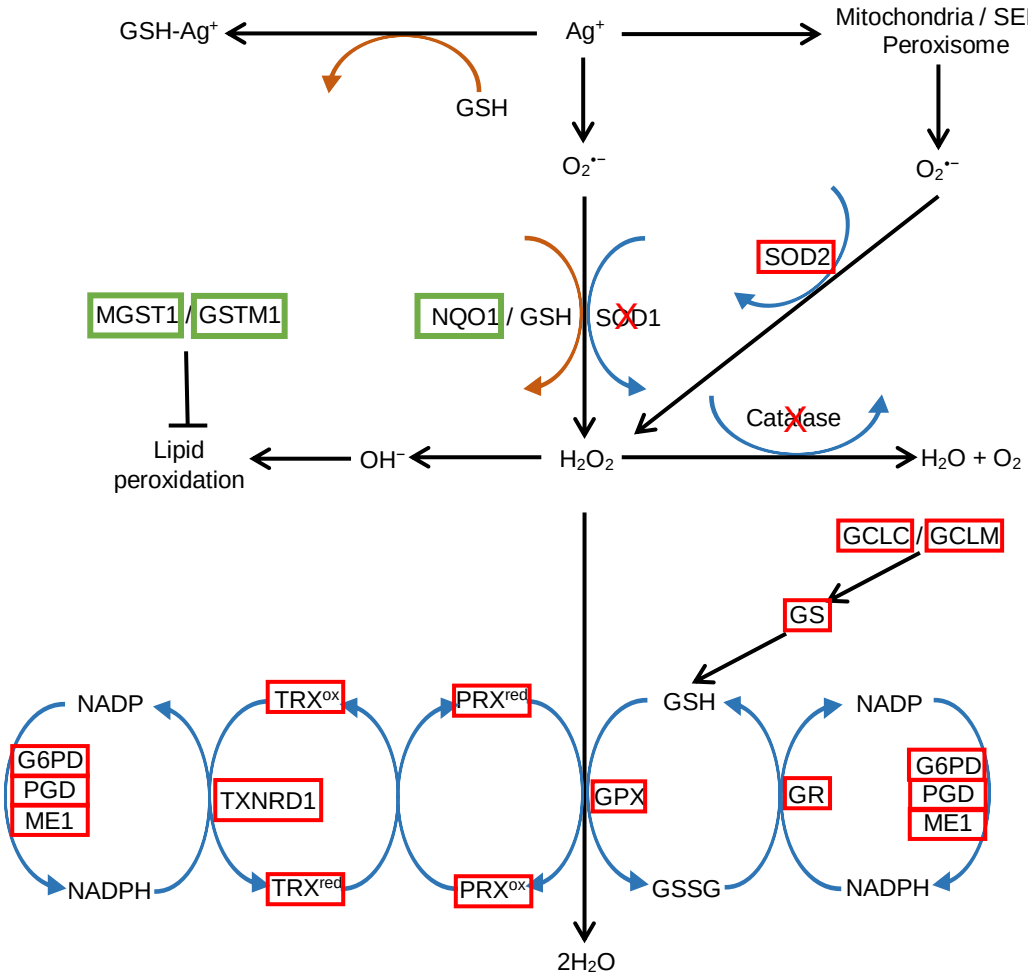

Figure 7.1: Mechanisms of ROS processing as a consequence of Ag^+ exposure.

Upregulation of proteins related to both the glutathione and peroxiredoxin/thioredoxin pathways implicates these systems in MSC tolerance to silver in order to maintain clonogenicity. However, lack of SOD1 and catalase expression indicates at the use of alternative mechanisms in the processing of superoxide and hydrogen peroxide under *in vitro* conditions of Ag^+ induced oxidative stress. Increased synthesis of MGST & GSTM during Ag^+ treatment also suggests at the generation of damaging hydroxyl radicals, a result of the Fenton reaction with intracellular iron (not shown (397)).

Significantly upregulated proteins are indicated with a green border (q<0.05), further upregulated proteins indicated with a red border.

Figure 7.2: DNA repair mechanisms in which protein components were upregulated in MSC CFU-f culture in the presence of Ag^+.

Several DNA repair processes were highlighted during this thesis as likely mechanisms employed by MSCs to restore DNA integrity during Ag^+ exposure. Although GG-NER, MMR and BER use many of the same components for the replacement and ligation of the newly synthesised strand, unique proteins are involved in the detection and control of each. Significantly upregulated proteins are indicated with a green border (q<0.05), those upregulated indicated with a red border.

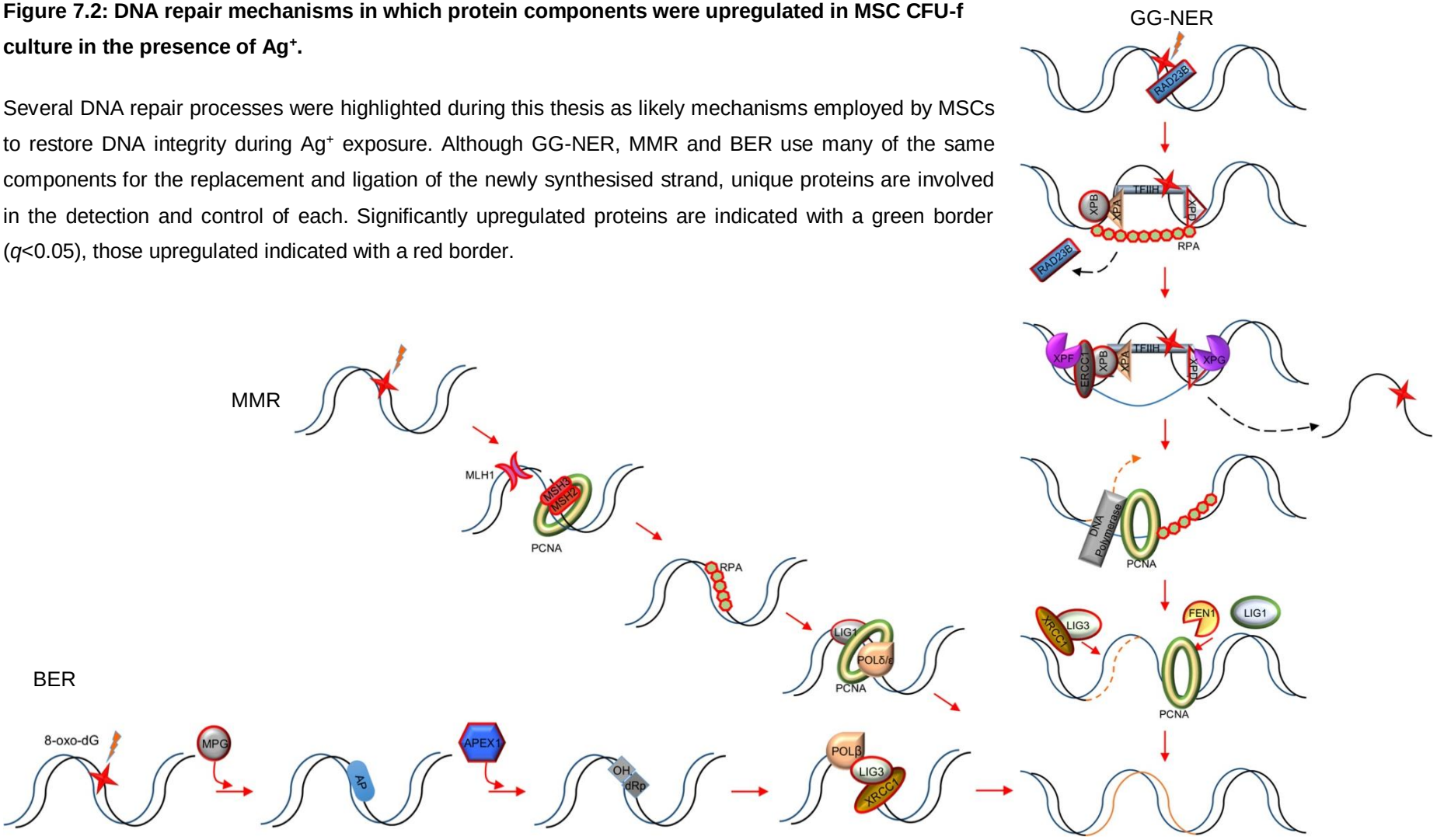

Appendix 1

Donor ID: HS509

Gender - Male
Age at donation - 28 years old
Ethnicity - African American
Tissue - Bone Marrow Aspirate

Cytotoxicity

WST-1	EdU
Viability of MSCs as a percentage of untreated control determined via WST-1 conversion. EC_{50} value of 32.84 µM. Results are plotted as mean percentage viability ±SEM and represent triplicate measurements.	N/A

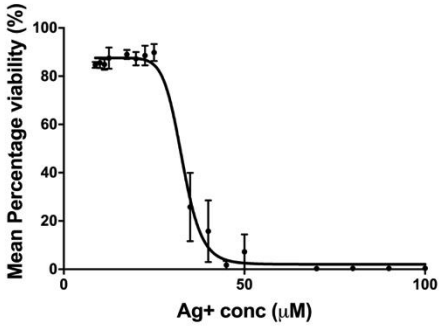

Differentiation - Culture expanded

Osteogenesis	Adipogenesis
N/A	N/A

Differentiation - CFU-f expanded

Osteogenesis	Adipogenesis
CFU-f check plate	CFU-f check plate

CFU-f formation

Day 0-3 Ag^+ exposure – CFU-f Number	Day 0-3 Ag^+ exposure – CFU-f Area
N/A	N/A
Continuous Ag^+ exposure –CFU-f Number	Continuous Ag^+ exposure – CFU-f Area
N/A	N/A

CFU-Ob formation – continuous Ag^+ exposure

CFU-Ob Number	CFU-Ob Area
N/A	N/A

Determination of CFU-f survival and continued decrease in number following replating

CFU-f Number	CFU-f Diameter (pixels)
N/A	N/A

Conditioned media

N/A	

qPCR – Oxidative stress pathway

N/A	

Proteomic analysis of CFU-f cultured in 10 µM Ag^+

N/A	

Oxidative stress pathway inhibition

Inhibition with PX-12	Inhibition with BSO
N/A	N/A

Recovery of CFU through addition of GSH-MEE

N/A	

Wnt signalling pathway reduction in CFU-f expanded in 10 µM Ag^+

N/A

Donor ID: HS674

Gender - Male
Age at donation - 25 years old
Ethnicity - African American
Tissue - Bone Marrow Aspirate

Cytotoxicity

WST-1

N/A

EdU

Incorporation of EdU presented as the mean percentage of cells detected using a secondary fluorescent probe ±SEM, and represent data from fifteen images per Ag^+ concentration.

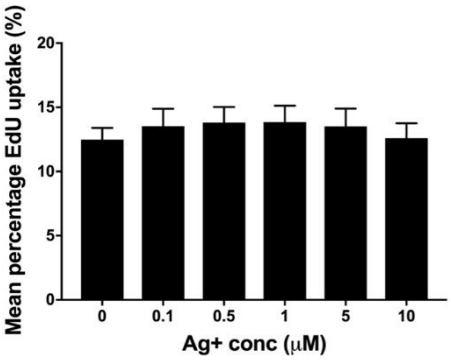

Differentiation - Culture expanded

Osteogenesis

Osteogenic differentiation in the presence of 10 µM Ag^+ for either the initial three days of culture (Ag^+ 10 µM (Day 0-3)) or for the entire differentiation period (Ag^+ 10 µM). ALP activity and DNA quantification were measured from cell lysates, providing normalised ALP. The results represent the mean ±SEM of triplicate measures.

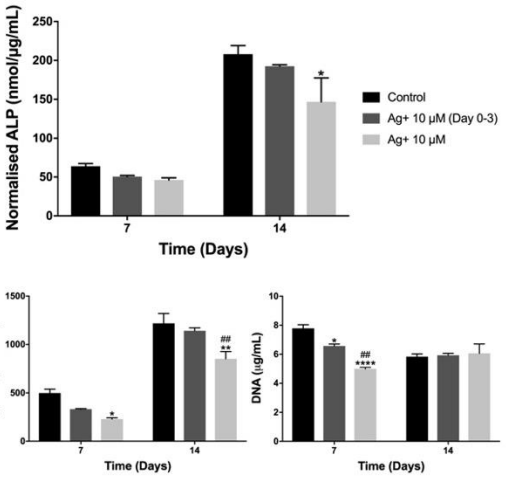

Adipogenesis

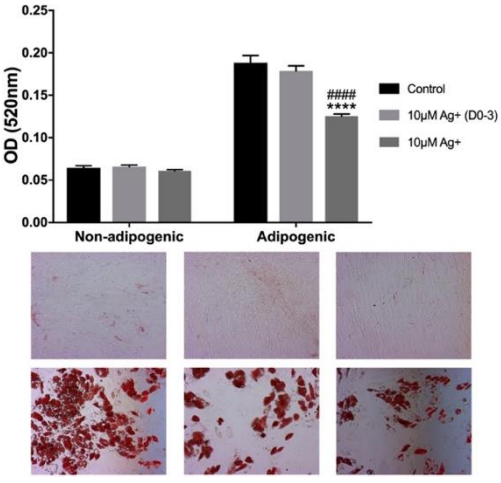

Differentiation - CFU-f expanded

Osteogenesis

Osteogenic differentiation of CFU-f derived MSCs expanded in the presence/absence of 10μM Ag^+ prior to differentiation (in Ag^+ free media). ALP activity and DNA quantification were measured from cell lysates, providing normalised ALP. The results represent the mean ±SEM of triplicate measures.
Check plate provides evidence of reduced CFU-f formation in presence of Ag^+.

CFU-f check plate

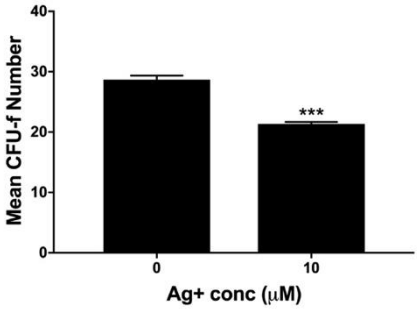

Data

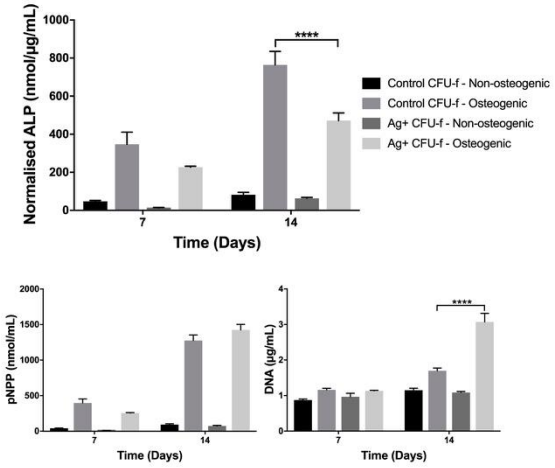

Adipogenesis

Adipogenic differentiation of CFU-f derived MSCs expanded in the presence/absence of 10μM Ag^+ prior to differentiation (in Ag^+ free media). Lipid bound Oil Red O was measured by optical density (520nm). The results represent the mean ±SEM of triplicate measures.
Check plate provides evidence of reduced CFU-f formation in presence of Ag^+.

CFU-f check plate

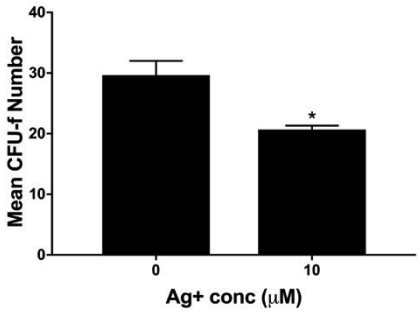

Data

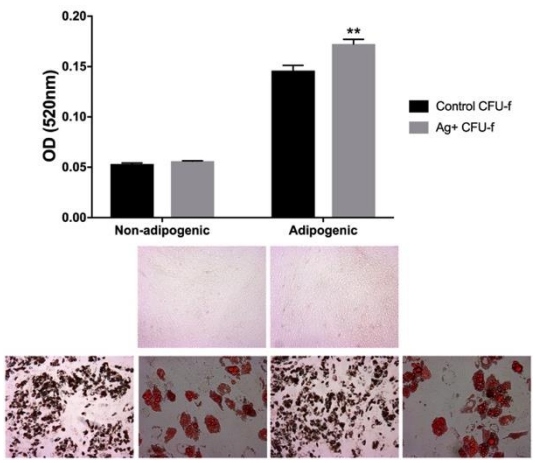

CFU-f formation

Characterisation of colony formation (CFU-f) of MSCs seeded at clonal density and cultured for the initial three days or continuously in the presence of ≤10 μM Ag^+. CFU-f number and total percentage CFU-f area presented as mean ±SEM of triplicate measures.

Day 0-3 Ag^+ exposure – CFU-f Number

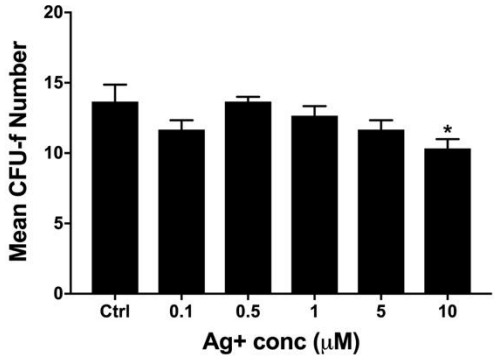

Day 0-3 Ag^+ exposure – CFU-f Area

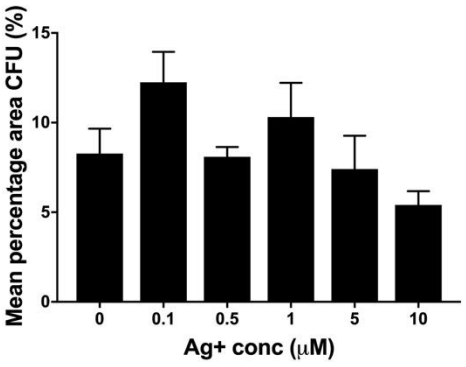

Continuous Ag^+ exposure –CFU-f Number

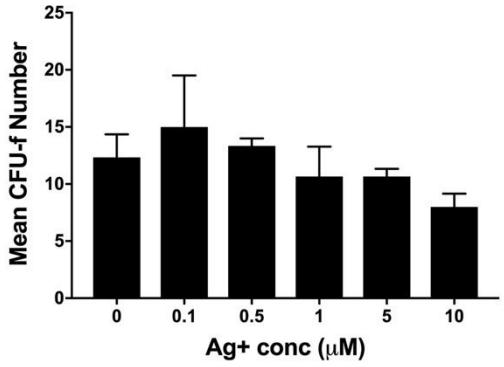

Continuous Ag^+ exposure – CFU-f Area

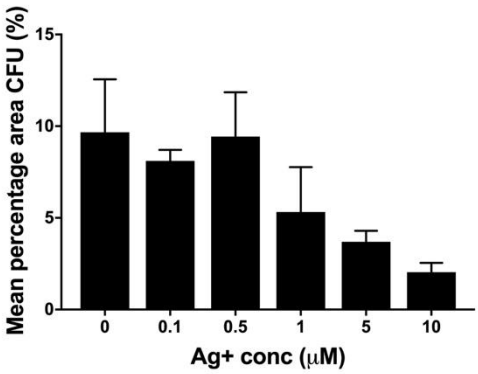

CFU-Ob formation – continuous Ag^+ exposure

Characterisation of alkaline phosphatase positive colony formation (CFU-Ob) of MSCs seeded at clonal density and cultured continuously in the presence of ≤10 μM Ag^+. CFU-Ob number and total percentage CFU-Ob area presented as mean ±SEM of triplicate measures.

CFU-Ob Number

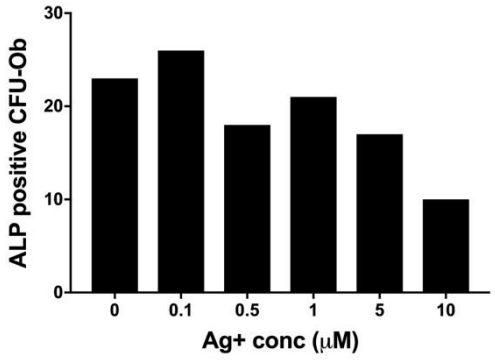

CFU-Ob Area

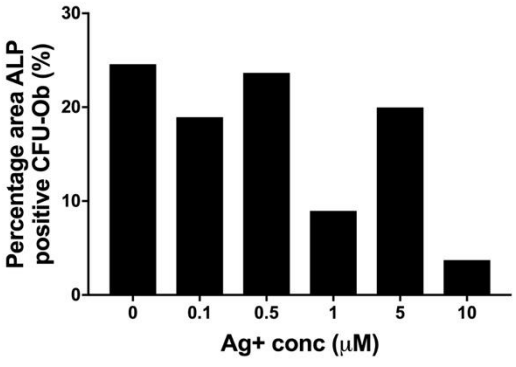

Determination of CFU-f survival and continued decrease in number following replating

CFU-f generation by MSCs during Stage 2 culture following pre-culture at clonal density. Ag^+ exposure during initial culture is represented on the x-axis with different Ag^+ exposures during Stage 2 displayed using individual bars, identified by the key. CFU-f number and CFU-f diameter presented as mean ±SEM of triplicate measures.

CFU-f Number

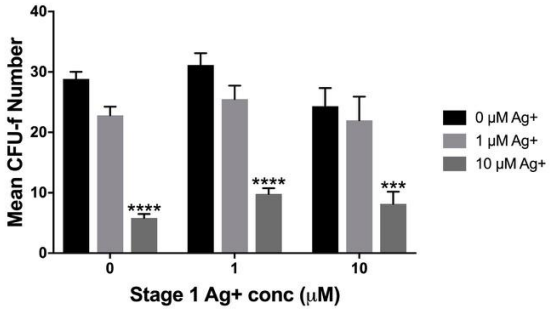

CFU-f Diameter (pixels)

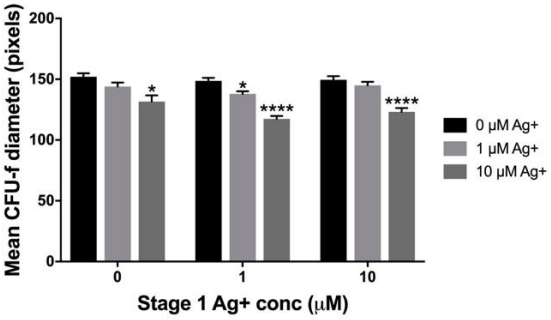

Conditioned media

N/A

qPCR – Oxidative stress pathway

Real-time PCR analysis of oxidative stress gene regulation associated with the response of primary MSCs cultured at clonal density in media containing 10 µM Ag^+.

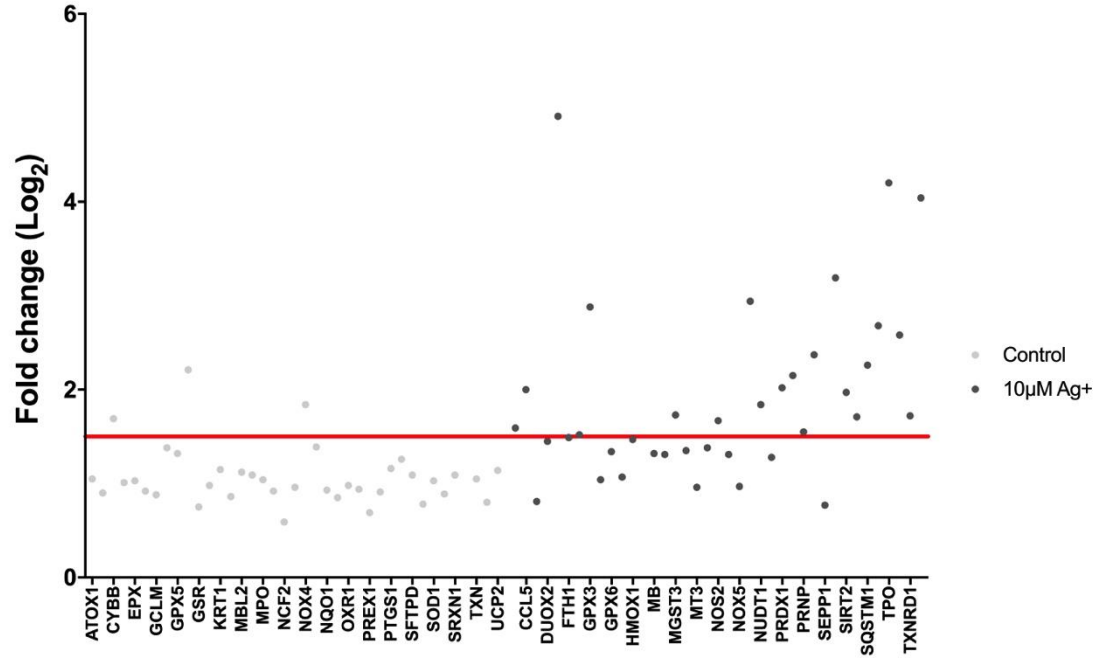

Proteomic analysis of CFU-f cultured in 10 µM Ag^+

N/A

Oxidative stress pathway inhibition

Potentiation of the Ag^+ induced ROS through addition of the thioredoxin inhibitor, PX-12 and the glutathione pathway inhibitor, BSO. Dose response of Ag^+ and BSO/PX-12. The results represent the mean CFU-f number ±SEM of triplicate measures.

Inhibition with PX-12

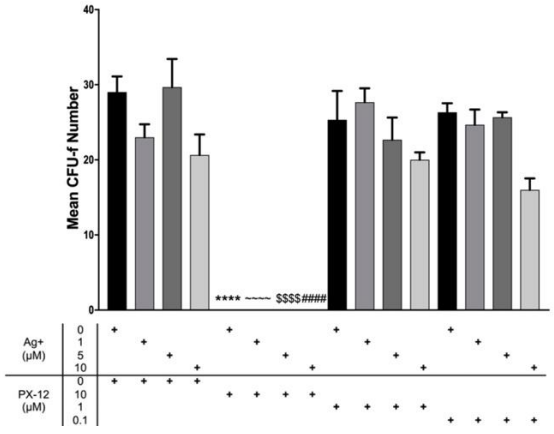

Inhibition with BSO

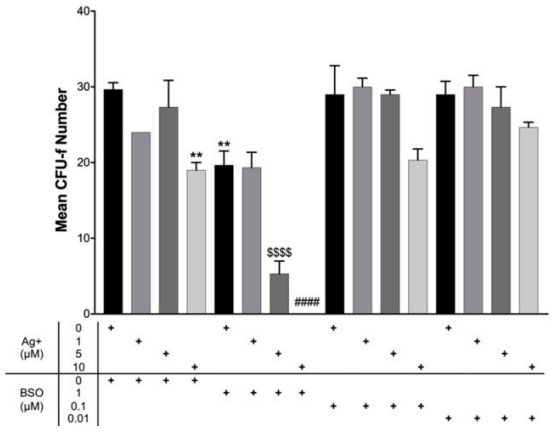

Recovery of CFU through addition of GSH-MEE

N/A

Wnt signalling pathway reduction in CFU-f expanded in 10 µM Ag^+

N/A

Donor ID: HS681

Gender - Female
Age at donation - 19 years old
Ethnicity - Hispanic
Tissue - Bone Marrow Aspirate

Cytotoxicity

WST-1	EdU Incorporation of EdU presented as the mean percentage of cells detected using a secondary fluorescent probe ±SEM, and represent data from fifteen images per Ag^+ concentration.
N/A	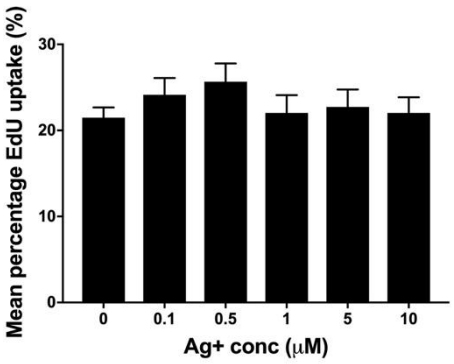

Differentiation - Culture expanded

Osteogenesis	Adipogenesis Adipogenic differentiation in the presence of 10 μM Ag^+ for either the initial three days of culture (10 μM Ag^+ (Day 0-3)) or for the entire differentiation period (10 μM Ag^+). Lipid bound Oil Red O was removed and measured by optical density (520nm). The results represent the mean OD_{520} ±SEM of triplicate measures.
N/A	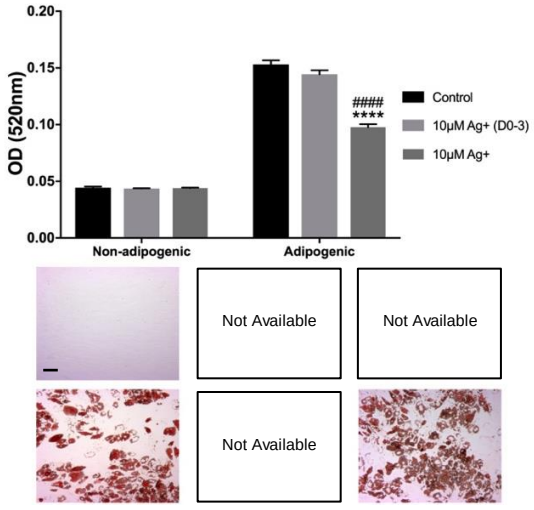

Differentiation - CFU-f expanded

Osteogenesis CFU-f check plate N/A	Adipogenesis CFU-f check plate N/A

CFU-f formation

Characterisation of colony formation (CFU-f) of MSCs seeded at clonal density and cultured for the initial three days or continuously in the presence of ≤10 μM Ag^+. CFU-f number and total percentage CFU-f area presented as mean ±SEM of triplicate measures.

Day 0-3 Ag^+ exposure – CFU-f Number	Day 0-3 Ag^+ exposure – CFU-f Area
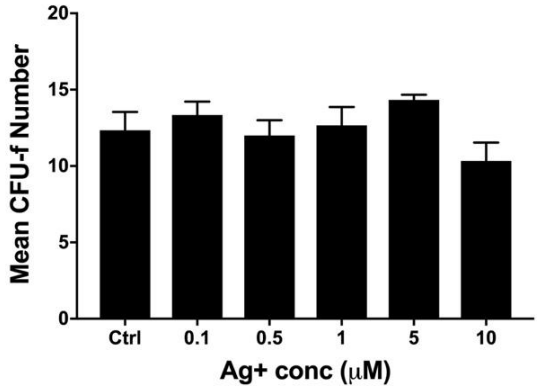	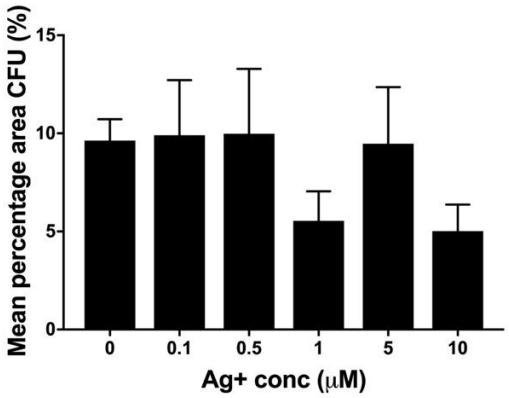
Continuous Ag^+ exposure –CFU-f Number	Continuous Ag^+ exposure – CFU-f Area
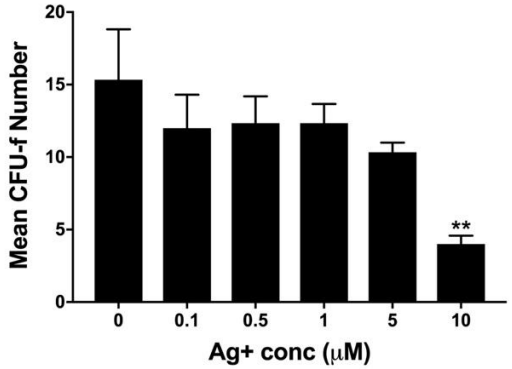	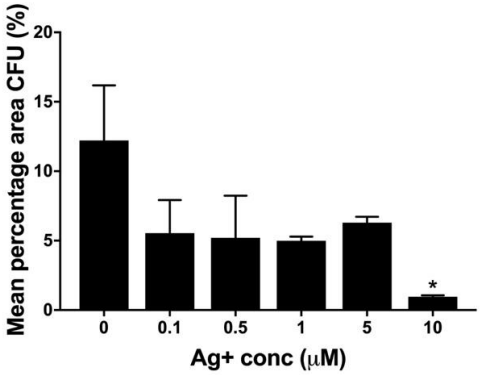

CFU-Ob formation – continuous Ag^+ exposure

CFU-Ob Number	CFU-Ob Area
N/A	N/A

Determination of CFU-f survival and continued decrease in number following replating

CFU-f Number	CFU-f Diameter (pixels)
N/A	N/A

Conditioned media

N/A

qPCR – Oxidative stress pathway

N/A

Proteomic analysis of CFU-f cultured in 10 μM Ag^+

N/A

Oxidative stress pathway inhibition

Inhibition with PX-12	Inhibition with BSO
N/A	N/A

Recovery of CFU through addition of GSH-MEE

N/A

Wnt signalling pathway reduction in CFU-f expanded in 10 μM Ag^+

N/A

Donor ID: HS726

Gender - Female
Age at donation - 32 years old
Ethnicity - Asian
Tissue - Bone Marrow Aspirate

Cytotoxicity

WST-1	EdU
N/A	N/A

Differentiation - Culture expanded

Osteogenesis	Adipogenesis
N/A	N/A

Differentiation - CFU-f expanded

Osteogenesis	Adipogenesis
CFU-f check plate	CFU-f check plate
N/A	N/A

CFU-f formation

Day 0-3 Ag^+ exposure – CFU-f Number	Day 0-3 Ag^+ exposure – CFU-f Area
N/A	N/A

Continuous Ag^+ exposure –CFU-f Number	Continuous Ag^+ exposure – CFU-f Area
N/A	N/A

CFU-Ob formation – continuous Ag^+ exposure

CFU-Ob Number	CFU-Ob Area
N/A	N/A

Determination of CFU-f survival and continued decrease in number following replating

CFU-f generation by MSCs during Stage 2 culture following pre-culture at clonal density. Ag^+ exposure during initial culture is represented on the x-axis with different Ag^+ exposures during Stage 2 displayed using individual bars, identified by the key. CFU-f number and CFU-f diameter presented as mean ±SEM of triplicate measures.

CFU-f Number

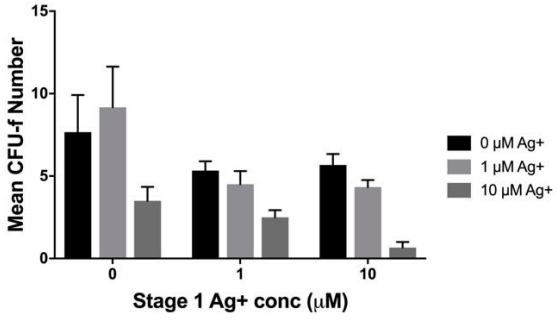

CFU-f Diameter (pixels)

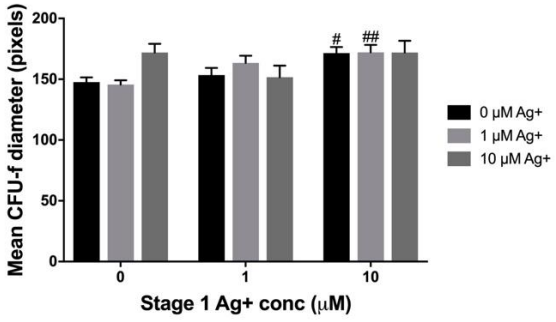

Conditioned media

N/A

qPCR – Oxidative stress pathway

N/A

Proteomic analysis of CFU-f cultured in 10 μM Ag^+

N/A

Oxidative stress pathway inhibition

Potentiation of the Ag^+ induced ROS through addition of the thioredoxin inhibitor, PX-12 and the glutathione pathway inhibitor, BSO. Dose response of Ag^+ and BSO/PX-12. The results represent the mean CFU-f number ±SEM of triplicate measures.

Inhibition with PX-12

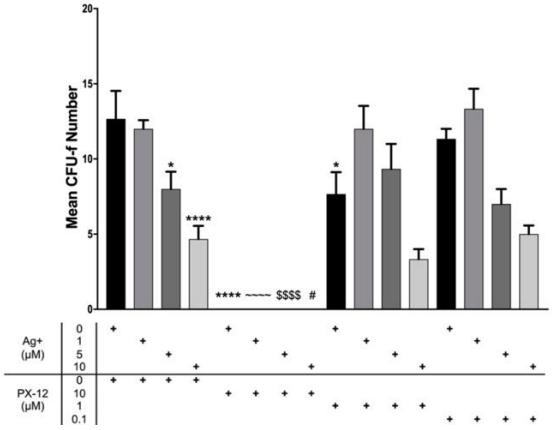

Inhibition with BSO

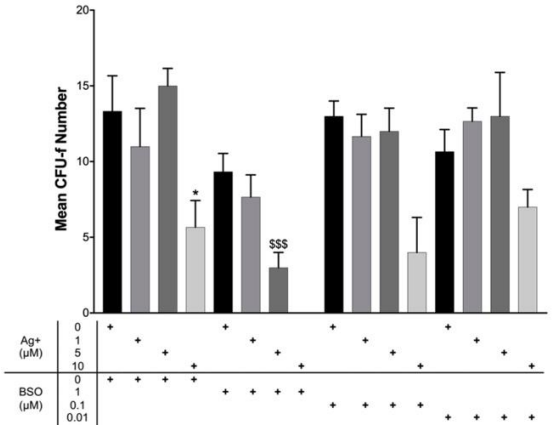

Recovery of CFU through addition of GSH-MEE

N/A

Wnt signalling pathway reduction in CFU-f expanded in 10 μM Ag^+

N/A

Donor ID: HS729

Gender - Female
Age at donation - 20 years old
Ethnicity - Unknown
Tissue - Bone Marrow Aspirate

Cytotoxicity

WST-1	EdU
N/A	Incorporation of EdU presented as the mean percentage of cells detected using a secondary fluorescent probe ±SEM, and represent data from fifteen images per Ag^+ concentration. 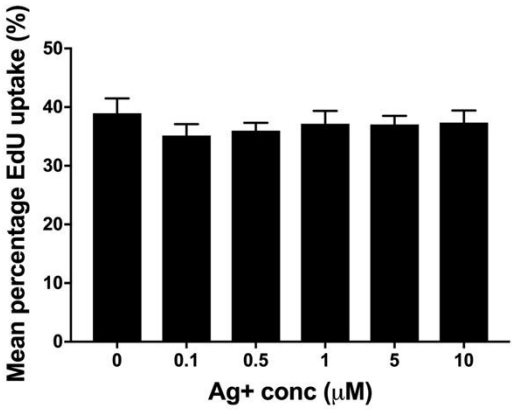

Differentiation - Culture expanded

Osteogenesis	Adipogenesis
Osteogenic differentiation in the presence of 10 µM Ag^+ for either the initial three days of culture (Ag^+ 10 µM (Day 0-3)) or for the entire differentiation period (Ag^+ 10 µM). ALP activity and DNA quantification were measured from cell lysates, providing normalised ALP. The results represent the mean ±SEM of triplicate measures. 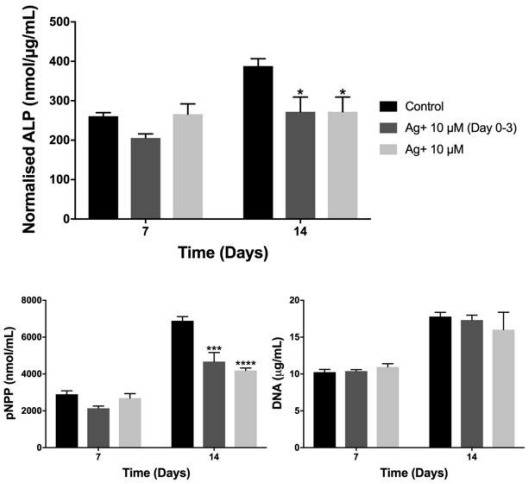	N/A

Differentiation - CFU-f expanded

Osteogenesis	Adipogenesis
N/A	N/A

CFU-f formation

Characterisation of colony formation (CFU-f) of MSCs seeded at clonal density and cultured for the initial three days or continuously in the presence of ≤10 μM Ag^+. CFU-f number and total percentage CFU-f area presented as mean ±SEM of triplicate measures.

Day 0-3 Ag^+ exposure – CFU-f Number

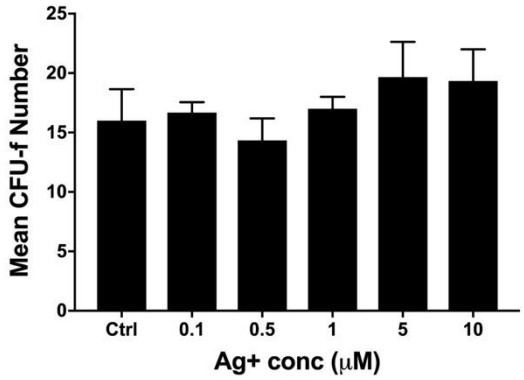

Day 0-3 Ag^+ exposure – CFU-f Area

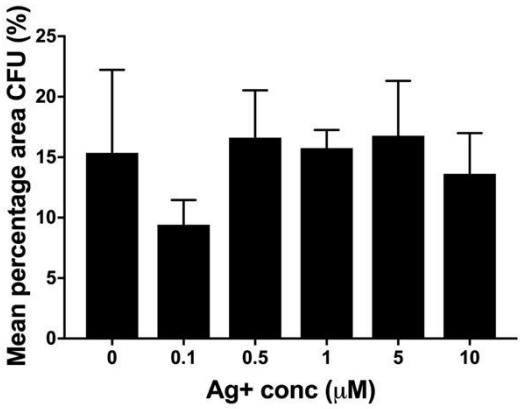

Continuous Ag^+ exposure –CFU-f Number

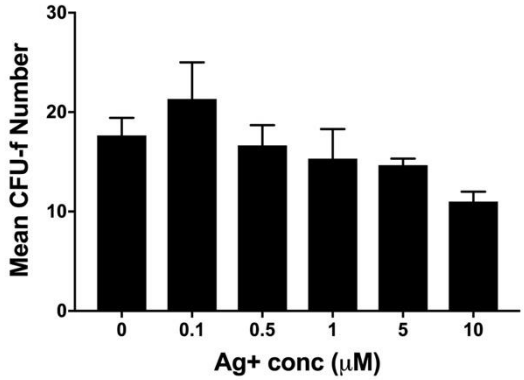

Continuous Ag^+ exposure – CFU-f Area

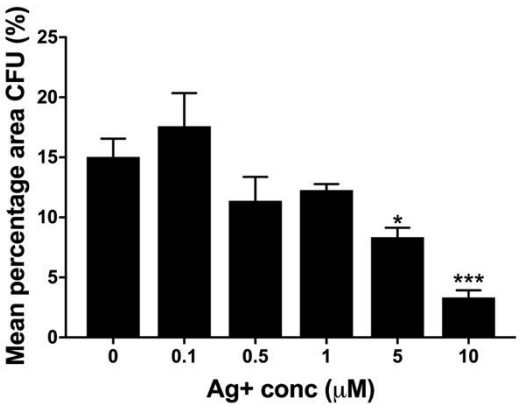

CFU-Ob formation – continuous Ag^+ exposure

Characterisation of alkaline phosphatase positive colony formation (CFU-Ob) of MSCs seeded at clonal density and cultured continuously in the presence of ≤10 μM Ag^+. CFU-Ob number and total percentage CFU-Ob area presented as mean ±SEM of triplicate measures.

CFU-Ob Number

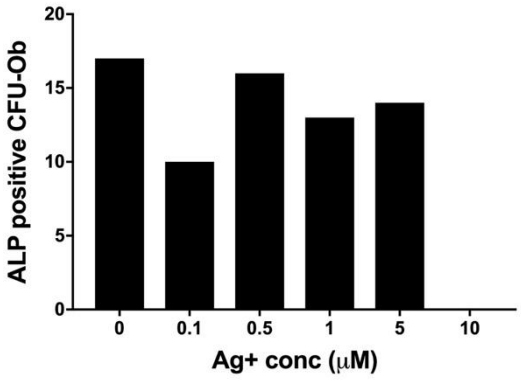

CFU-Ob Area

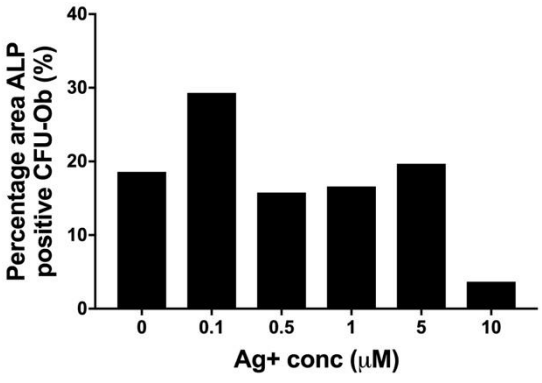

Determination of CFU-f survival and continued decrease in number following replating

CFU-f Number	CFU-f Diameter (pixels)
N/A	N/A

Conditioned media

Characterisation of colony formation (CFU-f) of MSCs seeded at clonal density and cultured in the absence/presence of 10 μM Ag^+ applied in normal or conditioned media. CFU-f number presented as mean ±SEM of triplicate measures.

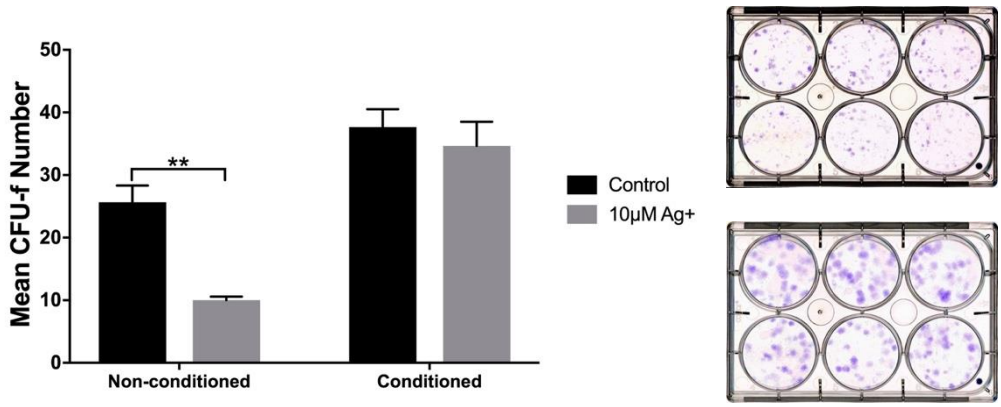

qPCR – Oxidative stress pathway

Real-time PCR analysis of oxidative stress gene regulation associated with the response of primary MSCs cultured at clonal density in media containing 10 μM Ag^+.

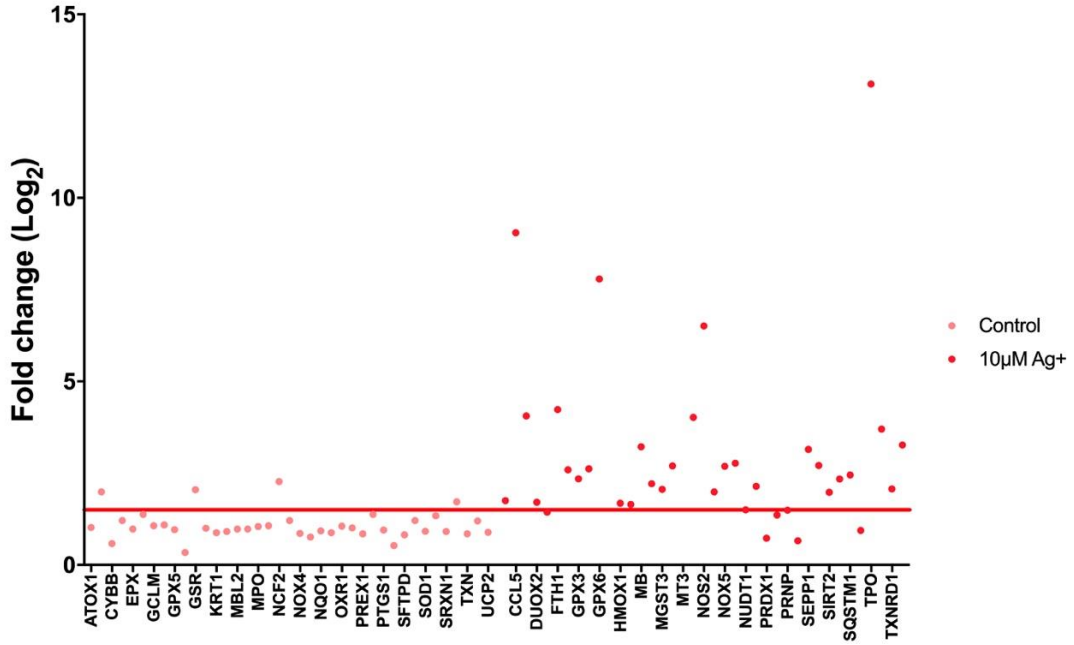

Proteomic analysis of CFU-f cultured in 10 μM Ag^+

N/A

Oxidative stress pathway inhibition

Inhibition of thioredoxin with PX-12	Inhibition glutathione synthesis with BSO
N/A	N/A

Recovery of CFU through addition of GSH-MEE

Mean CFU-f number of MSCs treated with a combination of 10 µM Ag^+, the glutathione pathway inhibitor, BSO, and 2 mM GSH-MEE.

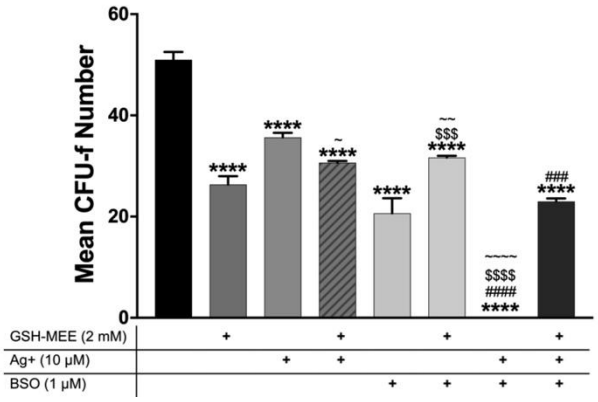

Wnt signalling pathway reduction in CFU-f expanded in 10 µM Ag^+

N/A

Donor ID: HS738

Gender - Male
Age at donation - 18 years old
Ethnicity - Hispanic
Tissue - Bone Marrow Aspirate

Cytotoxicity

WST-1	EdU
N/A	N/A

Differentiation - Culture expanded

Osteogenesis	Adipogenesis
	Adipogenic differentiation in the presence of 10 µM Ag^+ for either the initial three days of culture (10 µM Ag^+ (Day 0-3)) or for the entire differentiation period (10 µM Ag^+). Lipid bound Oil Red O was removed and measured by optical density (520nm). The results represent the mean OD_{520} ±SEM of triplicate measures.
N/A	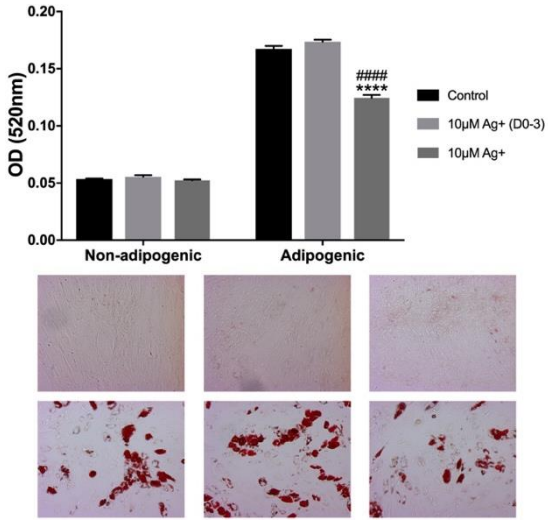

Differentiation - CFU-f expanded

Osteogenesis	Adipogenesis
Osteogenic differentiation of CFU-f derived MSCs expanded in the presence/absence of 10µM Ag^+ prior to differentiation (in Ag^+ free media). ALP activity and DNA quantification were measured from cell lysates, providing normalised ALP. The results represent the mean ±SEM of triplicate measures. Check plate provides evidence of reduced CFU-f formation in presence of Ag^+.	Adipogenic differentiation of CFU-f derived MSCs expanded in the presence/absence of 10µM Ag^+ prior to differentiation (in Ag^+ free media). Lipid bound Oil Red O was measured by optical density (520nm). The results represent the mean ±SEM of triplicate measures. Check plate provides evidence of reduced CFU-f formation in presence of Ag^+.
CFU-f check plate	CFU-f check plate
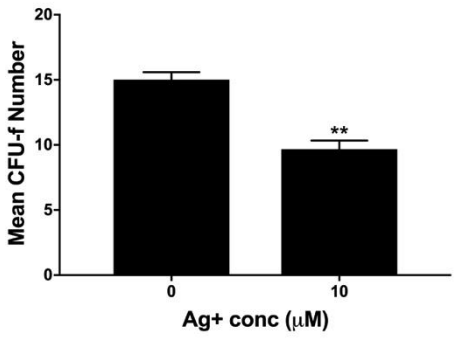	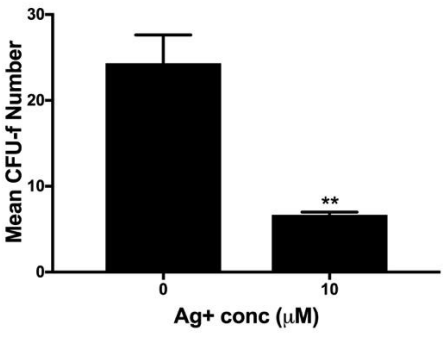

Data

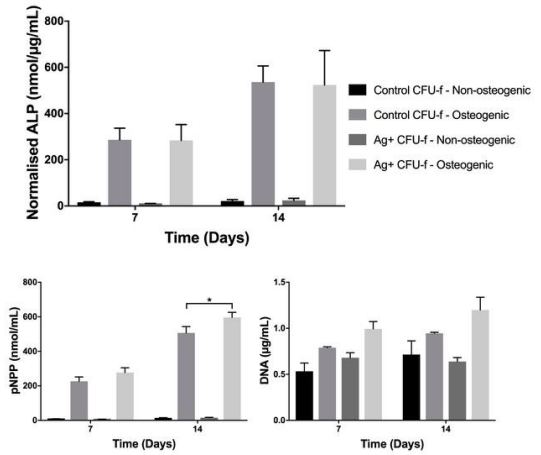

Data

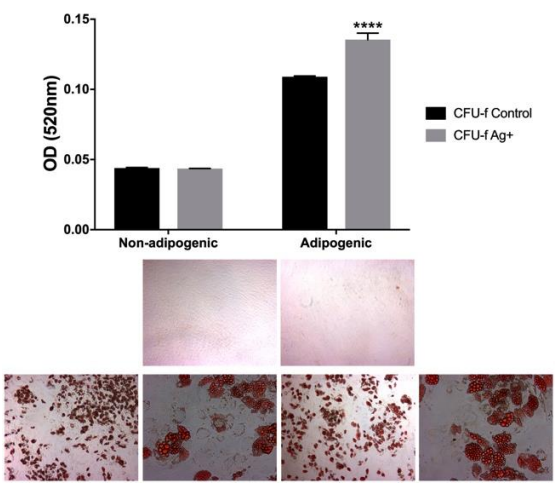

CFU-f formation

Day 0-3 Ag^+ exposure – CFU-f Number	Day 0-3 Ag^+ exposure – CFU-f Area
N/A	N/A
Continuous Ag^+ exposure –CFU-f Number	Continuous Ag^+ exposure – CFU-f Area
N/A	N/A

CFU-Ob formation – continuous Ag^+ exposure

Characterisation of alkaline phosphatase positive colony formation (CFU-Ob) of MSCs seeded at clonal density and cultured continuously in the presence of ≤10 μM Ag^+. CFU-Ob number and total percentage CFU-Ob area presented as mean ±SEM of triplicate measures.

CFU-Ob Number

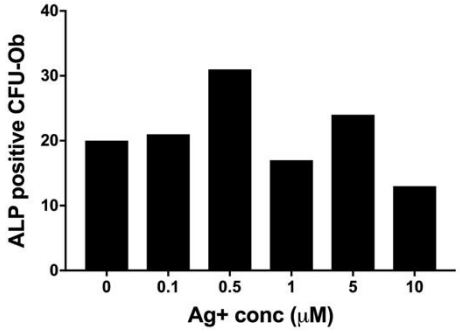

CFU-Ob Area

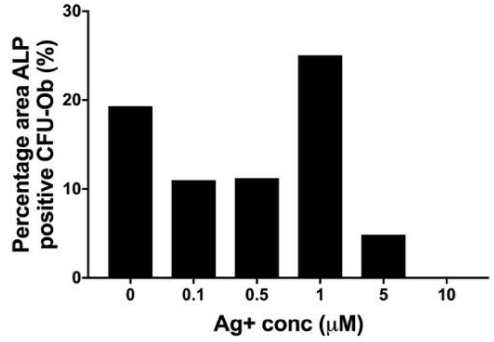

Determination of CFU-f survival and continued decrease in number following replating

CFU-f generation by MSCs during Stage 2 culture following pre-culture at clonal density. Ag^+ exposure during initial culture is represented on the x-axis with different Ag^+ exposures during Stage 2 displayed using individual bars, identified by the key. CFU-f number and CFU-f diameter presented as mean ±SEM of triplicate measures.

CFU-f Number

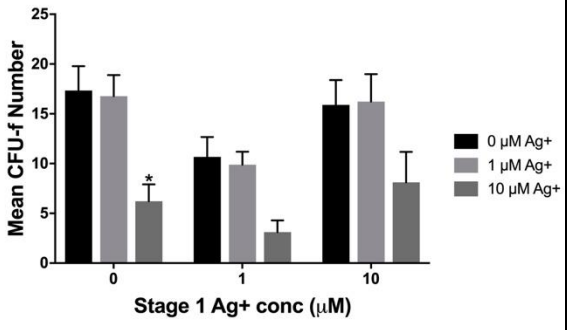

CFU-f Diameter (pixels)

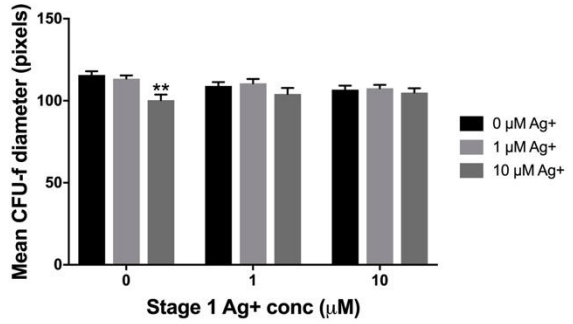

Conditioned media

Characterisation of colony formation (CFU-f) of MSCs seeded at clonal density and cultured in the absence/presence of 10 µM Ag^+ applied in normal or conditioned media. CFU-f number presented as mean ±SEM of triplicate measures.

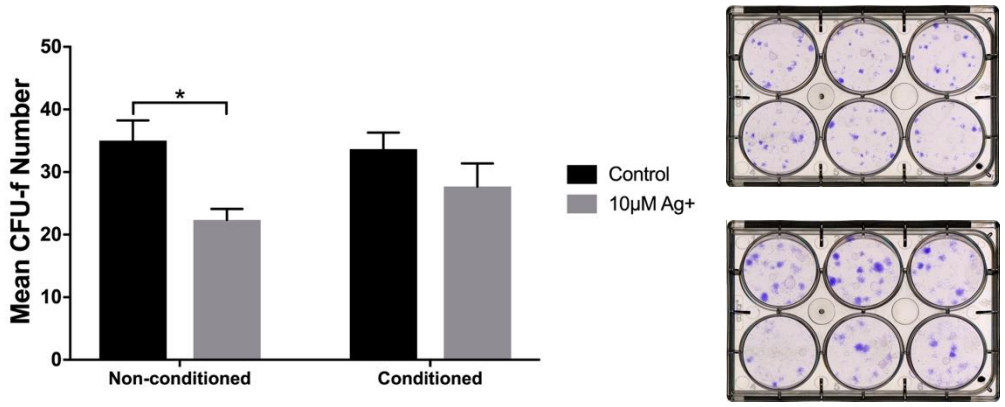

qPCR – Oxidative stress pathway

N/A

Proteomic analysis of CFU-f cultured in 10 µM Ag^+

N/A

Oxidative stress pathway inhibition

Inhibition with PX-12	Inhibition with BSO
N/A	N/A

Recovery of CFU through addition of GSH-MEE

Mean CFU-f number of MSCs treated with a combination of 10 µM Ag^+, the glutathione pathway inhibitor, BSO, and 2 mM GSH-MEE.

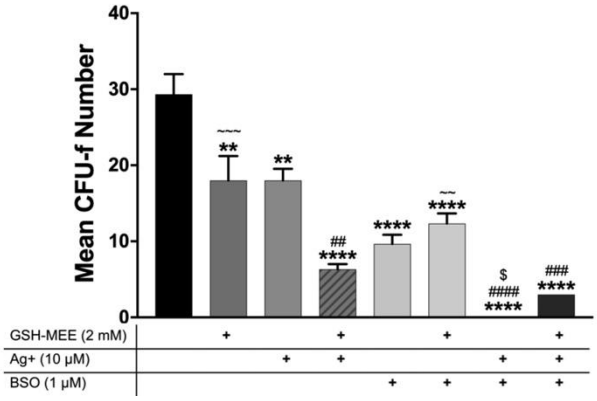

Wnt signalling pathway reduction in CFU-f expanded in 10 µM Ag^+

N/A

Donor ID: HS739

Gender - Male
Age at donation - 38 years old
Ethnicity - Hispanic
Tissue - Bone Marrow Aspirate

Cytotoxicity

WST-1

Viability of MSCs as a percentage of untreated control determined via WST-1 conversion. EC_{50} value of 33.93 µM. Results are plotted as mean percentage viability ±SEM and represent triplicate measurements.

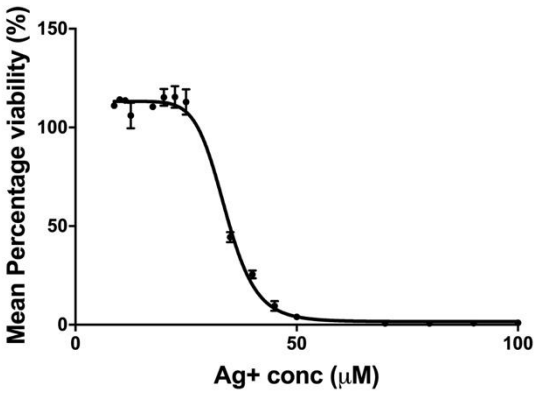

EdU

N/A

Differentiation - Culture expanded

Osteogenesis

Osteogenic differentiation in the presence of 10 µM Ag^+ for either the initial three days of culture (Ag^+ 10 µM (Day 0-3)) or for the entire differentiation period (Ag^+ 10 µM). ALP activity and DNA quantification were measured from cell lysates, providing normalised ALP. The results represent the mean ±SEM of triplicate measures.

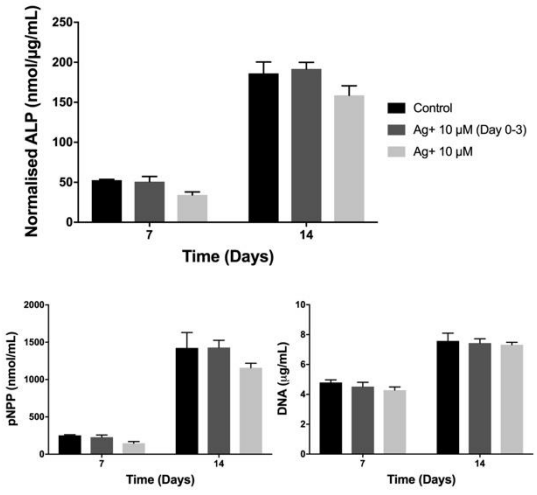

Adipogenesis

Adipogenic differentiation in the presence of 10 µM Ag^+ for either the initial three days of culture (10 µM Ag^+ (Day 0-3)) or for the entire differentiation period (10 µM Ag^+). Lipid bound Oil Red O was removed and measured by optical density (520nm). The results represent the mean OD_{520} ±SEM of triplicate measures.

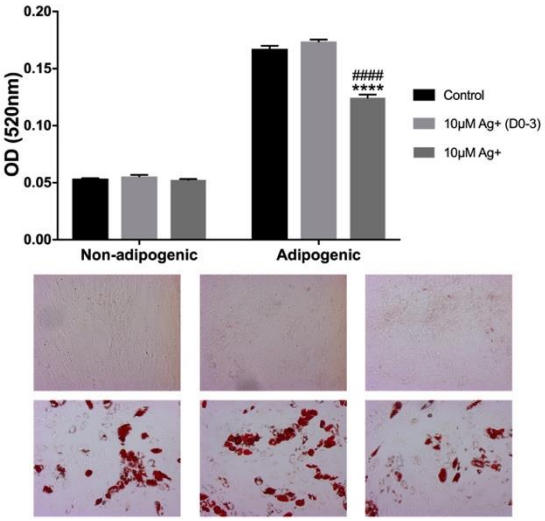

Differentiation - CFU-f expanded

Osteogenesis

Osteogenic differentiation of CFU-f derived MSCs expanded in the presence/absence of 10μM Ag^+ prior to differentiation (in Ag^+ free media). ALP activity and DNA quantification were measured from cell lysates, providing normalised ALP. The results represent the mean ±SEM of triplicate measures.
Check plate provides evidence of reduced CFU-f formation in presence of Ag^+.

CFU-f check plate

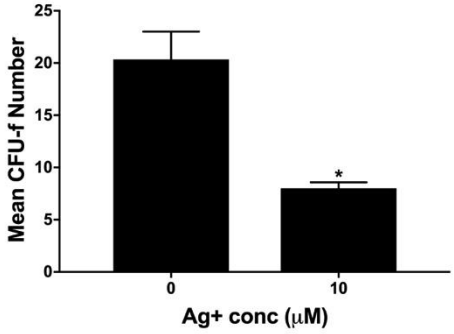

Data

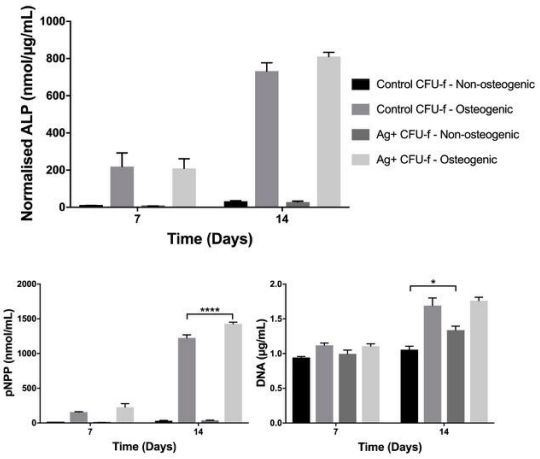

Adipogenesis

Adipogenic differentiation of CFU-f derived MSCs expanded in the presence/absence of 10μM Ag^+ prior to differentiation (in Ag^+ free media). Lipid bound Oil Red O was measured by optical density (520nm). The results represent the mean ±SEM of triplicate measures.
Check plate provides evidence of reduced CFU-f formation in presence of Ag^+.

CFU-f check plate

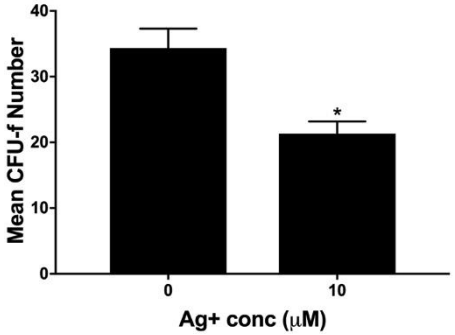

Data

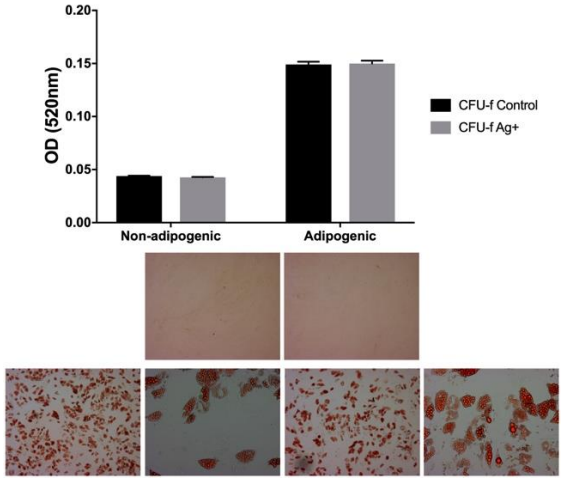

CFU-f formation

Day 0-3 Ag^+ exposure – CFU-f Number N/A	Day 0-3 Ag^+ exposure – CFU-f Area N/A
Continuous Ag^+ exposure –CFU-f Number N/A	Continuous Ag^+ exposure – CFU-f Area N/A

CFU-Ob formation – continuous Ag^+ exposure

CFU-Ob Number N/A	CFU-Ob Area N/A

Determination of CFU-f survival and continued decrease in number following replating

CFU-f Number N/A	CFU-f Diameter (pixels) N/A

Conditioned media

Characterisation of colony formation (CFU-f) of MSCs seeded at clonal density and cultured in the absence/presence of 10 μM Ag^+ applied in normal or conditioned media. CFU-f number presented as mean ±SEM of triplicate measures.

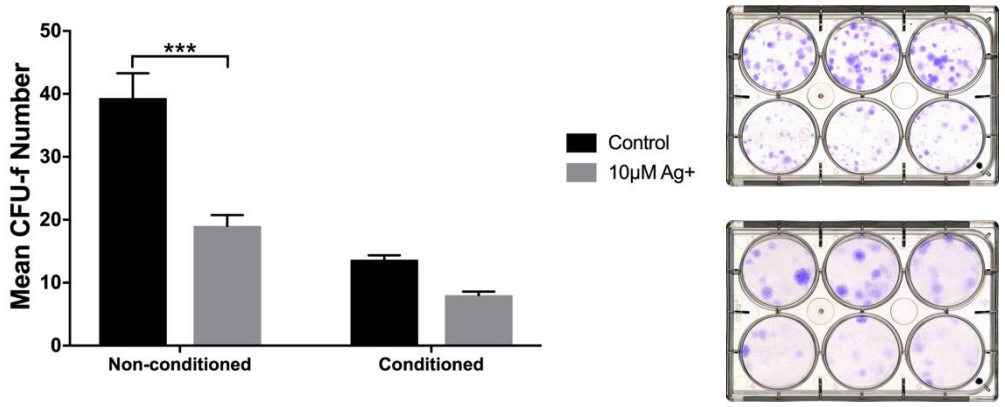

qPCR – Oxidative stress pathway

Real-time PCR analysis of oxidative stress gene regulation associated with the response of primary MSCs cultured at clonal density in media containing 10 μM Ag^+.

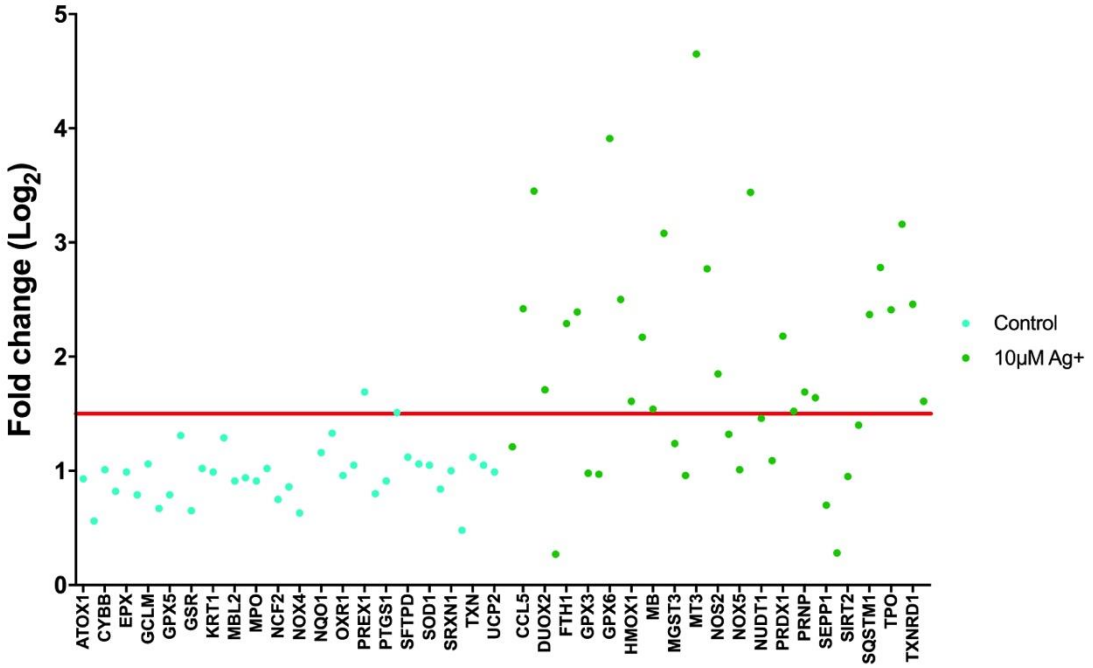

Proteomic analysis of CFU-f cultured in 10 μM Ag^+

N/A

Oxidative stress pathway inhibition

Potentiation of the Ag^+ induced ROS through addition of the thioredoxin inhibitor, PX-12 and the glutathione pathway inhibitor, BSO. Dose response of Ag^+ and BSO/PX-12. The results represent the mean CFU-f number ±SEM of triplicate measures.

Inhibition with PX-12

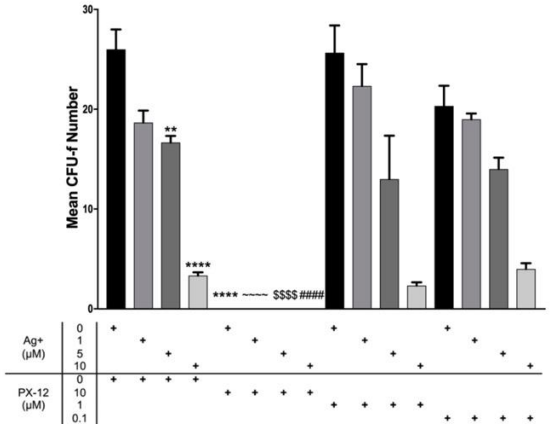

Inhibition with BSO

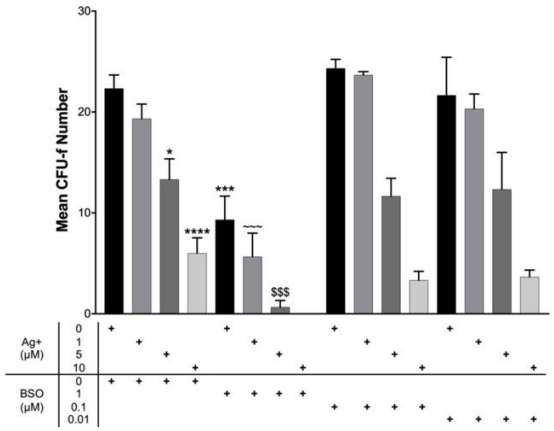

Recovery of CFU through addition of GSH-MEE

Mean CFU-f number of MSCs treated with a combination of 10 μM Ag^+, the glutathione pathway inhibitor, BSO, and 2 mM GSH-MEE.

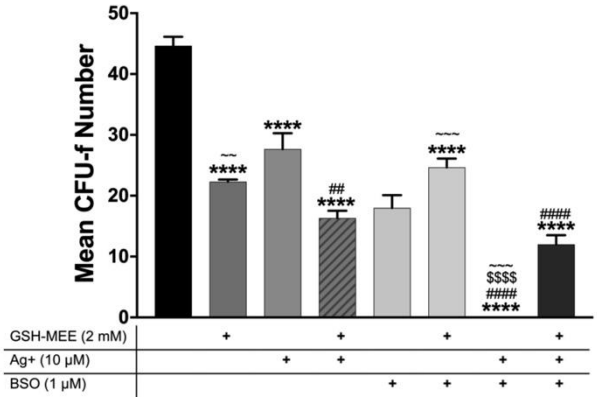

Wnt signalling pathway reduction in CFU-f expanded in 10 μM Ag^+

N/A

Donor ID: K224

Gender - Female
Age at donation - 74 years old
Ethnicity - N/A
Tissue - Bone from knee arthroplasty

Cytotoxicity	
WST-1 Viability of MSCs as a percentage of untreated control determined via WST-1 conversion. EC_{50} value of 32.42 µM. Results are plotted as mean percentage viability ±SEM and represent triplicate measurements. 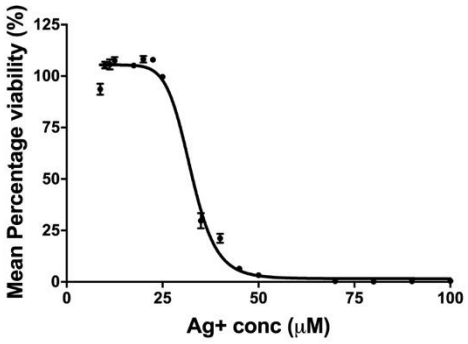 	EdU N/A

Differentiation - Culture expanded	
Osteogenesis	Adipogenesis

Differentiation - CFU-f expanded	
Osteogenesis CFU-f check plate	Adipogenesis CFU-f check plate

CFU-f formation	
Day 0-3 Ag^+ exposure – CFU-f Number N/A	Day 0-3 Ag^+ exposure – CFU-f Area N/A
Continuous Ag^+ exposure –CFU-f Number N/A	Continuous Ag^+ exposure – CFU-f Area N/A

CFU-Ob formation – continuous Ag^+ exposure	
CFU-Ob Number N/A	CFU-Ob Area N/A

Determination of CFU-f survival and continued decrease in number following replating	
CFU-f Number N/A	CFU-f Diameter (pixels) N/A

Conditioned media	
N/A	

qPCR – Oxidative stress pathway
N/A

Proteomic analysis of CFU-f cultured in 10 µM Ag^+
N/A

Oxidative stress pathway inhibition

Inhibition with PX-12	Inhibition with BSO
N/A	N/A

Recovery of CFU through addition of GSH-MEE

N/A

Wnt signalling pathway reduction in CFU-f expanded in 10 µM Ag^+

N/A

Donor ID: Y201 (and GFP-Y201)

Gender - N/A
Age at donation - N/A
Ethnicity - N/A
Tissue - N/A

Cytotoxicity

WST-1	EdU
N/A	N/A

Differentiation - Culture expanded

Osteogenesis	Adipogenesis
N/A	N/A

Differentiation - CFU-f expanded

Osteogenesis	Adipogenesis
N/A	N/A

CFU-f formation

Characterisation of colony formation (CFU-f) of MSCs seeded at clonal density and cultured for the initial three days or continuously in the presence of ≤10 μM Ag^+. CFU-f number and total percentage CFU-f area presented as mean ±SEM of triplicate measures.

Day 0-3 Ag^+ exposure – CFU-f Number	Day 0-3 Ag^+ exposure – CFU-f Area
N/A	N/A
Continuous Ag^+ exposure –CFU-f Number	Continuous Ag^+ exposure – CFU-f Area

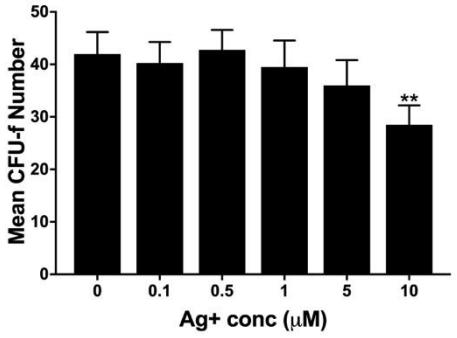

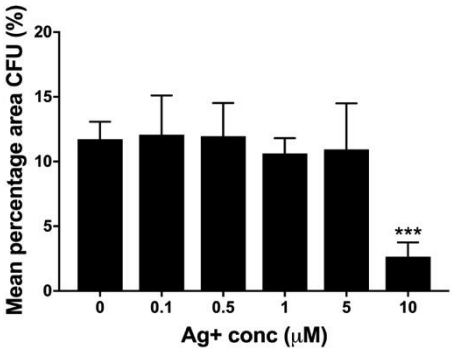

CFU-Ob formation – continuous Ag^+ exposure

CFU-Ob Number	CFU-Ob Area
N/A	N/A

Determination of CFU-f survival and continued decrease in number following replating

CFU-f Number	CFU-f Diameter (pixels)
N/A	N/A

Conditioned media

Characterisation of colony formation (CFU-f) of MSCs seeded at clonal density and cultured in the absence/presence of 10 μM Ag^+ applied in normal or conditioned media. CFU-f number presented as mean ±SEM of triplicate measures.

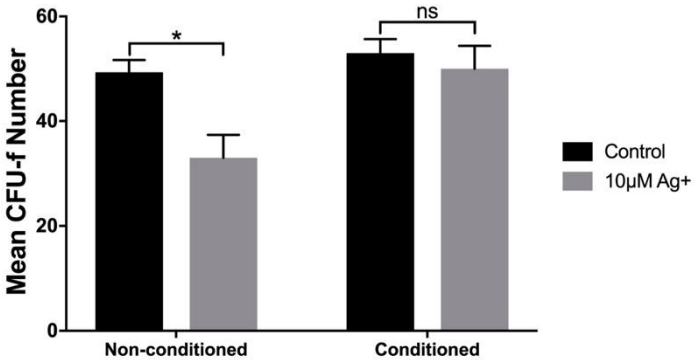

qPCR – Oxidative stress pathway

N/A

Proteomic analysis of CFU-f cultured in 10 μM Ag^+

Proteomic identification and fold-change of proteins in Ag^+ and control CFU-f (Y201). Representations of protein fold-changes (< -0.5 - >0.5) following Ag^+ treatment. Less than 0.5-fold increase/decrease determined as 'No change'.

Volcano plot of proteomic data for control and Ag^+ treated CFU-f (Y201).

Proteomic identification of 5050 proteins illustrated according to statistical significance. 15.19% of proteins were significantly differentially regulated assuming a q-value of <0.05 (orange), reducing to 2.17% (green) when allowing for correction (Benjamini & Hochberg).

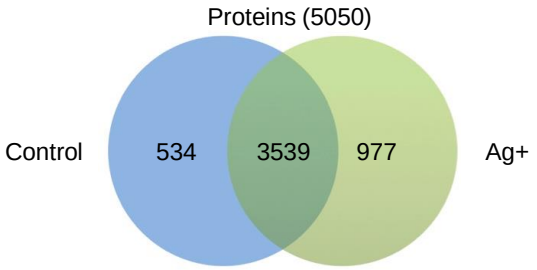

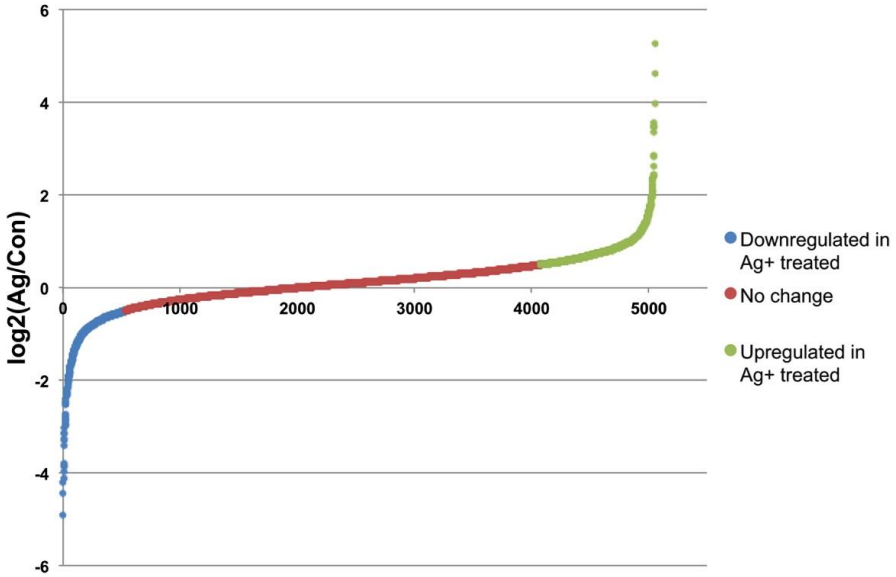

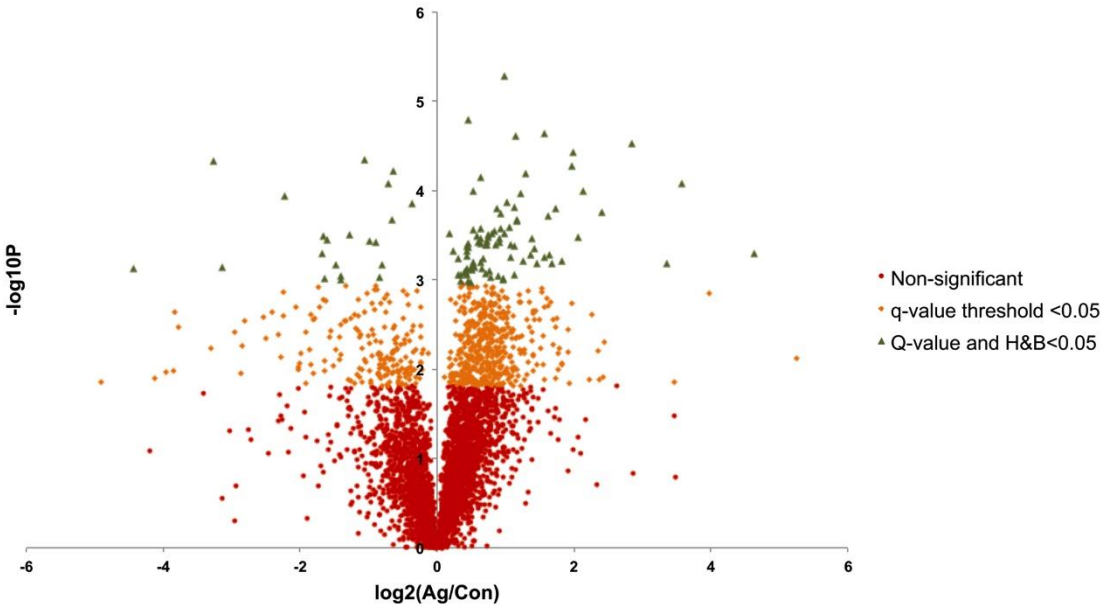

Oxidative stress pathway inhibition

Inhibition with PX-12	Inhibition with BSO
N/A	N/A

Recovery of CFU through addition of GSH-MEE

N/A	

Wnt signalling pathway reduction in CFU-f expanded in 10 µM Ag^+

Response of GFP-Y201 MSCs to Wnt3a following expansion as CFU-f in the presence/absence of 10µM Ag^+ assessed via GFP production. GFP activity and protein quantification were measured from cell lysates, providing normalised GFP. The results represent the mean ±SEM of triplicate measures.
Check plate provides evidence of reduced CFU-f formation in presence of Ag^+.

CFU-f check plate

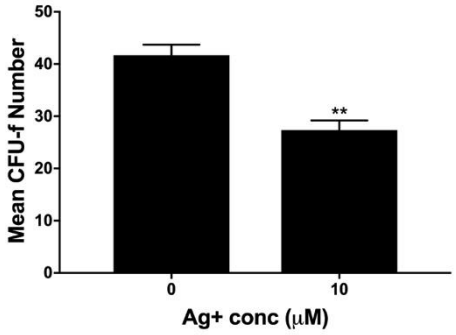

Data

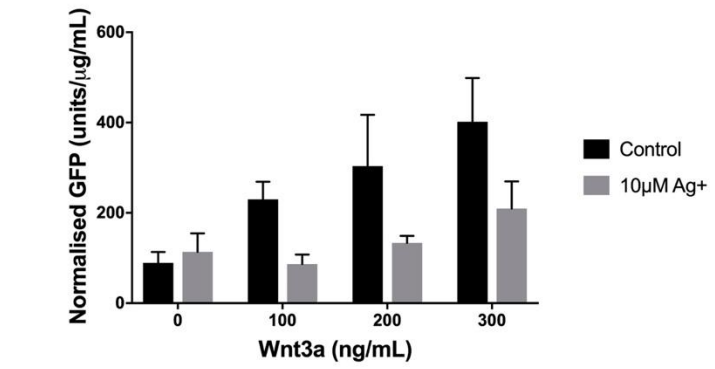

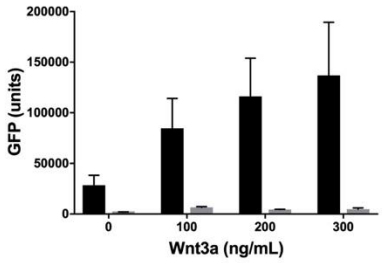

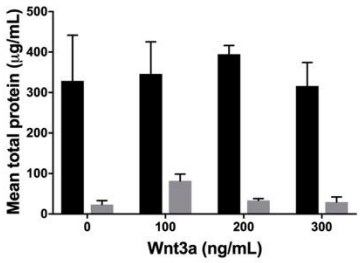

Donor ID: HeLa

Positive control culture for antibody identification of GCLM and TRX.

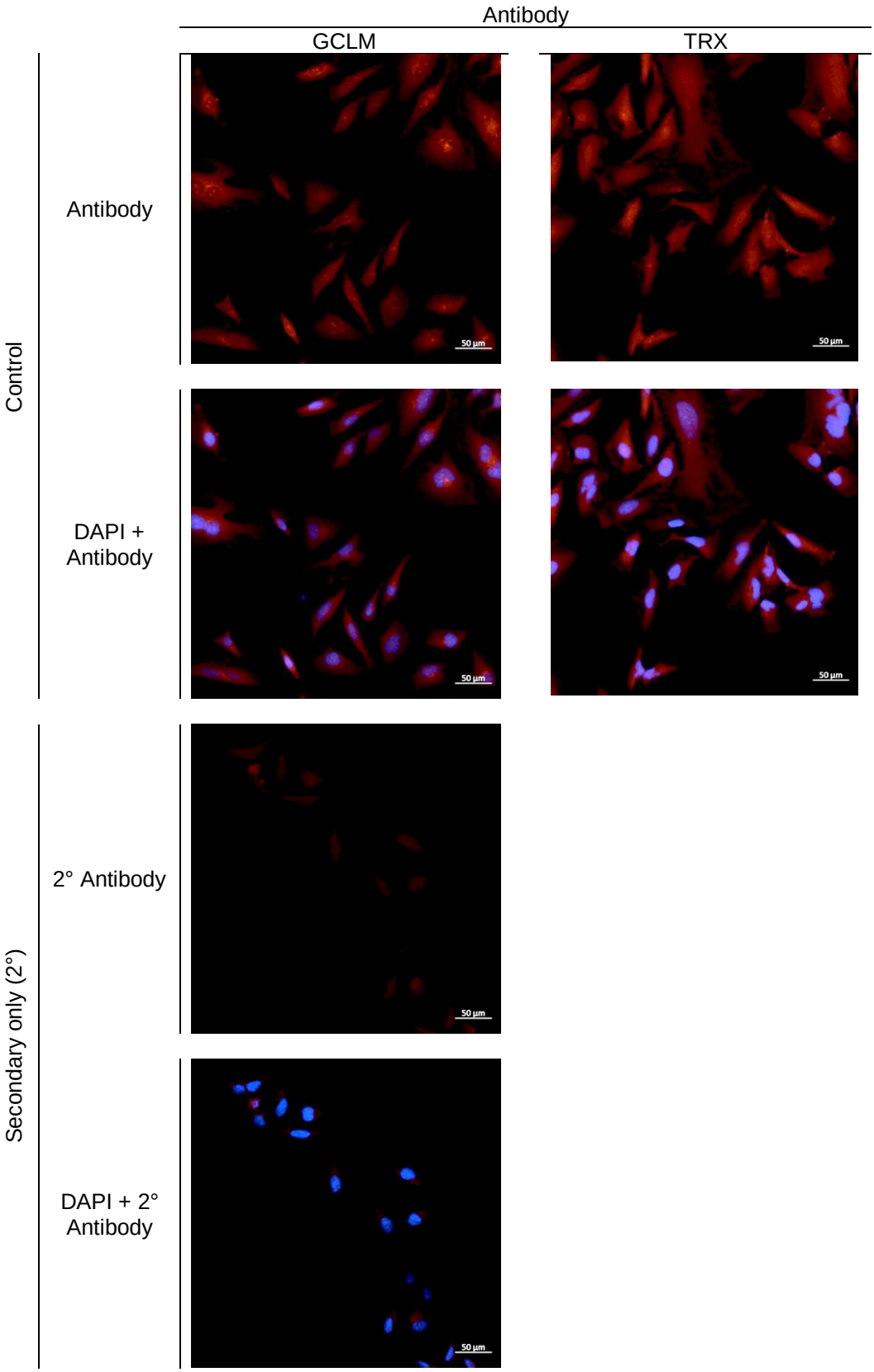

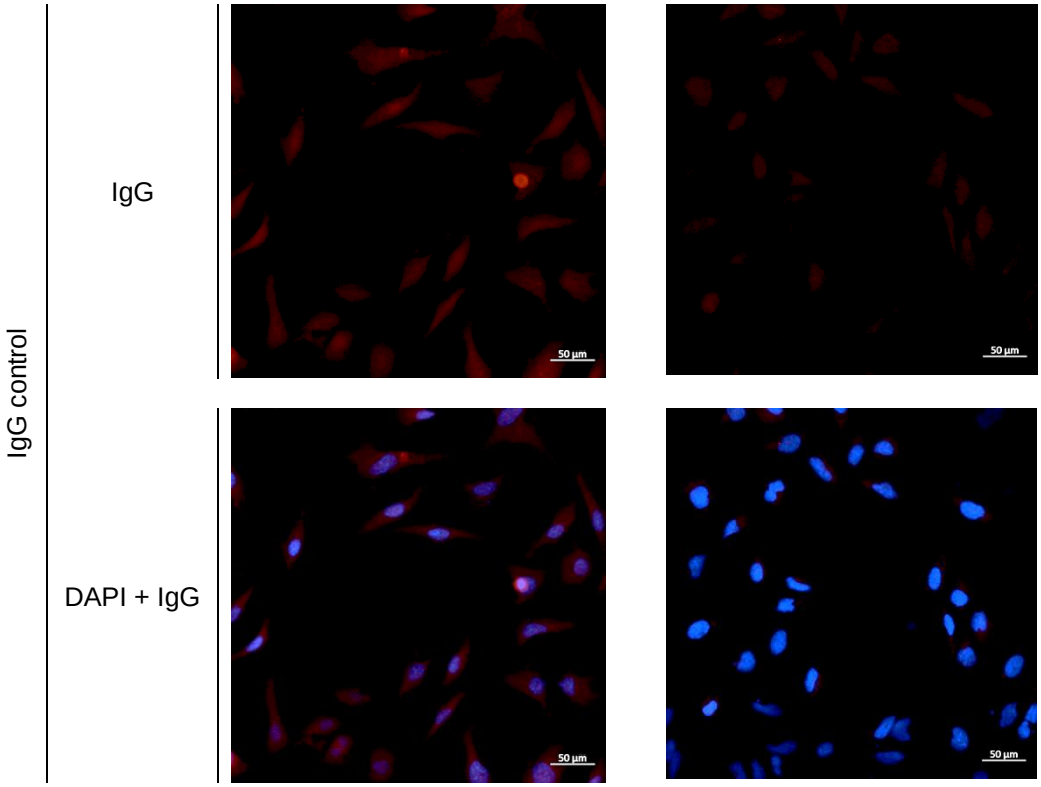
IgG control
IgG
DAPI + IgG
50 µm
50 µm
50 µm
50 µm

8 List of Abbreviations

AA	Ascorbic Acid
αMEM	Minimum Essential Medium Eagle - alpha modification
Ag^+	Silver
Ag_2SO_4	Silver sulphate
$AgNO_3$	Silver nitrate
AgNP	Silver nanoparticle
ALP	Alkaline phosphatase
βGP	β-glycerophosphate
BSA	Bovine Serum Albumin
BSO	L-Buthionine-sulfoxamine
CAUTI	Catheter Associated Urinary Tract Infection
CFU-f	Colony-forming unit fibroblast
DAPI	4', 6-diamidino-2-phenylindole
Dex	Dexamethasone
DMEM	Dulbecco's Modified Eagles Media
dsDNA	Double stranded deoxyribonucleic acid
EC_{50}	Dose causing response in 50% of subjects
eGFP	Enhanced green fluorescent protein
EPS	Extracellular polymeric substance
FBS	Foetal Bovine Serum
FDR	False Detection Rate
GSH-MEE	Glutathione monoethyl ester

OH^-	Hydroxyl radical
ICP-MS	Inductively Coupled Plasma Mass Spectrometry
ID_{50}	Dose causing infection in 50% of subjects
i.v.	Intravenous
LOS	Length of stay
µCT	Micro computed tomography
miRNA	Micro ribonucleic acid
MBC	Minimum bactericidal concentration
MSC	Mesenchymal Stromal Cell
NOAEL	No Observable Adverse Effect Level
PBS	Phosphate Buffered Saline
pNPP	p-nitrophenyl-phosphate
qPCR	Real-time Polymerase Chain Reaction (quantitative)
ROS	Reactive Oxygen Species
RT	Room Temperature
SD	Standard Deviation
SEM	Standard Error Mean
$O_2^{\bullet-}$	Superoxide
SSI	Surgical Site Infection
Wnt	Member of the Wnt family of ligands
WHO	World Health Organisation
Y201	Clonal mesenchymal stromal cell line
Y201-Wnt	Wnt reporter Y201 mesenchymal stromal cell

9 References

1. Donaldson LJ, Reckless IP, Scholes S, Mindell JS, Shelton NJ. The epidemiology of fractures in England. J Epidemiol Community Health. 2008;62(2):174–80.

2. Johansen A, Evans RJ, Stone MD, Richmond PW, Lo SV, Woodhouse KW. Fracture incidence in England and Wales: A study based on the population of Cardiff. Injury. 1997;28(9–10):655–60.

3. Van Staa TP, Dennison EM, Leufkens HGM, Cooper C. Epidemiology of fractures in England and Wales. Bone. 2001;29(6):517–22.

4. Meling T, Harboe K, Søreide K. Incidence of traumatic long-bone fractures requiring in-hospital management: A prospective age- and gender-specific analysis of 4890 fractures. Injury. 2009;40(11):1212–9.

5. Bong MR, Koval KJ, Egol KA. The history of intramedullary nailing. Bull NYU Hosp Jt Dis. 2006;64(3–4):94–7.

6. Whittle AP. A century of tibial intramedullary nailing. Curr Orthop Pract. 2018;29(1):6–10.

7. Claes L, Recknagel S, Ignatius A. Fracture healing under healthy and inflammatory conditions. Nat Rev Rheumatol. 2012;8(3):133–43.

8. Goodman SB, Yao Z, Keeney M, Yang F. The future of biologic coatings for orthopaedic implants. Biomaterials. 2013;34(13):3174–83.

9. Gustilo RB, Anderson JT. Prevention of infection in the treatment of one thousand and twenty-five open fractures of long bones : retrospective and prospective analyses. J Bone Jt Surg. 1976;58(4):453–8.

10. Gustilo RB, Mendoza RM, Williams DN. Problems in the management of type III (severe) open fractures: a new classification of type III open fractures. J Trauma. 1984;24(8):742–6.

11. Nanchahal J, Nayagam S, Khan U, Moran C, Barrett S, Sanderson F, et al. Standards for the management of open fractures of the lower limbs. BAPRAS; 2009.

12. Bennett AR, Smith KD. Open fractures. Orthop Trauma. 2013;27(1):9–14.

13. Yates JB, Fountain JR. Fractures of the femur and tibial shaft. Surgery. 2016;34(9):444–52.

14. Keating JF, Simpson AHRW, Robinson CM. The management of fractures with bone loss. J Bone Jt Surg Br. 2005;87–B(2):142–50.

15. Tanner MC, Heller R, Westhauser F, Miska M, Ferbert T, Fischer C, et al. Evaluation of the clinical effectiveness of bioactive glass (S53P4) in the treatment of non-unions of the tibia and femur: Study protocol of a randomized controlled non-inferiority trial. Trials. Trials; 2018;19(1):1–9.

16. Cuthbert RJ, Churchman SM, Tan HB, McGonagle D, Jones E, Giannoudis P V. Induced periosteum a complex cellular scaffold for the treatment of large bone defects. Bone. 2013;57(2):484–92.

17. Court-Brown CM, Bugler KE, Clement ND, Duckworth AD, McQueen MM. The epidemiology of open fractures in adults. A 15-year review. Injury. 2012;43(6):891–7.

18. Weber D, Dulai SK, Bergman J, Buckley R, Beaupre LA. Time to initial operative treatment following open fracture does not impact development of deep infection: a prospective cohort study of 736 subjects. J Orthop Trauma. 2014;28(11):613–9.

19. Weiss RJ, Montgomery SM, Ehlin A, Dabbagh Z Al, Stark A, Jansson KÅ. Decreasing incidence of tibial shaft fractures between 1998 and 2004: Information based on 10,627 Swedish inpatients. Acta Orthop. 2008;79(4):526–33.

20. Court-Brown CM, Rimmer S, Prakash U, McQueen MM. The epidemiology of

open long bone fractures. Injury. 1998;29(7):529–34.

21. Papakostidis C, Kanakaris NK, Pretel J, Faour O, Morell DJ, Giannoudis P V. Prevalence of complications of open tibial shaft fractures stratified as per the Gustilo-Anderson classification. Injury. 2011;42(12):1408–15.

22. Sfeir C, Ho L, Doll BA, Azari K, Hollinger JO. Fracture Repair. In: Bone Regeneration and Repair: Biology and Clinical Applications. 2005. p. 21–44.

23. Schindeler A, McDonald MM, Bokko P, Little DG. Bone remodeling during fracture repair: The cellular picture. Semin Cell Dev Biol. 2008;19(5):459–66.

24. Al-Aql ZS, Alagl AS, Graves DT, Gerstenfeld LC, Einhorn TA. Molecular Mechanisms Controlling Bone Formation During Fracture Healing and Distraction Osteogenesis. J Dent Res. 2008;87(2):107–18.

25. Loi F, Córdova LA, Pajarinen J, Lin T, Yao Z, Goodman SB. Inflammation, fracture and bone repair. Bone. 2016;86:119–30.

26. Gerstenfeld LC, Shapiro FD. Expression of bone-specific genes by hypertrophic chondrocytes: Implications of the complex functions of the hypertrophic chondrocyte during endochondral bone development. J Cell Biochem. 1996;62(1):1–9.

27. Andrew JG, Andrew SM, Freemont AJ, Marsh DR. Inflammatory cells in normal human fracture healing. Acta Orthop Scand. 1994;65(4):462–6.

28. Bastian O, Pillay J, Alblas J, Leenen L, Koenderman L, Blokhuis T. Systemic inflammation and fracture healing. J Leukoc Biol. 2011;89(5):669–73.

29. Xing Z, Lu C, Hu D, Yu Y -y., Wang X, Colnot C, et al. Multiple roles for CCR2 during fracture healing. Dis Model Mech. 2010;3(7–8):451–8.

30. Granero-Moltó F, Weis JA, Miga MI, Landis B, Myers TJ, O'Rear L, et al. Regenerative effects of transplanted mesenchymal stem cells in fracture healing. Stem Cells. 2009;27(8):1887–98.

31. Schmid GJ, Kobayashi C, Sandell LJ, Ornitz DM. Fibroblast growth factor expression during skeletal fracture healing in mice. Dev Dyn. 2009;238(3):766–74.

32. Kon T, Cho TJ, Aizawa T, Yamazaki M, Nooh N, Graves D, et al. Expression of osteoprotegerin, receptor activator of NF-κB ligand (osteoprotegerin ligand) and related proinflammatory cytokines during fracture healing. J Bone Miner Res. 2001;16(6):1004–14.

33. Kolar P, Gaber T, Perka C, Duda GN, Buttgereit F. Human early fracture hematoma is characterized by inflammation and hypoxia. Clin Orthop Relat Res. 2011;469(11):3118–26.

34. Tseng WP, Yang SN, Lai CH, Tang CH. Hypoxia induces BMP-2 expression via ILK, Akt, mTOR, and HIF-1 pathways in osteoblasts. J Cell Physiol. 2010;223(3):810–8.

35. Lee CM, Genetos DC, Wong A, Yellowley CE. Prostaglandin expression profile in hypoxic osteoblastic cells. J Bone Miner Metab. 2010;28(1):8–16.

36. Gerstenfeld LC, Cullinane DM, Barnes GL, Graves DT, Einhorn TA. Fracture healing as a post-natal developmental process: Molecular, spatial, and temporal aspects of its regulation. J Cell Biochem. 2003;88(5):873–84.

37. Keller J, Klamer A, Bak B, Suder P. Effect of local prostaglandin E2 on fracture callus in rabbits. Acta Orthop Scand. 1993;64(1):59–63.

38. Tsuji K, Bandyopadhyay A, Harfe BD, Cox K, Kakar S, Gerstenfeld L, et al. BMP2 activity, although dispensable for bone formation, is required for the initiation of fracture healing. Nat Genet. 2006;38(12):1424–9.

39. Bourque WT, Gross M, Hall BK. Expression of four growth factors during fracture repair. Int J Dev Biol. 1993;37(4):573–9.

40. Köttstorfer J, Thomas A, Gregori M, Kecht M, Kaiser G, Eipeldauer S, et al. Are OPG and RANKL involved in human fracture healing? J Orthop Res.

2014;32(12):1557–61.

41. Liu R, Birke O, Morse A, Peacock L, Mikulec K, Little DG, et al. Myogenic progenitors contribute to open but not closed fracture repair. BMC Musculoskelet Disord. 2011;12:288.

42. Claes L, Maurer-Klein N, Henke T, Gerngross H, Melnyk M, Augat P. Moderate Soft Tissue Trauma Delays New Bone Formation Only in the Early Phase of Fracture Healing. J Orthop Res. 2006;24(6):1178–85.

43. Marsell R, Einhorn TA. The biology of fracture healing. Injury. 2011;42(6):551–5.

44. Gerstenfeld LC, Cho T-J, Kon T, Aizawa T, Tsay A, Fitch J, et al. Impaired Fracture Healing in the Absence of TNF-α Signaling: The Role of TNF-α in Endochondral Cartilage Resorption. J Bone Miner Res. 2003;18(9):1584–92.

45. Colnot C. Altered fracture repair in the absence of MMP9. Development. 2003;130(17):4123–33.

46. Trampuz A, Zimmerli W. Diagnosis and treatment of infections associated with fracture-fixation devices. Injury. 2006;37 Suppl 2:S59-66.

47. Von Eiff C, Jansen B, Kohnen W, Becker K. Infections associated with medical devices: Pathogenesis, management and prophylaxis. Drugs. 2005;65(2):179–214.

48. Metsemakers WJ, Smeets B, Nijs S, Hoekstra H. Infection after fracture fixation of the tibia: Analysis of healthcare utilization and related costs. Injury. 2017;48(6):1204–10.

49. Blick SS, Brumback RJ, Lakatos R, Poka A, Burgess AR. Early prophylactic bone grafting of high-energy tibial fractures. Clin Orthop Relat Res. 1989;(240):21–41.

50. Naique SB, Pearse M, Nanchahal J. Management of severe open tibial fractures: the need for combined orthopaedic and plastic surgical treatment in

specialist centres. J Bone Jt Surg Br. 2006;88(3):351–7.

51. Rajasekaran S, Naresh Babu J, Dheenadhayalan J, Shetty a P, Sundararajan SR, Kumar M, et al. A score for predicting salvage and outcome in Gustilo type-IIIA and type-IIIB open tibial fractures. J Bone Jt Surg Br. 2006;88(10):1351–60.

52. Yokoyama K, Itoman M, Uchino M, Fukushima K, Nitta H, Kojima Y. Immediate versus delayed intramedullary nailing for open fractures of the tibial shaft: A multivariate analysis of factors affecting deep infection and fracture healing. Indian J Orthop. 2008;42(4):410–9.

53. Tripuraneni BK, Ganga S, Quinn R, Gehlert R, Tripuraneni K, Ganga S, et al. The effect of time delay to surgical debridement of open tibia shaft fractures on infection rate. Orthopedics. 2008;31(12):6–11.

54. Yusof NM, Khalid KA, Zulkifly AH, Zakaria Z, Amin MAM, Awang MS, et al. Factors associated with the outcome of open tibial fractures. Malays J Med Sci. 2013;20(5):47–53.

55. Matos MA, Catro-Filho RN, da Silva BVP. Risk factors associated with infection in tibial open fractures. Rev Fac Ciencias Medicas. 2013;70(1):14–8.

56. Madhuchandra P, Rafi M, Devadoss S, Devadoss A. Predictability of salvage and outcome of Gustilo and Anderson type-IIIA and type-IIIB open tibial fractures using Ganga Hospital Scoring system. Injury. 2015;46(2):282–7.

57. Yokoyama K, Shindo M, Itoman M, Yamamoto M. Immediate internal fixation for open fractures of the long bones of the upper and lower extremities. J Trauma Acute Care Surg. 1994;37(2).

58. Court-Brown CM, Keating JF, McQueen MM. Infection after intramedullary nailing of the tibia. Incidence and protocol for management. J Bone Jt Surg Br. 1992;74(5):770–4.

59. Sanders R, Jersinovich I, Anglen J, DiPasquale T, Herscovici D. The treatment of open tibial shaft fractures using an interlocked intramedullary nail without

reaming. J Orthop Trauma. 1994;8(6):504–10.

60. Singer R, Kellan J. Open tibial diaphyseal fractures: Results of unreamed locked intramedullary nailing. Clin Orthop Relat Res. 1995;315:114–8.

61. Cole JD, Ansel LJ, Schwartzberg R. A sequential protocol for management of severe open tibial fractures. Clin Orthop Relat Res. 1995;315:84–103.

62. Ostermann P, Seligson D, Henry S. Local antibiotic therapy for severe open fractures. A review of 1085 consecutive cases. J Bone Jt Surg Br. 1995;77(1):93–7.

63. Oh CW, Park BC, Ihn JC, Park HJ. Primary unreamed intramedullary nailing for open fractures of the tibia. Int Orthop. 2001;24(6):338–41.

64. Joshi D, Ahmed A, Krishna L, Lal Y. Unreamed Interlocking Nailing in Open Fractures of Tibia. J Orthop Surg. 2004 Dec 4;12(2):216–21.

65. Djahangiri A, Garofalo R, Chevalley F, Leyvraz P-F, Wettstein M, Borens O, et al. Closed and open grade I and II tibial shaft fractures treated by reamed intramedullary nailing. Med Princ Pract. 2006;15(4):293–8.

66. Elek SD, Conen PE. The virulence of Staphylococcus pyogenes for man. A study of the problems of wound infection. Br J Exp Pathol. 1957;38(6):573–86.

67. Gristina AG, Rovere GD, Shoji H, Nicastro JF. An in vitro study of bacterial response to inert and reactive metals and to methyl methacrylate. J Biomed Mater Res. 1976;10(2):273–81.

68. Gristina AG, Costerton JW, McGainty PLJ. Bacteria-Laden Biofilms: A hazard of orthopedic prostheses. Infect Surg. 1984;655–62.

69. Verheyen CCPM, Dhert WJA, de Blieck-Hogervorst JMA, van der Reijden TJK, Petit PLC, de Groot K. Adherence to a metal, polymer and composite by Staphylococcus aureus and Staphylococcus epidermidis. Biomaterials. 1993;14(5):383–91.

70. Moriarty TF, Debefve L, Boure L, Campoccia D, Schlegel U, Richards RG. Influence of material and microtopography on the development of local infection in vivo: Experimental investigation in rabbits. Int J Artif Organs. 2009;32(9):663–70.

71. Metsemakers WJ, Schmid T, Zeiter S, Ernst M, Keller I, Cosmelli N, et al. Titanium and steel fracture fixation plates with different surface topographies: Influence on infection rate in a rabbit fracture model. Injury. 2016;47(3):633–9.

72. Gallo J, Holinka M, Moucha CS. Antibacterial surface treatment for orthopaedic implants. Int J Mol Sci. 2014;15(8):13849–80.

73. Kendall K, Roberts AD. Van der Waals forces influencing adhesion of cells. Philos Trans R Soc B Biol Sci. 2015;370(1661).

74. Arens S, Schlegel U, Printzen G, Ziegler W, Perren SM, Hansis M. Influence of materials for fixation implants on local infection: An experimental study of steel versus titanium DCP in rabbits. J Bone Jt Surg. 1996;78–B(4):647–51.

75. Sheehan E, Mckenna J, Mulhall KJ, Marks P, McCormack D. Adhesion of Staphylococcus to orthopaedic metals, an in vivo study. J Orthop Res. 2004;22:39–43.

76. Chang CC, Merritt K. Infection at the site of implanted materials with and without preadhered bacteria. J Orthop Res. 1994;12(4):526–31.

77. Melcher GA, Hauke C, Metzdorf A, Perren SM, Printzen G, Schlegel U, et al. Infection after intramedullary nailing: An experimental investigation on rabbits. Injury. 1996;27(Supp 3):SC23-26.

78. Melcher GA, Claudi B, Schlegel U, Perren SM, Printzen G, Munzinger J. Influence of type of medullary nail on the development of local infection. J Bone Jt Surg. 1994;76(6):955–9.

79. Horn J, Schlegel U, Krettek C, Ito K. Infection resistance of unreamed solid, hollow slotted and cannulated intramedullary nails: An in-vivo experimental

comparison. J Orthop Res. 2005;23(4):810–5.

80. Panti JPL, Geronilla M, Arada EC. Clinical outcomes of patients with isolated femoral shaft fractures treated with S.I.G.N interlock nails versus Cannulated Interlock Intramedullary nails. J Orthop. 2013;10(4):182–7.

81. Donlan RM. Biofilms: Microbial life on surfaces. Emerg Infect Dis. 2002;8(9):881–90.

82. Costerton JW, Geesey GG, Cheng KJ. How bacteria stick. Sci Am. 1978;238(1):86–95.

83. Cheung AL, Fischetti VA. The role of fibrinogen in Staphylococcal adherence to catheters in vitro. J Infect Dis. 1990;161(6):1177–86.

84. Galanakos SP, Papadakis S a., Kateros K, Papakostas I, Macheras G. Biofilm and orthopaedic practice: the world of microbes in a world of implants. Orthop Trauma. 2009;23(3):175–9.

85. Sutherland IW. Biofilm exopolysaccharides: A strong and sticky framework. Microbiology. 2001;147(1):3–9.

86. Ventola CL. The Antibiotic Resistance Crisis. Part 1: Causes and Threats. Pharm Ther. 2015;40(4):277–83.

87. Høiby N, Bjarnsholt T, Givskov M, Molin S, Ciofu O. Antibiotic resistance of bacterial biofilms. Int J Antimicrob Agents. 2010;35(4):322–32.

88. Williams I, Venables WA, Lloyd D, Paul F, Critchley I. The effects of adherence to silicone surfaces on antibiotic susceptibility in Staphylococcus aureus. Microbiology. 1997;143(7):2407–13.

89. Hoffman LR, D'Argenio DA, MacCoss MJ, Zhang Z, Jones RA, Miller SI. Aminoglycoside antibiotics induce bacterial biofilm formation. Nature. 2005;436:1171–5.

90. Costerton JW, Stewart PS, Greenberg EP. Bacterial biofilms: a common cause of persistent infections. Science. 1999;284:1318–22.

91. Singh R, Ray P, Das A, Sharma M. Penetration of antibiotics through Staphylococcus aureus and Staphylococcus epidermidis biofilms. J Antimicrob Chemother. 2010;65(9):1955–8.

92. Donlan RM. Biofilm Formation: A Clinically Relevant Microbiological Process. Clin Infect Dis. 2001;33(8):1387–92.

93. Liu X, Roe F, Jesaitis A, Lewandowski Z. Resistance of biofilms to the catalase inhibitor 3-amino-1,2,4-triazole. Biotechnol Bioeng. 1998;59(2):156–62.

94. Brown MRW, Allison DG, Gilbert P. Resistance of bacterial biofilms to antibiotics: a growth-rate related effect? J Antimicrob Chemother. 1988;22:777–83.

95. Bennett PM. Plasmid encoded antibiotic resistance: Acquisition and transfer of antibiotic resistance genes in bacteria. Br J Pharmacol. 2008;153(Suppl. 1):S347-357.

96. Marrie TJ, Nelligan J, Costerton JW. A scanning and transmission electron microscopic study of an infected endocardial pacemaker lead. Circulation. 1982;66(6):1339–42.

97. Otchwemah R, Grams V, Tjardes T, Shafizadeh S, Bäthis H, Maegele M, et al. Bacterial contamination of open fractures – pathogens, antibiotic resistances and therapeutic regimes in four hospitals of the trauma network Cologne, Germany. Injury. 2015 Oct;46:S104–8.

98. Hoff WS, Bonadies JA, Cachecho R, Dorlac WC. East Practice Management Guidelines Work Group: Update to Practice Management Guidelines for Prophylactic Antibiotic Use in Open Fractures. J Trauma Inj Infect Crit Care. 2011;70(3):751–4.

99. Olesen UK, Pedersen NJ, Eckardt H, Lykke-Meyer L, Bonde CT, Singh UM, et

al. The cost of infection in severe open tibial fractures treated with a free flap. Int Orthop. International Orthopaedics; 2017;41(5):1049–55.

100. Thakore R V., Greenberg SE, Shi H, Foxx AM, Francois EL, Prablek MA, et al. Surgical site infection in orthopedic trauma: A case-control study evaluating risk factors and cost. J Clin Orthop Trauma. 2015;6(4):220–6.

101. Jenks PJ, Laurent M, McQuarry S, Watkins R. Clinical and economic burden of surgical site infection (SSI) and predicted financial consequences of elimination of SSI from an English hospital. J Hosp Infect. 2014;86(1):24–33.

102. Alt V. Antimicrobial coated implants in trauma and orthopaedics–A clinical review and risk-benefit analysis. Injury. 2017;48(3):599–607.

103. Edwards C, Counsell A, Boulton C, Moran CG. Early infection after hip fracture surgery: Risk factors, costs and outcome. J Bone Jt Surg Br. 2008;90–B(6):770–7.

104. Campoccia D, Montanaro L, Arciola CR. A review of the biomaterials technologies for infection-resistant surfaces. Biomaterials. 2013;34(34):8533–54.

105. Mah T-FC, Toole GAO. Mechanisms of biofilm resistance to antimicrobial agents. Trends Microbiol. 2001;9(1):34–9.

106. Fuchs T, Stange R, Schmidmaier G, Raschke MJ. The use of gentamicin-coated nails in the tibia: Preliminary results of a prospective study. Arch Orthop Trauma Surg. 2011;131(10):1419–25.

107. Metsemakers WJ, Reul M, Nijs S. The use of gentamicin-coated nails in complex open tibia fracture and revision cases: A retrospective analysis of a single centre case series and review of the literature. Injury. 2015;46(12):2433–7.

108. Antoci Jr. V, King SB, Jose B, Parvizi J, Zeiger AR, Wickstrom E, et al. Vancomycin Covalently Bonded to Titanium Alloy Prevents Bacterial Colonization. J Orthop Res. 2007;25(7):858–66.

109. Darouiche RO, Mansouri MD, Zakarevicz D, AlSharif A, Landon GC. In Vivo Efficacy of Antimicrobial-Coated Devices. J Bone Jt Surg. 2007;89(4):792.

110. Davidson H, Poon M, Saunders R, Shapiro IM, Hickok NJ, Adams CS. Tetracycline tethered to titanium inhibits colonization by Gram-negative bacteria. J Biomed Mater Res - Part B Appl Biomater. 2015;103(7):1381–9.

111. Nie B, Long T, Ao H, Zhou J, Tang T, Yue B. Covalent Immobilization of Enoxacin onto Titanium Implant Surfaces for Inhibiting Multiple Bacterial Species Infection and In Vivo Methicillin-Resistant Staphylococcus aureus Infection Prophylaxis. Antimicrob Agents Chemother. 2017;61(1):1–14.

112. Campoccia D, Montanaro L, Speziale P, Arciola CR. Antibiotic-loaded biomaterials and the risks for the spread of antibiotic resistance following their prophylactic and therapeutic clinical use. Biomaterials. 2010;31(25):6363–77.

113. Neut D, Van De Belt H, Van Horn JR, Van Der Mei HC, Busscher HJ. Residual gentamicin-release from antibiotic-loaded polymethylmethacrylate beads after 5 years of implantation. Biomaterials. 2003;24(10):1829–31.

114. Lansdown ABG. Silver in health care: antimicrobial effects and safety in use. In: Biofunctional Textiles and the Skin Current Problems in Dermatology. 2006. p. 17–34.

115. Chopra I. The increasing use of silver-based products as antimicrobial agents: a useful development or a cause for concern? J Antimicrob Chemother. 2007;59(4):587–90.

116. Percival SL, Bowler PG, Russell D. Bacterial resistance to silver in wound care. J Hosp Infect. 2005;60(1):1–7.

117. Radzig MA, Nadtochenko VA, Koksharova OA, Kiwi J, Lipasova VA, Khmel IA. Antibacterial effects of silver nanoparticles on gram-negative bacteria: Influence on the growth and biofilms formation, mechanisms of action. Colloids Surfaces B Biointerfaces. 2013;102:300–6.

118. Hachicho N, Hoffmann P, Ahlert K, Heipieper HJ. Effect of silver nanoparticles and silver ions on growth and adaptive response mechanisms of Pseudomonas putida mt-2. FEMS Microbiol Lett. 2014;355(1):71–7.

119. Heipieper HJ, Meinhardt F, Segura A. The cis-trans isomerase of unsaturated fatty acids in Pseudomonas and Vibrio: Biochemistry, molecular biology and physiological function of a unique stress adaptive mechanism. FEMS Microbiol Lett. 2003;229(1):1–7.

120. Jung WK, Koo HC, Kim KW, Shin S, Kim SH, Park YH. Antibacterial activity and mechanism of action of the silver ion in Staphylococcus aureus and Escherichia coli. Appl Environ Microbiol. 2008;74(7):2171–8.

121. Feng QL, Wu J, Chen GQ, Cui FZ, Kim TN, Kim JO. A mechanistic study of the antibacterial effect of silver ions on Escherichia coli and Staphylococcus aureus. J Biomed Mater Res. 2000;52(4):662–8.

122. Morones-Ramirez JR, Winkler JA, Spina CS, Collins JJ. Silver Enhances Antibiotic Activity Against Gram-Negative Bacteria. Sci Transl Med. 2013;5(190):1–11.

123. Schreurs WJA, Rosenberg H. Effect of Silver Ions on Transport and Retention of Phosphate by Escherichia coli. J Bacteriol. 1982;152(1):7–13.

124. Bragg PD, Rainnie DJ. The effect of silver ions on the respiratory chain of Escherichia coli. Can J Microbiol. 1974;20(6):883–9.

125. Yamanaka M, Hara K, Kudo J. Bactericidal Actions of a Silver Ion Solution on Escherichia coli, Studied by Energy-Filtering Transmission Electron Microscopy and Proteomic Analysis. Appl Environ Microbiol. 2005;71(11):7589–7593.

126. Anas A, Jiya J, Rameez MJ, Anand PB, Anantharaman MR, Nair S. Sequential interactions of silver-silica nanocomposite (Ag-SiO2NC) with cell wall, metabolism and genetic stability of Pseudomonas aeruginosa, a multiple antibiotic-resistant bacterium. Lett Appl Microbiol. 2013;56(1):57–62.

127. Silver S. Bacterial silver resistance: molecular biology and uses and misuses of silver compounds. FEMS Microbiol Rev. 2003;27(2–3):341–53.

128. Chaw KC, Manimaran M, Tay FEH. Role of Silver Ions in Destabilization of Intermolecular Adhesion Forces Measured by Atomic Force Microscopy in Staphylococcus epidermidis Biofilms. Antimicrob Agents Chemother. 2005;49(12):4853–9.

129. Hill KE, Malic S, McKee R, Rennison T, Harding KG, Williams DW, et al. An in vitro model of chronic wound biofilms to test wound dressings and assess antimicrobial susceptibilities. J Antimicrob Chemother. 2010;65(6):1195–206.

130. Bjarnsholt T, Kirketerp-Møller K, Kristiansen S, Phipps R, Nielsen AK, Jensen PØ, et al. Silver against Pseudomonas aeruginosa biofilms. APMIS. 2007;115(8):921–8.

131. Shahverdi AR, Fakhimi A, Shahverdi HR, Minaian S. Synthesis and effect of silver nanoparticles on the antibacterial activity of different antibiotics against Staphylococcus aureus and Escherichia coli. Nanomedicine Nanotechnology, Biol Med. 2007;3(2):168–71.

132. Birla SS, Tiwari V V., Gade AK, Ingle AP, Yadav AP, Rai MK. Fabrication of silver nanoparticles by Phoma glomerata and its combined effect against Escherichia coli, Pseudomonas aeruginosa and Staphylococcus aureus. Lett Appl Microbiol. 2009;48(2):173–9.

133. Kuehl R, Brunetto PS, Woischnig AK, Varisco M, Rajacic Z, Vosbeck J, et al. Preventing Implant-Associated infections by silver coating. Antimicrob Agents Chemother. 2016;60(4):2467–75.

134. International consensus. Appropriate use of silver dressings in wounds. An expert working group consensus. Wounds Int. 2012;

135. Biological evaluation of medical devices Part 1: Evaluation and testing within a risk management process (ISO10993-1: 2009).

136. Rupp ME, Fitzgerald T, Marion N, Helget V, Puumala S, Anderson JR, et al. Effect of silver-coated urinary catheters: Efficacy, cost-effectiveness, and antimicrobial resistance. Am J Infect Control. 2004;32(8):445–50.

137. Riley DK, Classen DC, Stevens LE, Burke JP. A large randomized clinical trial of a silver-impregnated urinary catheter: Lack of efficacy and Staphylococcal superinfection. Am J Med. 1995;98(4):349–56.

138. Wafa H, Grimer RJ, Reddy K, Jeys L, Abudu A, Carter SR, et al. Retrospective evaluation of the incidence of early periprosthetic infection with silver-treated endoprostheses in high-risk patients: case-control study. Bone Joint J. 2015;97–B(2):252–7.

139. Hardes J, Von Eiff C, Streitbuerger A, Balke M, Budny T, Henrichs MP, et al. Reduction of periprosthetic infection with silver-coated megaprostheses in patients with bone sarcoma. J Surg Oncol. 2010;101(5):389–95.

140. Donati F, Di Giacomo G, D'Adamio S, Ziranu A, Careri S, Rosa MA, et al. Silver-Coated Hip Megaprosthesis in Oncological Limb Savage Surgery. Biomed Res Int. 2016;2016.

141. Malawer MM, Chou LB. Prosthetic Survival and Clinical Results with Use of Large-Segment Replacements in the Treatment of High-Grade Bone Sarcomas. J Bone Jt Surgery Am. 1995;77(8):1154–65.

142. Jeys LM, Grimer RJ, Carter SR, Tillman RM. Risk of amputation following limb salvage surgery with endoprosthetic replacement, in a consecutive series of 1261 patients. Int Orthop. 2003;27(3):160–3.

143. Wilding CP, Cooper GA, Freeman AK, Parry MC, Jeys L. Can a Silver-Coated Arthrodesis Implant Provide a Viable Alternative to Above Knee Amputation in the Unsalvageable, Infected Total Knee Arthroplasty? J Arthroplasty. 2016;31(11):2542–7.

144. Bury NR. Chapter 19. Silver. In: Binding, Transport and Storage of Metal Ions in Biological Cells. 2014. p. 556–81.

145. Hardes J, Ahrens H, Gebert C, Streitbuerger A, Buerger H, Erren M, et al. Lack of toxicological side-effects in silver-coated megaprostheses in humans. Biomaterials. 2007;28(18):2869–75.

146. Glehr M, Leithner A, Friesenbichler J, Goessler W, Avian A, Andreou D, et al. Argyria following the use of silver-coated megaprostheses: no association between the development of local argyria and elevated silver levels. Bone Joint J. 2013;95–B(7):988–92.

147. Lansdown ABG. A pharmacological and toxicological profile of silver as an antimicrobial agent in medical devices. Adv Pharmacol Sci. 2010;2010:1–16.

148. Scoccianti G, Frenos F, Beltrami G, Campanacci DA, Capanna R. Levels of silver ions in body fluids and clinical results in silver-coated megaprostheses after tumour, trauma or failed arthroplasty. Injury. 2016;47:S11–6.

149. Gosheger G, Hardes J, Ahrens H, Streitburger A, Buerger H, Erren M, et al. Silver-coated megaendoprostheses in a rabbit model - an analysis of the infection rate and toxicological side effects. Biomaterials. 2004;25(24):5547–56.

150. De Feo CJ, Aller SG, Siluvai GS, Blackburn NJ, Unger VM. Three-dimensional structure of the human copper transporter hCTR1. PNAS. 2009;106(11):4237–42.

151. Bertinato J, Cheung L, Hoque R, Plouffe LJ. Ctr1 transports silver into mammalian cells. J Trace Elem Med Biol. 2010;24(3):178–84.

152. Behra R, Sigg L, Clift MJD, Herzog F, Minghetti M, Johnston B, et al. Bioavailability of silver nanoparticles and ions: from a chemical and biochemical perspective. J R Soc Interface. 2013;10(87):20130396.

153. Zhan D, Fan F-RF, Bard AJ. The Kv channel blocker 4-aminopyridine enhances Ag+ uptake: a scanning electrochemical microscopy study of single living cells. PNAS. 2008;105(34):12118–22.

154. Bury NR, Wood CM. Mechanism of branchial apical silver uptake by rainbow

trout is via the proton-coupled Na(+) channel. Am J Physiol. 1999;277(5):R1385–91.

155. Havelaar AC, De Gast IL, Snijders S, Beerens CEMT, Mancini GMS, Verheijen FW. Characterization of a heavy metal ion transporter in the lysosomal membrane. FEBS Lett. 1998;436(2):223–7.

156. Schieber M, Chandel NS. ROS function in redox signaling and oxidative stress. Curr Biol. 2014;24(10):R453–62.

157. Thannickal VJ, Fanburg BL. Reactive oxygen species in cell signaling. Am J Physiol Lung Cell Mol Physiol. 2000;279(78):1005–28.

158. Halliwell B, Cross CE. Oxygen-derived species: Their relation to human disease and environmental stress. Environ Health Perspect. 1994;102(Suppl. 10):5–12.

159. Holmström KM, Finkel T. Cellular mechanisms and physiological consequences of redox-dependent signalling. Nat Rev Mol Cell Biol. 2014;15(6):411–21.

160. Ke Q., Costa M. Hypoxia-Inducible Factor-1. Mol Pharmacol. 2006;70(5):1469–80.

161. Putker M, Madl T, Vos HR, de Ruiter H, Visscher M, van den Berg MCW, et al. Redox-Dependent Control of FOXO/DAF-16 by Transportin-1. Mol Cell. 2013;49(4):730–42.

162. Hayes JD, Dinkova-Kostova AT. The Nrf2 regulatory network provides an interface between redox and intermediary metabolism. Trends Biochem Sci. 2014;39(4):199–218.

163. Mittal M, Siddiqui MR, Tran K, Reddy SP, Malik AB. Reactive Oxygen Species in Inflammation and Tissue Injury. Antioxidants. 2014;20(7):1126–67.

164. Atashi F, Modarressi A, Pepper MS. The role of reactive oxygen species in mesenchymal stem cell adipogenic and osteogenic differentiation: a review. Stem Cells Dev. 2015;24(10):1150–63.

165. Bigarella CL, Liang R, Ghaffari S. Stem cells and the impact of ROS signaling. Development. 2014;141(22):4206–18.

166. Jeong S-G, Cho G-W. Endogenous ROS levels are increased in replicative senescence in human bone marrow mesenchymal stromal cells. Biochem Biophys Res Commun. 2015;460(4):971–6.

167. Chen C-T, Shih Y-R V., Kuo TK, Lee OK, Wei Y-H. Coordinated Changes of Mitochondrial Biogenesis and Antioxidant Enzymes During Osteogenic Differentiation of Human Mesenchymal Stem Cells. Stem Cells. 2008;26(4):960–8.

168. Almeida M, Han L, Martin-Millan M, O'Brien CA, Manolagas SC. Oxidative stress antagonizes Wnt signaling in osteoblast precursors by diverting β-catenin from T cell factor- to forkhead box O-mediated transcription. J Biol Chem. 2007;282(37):27298–305.

169. Kim W-K, Meliton V, Bourquard N, Hahn TJ, Parhami F. Hedgehog signaling and osteogenic differentiation in multipotent bone marrow stromal cells are inhibited by oxidative stress. J Cell Biochem. 2010;111(5):1199–209.

170. Spinella-Jaegle S, Rawadi G, Kawai S, Gallea S, Faucheu C, Mollat P, et al. Sonic hedgehog increases the commitment of pluripotent mesenchymal cells into the osteoblastic lineage and abolishes adipocytic differentiation. J Cell Sci. 2001;114(11):2085–94.

171. Yuasa T, Kataoka H, Kinto N, Iwamoto M, Enomoto-Iwamoto M, Iemura SI, et al. Sonic hedgehog is involved in osteoblast differentiation by cooperating with BMP-2. J Cell Physiol. 2002;193(2):225–32.

172. Miyaji T, Nakase T, Iwasaki M, Kuriyama K, Tamai N, Higuchi C, et al. Expression and distribution of transcripts for sonic hedgehog in the early phase of fracture repair. Histochem Cell Biol. 2003;119(3):233–7.

173. Horikiri Y, Shimo T, Kurio N, Okui T, Matsumoto K, Iwamoto M, et al. Sonic Hedgehog Regulates Osteoblast Function by Focal Adhesion Kinase Signaling

in the Process of Fracture Healing. PLoS One. 2013;8(10):1–13.

174. Ito H, Akiyama H, Shigeno C, Iyama K, Matsuoka H, Nakamura T. Hedgehog signaling molecules in bone marrow cells at the initial stage of fracture repair. Biochem Biophys Res Commun. 1999;262(2):443–51.

175. Garrett IR, Boyce BF, Oreffo C, Bonewald L, Poser J, Mundy GR. Oxygen-derived Free Radicals Stimulate Osteoclastic Bone Resorption in Rodent Bone In Vitro and In Vivo. J Clin Invest. 1990;85:632–9.

176. Bax BE, Alam ASMT, Banerji B, Bax CMR, Bevis PJR, Stevens CR, et al. Stimulation of osteoclastic bone resorption by hydrogen peroxide. Biochem Biophys Res Commun. 1992;183(3):1153–8.

177. Fraser JHE, Helfrich MH, Wallace HM, Ralston SH. Hydrogen peroxide, but not superoxide, stimulates bone resorption in mouse calvariae. Bone. 1996;19(3):223–6.

178. Rhee SG. Redox signaling: hydrogen peroxide as intracellular messenger. Exp Mol Med. 1999;31(2):53–9.

179. Ikeda F, Nishimura R, Matsubara T, Tanaka S, Inoue J, Reddy S V., et al. Critical roles of c-Jun signaling in regulation of NFAT family and RANKL-regulated osteoclast differentiation. J Clin Invest. 2004;114(4):475–84.

180. Lee NK, Choi YG, Baik JY, Han SY, Jeong D, Bae YS, et al. A crucial role for reactive oxygen species in RANKL-induced osteoclast differentiation. Blood. 2005;106(3):852–9.

181. Bai XC, Lu D, Liu AL, Zhang ZM, Li XM, Zou ZP, et al. Reactive oxygen species stimulates receptor activator of NF-kB ligand expression in osteoblast. J Biol Chem. 2005;280(17):17497–506.

182. Lean JM, Davies JT, Fuller K, Jagger CJ, Kirstein B, Partington GA, et al. A crucial role for thiol antioxidants in estrogen-deficiency bone loss. J Clin Invest. 2003;112(6):915–23.

183. Cortese-Krott MM, Münchow M, Pirev E, He F, Bozkurt A, Uciechowski P, et al. Silver ions induce oxidative stress and intracellular zinc release in human skin fibroblasts. Free Radic Biol Med. 2009;47:1570–7.

184. Friedenstein AJ, Piatetzky-Shapiro II, Petrakova K V. Osteogenesis in transplants of bone marrow cells. J Embryol Exp Morphol. 1966;16(3):381–90.

185. Friedenstein AJ, Chailakhjan RK, Lalykina KS. The Development of Fibroblast Colonies in Monolayer Cultures of Guinea-Pig Bone Marrow and Spleen Cells. Cell Tissue Kinet. 1970;3:393–403.

186. Bianco P, Kuznetsov SA, Riminucci M, Gehron Robey P. Postnatal Skeletal Stem Cells. Methods Enzymol. 2006;419:117–48.

187. Tuan RS, Boland G, Tuli R. Adult mesenchymal stem cells and cell-based tissue engineering. Arthritis Res Ther. 2003;5(1):32–45.

188. Caplan AI. Mesenchymal Stem Cells. J Orthop Res. 1991;9(5):641–50.

189. Bianco P, Riminucci M, Gronthos S, Robey PG. Bone marrow stromal stem cells: nature, biology, and potential applications. Stem Cells. 2001;19(3):180–92.

190. Bianco P, Robey PG, Simmons PJ. Mesenchymal Stem Cells: Revisiting History, Concepts, and Assays. Cell Stem Cell. 2008;2(4):313–9.

191. Pittenger MF. Multilineage Potential of Adult Human Mesenchymal Stem Cells. Science. 1999;284(5411):143–7.

192. Horwitz EM, Andreef M, Frassoni F. Mesenchymal Stromal Cells. Curr Opin Hematol. 2006;13(6):419–25.

193. Dominici M, Le Blanc K, Mueller I, Slaper-Cortenbach I, Marini FC, Krause DS, et al. Minimal criteria for defining multipotent mesenchymal stromal cells. The International Society for Cellular Therapy position statement. Cytotherapy. 2006;8(4):315–7.

194. Sacchetti B, Funari A, Michienzi S, Di Cesare S, Piersanti S, Saggio I, et al. Self-Renewing Osteoprogenitors in Bone Marrow Sinusoids Can Organize a Hematopoietic Microenvironment. Cell. 2007;131(2):324–36.

195. Simmons PJ, Torok-Storb B. Identification of stromal cell precursors in human bone marrow by a novel monoclonal antibody, STRO-1. Blood. 1991;78(1):55–62.

196. Gronthos S. Molecular and cellular characterisation of highly purified stromal stem cells derived from human bone marrow. J Cell Sci. 2003;116(9):1827–35.

197. Gammons M, Bienz M. Multiprotein complexes governing Wnt signal transduction. Curr Opin Cell Biol. 2018;51:42–9.

198. Gaur T, Lengner CJ, Hovhannisyan H, Bhat RA, Bodine PVN, Komm BS, et al. Canonical WNT signaling promotes osteogenesis by directly stimulating Runx2 gene expression. J Biol Chem. 2005;280(39):33132–40.

199. Bain G, Müller T, Wang X, Papkoff J. Activated β-catenin induces osteoblast differentiation of C3H10T1/2 cells and participates in BMP2 mediated signal transduction. Biochem Biophys Res Commun. 2003;301(1):84–91.

200. Bennett CN, Longo KA, Wright WS, Suva LJ, Lane TF, Hankenson KD, et al. Regulation of osteoblastogenesis and bone mass by Wnt10b. PNAS. 2005;102(9):3324–9.

201. De Boer J, Siddappa R, Gaspar C, Van Apeldoorn A, Fodde R, Van Blitterswijk C. Wnt signaling inhibits osteogenic differentiation of human mesenchymal stem cells. Bone. 2004;34(5):818–26.

202. Ducy P, Zhang R, Geoffroy V, Ridall AL, Karsenty G. Osf2/Cbfa1: A transcriptional activator of osteoblast differentiation. Cell. 1997;89(5):747–54.

203. M. Bruderer, R.G. Richards MA and MJS. Role and Regulation of Runx2 in Osteogenesis. Eur Cells Mater. 2014;28:269–86.

204. Liu TM, Lee EH. Transcriptional regulatory cascades in Runx2-dependent bone development. Tissue Eng Part B Rev. 2013;19(3):254–63.

205. Hong D, Chen H-X, Xue Y, Li D-M, Wan X-C, Ge R, et al. Osteoblastogenic effects of dexamethasone through upregulation of TAZ expression in rat mesenchymal stem cells. J Steroid Biochem Mol Biol. 2009;116(1–2):86–92.

206. Azzolin L, Zanconato F, Bresolin S, Forcato M, Basso G, Bicciato S, et al. Role of TAZ as mediator of wnt signaling. Cell. 2012;151(7):1443–56.

207. Phillips JE, Gersbach CA, Wojtowicz AM, García AJ. Glucocorticoid-induced osteogenesis is negatively regulated by Runx2/Cbfa1 serine phosphorylation. J Cell Sci. 2006;119(3):581–91.

208. Rosen ED, MacDougald OA. Adipocyte differentiation from the inside out. Nat Rev Mol Cell Biol. 2006;7(12):885–96.

209. El-Jack AK, Hamm JK, Paul F, Farmer SR. Reconstitution of Insulin-sensitive Glucose Transport in Fibroblasts Requires Expression of Both PPARγ and C/EBPα. J Biol Chem. 1999;274(12):7946–51.

210. Tang Q-Q, Otto TC, Lane MD. Commitment of C3H10T1/2 pluripotent stem cells to the adipocyte lineage. PNAS. 2004;101(26):9607–11.

211. Sottile V, Seuwen K. Bone morphogenetic protein-2 stimulates adipogenic differentiation of mesenchymal precursor cells in synergy with BRL 49653 (rosiglitazone). FEBS Lett. 2000;475(3):201–4.

212. Kang Q, Song W-X, Luo Q, Tang N, Luo J, Luo X, et al. A Comprehensive Analysis of the Dual Roles of BMPs in Regulating Adipogenic and Osteogenic Differentiation of Mesenchymal Progenitor Cells. Stem Cells Dev. 2009;18(4):545–58.

213. Choy L, Derynck R. Transforming growth factor-β inhibits adipocyte differentiation by Smad3 interacting with CCAAT/enhancer-binding protein (C/EBP) and repressing C/EBP transactivation function. J Biol Chem.

2003;278(11):9609–19.

214. Hong J-H, Hwang ES, McManus MT, Amsterdam A, Tian Y, Kalmukova R, et al. TAZ, a Transcriptional Modulator of Mesenchymal Stem Cell Differentiation. Science. 2005;309(5737):1074–8.

215. Etheridge SL, Spencer GJ, Heath DJ, Genever PG. Expression profiling and functional analysis of wnt signaling mechanisms in mesenchymal stem cells. Stem Cells. 2004;22(5):849–60.

216. Ross SE, Hemati N, Longo KA, Bennett CN, Lucas PC, Erickson RL, et al. Inhibition of adipogensis by Wnt signaling. Science. 2000;289(5481):950–3.

217. Bennett CN, Ross SE, Longo KA, Bajnok L, Hemati N, Johnson KW, et al. Regulation of Wnt signaling during adipogenesis. J Biol Chem. 2002;277(34):30998–1004.

218. Barry F, Boynton RE, Liu B, Murphy JM. Chondrogenic differentiationof mesenchymal stem cells from bone marrow: Differentiation-dependent gene expression of matrix components. Exp Cell Res. 2001;268:189–200.

219. Watanabe H, De Caestecker MP, Yamada Y. Transcriptional Cross-talk between Smad, ERK1/2, and p38 Mitogen-activated Protein Kinase Pathways Regulates Transforming Growth Factor-b-induced Aggrecan Gene Expression in Chondrogenic ATDC5 Cells. J Biol Chem. 2001;276(17):14466–73.

220. Coricor G, Serra R. TGF-β regulates phosphorylation and stabilization of Sox9 protein in chondrocytes through p38 and Smad dependent mechanisms. Sci Rep. 2016;6:1–11.

221. Bell DM, Leung KKH, Wheatley SC, Ling Jim Ng, Zhou S, Kam Wing Ling, et al. SOX9 directly regulates the type-II collagen gene. Nat Genet. 1997;16(2):174–8.

222. Akiyama H. Control of chondrogenesis by the transcription factor Sox9. Mod Rheumatol. 2008;18(3):213–9.

223. Denker AE, Haas AR, Nicoll SB, Tuan RS. Chondrogenic differentiation of murine C3H10T1/2 multipotential mesenchymal cells: I. Stimulation by bone morphogenetic protein-2 in high-density micromass cultures. Differentiation. International Society of Differentiation; 1999;64(2):67–76.

224. Sekiya I, Larson BL, Vuoristo JT, Reger RL, Prockop DJ. Comparison of effect of BMP-2, -4, and -6 on in vitro cartilage formation of human adult stem cells from bone marrow stroma. Cell Tissue Res. 2005;320(2):269–76.

225. Komatsu DE, Hadjiargyrou M. Activation of the transcription factor HIF-1 and its target genes, VEGF, HO-1, iNOS, during fracture repair. Bone. 2004;34(4):680–8.

226. Schipani E. Hypoxia and HIF-1α in chondrogenesis. Semin Cell Dev Biol. 2005;16(4–5):539–46.

227. Pfander D. HIF-1α controls extracellular matrix synthesis by epiphyseal chondrocytes. J Cell Sci. 2003;116(9):1819–26.

228. Amarilio R, Viukov S V., Sharir A, Eshkar-Oren I, Johnson RS, Zelzer E. HIF1α regulation of Sox9 is necessary to maintain differentiation of hypoxic prechondrogenic cells during early skeletogenesis. Development. 2007;134(21):3917–28.

229. Dy P, Wang W, Bhattaram P, Wang Q, Wang L, Ballock RT, et al. Sox9 Directs Hypertrophic Maturation and Blocks Osteoblast Differentiation of Growth Plate Chondrocytes. Dev Cell. 2012;22(3):597–609.

230. Inada M, Yasui T, Nomura S, Miyake S, Deguchi K, Himeno M, et al. Maturational disturbance of chondrocytes in Cbfa1-deficient mice. Dev Dyn. 1999;214(4):279–90.

231. Wataha JC, Hanks CT, Craig RG. The in vitro effects of metal cations on eukaryotic cell metabolism. J Biomed Mater Res. 1991;25(9):1133–49.

232. Wataha JC, Hanks CT, Craig RG. The effect of cell monolayer density on the

cytotoxicity of metal ions which are released from dental alloys. Dent Mater. 1993;9(3):172–6.

233. Wataha JC, Hanks CT, Sun Z. Effect of cell line on in vitro metal ion cytotoxicity. Dent Mater. 1994;10(3):156–61.

234. Schedle A, Samorapoompichit P, Rausch-Fan XH, Franz A, Fureder W, Sperr WR, et al. Response of L-929 Fibroblasts, Human Gingival Fibroblasts, and Human Tissue Mast Cells to Various Metal Cations. J Dent Res. 1995;74(8):1513–20.

235. Wataha JC, Hanks CT, Craig RG. In vitro effects of metal ions on cellular metabolism and the correlation between these effects and the uptake of the ions. J Biomed Mater Res. 1994;28(4):427–33.

236. Boonkaew B, Kempf M, Kimble R, Cuttle L. Cytotoxicity testing of silver-containing burn treatments using primary and immortal skin cells. Burns. 2014;40(8):1562–9.

237. Schedle A, Samorapoompichit P, Fu W, Franz A, Sperr WR, Sperr W. Metal ion-induced toxic histamine release from human basophils and mast cells. J Biomed Mater Res. 1998;39(4):560–7.

238. Pauksch L, Hartmann S, Rohnke M, Szalay G, Alt V, Schnettler R, et al. Biocompatibility of silver nanoparticles and silver ions in primary human mesenchymal stem cells and osteoblasts. Acta Biomater. 2014;10(1):439–49.

239. Contreras RG, Vilchis JRS, Sakagami H, Nakamura Y, Nakamura Y, Hibino Y, et al. Type of cell death induced by seven metals in cultured mouse osteoblastic cells. In Vivo (Brooklyn). 2010;24(4):507–12.

240. Hidalgo E, Domínguez C. Study of cytotoxicity mechanisms of silver nitrate in human dermal fibroblasts. Toxicol Lett. 1998;98(3):169–79.

241. Locht LJ, Smidt K, Rungby J, Stoltenberg M, Larsen A. Uptake of silver from metallic silver surfaces induces cell death and a pro-inflammatory response in

cultured J774 macrophages. Histol Histopathol. 2011;26(6):689–97.

242. Mulley G, Jenkins ATA, Waterfield NR. Inactivation of the Antibacterial and Cytotoxic Properties of Silver Ions by Biologically Relevant Compounds. PLoS One. 2014;9(4):2–10.

243. Poon VKM, Burd A. In vitro cytotoxity of silver: implication for clinical wound care. Burns. 2004;30(2):140–7.

244. Wataha JC, Lockwood PE, Schedle A. Effect of silver, copper, mercury, and nickel ions on cellular proliferation during extended, low-dose exposures. J Biomed Mater Res. 2000;52(2):360–4.

245. Miyayama T, Arai Y, Suzuki N, Hirano S. Mitochondrial electron transport is inhibited by disappearance of metallothionein in human bronchial epithelial cells following exposure to silver nitrate. Toxicology. 2013;305:20–9.

246. Zheng Y, Li J, Liu X, Sun J. Antimicrobial and osteogenic effect of Ag-implanted titanium with a nanostructured surface. Int J Nanomedicine. 2012;7:875–84.

247. Kawata K, Osawa M, Okabe S. In vitro toxicity of silver nanoparticles at noncytotoxic doses to HepG2 human hepatoma cells. Environ Sci Technol. 2009;43(15):6046–51.

248. Kim S, Choi JE, Choi J, Chung K-H, Park K, Yi J, et al. Oxidative stress-dependent toxicity of silver nanoparticles in human hepatoma cells. Toxicol Vitr. 2009;23(6):1076–84.

249. Albers CE, Hofstetter W, Siebenrock KA, Landmann R, Klenke FM. In vitro cytotoxicity of silver nanoparticles on osteoblasts and osteoclasts at antibacterial concentrations. Nanotoxicology. 2013;7(1):30–6.

250. Inoue T, Suzuki Y, Yoshimaru T, Ra C. Ca2+-dependent mast cell death induced by Ag (I) via cardiolipin oxidation and ATP depletion. J Leukoc Biol. 2009;86(1):167–79.

251. Jiang X, Foldbjerg R, Miclaus T, Wang L, Singh R, Hayashi Y, et al. Multi-platform genotoxicity analysis of silver nanoparticles in the model cell line CHO-K1. Toxicol Lett. 2013;222(1):55–63.

252. Beer C, Foldbjerg R, Hayashi Y, Sutherland DS, Autrup H. Toxicity of silver nanoparticles - nanoparticle or silver ion? Toxicol Lett. 2012;208(3):286–92.

253. Foldbjerg R, Olesen P, Hougaard M, Dang DA, Hoffmann HJ, Autrup H. PVP-coated silver nanoparticles and silver ions induce reactive oxygen species, apoptosis and necrosis in THP-1 monocytes. Toxicol Lett. 2009;190(2):156–62.

254. Gonçalves TS, Menezes LM De, Trindade C, Machado MDS, Thomas P, Fenech M, et al. Cytotoxicity and genotoxicity of orthodontic bands with or without silver soldered joints. Mutat Res Genet Toxicol Environ Mutagen. 2014;762:1–8.

255. Wataha JC, Lewis JB, Lockwood PE, Rakich DR. Effect of dental metal ions on glutathione levels in THP-1 human monocytes. J Oral Rehabil. 2000;27(6):508–16.

256. Bai X, Sandukas S, Appleford M, Ong JL, Rabiei A. Antibacterial effect and cytotoxicity of Ag-doped functionally graded hydroxyapatite coatings. J Biomed Mater Res Part B. 2012;100(2):553–61.

257. Fielding GA, Roy M, Bandyopadhyay A, Bose S. Antibacterial and biological characteristics of plasma sprayed silver and strontium doped hydroxyapatite coatings. Acta Biomater. 2012;8(8):3144–52.

258. Lim PN, Shi Z, Neoh KG, Ho B, Tay BY, Thian ES. The effects of silver, silicon-containing apatite towards bacteria and cell responses. Biomed Mater. 2014;9(1):015010.

259. Bostancioglu RB, Gurbuz M, Akyurekli AG, Dogan A, Koparal AS, Koparal AT. Adhesion profile and differentiation capacity of human adipose tissue derived mesenchymal stem cells grown on metal ion (Zn, Ag and Cu) doped hydroxyapatite nano-coated surfaces. Colloids Surfaces B Biointerfaces.

2017;155:415–28.

260. Zhao Y, Cao H, Qin H, Cheng T, Qian S, Cheng M, et al. Balancing the Osteogenic and Antibacterial Properties of Titanium by Codoping of Mg and Ag: An in Vitro and in Vivo Study. ACS Appl Mater Interfaces. 2015;7(32):17826–36.

261. Hardes J, Streitburger A, Ahrens H, Nusselt T, Gebert C, Winkelmann W, et al. The influence of elementary silver versus titanium on osteoblasts behaviour in vitro using human osteosarcoma cell lines. Sarcoma. 2007 Jan;2007:26539.

262. Cortizo MC, de Mele MFL, Cortizo AM. Metallic Dental Material Biocompatibility in Osteoblastlike Cells: Correlation with Metal Ion Release. Biol Trace Elem Res. 2004;100(2):151–68.

263. Qin H, Zhu C, An Z, Jiang Y, Zhao Y, Wang J, et al. Silver nanoparticles promote osteogenic differentiation of human urine-derived stem cells at noncytotoxic concentrations. Int J Nanomedicine. 2014;9:2469–78.

264. Sengstock C, Diendorf J, Epple M, Schildhauer TA, Köller M. Effect of silver nanoparticles on human mesenchymal stem cell differentiation. Beilstein J Nanotechnol. 2014;5:2058–69.

265. He W, Elkhooly TA, Liu X, Cavallaro A, Taheri S, Vasilev K, et al. Silver nanoparticle based coatings enhance adipogenesis compared to osteogenesis in human mesenchymal stem cells through oxidative stress. J Mater Chem B. Royal Society of Chemistry; 2016;4(8):1466–79.

266. James S, Fox J, Afsari F, Lee J, Clough S, Knight C, et al. Multiparameter Analysis of Human Bone Marrow Stromal Cells Identifies Distinct Immunomodulatory and Differentiation-Competent Subtypes. Stem Cell Reports. 2015;4(6):1004–15.

267. Guzmán C, Bagga M, Kaur A, Westermarck J, Abankwa D. ColonyArea: An ImageJ plugin to automatically quantify colony formation in clonogenic assays. PLoS One. 2014;9(3):14–7.

268. Nelson SK, Wataha JC, Lockwood PE. Accelerated toxicity testing of casting alloys and reduction of intraoral release of elements. J Prosthet Dent. 1999;81(6):715–20.

269. Roohani-Esfahani S-I, Wong KY, Lu Z, Juan Chen Y, Li JJ, Gronthos S, et al. Fabrication of a novel triphasic and bioactive ceramic and evaluation of its in vitro and in vivo cytocompatibility and osteogenesis. J Mater Chem B. 2014;2(13):1866.

270. Cheng H, Li Y, Huo K, Gao B, Xiong W. Long-lasting in vivo and in vitro antibacterial ability of nanostructured titania coating incorporated with silver nanoparticles. J Biomed Mater Res - Part A. 2014;102(10):3488–99.

271. Roe D, Karandikar B, Bonn-Savage N, Gibbins B, Roullet J-B. Antimicrobial surface functionalization of plastic catheters by silver nanoparticles. J Antimicrob Chemother. 2008;61(4):869–76.

272. Lischer S, Körner E, Balazs DJ, Shen D, Wick P, Grieder K, et al. Antibacterial burst-release from minimal Ag-containing plasma polymer coatings. J R Soc Interface. 2011;8:1019–30.

273. Fordham WR, Redmond S, Westerland A, Cortes EG, Walker C, Gallagher C, et al. Silver as a Bactericidal Coating for Biomedical Implants. Surf Coatings Technol. 2014;253:52–7.

274. Luo S-H, Xiao W, Wei X-J, Jia W-T, Zhang C-Q, Huang W-H, et al. In vitro evaluation of cytotoxicity of silver-containing borate bioactive glass. J Biomed Mater Res B Appl Biomater. 2010;95B(2):441–8.

275. Vernè E, Di Nunzio S, Bosetti M, Appendino P, Vitale Brovarone C, Maina G, et al. Surface characterization of silver-doped bioactive glass. Biomaterials. 2005;26(25):5111–9.

276. Ramstedt M, Ekstrand-Hammarström B, Shchukarev A V, Bucht A, Osterlund L, Welch M, et al. Bacterial and mammalian cell response to poly(3-sulfopropyl methacrylate) brushes loaded with silver halide salts. Biomaterials.

2009;30(8):1524–31.

277. Probst R, Lim J, Bird D, Pole G, Sato A, Claybaugh J. Gender differences in the blood volume of conscious Sprague-Dawley rats. J Am Assoc Lab Anim Sci. 2006;45(2):49–52.

278. McCabe A, Pickford M, Shawcross J. The History, Technical Specifications and Efficacy of Plasma Spray Coatings Applied to Joint Replacement Prostheses. Reconstr Rev. 2016;6(4):19–26.

279. Klaassen CD. Biliary excretion of silver in the rat, rabbit, and dog. Toxicol Appl Pharmacol. 1979;50(1):49–55.

280. Liu J, Liu Y, Habeebu SS, Klaassen CD. Susceptibility of MT-null mice to chronic CdCl2-induced nephrotoxicity indicates that renal injury is not mediated by the CdMT complex. Toxicol Sci. 1998;46(1):197–203.

281. Nordberg GF. Modulation of metal toxicity by metallothionein. Biol Trace Elem Res. 1989;21(I):131–5.

282. Roesijadi G. Metallothionein and its role in toxic metal regulation. Comp Biochem Physiol - C Pharmacol Toxicol Endocrinol. 1996;113(2):117–23.

283. Feldman S, Cousins R. Degradation of hepatic zinc-thionein after parenteral zinc administration. Biochem J. 1976;160(3):583–8.

284. Steinebach OM, Wolterbeek BT. Metallothionein biodegradation in rat hepatoma cells: a compartmental analysis aided 35S-radiotracer study. Biochim Biophys Acta. 1992;1116(2):155–65.

285. Kimura M, Otaki N, Yoshiki S, Suzuki M, Horiuchi N. The isolation of metallothionein and its protective role in cadmium poisoning. Arch Biochem Biophys. 1974;165(1):340–8.

286. Habeebu SS, Liu J, Liu Y, Klaassen CD. Metallothionein-null mice are more susceptible than wild-type mice to chronic CdCl(2)-induced bone injury. Toxicol

Sci. 2000;56(1):211–9.

287. Cherian MG, Goyer RA. Metallothioneins and their role in the metabolism and toxicity of metals. Life Sci. 1978;23:1–10.

288. Eagle H. Nutrition needs of mammalian cells in tissue culture. Science. 1955;122:501–4.

289. Eagle H. Amino acid metabolism in mammalian cell cultures. Science. 1959;130:432–7.

290. Morton HJ. A survey of commercially available tissue culture media. In Vitro. 1970;6(2):89–108.

291. Dulbecco R. Transformation of Cells in Vitro By DNA-Containing Viruses. JAMA. 1964;190(8):721–6.

292. Stanners CP, Eliceiri GL, Green H. Two Types of Ribosome in Mouse–Hamster Hybrid Cells. Nat New Biol. 1971;230(10):52–4.

293. Sotiropoulou PA, Perez SA, Salagianni M, Baxevanis CN, Papamichail M. Characterization of the Optimal Culture Conditions for Clinical Scale Production of Human Mesenchymal Stem Cells. Stem Cells. 2006;24:462–71.

294. Greulich C, Braun D, Peetsch A, Diendorf J, Siebers B, Epple M, et al. The toxic effect of silver ions and silver nanoparticles towards bacteria and human cells occurs in the same concentration range. RSC Adv. 2012;2:6981–7.

295. Samberg ME, Loboa EG, Oldenburg SJ, Monteiro-Riviere NA. Silver nanoparticles do not influence stem cell differentiation but cause minimal toxicity. Nanomedicine. 2012;7(8):1197–209.

296. Loza K, Sengstock C, Chernousova S, Köller M, Epple M. The predominant species of ionic silver in biological media is colloidally dispersed nanoparticulate silver chloride. RSC Adv. 2014;4:35290–7.

297. Jaiswal N, Haynesworth SE, Caplan AI, Bruder SP. Osteogenic differentiation of purified, culture-expanded human mesenchymal stem cells in vitro. J Cell Biochem. 1997;64(2):295–312.

298. Nöth U, Osyczka AM, Tuli R, Hickok NJ, Danielson KG, Tuan RS. Multilineage mesenchymal differentiation potential of human trabecular bone-derived cells. J Orthop Res. 2002;20(5):1060–9.

299. Sekiya I, Larson BBL, Smith JJR, Pochampally R, Cui J-G, Prockop DJ. Expansion of human adult stem cells from bone marrow stroma: conditions that maximize the yields of early progenitors and evaluate their quality. Stem Cells. 2002;20:530–41.

300. Both SK, Muijsenberg AJC van der, Blitterswijk CA van, Boer J de, Bruijn JD de. A Rapid and Efficient Method for Expansion of Human Mesenchymal Stem Cells. Tissue Eng. 2007;13(1):3–9.

301. Schierholz JM, Wachol-Drewek Z, Lucas LJ, Pulverer G. Activity of silver ions in different media. Zentralbl Bakteriol. 1998;287(4):411–20.

302. Zhang S, Du C, Wang Z, Han X, Zhang K, Liu L. Reduced cytotoxicity of silver ions to mammalian cells at high concentration due to the formation of silver chloride. Toxicol Vitr. 2013;27(2):739–44.

303. Gupta A, Maynes M, Silver S. Effects of halides on plasmid-mediated silver resistance in Escherichia coli. Appl Environ Microbiol. 1998;64(12):5042–5.

304. Zuberek M, Wojciechowska D, Krzyzanowski D, Meczynska-Wielgosz S, Kruszewski M, Grzelak A. Glucose availability determines silver nanoparticles toxicity in HepG2. J Nanobiotechnology. BioMed Central; 2015;13(1):72.

305. Biological evaluation of medical devices Part 5: Tests for in vitro cytotoxicity (ISO10993-5). 2009.

306. Cortizo MC, Mele MFL De, Cortizo AM, Fernández M, Mele L De, María A. Cytotoxicity of copper and silver ions on specific osteoblastic properties. Rev

CENIC Ciencias Biológicas. 2006;37(3):159–60.

307. Williams D, Askill I, Smith R. Protein absorption and desorption phenomena on clean metal surfaces. J Biomed Mater Res. 1985;19(3):313–20.

308. Kaiser J-P, Roesslein M, Diener L, Wichser A, Nowack B, Wick P. Cytotoxic effects of nanosilver are highly dependent on the chloride concentration and the presence of organic compounds in the cell culture media. J Nanobiotechnology. BioMed Central; 2017;15(1):5.

309. Struempler AW. Adsorption Characteristics of Silver, Lead, Cadmium, Zinc, and Nickel on Borosilicate Glass, Polyethylene, and Polypropylene Container Surfaces. Anal Chem. 1973;45(13):2251–4.

310. West FK, West PW. Adsorption of Traces of Silver on Container Surfaces. Anal Chem. 1966;38(11):1566–70.

311. Paasche G, Ceschi P, Löbler M, Rösl C, Gomes P, Hahn A, et al. Effects of metal ions on fibroblasts and spiral ganglion cells. J Neurosci Res. 2011;89(4):611–7.

312. Wu J, Wang L, He J, Zhu C. In vitro cytotoxicity of Cu^{2+}, Zn^{2+}, Ag^{+} and their mixtures on primary human endometrial epithelial cells. Contraception. 2012;85(5):509–18.

313. Lee JTY, Leng Y, Chow KL, Ren F, Ge X, Wang K, et al. Cell culture medium as an alternative to conventional simulated body fluid. Acta Biomater. 2011;7(6):2615–22.

314. Gao X, Topping VD, Keltner Z, Sprando RL, Yourick JJ. Toxicity of nano- and ionic silver to embryonic stem cells: A comparative toxicogenomic study. J Nanobiotechnology. BioMed Central; 2017;15(31):1–18.

315. Albers CE, Hofstetter W, Siebenrock KA, Landmann R, Klenke FM. In vitro cytotoxicity of silver nanoparticles on osteoblasts and osteoclasts at antibacterial concentrations. Nanotoxicology. 2013;7(1):30–6.

316. Lewis JB, Wataha JC, Randol TM, McCloud V V, Lockwood PE. Metal ions alter lipopolysaccharide-induced NF kappa B binding in monocytes. J Biomed Mater Res A. 2003;67(3):868–75.

317. Justesen J, Stenderup K, Ebbesen EN, Mosekilde L, Steiniche T, Kassem M. Adipocyte tissue volume in bone marrow is increased with aging and in patients with osteoporosis. Biogerontology. 2001;2(3):165–71.

318. Oreffo ROC, Bord S, Triffitt JT. Skeletal progenitor cells and ageing human populations. Clin Sci. 1998;94:594–55.

319. Moerman EJ, Teng K, Lipschitz DA, Lecka-Czernik B. Aging activates adipogenic and suppresses osteogenic programs in mesenchymal marrow stroma/stem cells: The role of PPAR-γ2 transcription factor and TGF-β/BMP signaling pathways. Aging Cell. 2004;3(6):379–89.

320. Zhou S, Greenberger JS, Epperly MW, Goff JP, Adler C, Leboff MS, et al. Age-related intrinsic changes in human bone-marrow-derived mesenchymal stem cells and their differentiation to osteoblasts. Aging Cell. 2008;7(3):335–43.

321. Stolzing A, Jones E, McGonagle D, Scutt A. Age-related changes in human bone marrow-derived mesenchymal stem cells: consequences for cell therapies. Mech Ageing Dev. 2008;129(3):163–73.

322. Golden TR, Hinerfeld DA, Melov S. Oxidative stress and aging: beyond correlation. Aging Cell. 2002;1(2):117–23.

323. Sengers BG, Dawson JI, Oreffo ROC. Characterisation of human bone marrow stromal cell heterogeneity for skeletal regeneration strategies using a two-stage colony assay and computational modelling. Bone. 2010;46(2):496–503.

324. Gronthos S, Simmons PJ. The growth factor requirements of STRO-1-positive human bone marrow stromal precursors under serum-deprived conditions in vitro. Blood. 1995;85(4):929–40.

325. Kuznetsov SA, Friedenstein AJ, Robey PG. Factors required for bone marrow

stromal fibroblast colony formation in vitro. Br J Haematol. 1997;97(3):561–70.

326. Montes R, Ligero G, Sanchez L, Catalina P, De La Cueva T, Nieto A, et al. Feeder-free maintenance of hESCs in mesenchymal stem cell-conditioned media: Distinct requirements for TGF-B and IGF-II. Cell Res. 2009;19(6):698–709.

327. Caplan AI, Dennis JE. Mesenchymal stem cells as trophic mediators. J Cell Biochem. 2006;98(5):1076–84.

328. Gnecchi M, Zhang Z, Ni A, Dzau VJ. Paracrine mechanisms in adult stem cell signaling and therapy. Circ Res. 2008;103(11):1204–19.

329. Nakagami H, Maeda K, Morishita R, Iguchi S, Nishikawa T, Takami Y, et al. Novel autologous cell therapy in ischemic limb disease through growth factor secretion by cultured adipose tissue-derived stromal cells. Arterioscler Thromb Vasc Biol. 2005;25(12):2542–7.

330. Lai RC, Arslan F, Lee MM, Sze NSK, Choo A, Chen TS, et al. Exosome secreted by MSC reduces myocardial ischemia/reperfusion injury. Stem Cell Res. 2010;4(3):214–22.

331. Timmers L, Lim SK, Hoefer IE, Arslan F, Lai RC, van Oorschot AAM, et al. Human mesenchymal stem cell-conditioned medium improves cardiac function following myocardial infarction. Stem Cell Res. 2011;6(3):206–14.

332. Kordelas L, Rebmann V, Ludwig AK, Radtke S, Ruesing J, Doeppner TR, et al. MSC-derived exosomes: A novel tool to treat therapy-refractory graft-versus-host disease. Leukemia. 2014;28(4):970–3.

333. Linero I, Chaparro O. Paracrine effect of mesenchymal stem cells derived from human adipose tissue in bone regeneration. PLoS One. 2014;9(9):1–12.

334. Kemp K, Hares K, Mallam E, Heesom KJ, Scolding N, Wilkins A. Mesenchymal stem cell-secreted superoxide dismutase promotes cerebellar neuronal survival. J Neurochem. 2010;114(6):1569–80.

335. Salic A, Mitchison TJ. A chemical method for fast and sensitive detection of DNA synthesis in vivo. Proc Natl Acad Sci. 2008 Feb 19;105(7):2415–20.

336. Qin H, Cao H, Zhao Y, Zhu C, Cheng T, Wang Q, et al. In vitro and in vivo anti-biofilm effects of silver nanoparticles immobilized on titanium. Biomaterials. 2014;1–12.

337. Kohlmeier F, Maya-Mendoza A, Jackson DA. EdU induces DNA damage response and cell death in mESC in culture. Chromosom Res. 2013;21(1):87–100.

338. Jiao ZH, Li M, Feng YX, Shi JC, Zhang J, Shao B. Hormesis effects of silver nanoparticles at non-cytotoxic doses to human hepatoma cells. PLoS One. 2014;9(7).

339. Yoshimaru T, Suzuki Y, Inoue T, Niide O, Ra C. Silver activates mast cells through reactive oxygen species production and a thiol-sensitive store-independent Ca2+ influx. Free Radic Biol Med. 2006;40:1949–59.

340. Li Y, Qin T, Ingle T, Yan J, He W, Yin JJ. Differential genotoxicity mechanisms of silver nanoparticles and silver ions. Arch Toxicol. 2016;

341. Shim I, Choi K, Hirano S. Oxidative stress and cytotoxic effects of silver ion in mouse lung macrophages J774.1 cells. J Appl Toxicol. 2017;37(4):471–8.

342. Dekkers S, Williams TD, Zhang J, Zhou J (Albert), Vandebriel RJ, De La Fonteyne LJJ, et al. Multi-omics approaches confirm metal ions mediate the main toxicological pathways of metal-bearing nanoparticles in lung epithelial A549 cells. Environ Sci Nano. 2018;5(6):1506–17.

343. Georgantzopoulou A, Serchi T, Cambier S, Leclercq CC, Renaut J, Shao J, et al. Effects of silver nanoparticles and ions on a co-culture model for the gastrointestinal epithelium. Part Fibre Toxicol. 2016;13(1).

344. Juling S, Böhmert L, Lichtenstein D, Oberemm A, Creutzenberg O, Thünemann AF, et al. Comparative proteomic analysis of hepatic effects induced by

nanosilver, silver ions and nanoparticle coating in rats. Food Chem Toxicol. 2018;113:255–66.

345. Dickinson DA, Forman HJ. Cellular glutathione and thiols metabolism. Biochem Pharmacol. 2002;64(5–6):1019–26.

346. Aquilano K, Baldelli S, Ciriolo MR. Glutathione: new roles in redox signaling for an old antioxidant. Front Pharmacol. 2014;5:196.

347. Wellner VP, Anderson ME, Puri RN, Jensen GL, Meister A. Radioprotection by glutathione ester: transport of glutathione ester into human lymphoid cells and fibroblasts. PNAS. 1984;81(15):4732–5.

348. Dunning S, ur Rehman A, Tiebosch MH, Hannivoort RA, Haijer FW, Woudenberg J, et al. Glutathione and antioxidant enzymes serve complementary roles in protecting activated hepatic stellate cells against hydrogen peroxide-induced cell death. Biochim Biophys Acta. 2013;1832(12):2027–34.

349. Iemata M, Takarada T, Hinoi E, Taniura H, Yoneda Y. Suppression by glutamate of proliferative activity through glutathione depletion mediated by the cystine/glutamate antiporter in mesenchymal C3H10T1/2 stem cells. J Cell Physiol. 2007;213(3):721–9.

350. Ito K, Hirao A, Arai F, Takubo K, Matsuoka S, Miyamoto K, et al. Reactive oxygen species act through p38 MAPK to limit the lifespan of hematopoietic stem cells. Nat Med. 2006;12(4):446–51.

351. Arai Y, Miyayama T, Hirano S. Difference in the toxicity mechanism between ion and nanoparticle forms of silver in the mouse lung and in macrophages. Toxicology. 2015;328(2015):84–92.

352. Tsan M, White JE, Rosano CL. Modulation of endothelial GSH concentrations: effect of exogenous GSH and GSH monoethyl ester. J Appl Physiol. 1989;66(3):1029–34.

353. Aminizadeh N, Tiraihi T, Mesbah-Namin SA, Taheri T. Stimulation of cell proliferation by glutathione monoethyl ester in aged bone marrow stromal cells is associated with the assistance of TERT gene expression and telomerase activity. Vitr Cell Dev Biol - Anim. 2016;52(7):772–81.

354. Guo W, Zhao Y, Zhang Z, Tan N, Zhao F, Ge C, et al. Disruption of xCT inhibits cell growth via the ROS/autophagy pathway in hepatocellular carcinoma. Cancer Lett. 2011;312(1):55–61.

355. Lu H, Samanta D, Xiang L, Zhang H, Hu H, Chen I, et al. Chemotherapy triggers HIF-1–dependent glutathione synthesis and copper chelation that induces the breast cancer stem cell phenotype. PNAS. 2015;112(33):E4600–9.

356. Espinosa-Diez C, Miguel V, Mennerich D, Kietzmann T, Sánchez-Pérez P, Cadenas S, et al. Antioxidant responses and cellular adjustments to oxidative stress. Redox Biol. 2015;6:183–97.

357. You BR, Shin HR, Park WH. PX-12 inhibits the growth of A549 lung cancer cells via G2/M phase arrest and ROS-dependent apoptosis. Int J Oncol. 2014;44(1):301–8.

358. Li GZ, Liang HF, Liao B, Zhang L, Ni YA, Zhou HH, et al. Px-12 inhibits the growth of hepatocelluar carcinoma by inducing S-phase arrest, ROS-dependent apoptosis and enhances 5-FU cytotoxicity. Am J Transl Res. 2015;7(9):1528–40.

359. von Mering C, Jensen LJ, Snel B, Hooper SD, Krupp M, Foglierini M, et al. STRING: Known and predicted protein-protein associations, integrated and transferred across organisms. Nucleic Acids Res. 2005;33:D433-437.

360. Szklarczyk D, Morris JH, Cook H, Kuhn M, Wyder S, Simonovic M, et al. The STRING database in 2017: Quality-controlled protein-protein association networks, made broadly accessible. Nucleic Acids Res. 2017;45:D362–8.

361. Huang DW, Sherman BT, Lempicki RA. Systematic and integrative analysis of large gene lists using DAVID bioinformatics resources. Nat Protoc. 2009;4(1):44–57.

362. Huang DW, Sherman BT, Lempicki RA. Bioinformatics enrichment tools: Paths toward the comprehensive functional analysis of large gene lists. Nucleic Acids Res. 2009;37(1):1–13.

363. Saleh F, Carstairs A, Etheridge SL, Genever P. Real-Time Analysis of Endogenous Wnt Signalling in 3D Mesenchymal Stromal Cells. Stem Cells Int. 2016;2016.

364. Siegel D, Gustafson DL, Dehn DL, Han JY, Boonchoong P, Berliner LJ, et al. NAD(P)H:Quinone Oxidoreductase 1: Role as a Superoxide Scavenger. Mol Pharmacol. 2004;65(5):1238–47.

365. Beckman JD, Chen C, Nguyen J, Thayanithy V, Subramanian S, Steer CJ, et al. Regulation of heme oxygenase-1 protein expression by miR-377 in combination with miR-217. J Biol Chem. 2011;286(5):3194–202.

366. Xin L, Wang J, Fan G, Che B, Wu Y, Guo S, et al. Oxidative Stress and Mitochondrial Injury-Mediated Cytotoxicity Induced by Silver Nanoparticles in Human A549 and HepG2 Cells. Environ Toxicol. 2016;31(12):1691–9.

367. Datta SR, Dudek H, Xu T, Masters S, Haian F, Gotoh Y, et al. Akt phosphorylation of BAD couples survival signals to the cell-intrinsic death machinery. Cell. 1997;91(2):231–41.

368. Song L, Webb NE, Song Y, Tuan RS. Identification and Functional Analysis of Candidate Genes Regulating Mesenchymal Stem Cell Self-Renewal and Multipotency. Stem Cells. 2006;24(7):1707–18.

369. Zhong N, Gersch RP, Hadjiargyrou M. Wnt signaling activation during bone regeneration and the role of Dishevelled in chondrocyte proliferation and differentiation. Bone. 2006;39(1):5–16.

370. Tokunaga A, Oya T, Ishii Y, Motomura H, Nakamura C, Ishizawa S, et al. PDGF receptor β is a potent regulator of mesenchymal stromal cell function. J Bone Miner Res. 2008;23(9):1519–28.

371. Rodrigues M, Griffith LG, Wells A. Growth factor regulation of proliferation and survival of multipotential stromal cells. Stem Cell Res Ther. 2010;1(4):32.

372. Zhang Y, Dépond M, He L, Foudi A, Kwarteng EO, Lauret E, et al. CXCR4/CXCL12 axis counteracts hematopoietic stem cell exhaustion through selective protection against oxidative stress. Sci Rep. 2016;6:1–13.

373. Chen D-J, Xu Y-M, Zheng W, Huang D-Y, Wong W-Y, Tai WC-S, et al. Proteomic analysis of secreted proteins by human bronchial epithelial cells in response to cadmium toxicity. Proteomics. 2015;15(17):3075–86.

374. Rawadi G, Vayssière B, Dunn F, Baron R. BMP-2 Controls Alkaline Phosphatase Expression and Osteoblast Mineralization by a Wnt Autocrine Loop. J Bone Miner Res. 2003;18(10):1842–53.

375. Day TF, Guo X, Garrett-Beal L, Yang Y. Wnt/β-Catenin Signaling in Mesenchymal Progenitors Controls Osteoblast and Chondrocyte Differentiation during Vertebrate Skeletogenesis. Dev Cell. 2005;8:739–50.

376. Macsai CE, Foster BK, Xian CJ. Roles of Wnt signalling in bone growth, remodelling, skeletal disorders and fracture repair. J Cell Physiol. 2008;215(3):578–87.

377. Hinoi E, Fujimori S, Wang L, Hojo H, Uno K, Yoneda Y. Nrf2 negatively regulates osteoblast differentiation via interfering with Runx2-dependent transcriptional activation. J Biol Chem. 2006;281(26):18015–24.

378. Kensler TW, Wakabayashi N, Biswal S. Cell Survival Responses to Environmental Stresses Via the Keap1-Nrf2-ARE Pathway. Annu Rev Pharmacol Toxicol. 2007;47(1):89–116.

379. Pi J, Leung L, Xue P, Wang W, Hou Y, Liu D, et al. Deficiency in the nuclear factor E2-related factor-2 transcription factor results in impaired adipogenesis and protects against diet-induced obesity. J Biol Chem. 2010;285(12):9292–300.

380. Hou Y, Xue P, Bai Y, Liu D, Woods CG, Yarborough K, et al. Nuclear factor

erythroid-derived factor 2-related factor 2 regulates transcription of CCAAT/enhancer-binding protein β during adipogenesis. Free Radic Biol Med. Elsevier Inc.; 2012;52(2):462–72.

381. Stewart D, Killeen E, Naquin R, Alam S, Alam J. Degradation of transcription factor Nrf2 via the ubiquitin-proteasome pathway and stabilization by cadmium. J Biol Chem. 2003;278(4):2396–402.

382. Haynesworth SE, Baber MA, Caplan AI. Cytokine Expression by Human Marrow-Derived Mesenchymal Progenitor Cells In Vitro: Effects of Dexamethasone and IL-1α. J Cell Physiol. 1996;166(3):585–92.

383. Liu CH, Hwang SM. Cytokine interactions in mesenchymal stem cells from cord blood. Cytokine. 2005;32(6):270–9.

384. Singhal RK, Anderson ME, Meister A. Glutathione, a first line of defense against cadmium toxicity. FASEB. 1987;1(3):220–3.

385. Mulier B, Rahman I, Watchorn T, Donaldson K, MacNee W, Jeffery PK. Hydrogen peroxide-induced epithelial injury: The protective role of intracellular nonprotein thiols (NPSH). Eur Respir J. 1998;11(2):384–91.

386. Cuypers A, Plusquin M, Remans T, Jozefczak M, Keunen E, Gielen H, et al. Cadmium stress: An oxidative challenge. BioMetals. 2010;23(5):927–40.

387. Hayes JD, Flanagan JU, Jowsey IR. Glutathione Transferases. Annu Rev Pharmacol Toxicol. 2005;45(1):51–88.

388. Marnett LJ, Riggins JN, West JD. Endogenous generation of reactive oxidants and electrophiles and their reactions with DNA and protein. J Clin Invest. 2003;111(5):583–93.

389. Iyama T, Wilson DM. DNA repair mechanisms in dividing and non-dividing cells. DNA Repair (Amst). Elsevier B.V.; 2013;12(8):620–36.

390. Hakem R. DNA-damage repair; the good, the bad, and the ugly. EMBO J.

2008;27(4):589–605.

391. Göktürk E, Turgut A, Baygu C, Gunal I, Seber S, Gulbas Z. Oxygen-free radicals impair fracture healing in rats. Acta Orthop. 1995;66(5):473–5.

392. Hernigou PH, Poignard A, Beaujean F, Rouard H. Percutaneous autologous bone- marrow grafting for nonunions. Influence of the number and concentration of progenitor cells. J Bone Jt Surg. 2005;87–A(7):1430–7.

393. Woolley JF, Stanicka J, Cotter TG. Recent advances in reactive oxygen species measurement in biological systems. Trends Biochem Sci. Elsevier Ltd; 2013;38(11):556–65.

394. Vandana S, Ram S, Ilavazhagan M, Kumar GD, Banerjee PK. Comparative cytoprotective activity of vitamin C, E and beta-carotene against chromium induced oxidative stress in murine macrophages. Biomed Pharmacother. 2006;60(2):71–6.

395. Gnanadhas DP, Thomas M Ben, Thomas R, Raichur AM, Chakravortty D. Interaction of silver nanoparticles with serum proteins affects their antimicrobial activity in vivo. Antimicrob Agents Chemother. 2013;57(10):4945–55.

396. Ambasudhan R, Nakamura T, Dolatabadi N, Sultan A, Yates JR, Masliah E, et al. Role of sulfiredoxin as a peroxiredoxin-2 denitrosylase in human iPSC-derived dopaminergic neurons. Proc Natl Acad Sci. 2016;113(47):E7564–71.

397. Tomanek L. Proteomic responses to environmentally induced oxidative stress. J Exp Biol. 2015;218(Pt 12):1867–79.